



University of Antwerp

LMPH | Laboratory of Microbiology,
Parasitology and Hygiene

Faculty of Pharmaceutical, Biomedical and Veterinary Sciences

Department of Pharmaceutical Sciences

**Investigating Mtr and MshC as
potential targets in the fight against
Mycobacterium abscessus infections**

**Het onderzoeken van Mtr en MshC als
mogelijke doelwitten in de strijd tegen
Mycobacterium abscessus infecties**

Thesis submitted to obtain the degree of
Doctor in Pharmaceutical Sciences at the University of Antwerp

Tatiana PILLER

April 2024, Antwerp

Promotors:

Prof. dr. Paul Cos

Dr. Linda De Vooght

© **Tatiana Piller.** “Investigating Mtr and MshC as potential targets in the fight against *Mycobacterium abscessus* infections”

All rights reserved. No part of this book may be reproduced, stored in a retrieval system or transmitted in any form by any means without the prior permission of the holder of the copyrights.

ISBN: 9789057288371

Depot number: D/2024/12.293/07

Front cover design: Tatiana Piller

The research described in this thesis was carried out in the Laboratory of Microbiology, Parasitology and Hygiene (LMPH) at the University of Antwerp, Belgium. The study was funded by an FWO-sb grant

**Dissertation submitted to obtain the degree of
Doctor in Pharmaceutical Sciences at the University of
Antwerp, Belgium to be defended by**

Tatiana PILLER

Promotors, University of Antwerp

Prof. dr. Paul Cos Promotor

Laboratory of Microbiology, Parasitology and Hygiene (LMPH)

Dr. Linda De Vooght Promotor

Laboratory of Microbiology, Parasitology and Hygiene (LMPH)

Members of the PhD Committee, University of Antwerp

Prof. dr. Wim Martinet Chair

Laboratory of Physiopharmacology

Prof. dr. ir. Yann Sterckx Member

Laboratory of Medical Biochemistry

External members of the PhD Jury

Prof. dr. Leen Rigouts

Unit of Microbiology, Institute of Tropical Medicine, Belgium

Prof. dr. Maria Salomé Gomes

*Instituto de Ciências Biomédicas Abel Salazar (ICBAS) and Instituto de
Investigação e Inovação em Saúde (i3S), Universidade do Porto, Portugal*

Tat's Lab Playlist

The Man Who Can't Be Moved The Script	4:01
People Libianca, Cian Ducrot	3:04
This Love Maroon 5	3:26
Dynamite BTS	3:19
We Don't Talk Anymore Charlie Puth, Selena Gomez	3:37
Every Second Mina Okabe	3:02
Standing Next To You Jungkook	3:26
Ocean Eyes Billie Eilish	3:20
Flowers Miley Cyrus	3:20
Sunroof Nicky Youre, Dazy	2:43
Way Back Home SHAUN	3:34
In The Stars Benson Boone	3:36
Smile Johnny Stimson	2:42
Wat Wil Je Van Mij Metejoor, Hannah Mae	3:19
17 Pink Sweat\$	2:40
Never Not Lauv	3:28
Strangers Kenya Grace	2:52
As It Was Harry Styles	2:47
About Damn Time Lizzo	3:11



Table of content

Abbreviations.....	1
Chapter I: Introduction.....	13
I.1 The everlasting fight against infectious diseases.....	15
I.2 <i>Mycobacterium abscessus</i> , an emerging pathogen.....	16
I.3 Redox homeostasis as drug target.....	35
I.4 Genetic engineering.....	39
Chapter II: Research objectives and outline.....	51
Chapter III: Generation and functional characterization of <i>mtr</i> and <i>mshC</i> overexpressing strains in <i>Mycobacterium abscessus</i>.....	57
Chapter IV: Implementation of the <i>Streptococcus thermophilus</i> CRISPRi-system to investigate the essentiality of <i>mtr</i> and <i>mshC</i> in <i>Mycobacterium abscessus</i>.....	91
Chapter V: Validating the p2NIL/pGOAL method in <i>Mycobacterium smegmatis</i>.....	121
Chapter VI: Creating <i>mtr</i> and <i>mshC</i> knockout strains to evaluate Mtr and MshC as potential drug targets.....	145
Chapter VII: Discussion and Summary.....	179
General discussion.....	181
Future perspectives.....	190
Conclusion.....	193
Summary/Samenvatting.....	194
References.....	199
Scientific curriculum vitae.....	219
Acknowledgements.....	221

Abbreviations

μF	microfarad
μg	microgram
μL	microliter
μm	micrometer
μM	micromolar
Ω	ohm

A

AcCys	acetylcysteine
AcCys-GlcN-Ins	acetylcysteine-glucosamine-inositol
ADS	albumin-dextrose-saline
AI	artificial intelligence
ATS	American Thoracic Society
Anti-TB	anti-tuberculosis
ATc	anhydrotetracycline
ATP	adenosine triphosphate

B

bp	base pairs
BleoR	bleomycin-resistant cassette

BLI bioluminescent imaging

BTS British Thoracic Society

C

CF cystic fibrosis

CFU colony-forming unit

CO₂ carbon dioxide

COVID-19 coronavirus disease

CRISPR-Cas Clustered Regularly Interspaced Short Palindromic Repeats–CRISPR associated proteins

CRISPR*i* Clustered Regular Short Palindromic Repeat or CRISPR interference

Cys-GlcN-Ins cysteine-glucosamine-inositol

D

dCas9 nuclease-deficient Cas9 protein

dCas9_{Spy} *Streptococcus pyogenes* dCas9

dCas9_{Sth1} *Streptococcus thermophilus* dCas9

DCO double cross-over

DEPC diethylpyrocarbonate

DMEM Dulbecco's modified Eagle's

DMSO	dimethyl sulfoxide
DNA	deoxyribonucleic acid
DNase	deoxyribonuclease
DPBS	Dulbecco's Phosphate Buffered Saline
dpi	days post-infection
dsDNA	double-stranded DNA

E

<i>E. coli</i>	<i>Escherichia coli</i>
<i>erm41</i>	erythromycin ribosomal methylase gene
ERS	European Respiratory Society
ESCMID	European Society of Clinical Microbiology and Infectious Diseases
ESH	ergothioneine

F

FAD	flavin adenine dinucleotide
For	forward

G

G	gauge
<i>G. mellonella</i>	<i>Galleria mellonella</i>

GlcN	N-glucosamine
GlcNAc	N-acetylglucosamine
GlcNAc-Ins-P	N-acetyl glucosamine myo-inositol-1-phosphate
GlcN-Ins	glucosamine inositol
GPL	glycopeptidolipid
GSH	glutathione

H

h	hours
H ₂ O ₂	hydrogen peroxide
Hifi	high fidelity
His	histidine
hpi	hours post-infection
<i>hsp60</i>	heat-shock protein 60
<i>hsp65</i>	heat-shock protein 65
HTS	high-throughput screen
HygR	hygromycin-resistant cassette
hygro	hygromycin

I

IC50	inhibitory concentration 50%
------	------------------------------

IC90	inhibitory concentration 90%
IDSA	Infectious Diseases Society of America
<i>i</i> FCS	heat-inactivated Fetal Calf Serum
Ins	inositol
Ins-P	inositol-phosphate
Int	integrase
<i>ITS</i>	internal transcribed spacer
IVIS	<i>in vivo</i> imaging system

K

kana	kanamycin
KanR	kanamycin-resistant cassette
<i>katA</i>	catalase gene
KD	knockdown
KO	knockout
kV	kilovolt

L

LB	Luria-Bertani
LMPH	Laboratory of Microbiology, Parasitology and Hygiene
LMW	low molecular weight

M

m	meter
<i>Mab</i>	<i>Mycobacterium abscessus</i>
MABC	<i>Mycobacterium abscessus</i> complex
MABC-PD	MABC pulmonary disease
MDR-TB	multidrug-resistant tuberculosis
mIHF	host-expressed integration host factor
min	minutes
mL	milliliter
mm	millimeter
mM	millimolar
mm ²	square millimeter
<i>mmp13</i>	mycobacterial membrane protein Large 3 gene
MOI	multiplication of infection
mRNA	messenger ribonucleic acid
MSH	mycothiol
MshA	glycosyltransferase
<i>mshA</i>	glycosyltransferase gene
MshA2	phosphatase
MshB	deacetylase
<i>mshB</i>	deacetylase gene
MshC	cysteine ligase

<i>mshC</i>	cysteine ligase gene
MshD	MSH synthase
<i>mshD</i>	MSH synthase gene
<i>Msm</i>	<i>Mycobacterium smegmatis</i>
MSSM	mycothione
<i>Mtb</i>	<i>Mycobacterium tuberculosis</i>
Mtr	mycothione reductase
<i>mtr</i>	mycothione reductase gene
MurNAc	N-acetylmuramic acid

N

NADP	nicotinamide adenine dinucleotide phosphate
NADPH	reduced nicotinamide adenine dinucleotide phosphate
NC	negative control
NCBI	National Center for Biotechnology Information
NEB	New England Biolabs
ng	nanogram
NPET	nascent peptide exit tunnel
nm	nanometer
nM	nanomolar
ns	non-significant

NTM nontuberculous mycobacteria

O

OADC oleic acid-albumin-catalase-dextrose

OD₆₀₀ optical density at 600 nm

OE overexpressor

Ohr organic hydroperoxide resistance protein

oligo oligonucleotide

ORBIT oligonucleotide-mediated recombineering followed by Bxb1 integrase targeting

ori origin of replication

P

P/S Penicillin-Streptomycin

PAM protospacer adjacent motif

PCR Polymerase chain reaction

PBP penicillin-binding proteins

Q

qPCR quantitative PCR

R

R	rough
R ²	coefficient of determination
RecT	RecT annealase
Rev	reverse
RGM	rapidly-growing mycobacteria
RLU	relative luminescence units
RNA	ribonucleic acid
RNAP	RNA polymerase
RNS	reactive nitrogen species
ROS	reactive oxygen species
rpm	rotation per minute
<i>rpoB</i>	β-subunit of RNA polymerase gene
<i>rRNA</i>	ribosomal RNA gene
RT	room temperature
RT-qPCR	real-time quantitative PCR

S

s	second
S	smooth
SCO	single cross-over

SEM	standard error of the mean
sgRNA	small guide RNA
SNPs	single nucleotide polymorphisms
<i>sodA</i>	superoxide dismutase
<i>Spy</i>	<i>Streptococcus pyogenes</i>
ssDNA	single-stranded DNA
ssRNA	single-stranded RNA
<i>Sth</i>	<i>Streptococcus thermophilus</i>
<i>Sth</i> CRISPRi	<i>Streptococcus thermophilus</i> CRISPR interference

T

Tc	tetracycline
TetR	tetracycline repressor
TNF	tumor necrosis factor
tRNA	transfer RNA

U

U	units
UDP-GlcNAc	uridine diphosphate N-acetylglucosamine

V

VPC viable plate count

W

w/v weight per volume

WGS whole genome sequencing

WHO World Health Organization

WT wild-type

CHAPTER I

Introduction



I. Introduction

I.1 The everlasting fight against infectious diseases

At least once every year, the majority of the population becomes sick with an infectious disease. Fortunately, most of the infectious diseases we encounter nowadays are easily treatable and curable after a short visit to a pharmacist or medical doctor that provides drugs that quickly alleviate the symptoms and/or kill the disease-causing pathogen. However, this has not always been the case. In the 19th century, people lived surrounded by many infectious diseases that were still untreatable. Getting sick with one would lead to the development of serious illness and often death. Infectious diseases were responsible for a high percentage of morbidity and mortality worldwide with an average life expectancy of 47 years (1). This all changed in the early 20th century with the discovery of antibiotics, significantly decreasing the deaths caused by bacterial infections (2, 3). The outcome of infections was even further improved with the discovery and approval of the first antiviral drug in 1963, targeting viral infectious diseases (4). Antimicrobial drugs have become part of our daily lives and are used to treat and cure a variety of infectious diseases globally.

When the coronavirus disease (COVID-19) pandemic started in the beginning of 2020, very limited resources were available to treat the disease, leading not only to severe illness and death, but also a mandatory lockdown, economic crisis, and worldwide panic. According to the World Health Organization (WHO), the COVID-19 pandemic resulted in the death of nearly 7 million people while causing immense suffering to an even higher amount of people worldwide (5). This global ordeal gave us a bitter taste of how life was before the development of antimicrobial drugs while further establishing the importance of medical advances and the emergence of novel drugs to fight infectious diseases (3).

Beside COVID-19, many other infectious diseases need our attention as they are still incurable, untreatable, or suffer suboptimal treatment. An example of such a

disease is caused by *Mycobacterium abscessus* (*Mab*), an emerging human pathogen often referred to as the “antibiotic nightmare” (6).

I.2 *Mycobacterium abscessus*, an emerging pathogen

Mycobacterium abscessus complex (MABC) is a group of aerobic, rod-shaped, rapidly-growing mycobacteria (RGM) and is the most common rapidly-growing nontuberculous mycobacteria (NTM) causing disease and respiratory infections worldwide (7–11). NTMs are mainly originating from the environment where they are ubiquitous and unlike the infamous *M. tuberculosis* (*Mtb*), person-to-person transmission is uncommon (12). Among the NTM species, MABC is considered the most difficult to treat as it is highly resistant and the most alarming nosocomial pathogen due to its opportunistic nature, predominantly infecting immunocompromised patients or patients with a preexisting lung condition (7–9). Although it is often considered a mere opportunistic pathogen, MABC is believed to possess various disconcerting features driving its evolution into a true human pathogen (13).

The incidence of NTM infections have been rapidly increasing over the last two decades in all types of populations, especially among cystic fibrosis (CF) patients for which the global incidence raised from 3.3% to 22.6% together with increasing morbidity and mortality. MABC infections are most frequent in the European CF population, particularly in younger CF patients (9, 13, 14). Hereby, the prevalence of MABC infections in pediatric CF patients in European centers is fluctuating between 3.4 and 5.8% (15). In the general population, an overall increasing trend in NTM incidence was observed worldwide based on 48 studies originating from more than 18 countries (**Figure I.1a**). Out of the 48 studies, 23 studies reported MABC incidence trend data of which two-thirds indicated an increase in incidence over time (**Figure I.1b**). An increase in incidence is likely the result of a longer life expectancy of the worldwide population, an intensification of immunosuppressive therapy, an improvement of mycobacterial diagnostics, and an increasing

awareness of NTMs (16). Furthermore, the prevalence of NTM infections vary widely according to the geographic region, with the annual prevalence going as high as 65 cases per 100,000 individuals in certain regions (17). However, the incidence and prevalence of NTM and MABC infections is underestimated due to the regular misdiagnosis, in which NTM infections are repeatedly mistaken as multidrug-resistant tuberculosis (MDR-TB), together with the missing data from various countries, intensifying the urgent need of a standardized format to provide data on NTM incidence and prevalence (9, 16, 18). From all NTM isolations worldwide, MABC accounted for 16% in Asia, 12% in Oceania, 5.7% in South America, 3.2% in North America and 2.9% in Europe while no precise percentage is known for Africa. With a total isolation frequency and clinical relevance of 61%, it is one of the most clinically relevant species among NTMs (18).

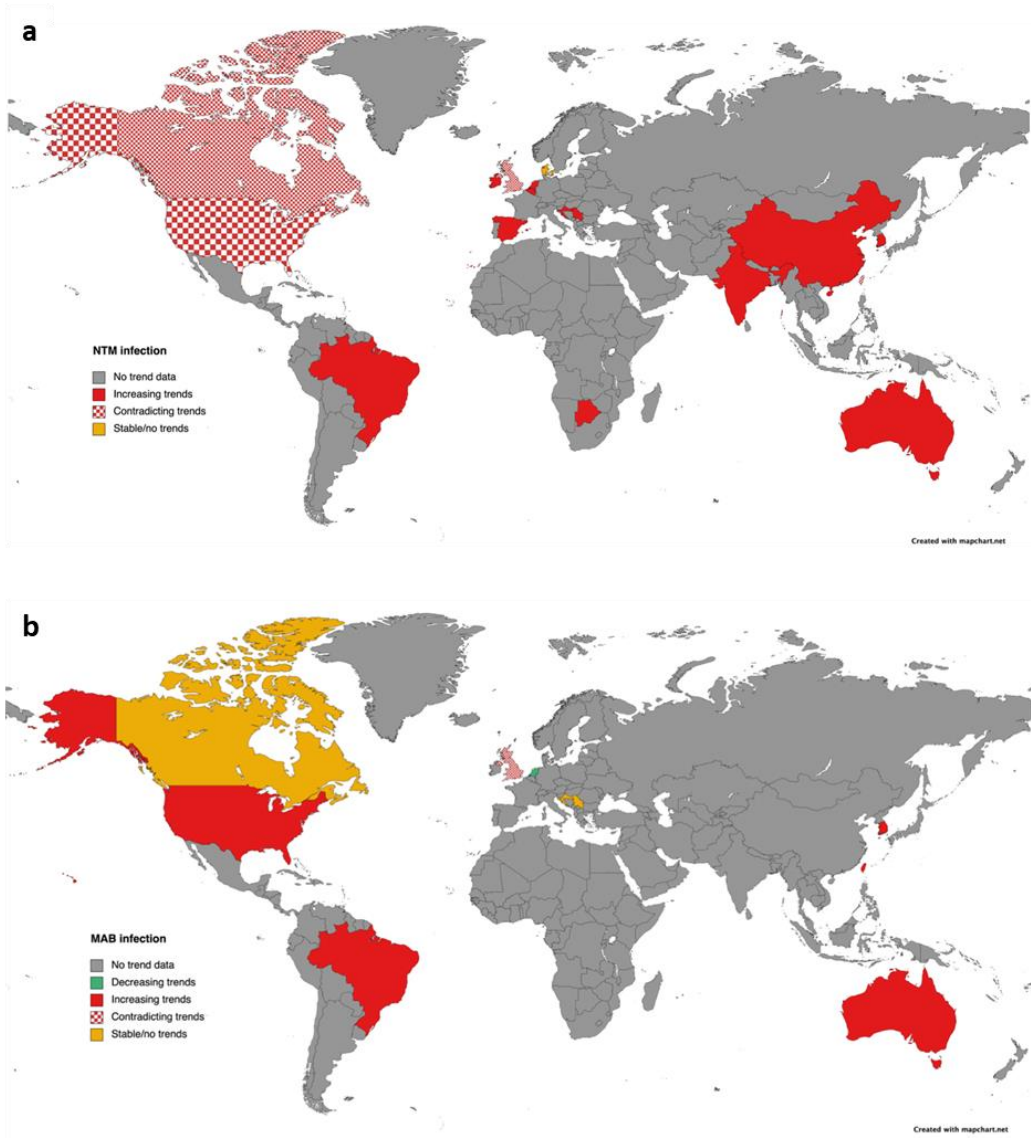


Figure I.1. Trend data of the incidence of NTM (a) and MABC (b) worldwide. Overall, increasing trends were detected for the incidence of both NTM and MABC infection. Gray colors represent the countries for which no trend data is available, red colors represent increasing trends, a red-white checkered area represents contradicting trends (i.e., both increasing, stable and/or decreasing), and yellow represents stable trends. Figure adapted from Dahl et al. (16).

MABC is a species belonging to the phylum *Actinobacteria* and comprises three subspecies: *M. abscessus bollettii*, *M. abscessus massiliense*, and *M. abscessus abscessus*, with the latter being the most common among the subspecies (45-65%) (19–21). Members of this species are Gram-positive, acid-fast bacteria containing high G+C content in their DNA (7, 21). Their cell wall is very thick and is composed of an inner single-lipid cell membrane, a peptidoglycan layer, an arabinogalactan layer, mycolic acids, and an outer capsule-like membrane containing glycolipids (**Figure I.2**). Peptidoglycan is made of linked N-acetylglucosamine (GlcNAc) and N-acetylmuramic acid (MurNAc) residues and functions as a layer to provide rigidity and osmotic stability to the bacteria (22, 23). The arabinogalactan layer consists of polysaccharides whereas mycolic acids are long chains of fatty acids, both contributing to the impermeability of the cell wall (10, 23–25). Other components such as porins, proteins transporting hydrophilic molecules into the bacteria, and lipoarabinomannan, glycoconjugates modulating host immune response during infection, are also present in the mycobacterial cell wall (23, 26).

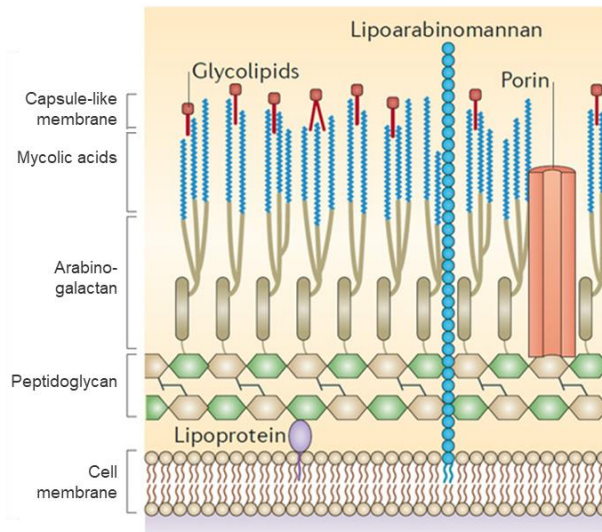


Figure I.2. Schematic representation of the acid-fast cell wall of MABC. The thick, impermeable, acid-fast cell wall consists of an inner cell membrane, a peptidoglycan layer, an arabinogalactan layer, mycolic acids and a capsule-like membrane containing glycolipids. Porins, lipoproteins and lipoarabinomannan are also present in the cell wall. Adapted from Brown et al (27).

Colonies formed by MABC can be found as two distinct phenotypes: a smooth (S) and rough (R) phenotype. While S colonies are round, uniform and glossy, R colonies are irregular, corded and dry (**Figure I.3**). These phenotypes are dependent on the presence or absence of glycopeptidolipids (GPLs), a vast array of complex glycolipids on the outer layer of the cell envelope, in which presence of GPLs results in a S phenotype whereas lack of GPLs lead to a R phenotype (28, 29). Absence of GPLs in MABC is a result of irreversible mutations in the mycobacterial genes responsible for GPL synthesis, i.e. nonribosomal peptide synthetases genes, and genes responsible for GPL transport, i.e. *mmp14* genes (30, 31).

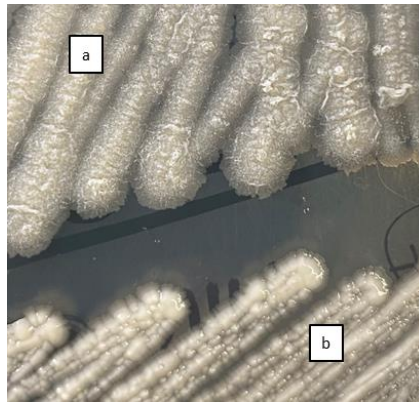


Figure I.3. Illustration of the distinct colony phenotypes of MABC on 7H10 agar. Rough (a) colonies have an irregular and dry look while smooth (b) colonies are round and glossy. Figure from López-Roa et al. (13).

I.2.1 Pathogenesis and risk factors

Members of MABC are widely spread throughout the environment and can be found in both natural, or human-made environments or any healthcare setting. Such environments include water, soil, dust, air, water distribution systems, household plumbing, cigarettes and contaminated healthcare materials (28, 32). It is believed that MABC can even persist in the environment by surviving and replicating within free-living amoeba, hereby being protected while preparing to infect another host (13). Infection of a host mainly occurs through penetration of

the skin via a wound or inhalation of aerosols with contaminated soil or water (11, 33). Moreover, recent studies demonstrated the occurrence of person-to-person transmission between CF patients in a healthcare setting, raising concerns regarding the ability of the pathogen to spread and the impact it will have on public health (13, 18).

After penetration of the host, the intruding pathogen encounters the host's first-line of defense, the innate immune system (**Figure I.4**) (34). Here, phagocytic cells of the skin and lungs, such as macrophages and neutrophils, will take up the bacteria as a bactericidal response (13). To evade the immune system and survive within the cells, the S and R morphologies of MABC will interact differently with the immune cells, leading to distinct disease outcomes (26). The S variants are phagocytized by macrophages individually and kept in "loner phagosomes" (13, 28). Within the phagosomes, they can resist phagosomal degradation and survive for an extended period by limiting phagosomal acidification and disrupting the phagosomal membrane integrity. Eventually, the production of inflammatory cytokines, such as tumor necrosis factor (TNF), is induced and B- and T-lymphocytes are recruited to form a granuloma (26, 28, 35). On the other hand, the R variants are phagocytized in small clusters, creating phagosomes containing a large number of bacteria or "social phagosomes". These variants are resistant to phagolysosomal degradation after the fusion of the phagosome with the lysosome, causing activation of autophagy followed by apoptosis. Subsequently, the R variant is released into the extracellular environment to freely replicate and form extensive serpentine cords which can resist recurrent phagocytosis, provoking inflammation and abscess formation. Furthermore, MABC can switch from a S to a R morphology, hereby transitioning from a colonizing phenotype to an invasive phenotype. In immunocompromised patients, MABC can also spread to other organs causing a disseminated infection (26, 28).

Another crucial strategy of MABC pathogenesis is the formation of biofilms, making the pathogen more resistant to antibiotics and disinfectants, and contributing to its transmission (13, 28, 36). In patients with pre-existing lung

Chapter I

disease, MABC biofilms can colonize a host before progressing to an invasive disease (13). The R variants form pellicular biofilms characterized by a high mechanical resistance while the S variants generate non-invasive biofilms that are more pliant under physical forces (13, 37).

Although the mechanism of pathogenesis is not yet fully understood, the risk and predisposing host factors for MABC infection are well known (13). Here, a distinction can be made between acquired, genetic and additional predisposing risk factors. Acquired risk factors can be classified as anatomic lung or immune abnormalities acquired during the lifetime of a host without underlying genetic cause and include the use of steroids, smoking and organ transplantation. Genetic risk factors are a result of genetic disorders that can cause a host to be more susceptible to disease, such as CF. Other predisposing risk factors are malnutrition, age, and recurrent NTM infections leading to a reduced immunity (28, 35).

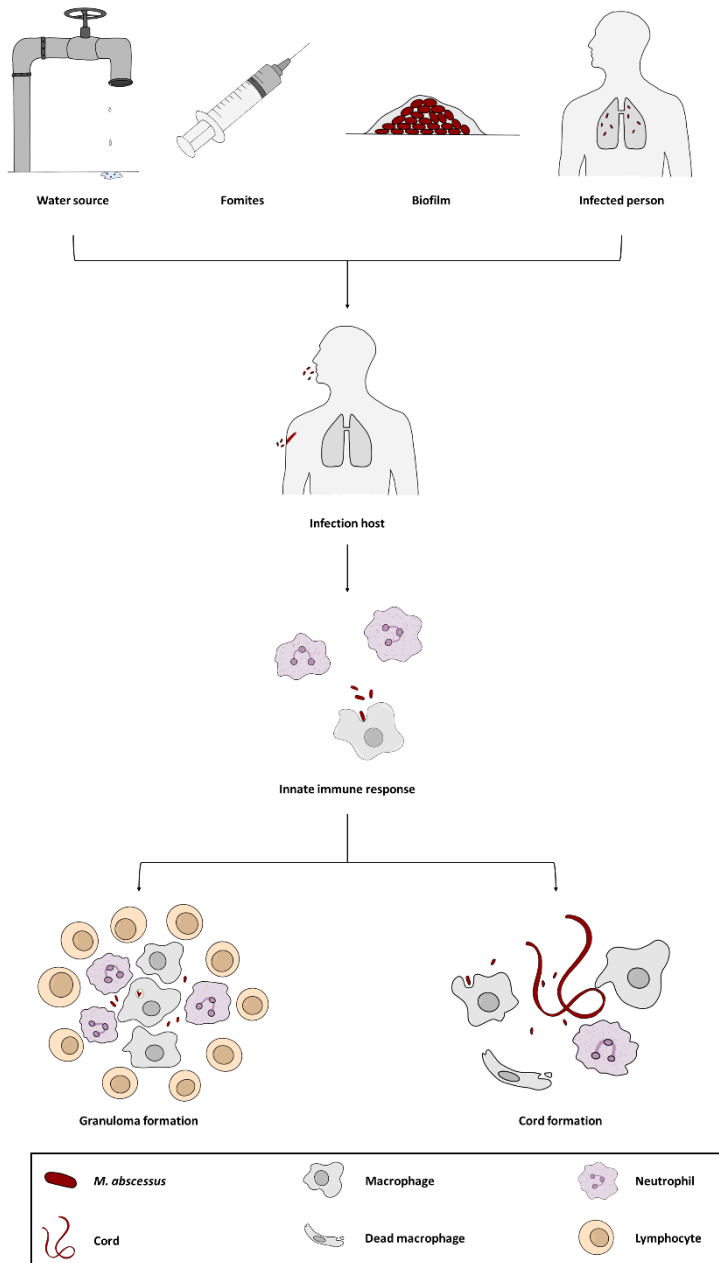


Figure I.4. MABC infection cycle. MABC is widely spread in the environment and can be transmitted through water sources (environment water, plumbing systems), fomites (dust, healthcare materials), biofilms and infected persons. Infection of a host can occur after inhalation of the pathogen or through entry via open wounds. Once infected, the innate immune system will be activated and phagocytize the pathogen. The smooth (S) MABC form will resist phagosomal degradation and lead to the production of a granuloma. Rough (R) MABC will activate apoptosis of the phagocytized cells, form cords to resist recurrent phagocytosis and provoke inflammation. Designed using iArtBook.

I.2.2 Clinical presentation

The clinical presentation of MABC infections is mainly dependent on the course of the infection and can be categorized as pulmonary, skin and tissue, or disseminated disease (**Figure I.5**).

MABC pulmonary disease (MABC-PD) is most common amongst CF patients or patients with preexisting conditions and can range from asymptomatic to chronic progressive lung disease (7, 28). Symptoms of MABC-PD are often labeled as non-specific as they include chronic cough, sputum, hemoptysis and fatigue (19). Radiographically, MABC-PD can be present as two distinguished forms: a nodular bronchiectasis form or fibrocavitary form (18, 19). Nodular bronchiectasis occurs in the middle lobe of the right lung or the lingual of the left lung of mostly non-smoking postmenopausal women and is characterized by multiple small nodules. It is a progressive disease that is accompanied by a decline in pulmonary function, decreased quality of life and ultimately death in some patients (18, 38). The fibrocavitary form is a fast progressive disease present as cavitary lesions invading the upper lobe of predominantly older men with underlying lung disease, leading to the rapid destruction of the lung. While both forms are common in MABC-PD, the nodular bronchiectasis form is predominant (18, 39).

Skin and soft tissue disease include the infection of the skin, cartilage, tendons and fat layers, and is generally a localized disease with symptoms such as redness and swelling (33, 39). Unlike MABC-PD, skin and soft tissue disease can be found in healthy individuals without preexisting conditions, mostly in a healthcare settings (28, 40).

MABC can also cause infections in the muscles, bones, joints, lymph nodes and internal organs, causing a disseminated disease (35). Disseminated disease predominantly occurs in patients with preexisting conditions including HIV or other immunosuppressive conditions (41).

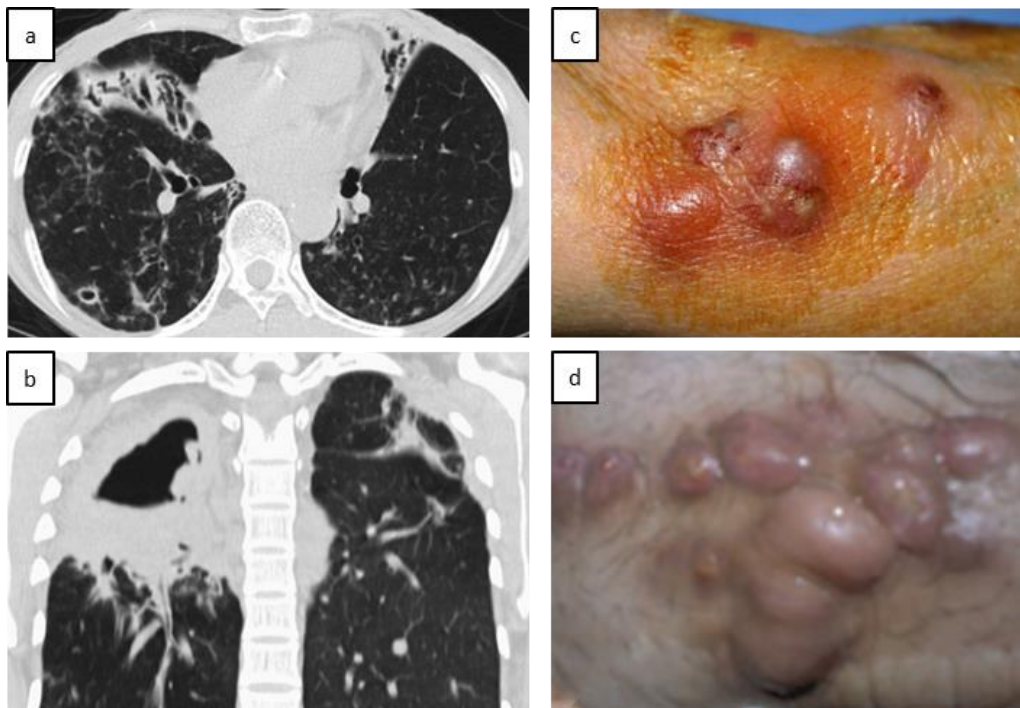


Figure 1.5. Overview of the different clinical presentations of MABC disease. a) Chest high-resolution computed tomography of the nodular bronchiectasis form of MABC pulmonary disease (MABC-PD). **b)** Chest high-resolution computed tomography of the fibrocavitary form of MABC-PD. **c)** Skin disease characterized by small nodules on the forearm. **d)** Nodular lesion of a post-kidney transplant surgical wound. Adapted from Sepulcri et al, Koh et al, and Kwon et al (19, 33, 42).

1.2.3 Diagnosis

Because NTM-PD is regularly mistaken for MDR-TB and due to the close relation of some RGM species, correct differentiation between mycobacterial species is of utmost importance (33, 43). Therefore, diagnosis of MABC disease relies on clinical (symptoms), microbiologic (cultures), and radiologic (imaging) criteria (38). Mycobacterial cultures are recognized as the golden standard in which a sputum sample or skin biopsy can be used to grow the pathogen, combined with fluorescent or Ziehl-Neelsen staining methods to confirm the presence of mycobacteria (18, 33, 44). For a more precise identification, molecular methods can be employed after culture growth. This is established by amplifying targets

that are distinct in the different mycobacterial species, including β -subunit of RNA Polymerase (*rpoB*), *gyrB*, heat-shock protein 65 (*hsp65*), internal transcribed spacer (*ITS*), superoxide dismutase (*sodA*), and 16S – 23S rRNA gene spacer. Furthermore, mass spectrometry can be implemented to differentiate between MABC and other RGM, however, cannot distinguish between the subspecies of MABC (18). Finally, genotyping methods and whole-genome sequencing (WGS) allow the identification of specific strains and facilitate phylogenetic studies (18, 33). Nevertheless, identification of mycobacterial species remains difficult and slow, requiring the development of novel laboratory methods to tackle these infections (33, 44).

I.2.4 Treatment

Treatment of MABC infections is challenging as to date there is no standard treatment available (45). However, in recent years, the American Thoracic Society (ATS)/European Respiratory Society (ERS)/European Society of Clinical Microbiology and Infectious Diseases (ESCMID)/Infectious Diseases Society of America (IDSA) and British Thoracic Society (BTS) published guidelines that recommend a multidrug therapy, including a macrolide together with one or more parenteral drugs (amikacin, ceftazidime or imipenem), characterized by two phases (46, 47). The first phase comprises an initial treatment phase of at least 4 weeks that includes the administration of 2 to 3 intravenous antibiotics (amikacin, tigecycline and if tolerated imipenem) in combination with an oral macrolide (clarithromycin or azithromycin) for macrolide-sensitive isolates. The second phase involves a continuation phase with nebulized amikacin, an oral macrolide and 1 to 3 oral antibiotics (linezolid, clofazimine, minocycline, cotrimoxazole, or moxifloxacin) depending on the patients tolerance and drug susceptibility (47, 48). The guidelines also suggest *in vitro* susceptibility testing of various antibiotics prior to treatment for selection of the appropriate antibiotics while combining the multidrug therapy with surgical lung resection for localized lung disease (35, 49).

The duration of the treatment is 18 to 24 months and requires a minimum of 12 months of negative sputum culture (47, 50).

Although the complete list of recommended antibiotics against MABC infections originate from different antibiotic groups while exhibiting different mode-of-actions, the most important ones, being macrolides and the parental drugs, can be classified into three classes of antibiotics: macrolide (clarithromycin and azithromycin), aminoglycoside (amikacin) and beta-lactam (cefoxitin and imipenem) antibiotics.

Macrolides

Macrolides are a group of antibiotics that are widely used to treat respiratory tract infections. The structure of macrolides consists of a large macrocyclic lactone ring with one or multiple amino-sugar side groups attached via glycosidic bonds (**Figure I.6a**). They can be characterized by the size of the lactone ring with clinically used macrolides presenting a 14-, 15- or 16-membered lactone ring (51, 52). Macrolides disrupt bacterial growth through inhibition of protein synthesis. They will bind to the 50S ribosomal subunit next to the nascent peptide exit tunnel (NPET), a tunnel where the newly synthesized polypeptides pass through before being released from the ribosome, hereby blocking the tunnel (52, 53). Binding of the macrolides to the 50S subunit will ultimately result in inhibiting elongation of the peptide chain, inhibiting the formation of a large 50S subunit, inhibiting peptide bond formation and promoting dissociation of peptidyl tRNA from the ribosome (54). Beside their antimicrobial effect, macrolides are also believed to have an immunomodulatory effect in respiratory diseases (52).

Aminoglycosides

Aminoglycosides are broad-spectrum antibiotics that are active against a wide range of Gram-positive and Gram-negative bacteria. This class of antibiotics is only active against aerobic bacteria as they need an active electron transport to be taken up into cells (55). The general structure of aminoglycosides contains a core amino-sugar structure linked by glycosidic bonds to an inositol derivative, totally

consisting of multiple free hydroxyl and at least two amino groups (**Figure I.6b**)(55, 56). Their mode of action is characterized by binding the A-site of the 16S ribosomal RNA of the 30S ribosome, consequently causing genetic code misread, inhibition of the protein synthesis, and a disruption of the integrity of the cell membrane (55, 57).

Beta-lactams

Beta-lactams are one of the largest and oldest classes of antibiotics that are successfully being used for the treatment of many bacterial species (57, 58). Their structure consists of a beta-lactam ring which is needed for activity (**Figure I.6c**)(57, 59). This class of antibiotics acts as an irreversible inhibitor by mimicking the substrate of the transpeptidase peptide, an enzyme belonging to the penicillin-binding proteins (PBP) cross-linking the peptidoglycan components of the bacterial cell wall. After binding to the transpeptidase peptide, beta-lactams will inhibit the transpeptidase activity, hereby inhibiting the cell wall biosynthesis, disrupting the integrity of the cell wall and causing cell lysis (57, 58).

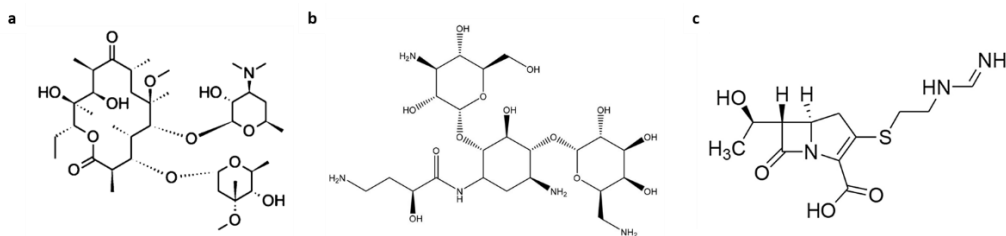


Figure I.6. Structure of important recommended antibiotics against MABC infections. Chemical structure of azithromycin (macrolide)(a), amikacin (aminoglycoside)(b), and imipenem (beta-lactam)(c). Figure adapted from Glanzer et al., Isanga et al., and El-Gamal et al. (60–62).

I.2.5 Treatment shortcomings

Despite the guidelines, MABC infections remain extremely difficult to treat due to the limited availability of therapeutic options (35). This is the result of MABC being extensively resistant to a variety of antibiotics, including the first-line anti-TB drugs such as isoniazid, rifampin, ethambutol and pyrazinamide (47). The intrinsic

resistance of MABC is mainly due to the mycobacterial cell wall. The cell wall acts as an effective barrier against antibiotics and other hydrophilic and lipophilic agents because of its thick, lipid-rich nature. Beside its protective characteristics, the cell wall also contains various efflux pumps that actively transport toxic compounds back to the extracellular environment (40). Another common resistance mechanism among MABC is macrolide resistance, which is caused by inducible resistance due to the presence of the erythromycin ribosomal methylase gene (*erm41*) or acquired resistance as a result of a mutation in the 23S ribosomal RNA gene (*rRNA*) (49, 50). MABC also produces a number of target-modifying enzymes and transcriptional regulators that promote supplementary antibiotic resistance (40). Furthermore, treatment of MABC often leads to serious adverse drug effects, eventually causing poor patient-compliance and further development of acquired drug resistance (50, 63). The adverse drug effects are usually antibiotic-related toxicity and include dyspnea, ototoxicity, nephrotoxicity, hepatotoxicity, cytopenia, vestibular toxicity, cough and electrolyte disturbance (45, 64). Altogether, these factors are accountable for a treatment success rate of only 45.6% (45). Because of the low treatment efficacy and limited treatment options, MABC disease remains a chronic and incurable disease for most patients. Hence, a more realistic treatment goal is often based on symptomatic improvement, reduction of radiographic infiltrates in the lung, and lowering of the sputum culture positivity (47).

The lack of an optimal treatment for MABC reinforces the need for novel anti-mycobacterials and anti-mycobacterial targets that could shorten the treatment, reduce adverse drug effects, and prevent further development of drug resistance. Unfortunately, because of the many challenges of drug discovery and the highly antibiotic resistant profile of MABC, the current anti-MABC drug pipeline remains scarce (50).

I.2.6 Anti-MABC drugs in the clinical pipeline

To enhance the clinical drug pipeline of MABC, two strategies can be applied: drug discovery or drug repurposing. The first strategy, drug discovery, relies on the discovery of *de novo* drugs starting from the identification of a drug target or lead optimization. To date, *de novo* drug discovery is essential for MABC disease, however, remains limited as this strategy requires an extensive amount of resources, is time-consuming, and is an expensive process. A faster strategy for developing drugs against MABC is drug repurposing. This strategy repurposes previously established and approved anti-tuberculosis (anti-TB) drugs for their use against MABC. Due to its low cost and short development time, it is an appealing strategy to surpass the rapidly emerging drug resistance in MABC (50, 65). By utilizing both strategies, the most promising leads for the development of anti-MABC drugs are currently in Phase I or II of the clinical drug pipeline. Phase I comprises three leads (benzimidazole SPR720, delpazolid and gallium nitrate) whereas Phase II holds five (inhaled nitric oxide, tigecycline, liposomal amikacin, bedaquiline and omadacycline) (**Figure I.7**) (65).

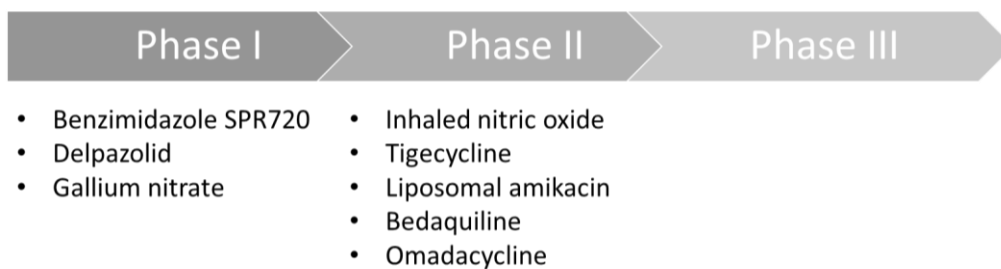


Figure I.7. Clinical drug pipeline of the emerging anti-MABC drugs. Anti-MABC drugs currently under investigation in Phase I are benzimidazole SPR720, delpazolid and gallium nitrate, while inhaled nitric oxide, tigecycline, liposomal amikacin, bedaquiline and omadacycline are currently in Phase II of the clinical pipeline. Adapted from Egorova et al (65).

Benzimidazole SPR720

Benzimidazole SPR720 is a prodrug derived from the compound SRP719, which is a second-generation aminobenzimidazole that was identified during the process of optimization of an analog. This compound inhibits a broad range of bacteria, including Gram-positive and -negative pathogens, by targeting DNA gyrase B and topoisomerase IV (65).

Delpazolid

Delpazolid is a novel antibiotic belonging to the class of oxazolidinone. It was discovered during the process of optimization of linezolid and inhibits the protein synthesis by targeting the 50S subunit of the ribosome (65).

Gallium nitrate

Gallium nitrate is a compound that was recently proven to inhibit the growth of MABC and other NTMs, and is being tested for intravenous use in CF patients having an additional NTM infection. It inhibits iron-dependent enzymes by competing with iron (65).

Inhaled nitric oxide

Inhaled nitric oxide is a drug under investigation for CF patients with refractory MABC lung infection. Its efficacy still needs to be improved while simultaneously reducing the adverse drug effects of a high dose of nitric oxide (65).

Tigecycline

Tigecycline is a glycylicycline antibiotic that is structurally similar to tetracyclines but was developed to overcome the resistance mechanisms known for tetracyclines (66, 67). It prevents translation by targeting the 30S ribosomal subunit and inhibiting peptide elongation (66). It is highly efficient against MABC-PD and is evolved to be one of the recommended antibiotics to treat this disease (40). Moreover, a study showed that tigecycline is also active against other rapid-growing NTMs (64).

Liposomal amikacin

Liposomal amikacin exists as amikacin encapsulated in liposomes and delivered into the patient by inhalation of aerosols containing the liposomes. This system is implemented to reduce the adverse drug effects of amikacin while increasing the drug concentration. Treatment of various patients in a recent study demonstrated that liposomal amikacin can serve to cure MABC disease (35).

Bedaquiline

Bedaquiline is a diarylquinoline containing a core of three aromatic groups (naphthyl, 6-bromoquinoline and phenyl) and was proven to inhibit the ATP synthase of mycobacteria by targeting the c subunit of ATP synthase (**Figure I.8**) (68, 69). It is a drug used to treat MDR-TB and is being repurposed for use in MABC (40, 64). Bedaquiline displays promising activity against MABC *in vitro* along with *in vitro* synergistic activity when combined with some antibiotics, including clofazimine. However, *in vivo* efficacy studies are not convincing and, so far, elaborated clinical data on the efficacy is still missing (65, 70). Furthermore, use of bedaquiline as a combination therapy *in vitro* can also have a negative impact on certain antibiotics, including β -lactams, in which the bactericidal potency of these antibiotics is decreased (65).

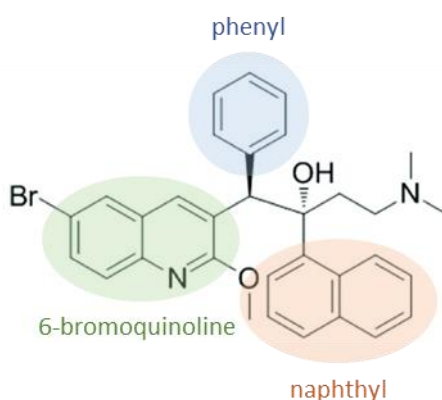


Figure I.8. Chemical structure of bedaquiline. Bedaquiline is a diarylquinoline with in the core three aromatic groups: a naphthyl, a 6-bromoquinoline and a phenyl ring. Figure adapted from Pinheiro et al. (71).

Omadacycline

Omadacycline is a tetracycline analogue used for the treatment of bacterial pneumonia as well as acute skin and tissue infections. It demonstrated an effective activity against NTMs, including MABC (64).

1.2.7 Target-based drug discovery

Drug discovery has been constantly evolving and adapting over the years but remains a complex and expensive process (72, 73). There are two main approaches to drug discovery, i.e. target-based or phenotypic-based. While a target-based approach advances from target identification to screening of drug candidates, a phenotypic approach will start from a drug candidate followed by identification of its target (72–74). Although a target-based approach is time-consuming, expensive and laborious, target identification and validation of the target suitability by establishing the lack of human orthologues, the absence of pre-existing drug resistance and a favorable localization are indispensable steps in drug discovery but not always possible in a phenotypic-based approach (73, 75). The target-based approach consists of the following chronological steps; target selection and validation, *in silico* virtual screening of compounds against the target, target expression and purification, testing potential inhibitors in *in vitro* inhibition assays, and testing potential inhibitors in whole-cell assays (**Figure I.9**)(76).

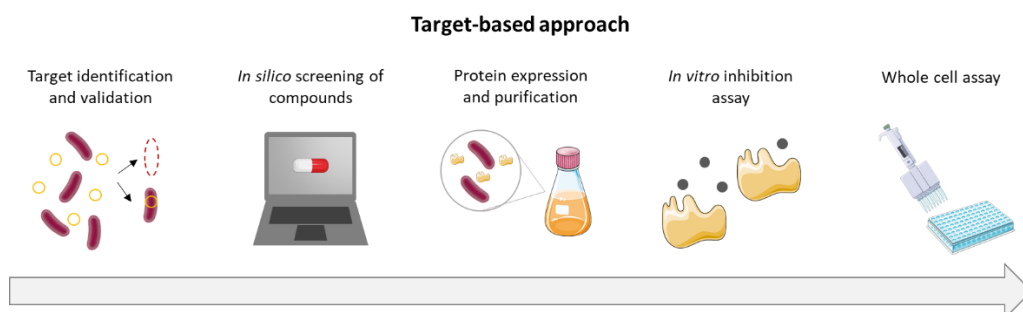


Figure I.9. Pathway of a target-based approach. Figure created with PowerPoint and based on Dalberto et al. (76). Some images originating from Servier Medical Art.

Thus, the first step of a target-based approach is the selection and validation of a drug target (76). Drug target selection mainly comprises of a single gene, gene product or molecular mechanism required for bacterial survival, virulence or pathogenesis, and are commonly essential genes (72, 77). Essential targets are targets that are indispensable for the bacterial growth and/or survival. However, some targets are only essential under certain growth conditions and are categorized as conditionally essential (78). To determine the degree of essentiality of a mycobacterial target (i.e. essential, conditionally essential or nonessential), mycobacteria are usually first genetically modified to alter the expression of the target and subsequently tested in different growth conditions (76, 79). These growth conditions include conditions relevant during host infection and can be divided into *in vitro* and *in vivo* models. Recognized mycobacterial *in vitro* models include non-replicating (nutrient starvation, acidic pH conditions, hypoxia conditions and stress conditions), antibiotic susceptibility testing, and macrophage infection models. *In vivo* models, on the other hand, are applied to more closely mimic the infection environment and are mostly animal models, including zebrafish and mice (80, 81). A more recently established mycobacterial *in vivo* model is the *Galleria mellonella* (*G. mellonella*) larva, i.e. an invertebrate insect that does not present ethical restrictions, is easily manipulated and maintained, is unexpensive, and has innate immune defenses presenting both cellular and humoral responses (82, 83). Furthermore, *G. mellonella* larvae infected with MABC demonstrate granuloma-like structures that are similar to the granulomas seen in human MABC-PD infections and are widely used to assess bacterial virulence (83, 84). The main limitation of this model is the lack of standardized procedures since variations in supplier, breeding conditions, maintenance, and infection method of the larvae can result in experimental differences. Moreover, although *G. mellonella* larvae present cellular and humoral immune responses, an adaptive immune system is absent (83, 85).

I.3 Redox homeostasis as drug target

The bacterial redox homeostasis is a process maintaining a balanced redox state inside the bacteria (86). However, the redox state can become unbalanced when mycobacteria are exposed to redox stress which can cause severe damage to cellular components (87, 88). To avoid damage, mycobacteria carry antioxidants that enable the neutralization of redox stress (87).

I.3.1 Redox stress

Almost all living organisms on earth need oxygen to survive (89). These aerobic organisms utilize aerobic respiration to generate adenosine triphosphate (ATP) hereby supplying the organism with energy. During such reactions, oxygen or nitrogen radicals that are highly reactive and quickly oxidized (i.e. reactive oxygen species (ROS) or reactive nitrogen species (RNS)), can be formed as byproducts, generating an imbalance in reductive and oxidative species termed redox stress (87, 90, 91). Redox stress is not only generated from intrinsic biological reactions, but can also originate from extrinsic factors, including metals, xenobiotics, antibiotics, alkylating agents, acidic pH, nutrient starvation and hypoxia, and is capable of causing damage to the DNA, RNA, lipids and proteins leading to cell death (87, 89, 92, 93).

When mycobacteria infect a host, they are exposed to a variety of redox stresses generated by their own aerobic respiration and/or by the host's immune system (88). The innate immune system is the first to be activated when mycobacteria enter the host after which macrophages and neutrophils are able to phagocytose the pathogen (94). Once phagocytosed, these activated cells retain the pathogen in an acidic environment and release a large amount of ROS and RNS to kill the invading pathogen (94–97). In order for mycobacteria to counteract the effect of redox stress, the pathogen developed antioxidants that can undergo reversible oxidation and thus maintain a balanced redox homeostasis (86, 87). When there is

an imbalance between oxidants (ROS and RNS) and antioxidants in favor of the oxidants, the term oxidative stress is used (98, 99).

I.3.2 Mycothiol biosynthesis and recycling pathway

Mycothiol (MSH) is the main low molecular weight (LMW) thiol present in mycobacteria and a glutathione (GSH) analogue that can only be found in *Actinomycetes* (89, 100). These thiols both present a similar function, however, differ in structure (**Figure I.10**)(101, 102).

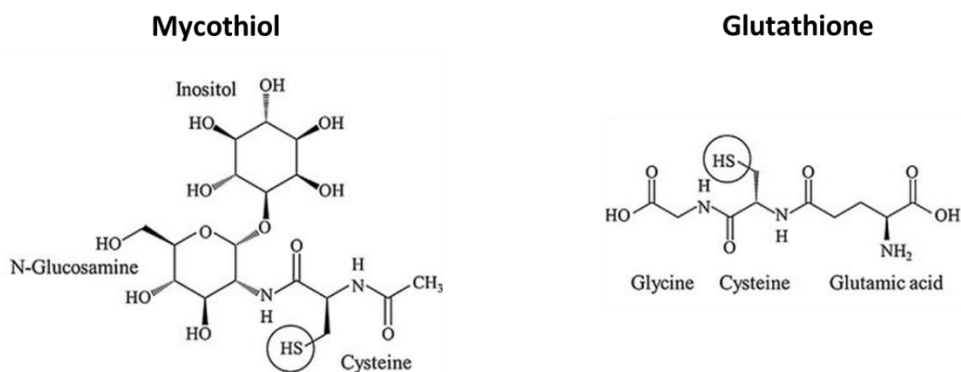


Figure I.10. Structure of MSH and GSH. MSH is a pseudo-disaccharide consisting of inositol (Ins), N-glucosamine (GlcN) and acetylcysteine (AcCys), while GSH is a tripeptide that includes a glycine, cysteine and glutamic acid. Figure adapted from Eberle et al. (103).

MSH acts as an antioxidant for the neutralization of ROS, RNS and other reactive intermediates generated during oxidative stress conditions by serving as an electron donor (89, 104). Furthermore, it also acts as a cofactor in various other reactions such as detoxification of formaldehyde or arsenate reduction (105). MSH biosynthesis is characterized by a five-step process that involves five enzymes: a glycosyltransferase (MshA), a phosphatase (MshA2), a deacetylase (MshB), a cysteine ligase (MshC) and an MSH synthase (MshD) (**Figure I.11**). First, MshA combines inositol-phosphate (Ins-P) with uridine diphosphate N-acetylglucosamine (UDP-GlcNAc) to form N-acetyl glucosamine myo-isonitol-1-phosphate (GlcNAc-Ins-P). Then, GlcNAc-Ins-P is dephosphorylated and

deacetylated by MshA2 and MshB, respectively, generating glucosamine inositol (GlcN-Ins) after which a cysteine amino group is added by MshC in an ATP-dependent manner, composing Cys-GlcN-Ins. Finally, MshD acetylates the cysteine to yield MSH or acetylcysteine-glucosamine-inositol (AcCys-GlcN-Ins) (88, 89, 100). When the generated MSH later encounters a reactive oxidant, it will donate electrons to neutralize the oxidant while becoming oxidized to form mycothione or MSSM. To keep a balanced redox homeostasis, MSSM is then reduced back to MSH by mycothione reductase (Mtr).

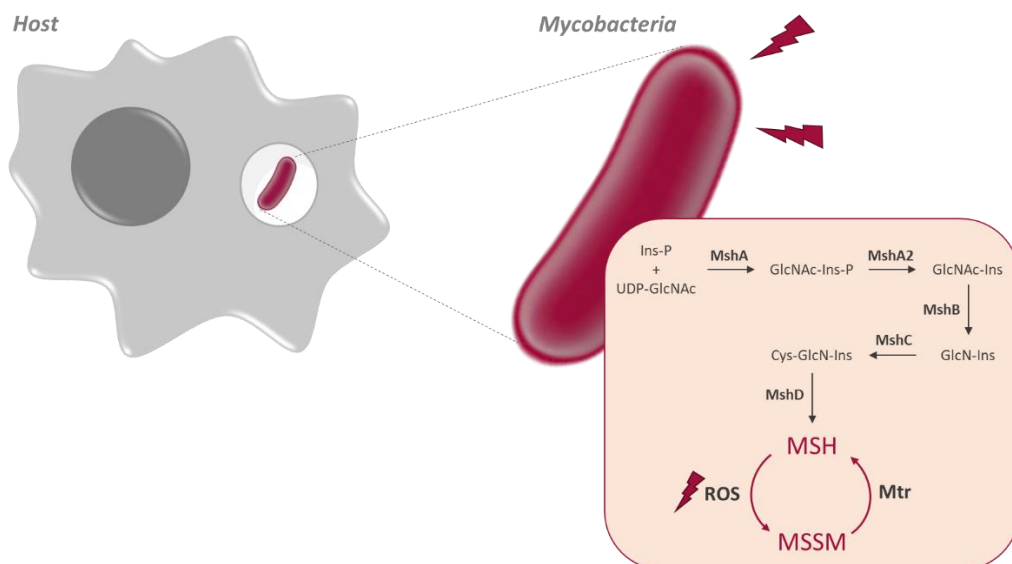


Figure I.11. Mycothiol biosynthesis and recycling process. Mycothiol (MSH) is synthesized in a five-step process involving a glycosyltransferase (MshA), a phosphatase (MshA2), a deacetylase (MshB), a cysteine ligase (MshC) and an MSH synthase (MshD). Once synthesized, mycothiol will act as an antioxidant to neutralize ROS, RNS and other reactive intermediates generated during stress conditions or by the host's immune system as a defense mechanism against the intruding pathogen, oxidizing MSH into mycothione (MSSM). To keep a stable redox homeostasis, MSSM is then reduced back into MSH by Mtr. Designed using PowerPoint. Ins-P: inositol-phosphate, UDP-GlcNAc; diphosphate N-acetylglucosamine, GlcNAc-Ins-P: myo-isonitol-1-phosphate, GlcN-Ins: glucosamine inositol, Cys-GlcN-Ins: cysteine-glucosamine-inositol, AcCys-GlcN-Ins: acetylcysteine-glucosamine-inositol

Mtr reduces MSSM in a NADP-dependent manner by using flavin adenine dinucleotide (FAD) as a cofactor and its bound redox-active disulfide. The reduction occurs via a ping-pong kinetic mechanism composed of a reductive and oxidative half-reaction (**Figure I.12**). During the reductive half-reaction, electrons are transferred from NADPH to the redox-active disulfide via FAD, generating a two-electron reduced Mtr enzyme. The oxidative half-reaction includes binding of the oxidized MSSM to the reduced enzyme to form a mixed disulfide followed by the release of two reduced MSH and a reformed redox active disulfide on Mtr (106, 107). Similar to Mtr, MshC also functions via a ping-pong kinetic mechanism. During this mechanism, ATP and cysteine will first bind MshC to form a complex followed by binding of the complex to GlcN-Ins and the release of Cys-GlcN-Ins and AMP (108). While the 3D-structure of Mtr is still unknown, the structure of MshC was uncovered in *M. smegmatis* (*Msm*) and shown to contain a Rossmann fold catalytic domain (109).

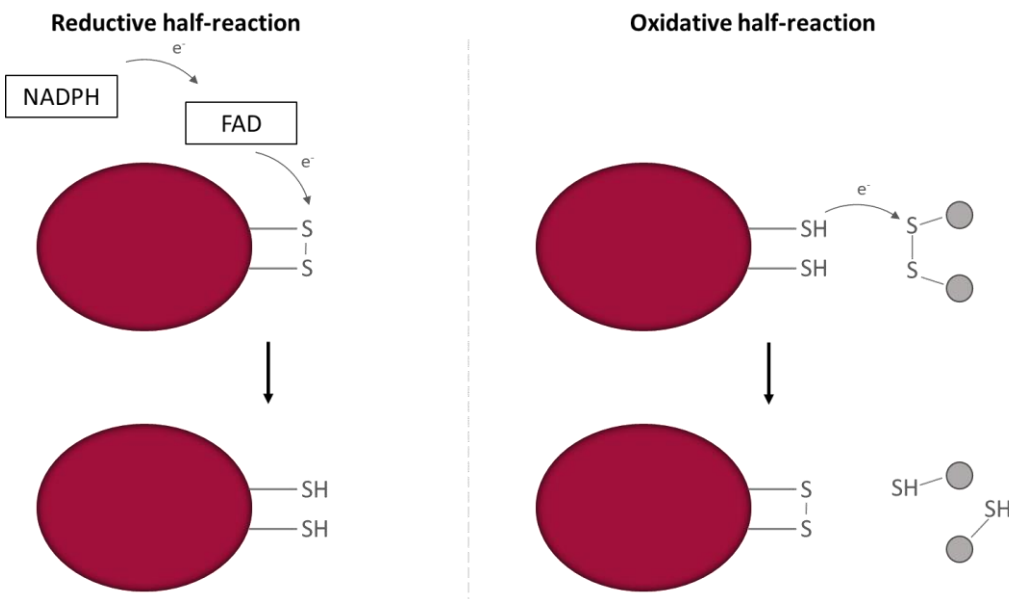


Figure I.12. Mechanism of action of Mtr. Mtr reduces MSSM via a ping-pong kinetic mechanism consisting of a reductive and oxidative half-reaction. First, the reductive half-reaction ensures the transfer of electrons from NADPH to Mtr by using FAD, generating a reduced Mtr enzyme. Then, during the oxidative half-reaction the reduced Mtr binds to MSSM and releases two reduced MSH. Designed with PowerPoint.

To date, it is not known whether the *mtr* and *mshC* genes are essential for MABC, however, their essentiality has been investigated in *Msm* and *Mtb*. While both genes are non-essential for *Msm* (110, 111), *mshC* is essential for *Mtb* whereas there is controversy about *mtr* essentiality in this pathogen (107, 112). In the recent years, dequalinium and NTF1836 were presented as novel MshC inhibitors demonstrating activity against *Mtb* but are far from ideal since they are cytotoxic for mammalian cells (100, 113, 114).

Because of the important role of MSH and the MSH biosynthesis and recycling enzymes in the maintenance of a balanced redox homeostasis and their uniqueness for *Actinomycetes*, these enzymes have been suggested as potential targets for developing anti-mycobacterial drugs in the fight against mycobacterial infections (100). To approve a novel target, potential targets need to be validated first with the help of genetic engineering techniques (115).

1.4 Genetic engineering

Genetic engineering is a widely used technique which is crucial to elucidate mycobacterial pathogenesis and disease, while being indispensable for the identification and validation of novel drug targets for anti-mycobacterial drugs (115, 116). By using genetic editing methods to manipulate the mycobacterial genome by producing knockouts, knockdowns or overexpression of particular genes, individual gene function and their involvement in the virulence and pathogenesis of the bacteria can be investigated (115, 117, 118). Essential genes are especially interesting as drug targets, however, knockout mutants of essential genes are not viable and require the insertion of an inducible second copy present on another location on the genome (119). Genetic engineering of mycobacteria remains a challenge due to the limited availability of selection drugs as a result of the highly resistant nature of these pathogens, the low transformation efficiency of mycobacteria, the thick and lipid-rich cell wall, the low efficiency of homologous repair within the bacteria and the time-consuming feature of gene editing (117,

118, 120–122). Nonetheless, significant improvements have been made over the last years in the development of genetic engineering techniques to more efficiently generate mutations in mycobacteria (115).

Several recombineering systems are commonly used for genetic engineering, including homologous recombination and site-specific recombination (**Figure I.13**) (123). Homologous recombination is a process mediated by the exchange of nucleotides between two homologous DNA sequences. These DNA sequences can be circular or linear, either double-stranded DNA (dsDNA), single-stranded DNA (ssDNA) or single-stranded RNA (ssRNA) (124, 125). To perform homologous recombination between a target gene and an editing substrate, implementation of endogenously expressed recombination enzymes (e.g. allelic exchange), a strain capable of recombination, or a phage recombination system are required (125). Site-specific recombination, on the other hand, is a process in which DNA is cleaved and reassembled at specific DNA sites without any DNA synthesis or degradation needed (126, 127). This process occurs between specific DNA sites that do not necessarily require homology and is executed by proteins such as integrases (127–129). Unlike homologous recombination, site-specific recombination is characterized by the integration of a DNA sequence into the specific DNA site rather than an exchange between two DNA sequences (115). A well-known site in the mycobacterial genome for site-specific recombination is the L5 integration site (130).

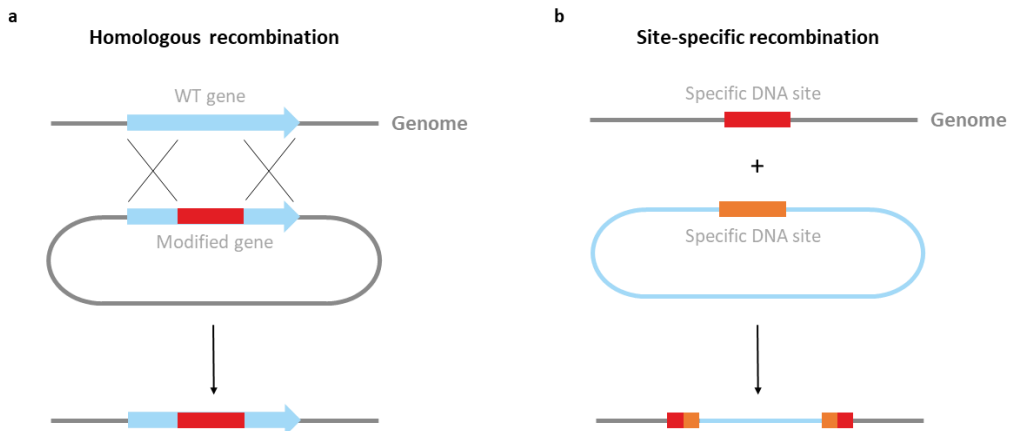


Figure I.13. Schematic representation of homologous and site-specific recombination. a) Homologous recombination occurs between two sequences that share some homology and is carried out by recombination enzymes. **b)** Site-specific recombination is mediated by DNA cleavage and reassembly at specific DNA sites. This process does not necessarily need homologous sequences for the recombination to occur but requires an integrase. Designed using PowerPoint.

I.4.1 L5 integration

The mycobacteriophage L5 is a temperate phage that infects mycobacteria to form stable lysogens via site-specific recombination (115, 131). Recombination occurs between the phage attachment site in the mycobacteriophage genome, *attP*, and the bacterial attachment site in the mycobacterial genome, *attB*, and is dependent on mycobacteriophage-expressed integrase (Int) as well as the host-expressed integration host factor (mIHF) (115, 132). Soon after its discovery, this mycobacteriophage system was transformed into a useful tool to manipulate the genome of mycobacteria (132). An example of a system using the L5 integration is the pMV306 vector, a vector containing an *attP* phage attachment site that integrates into the *attB* bacterial attachment site or L5 site with the help of a pBS-Int suicide plasmid expressing the mycobacteriophage L5 integrase (133, 134). A suicide plasmid is a plasmid unable of replicating within a host species (135). After integration of the pMV306 vector into the *attB* site, the vector is flanked by an *attL* site on his left side and an *attR* site on his right side (115). The pMV306 vector is

widely used to generate overexpressing or complementing mycobacterial strains as genes can easily be cloned into the vector and expressed by the promoter present on the vector (136, 137). Promoters present on these vectors can be either constitutive or inducible and mostly consist of a strong mycobacterial promoter such as heat-shock protein 60 (*hsp60*) or G13 (138–141). A constitutive promoter will continuously express the genes introduced on the integrating vector whereas an inducible promoter utilizes a tetracycline-controlled Tet-On or Tet-Off gene expression system to control the expression of the genes. After administration of tetracycline (Tc) or other Tc-derivatives such as anhydrotetracycline (ATc), a Tet-On system starts the expression of the genes present on the vector while a Tet-off system pauses gene expression (141, 142).

I.4.2 CRISPR*i*

CRISPR-Cas (Clustered Regularly Interspaced Short Palindromic Repeats–CRISPR associated proteins) is a system found in various bacteria as part of the adaptive immune system against invasive or foreign genetic elements that was adapted as a gene editing tool for both prokaryotic and eukaryotic cells (143, 144). Later, CRISPR-Cas was repurposed as a tool for silencing the expression of genes, termed CRISPR interference (CRISPR*i*), enabling the functional investigation of essential or other specific genes (145–147). To perform CRISPR*i* gene silencing, three components are necessary: a single guide RNA (sgRNA) containing a sequence complementary to the target sequence, a nuclease-deficient Cas9 protein (dCas9) inactivated by two point mutations within its RuvC and HNH nuclease domains, and a Cas9-permissible protospacer adjacent motif (PAM) (**Figure I.14**) (146, 148). The sgRNA and dCas9 protein are expressed from a single plasmid inside mycobacteria after integration of the plasmid in the L5 integration site of the mycobacterial genome (149). When expressed, the sgRNA forms a complex with the dCas9, sgRNA-dCas9, which is guided by the sgRNA to the complementary target sequence on the bacterial genome. Then, the sgRNA-dCas9 complex binds to the target sequence adjacent to a PAM motif hereby repressing gene transcription

by causing a steric block for transcription elongation or initiation by RNA polymerase and other transcription factors (146, 148, 150). The PAM sequence is an important component required for sgRNA-dCas9 to successfully target and bind the complementary target sequence (151). The most used and fully exploited dCas9 proteins are codon optimized and originate from two pathogens, *Streptococcus pyogenes* dCas9 (dCas9_{spy}) or *Streptococcus thermophilus* dCas9 (dCas9_{sth1}) (148). The CRISPRi system can be used to target either a promoter or an open reading frame of a gene (150).

CRISPRi shares many properties with CRISPR-Cas including being programmable, specific and highly efficient (147). Moreover, CRISPRi allows the simultaneous silencing of multiple genes, helping in the investigation of genetic interactions (146). Additionally, this system can also be used for essential genes that are extremely sensitive to knockdown as the degree of gene repression can also be controlled. Finally, knockdown of the gene of interest is both inducible and reversible. Nevertheless, using this system can also be accompanied by some unwanted outcomes including a bad-seed effect, a polar effect, toxicity and off-target. A bad-seed effect occurs when the last 5 nucleotides of a sgRNA produces a strong fitness defect while a polar effect is characterized by the repression of the expression of all genes in an operon downstream from the gene of interest. Another limitation of CRISPRi is the restricted amount of sequences that can be targeted due to the requirement of a PAM sequence (147, 152).

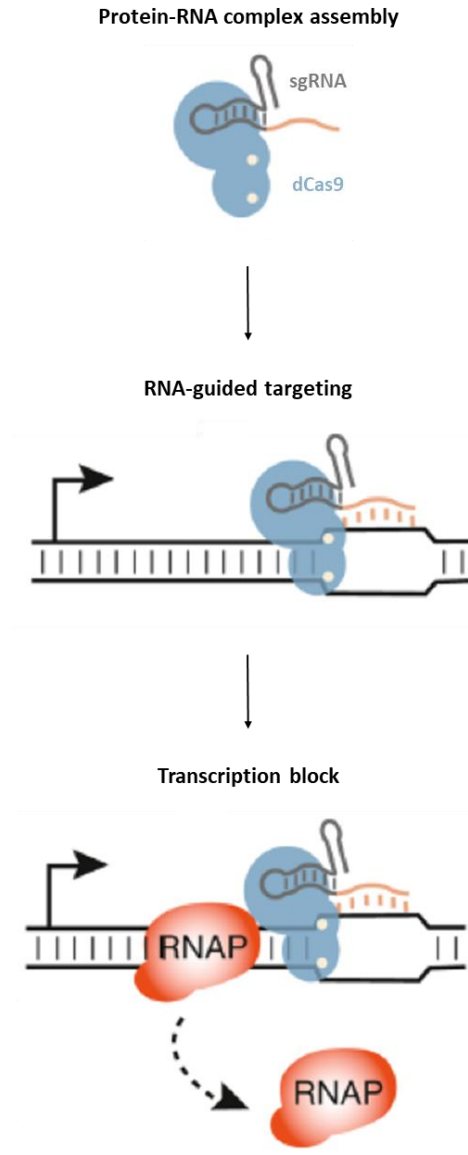


Figure I.14. CRISPRi gene silencing. During CRISPRi gene silencing, a small guide RNA (sgRNA) possessing a sequence complementary to the target sequence will bind to a nuclease-inactivated Cas9 protein (dCas9) and form a protein-RNA complex. Next, the sgRNA will guide the complex to bind to the target sequence. After binding to the target sequence, the complex will hinder the transcription by causing a block for the RNA polymerase (RNAP). Adapted from Qi et al. (153).

I.4.3 p2NIL/pGOAL system

To significantly improve the effectiveness of producing mutations in the mycobacterial genome, Parish and Stoker developed a new system in 2000 called the p2NIL/pGOAL system (116, 154). This system applies a two-step allelic exchange procedure relying on RecA-mediated homologous recombination and involves the replacement of a gene of interest with a modified version, hereby causing loss of function of the gene of interest (**Figure I.15**) (119). Replacement of the gene of interest is accomplished with the use of a p2NIL suicide vector constructed by cloning a marker cassette (antibiotic-resistant cassette, *lacZ* and *sacB*) from a pGOAL vector together with the modified gene of interest containing a 1 kb flanking region into the p2NIL vector (154, 155). Then, a two-step allelic exchange strategy is implemented composed of a single cross-over (SCO) and double cross-over (DCO) event. During the SCO event, the entire p2NIL vector will be incorporated into the mycobacterial genome, generating a strain that contains the marker cassette and both the wild-type (WT) and modified copies of the gene of interest (156). As a result of the *lacZ* marker gene, SCO transformants with an integrated vector will turn blue in the presence of X-Gal (120). Next, the genome is forced to remove *sacB*, a negative selection marker rendering the bacteria sensitive to sucrose, by undergoing a DCO event (116, 120). This recombination event will also be responsible for the removal of one of both copies of the gene of interest, giving rise to a strain containing either the modified gene or the WT gene (156). If the modified copy of the gene is retained, a mutant is successfully created (119). Mutants generated with the p2NIL/pGOAL system are characterized by a gene deletion marked with a drug resistance gene, an unmarked gene deletion, or the introduction of a point mutation into the target gene (156).

The use of the p2NIL/pGOAL two-step strategy has several advantages in comparison to a one-step strategy. First, a two-step strategy enables the creation of unmarked mutants, offering the possibility of deleting several genes in one strain without the need to find another resistance marker. The generation of unmarked mutants also enables the production of vaccines without including a

drug resistance gene (154). Secondly, a two-step strategy is more efficient for use in slow-growing species with a lower frequency of homologous recombination, but are also applicable to other bacterial species (154, 155). Finally, the use of *lacZ* and *sacB* as selection markers facilitate the selection of both SCO and DCO recombinants and reduce the number of colonies needed to be tested (154). However, as a result of an inefficient homologous repair together with a lower probability of homologous recombination when using a nonreplicating vector, SCO recombinants are difficult to produce (115, 121). Moreover, selection of mutants can be complex after the frequent spontaneous inactivation of *sacB* (115). Lastly, the procedures involved in performing the p2NIL/pGOAL technique are time-consuming and labor-intensive (121).

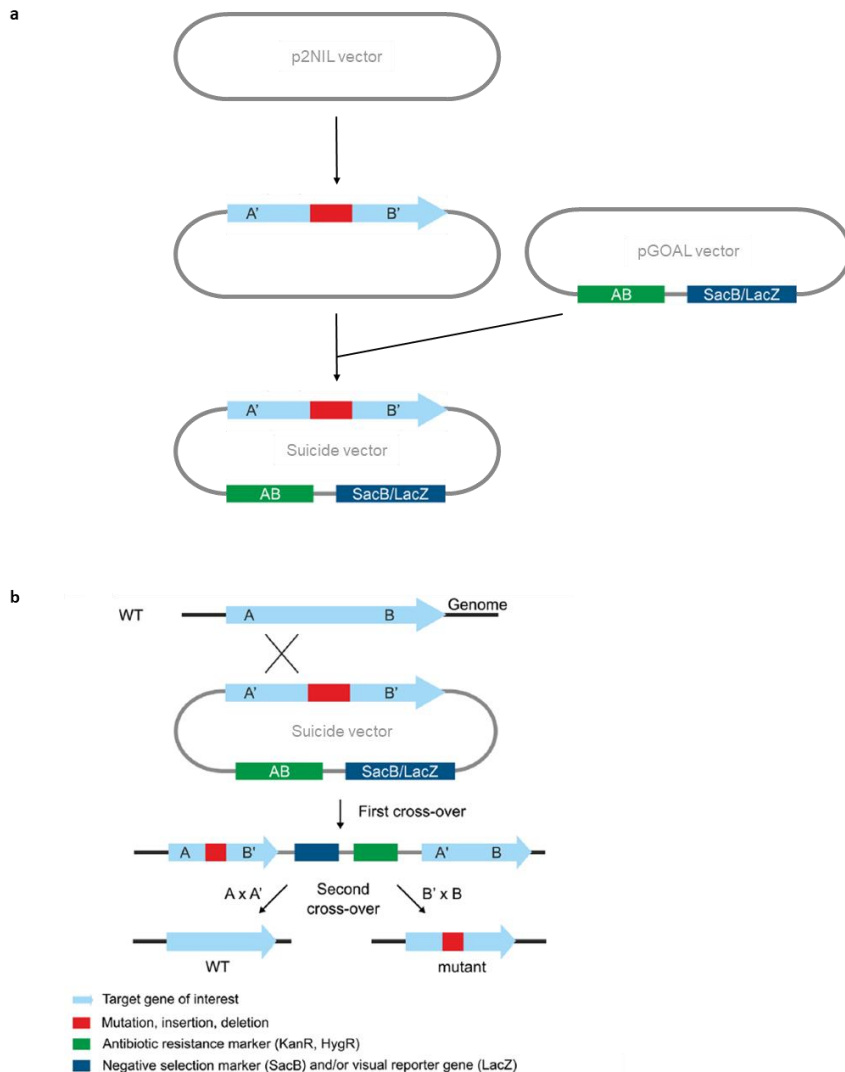


Figure I.15. p2NIL/pGOAL system. a) A nonreplicating suicide vector is generated by first inserting a modified copy of the gene of interest, containing flanking regions, into the p2NIL vector followed by the incorporation of a marker cassette originating from the pGOAL vector. **b)** A mutant is created in a two-step allelic exchange strategy. First, a single cross-over (SCO) event incorporates the suicide vector into the genome of the bacteria by homologous recombination, generating a mutant containing a wild-type (WT) and a modified copy of the gene of interest. Next, a second cross-over or double cross-over (DCO) event removes the marker cassette together with one copy of the gene of interest. If the modified copy is retained, a mutant is successfully created. Adapted from Borgers et al. (120).

I.4.4 ORBIT system

The “oligonucleotide-mediated recombineering followed by Bxb1 integrase targeting” or ORBIT system is a recent system described to efficiently engineer the genome of mycobacteria and was developed by combining two recombination methods, homologous recombination and site-specific integration (116, 157). This chromosomal engineering system is the first to enable the production of a drug-selectable recombinant without the need to generate target-specific dsDNA plasmids or PCR-generated recombinant substrates (123). To create a drug-selectable recombinant, a plasmid carrying a Che9c phage RecT annealase and a Bxb1 phage integrase is first transformed and expressed into mycobacteria. Then, a single-stranded “targeting oligonucleotide” is synthesized harboring a Bxb1 phage *attP* site flanked by 45 to 70 bp homologous to the chromosomal target sequence, hereby determining the exact location of insertion. This “targeting oligonucleotide” is cotransformed into mycobacteria with a nonreplicating “payload” plasmid containing a Bxb1 *attB* site and a selectable marker. After transformation, the DNA fragments are inserted into the genome in a two-step approach (**figure 1.16**). First, the Che9c RecT annealase anneals the “targeting oligonucleotide” to the lagging strand of the replicating fork via homologous recombination, thereby incorporating the *attP* site into the target sequence. During the second step, site-specific recombination occurs between *attB* and *attP* in which Bxb1 integrase inserts the “payload” plasmid into the *attP* site previously integrated by the oligonucleotide during the first step (115, 120, 123). The ORBIT system can be used to generate chromosomally tagged genes, promoter replacement or gene deletions. For the latter, the oligonucleotide synthesized will replace the target gene by an *attP* site (120).

The usage of this recently discovered system comes with many advantages. As the ORBIT system only requires the synthesis of a “targeting oligonucleotide”, it is an appropriate system to construct a library of mutants. Moreover, since no dsDNA is required, the flanked homologies is significantly reduced. Finally, the generated mutation is selectable and the generated mutant can be tagged by a particular

sequence added to the oligonucleotide (120, 125). However, this system is also characterized by a few disadvantages, including the need of an electroporation step limiting the overall efficiency. Additionally, after implementing the ORBIT system, a vector and antibiotic resistance markers or an *attP* site remain within the mutant while removal is time-consuming (120, 125, 157).

Deletion of target gene with ORBIT

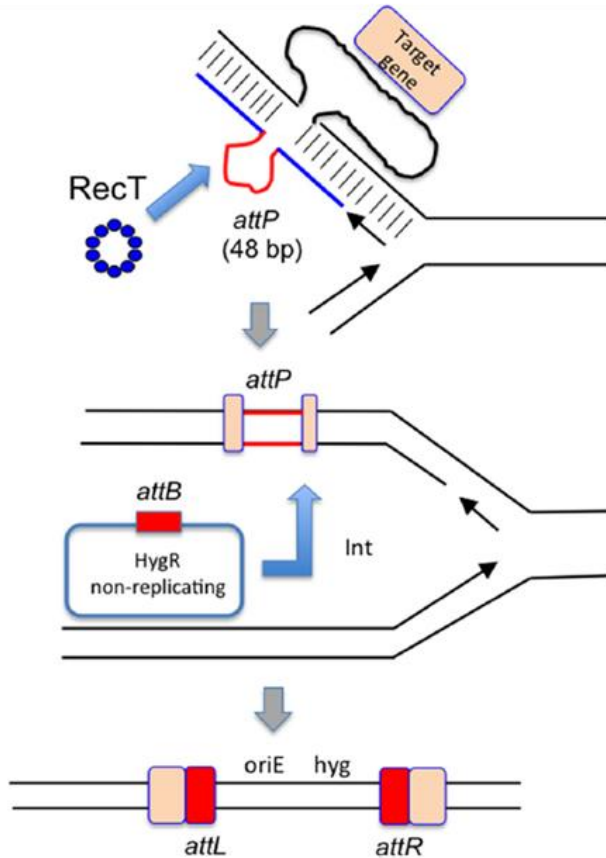


Figure I.16. Deletion of a target gene with the ORBIT system. Deletion of genes with the ORBIT (“oligonucleotide-mediated recombineering followed by Bxb1 integrase targeting”) system is performed via a two-step strategy. First, RecT annealase (RecT) facilitate the annealing of a “targeting oligonucleotide” containing a Bxb1 *attP* site (red line), flanking by sequences homologous to the targeting sequence (blue line), to the lagging strand of the replication fork. After DNA replication, the “targeting oligonucleotide” will be integrated into the genome by homologous recombination. The second step implies site-specific recombination driven by Bxb1 integrase (Int) in which the *attB* site of a nonreplicating “payload” plasmid containing a hygromycin-resistant cassette (HygR) will be incorporated into the previously inserted *attP* site. In order to delete a target gene, the oligonucleotide is designed such that the *attP* site will replace the target gene. Adapted from Murphey et al. (123).

CHAPTER II

Research objectives and outline



II. Research objectives and outline

MABC is the most common rapidly-growing NTM that causes respiratory infections in human. These infections have been increasing worldwide over the last two decades, especially among CF patients, leading to a higher morbidity and mortality associated with this pathogen (9). Treatment of MABC infections remains challenging as the recommended therapy demonstrates an average treatment success rate of only 45.6% (45). Treatment failure occurs as a cohesion of several different elements: i) the duration of the treatment is lengthy as it requires a multidrug therapy for 18 to 24 months (50), ii) the recommended treatment frequently causes severe antibiotic-related side effects, such as hepato-, nephron- and ototoxicity (40, 64), iii) the thick, lipid-rich cell wall of mycobacteria acts as barrier against antibiotics (40), and iv) most members of MABC developed inducible or acquired bacterial resistance against macrolides, an important antibiotic class used against MABC infections, or other antibiotics (40, 49). As a result of the low efficacy of the available treatment and the limited antibiotic options, MABC disease remains incurable for most patients (47). To improve MABC treatment and avoid the further development of drug resistance, novel anti-mycobacterials and anti-mycobacterial targets need to be explored (50).

An interesting novel anti-mycobacterial target is the MSH biosynthesis and recycling pathway. MSH is the main LMW thiol of mycobacteria and acts as an antioxidant for the neutralization of ROS and RNS (89). ROS, RNS and other reactive intermediates are generated during oxidative stress conditions encountered when infecting a host or caused by the bacteria's own aerobic respiration (87, 88). Accordingly, MSH and the MSH biosynthesis and recycling enzymes are of great importance for the survival of mycobacteria within a host (158). To tackle both the biosynthesis and recycling pathway of MSH, one enzyme of each pathway was selected as a potential target. Hereby, two key enzymes of the MSH biosynthesis and recycling pathway are Mtr and MshC. While Mtr is the only enzyme responsible for the recycling of MSH after neutralization of reactive species, MshC establishes the penultimate step of the MSH biosynthesis and is

essential to maintain a balanced redox homeostasis (100, 106). Furthermore, *mshC* is believed to be the only essential gene of the biosynthesis pathway in *Mtb* (112, 159).

Since targets for anti-mycobacterial drugs are commonly essential genes, it is of utmost importance to investigate the essentiality of novel potential targets. Simultaneously, it is also crucial to determine the degree of essentiality of these targets, as certain genes can be essential for the survival of MABC under specific clinically relevant conditions, i.e. conditionally essential, and hereby have the potential to become valuable targets as well. Up to date, it is not yet known whether *mtr* and *mshC* are essential genes for the survival of MABC in favorable or stress-related conditions nor whether they truly are potential good targets for anti-mycobacterial drugs. Therefore, the main objective of this thesis was to investigate and validate **Mtr and MshC as potential targets for anti-MABC drugs**. This was achieved by employing different genetic engineering techniques to produce a panel of strains with variable expression of both genes of interest. Since *M. abscessus abscessus* is the most common amongst the subspecies, it is the most relevant for conducting research. A widely used reference strain of this subspecies for drug discovery is the *M. abscessus (Mab)* ATCC 19977 strain (160, 161). To achieve the main objective, three sub-objectives were applied:

- i. to create a panel of recombinant *Mab* strains having a differential expression of *mtr* or *mshC*,
- ii. to determine the role of *mtr* and *mshC* during stress conditions,
- iii. to evaluate the role of *mtr* and *mshC* during infection.

First, **Chapter III** focusses on the development of both *mtr* and *mshC* overexpressing strains by integrating a pMV306 vector, containing an extra copy of the genes, in the mycobacterial L5 integration site. As these genes are part of a protective pathway within *Mab*, their overexpression would allow us to learn more about the protective function of *mtr* and *mshC* during stress conditions and

infection. Next, to determine the essentiality of both *mtr* and *mshC*, **Chapter IV** aims to produce *mtr* and *mshC* knockdown strains using the CRISPRi system while **Chapters V** and **VI** aim at creating *mtr* and *mshC* knockout strains. Hereby, **Chapter V** first investigates the efficiency of the p2NIL/pGOAL method for the generation of mycobacterial knockout strains by validating this method in *Msm*, i.e. a mycobacterial species that is widely used as an alternative model for mycobacterial studies. After validation and selection of the best method for creating knockout strains in mycobacteria, the selected method, i.e. the ORBIT system, is applied in **Chapter VI** to generate *mtr* and *mshC* knockout strains in *Mab*. In this chapter, the genes are evaluated based on their importance for the survival of *Mab* in different stress conditions and during infection, and investigated as potential novel drug targets for anti-mycobacterials. Finally, **Chapter VII** reviews all the obtained results in a general discussion while also covering the future perspectives of this thesis.

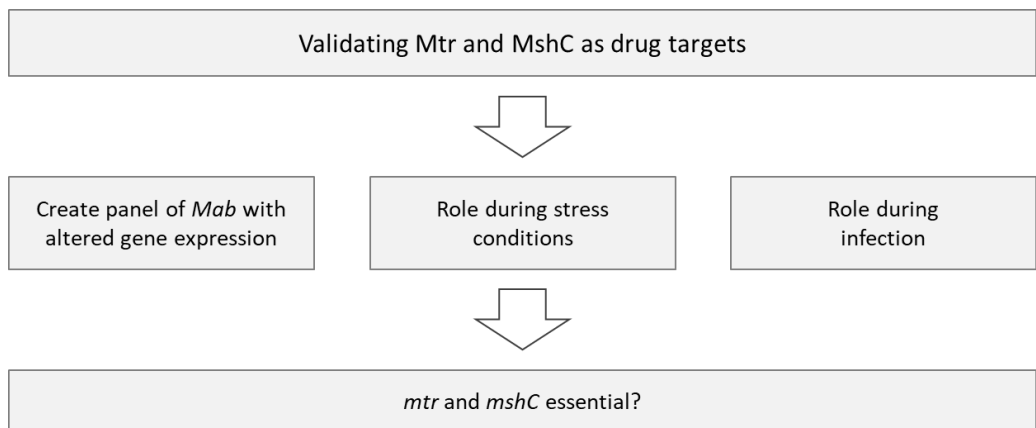


Figure II.1. Overview of the objectives of this thesis.

CHAPTER III

Generation and functional characterization
of *mtr* and *mshC* overexpressing strains in
Mycobacterium abscessus



The BLI results presented in this chapter have been submitted to mSphere as:

Bento C, Van Calster K, Piller T, Oliveira G, De Vooght L, Cappoen D, Cos P, Gomes M S, Silva T. Characterization of novel double-reporter strains of *Mycobacterium abscessus* for drug discovery: a study in mScarlet. **Submitted**

Author contributions:

Tatiana Piller¹: conceptualization, methodology, investigation and formal analysis.

Iris Jacobs¹, my master thesis student working on this project: helped with the investigation and formal analysis of the *mshC* overexpressing strain.

Clara Bento^{2,3,4}, characterized the *Mab* FF_scarlet strain used in the BLI experiment.

Kevin Van Calster¹, generated the *Mab* FF_scarlet strain used in the BLI experiment.

Linda De Vooght¹: conceptualization, methodology, formal analysis and supervision.

Paul Cos¹: conceptualization, methodology, formal analysis and supervision.

¹Laboratory of Microbiology, Parasitology and Hygiene (LMPH), University of Antwerp, Belgium ²i3S – Instituto de Investigação e Inovação e Saúde, Universidade do Porto, Portugal

³IBMC – Instituto de Biologia Celular e Molecular, Universidade do Porto, Portugal

⁴Programa Doutoral em Biologia Molecular e Celular (MCBiology), Instituto de Ciências Biomédicas Abel Salazar da Universidade do Porto, Portugal

III. Generation and functional characterization of *mtr* and *mshC* overexpressing strains in *Mycobacterium abscessus*

III.1 Abstract

MSH is an important antioxidant in mycobacteria capable of detoxifying reactive intermediates. Several studies already highlighted the benefits of increased MSH levels or levels of its analogs in a diverse range of bacteria, however, this was not yet accomplished for *Mab*. In this study, two key enzymes of the MSH biosynthesis and recycling pathway, Mtr and MshC, were selected to generate *mtr* and *mshC* overexpressing strains and to characterize their survival during stress conditions and infection. Our findings demonstrated that overexpressing only part of the MSH biosynthesis or recycling pathway does not lead to a general increase in intracellular reduced thiol levels, which may be due to the failed translation of higher levels of the MSH biosynthesis or recycling enzymes to higher MSH levels or due to a compensation mechanism leading to a reduction of the overall thiol levels. Furthermore, higher expression levels of *mtr* or *mshC* were not proven to be beneficial for *Mab* as *mtr* and *mshC* overexpressing strains showed a reduced ability to grow in the nutrient-poor medium Sauton and proliferation was not enhanced after exposure to oxidative stress or during infection in macrophages and *G. mellonella* larvae.

III.2 Introduction

To learn more about the function of a particular gene or gene product, genetic engineering approaches can be used to alter the expression of genes (162). An overexpressing approach enables the study of both essential and non-essential genes and is beneficial for understanding the function of genes involved in

certain mechanisms, including stress tolerance. Hereby, the overexpression of these genes can help the pathogen to adapt to stress conditions (162, 163).

Thiols are important intracellular components for all kind of life forms to maintain redox balance. While most eukaryotes and a large number of prokaryotes possess GSH to conserve this balance, mycobacteria lack this low-molecular weight thiol and instead rely on other types of thiols including MSH (164). MSH acts as an antioxidant that is capable of detoxifying reactive intermediates such as ROS which are mainly released due to aerobic respiration or by the host's immune system, i.e. macrophages, as a defense mechanism (88, 104, 165). Biosynthesis of MSH involves a five-step pathway conducted by a glycosyltransferase (MshA), a phosphatase (MshA2), a deacetylase (MshB), a cysteine ligase (MshC) and an MSH-synthase (MshD) (100, 106). Once MSH is synthesized and neutralizes reactive intermediates, it will become oxidized to MSSM. Then, to maintain a balanced redox homeostasis, Mtr will reduce MSSM back to MSH (107, 166).

Some studies have already highlighted the importance of MSH for the survival of *Msm* and *Mtb* and its role in the protection against oxidative stress. Hereby, *Msm* and *Mtb* showing reduced or deficient levels of MSH become more sensitive to free radicals and antibiotics (167–169). Furthermore, the overexpression of *mtr* was shown to enhance the fitness of *Corynebacterium glutamicum*, a bacteria belonging to the same order as *Mycobacterium*, during stress conditions (170, 171). Given previously mentioned findings and the fact that MSH plays a role in neutralizing reactive intermediates, enzymes of both the biosynthesis and the recycling pathways, Mtr and MshC, were selected to investigate their importance in protecting *Mab*. Hereby, we suggest the hypothesis that by overexpressing either *mtr* or *mshC*, the fitness of *Mab* would be increased during stress conditions or during infection. In this study, the pMV306 plasmid was used to integrate an extra copy of *mtr* or *mshC* into the genome of *Mab*, hereby generating novel *mtr* and *mshC* overexpressing strains. Our findings show that the overexpression of *mtr* or *mshC* is not favorable for

Mab as proliferation of both strains remains unaltered after exposure to oxidative stress or during infection in macrophages and *G. mellonella* larvae.

III.3 Material and methods

Bacterial strains, media and culture conditions

Escherichia coli (*E. coli*) DH5 α cultures were grown in Luria-Bertani (LB) broth (Sigma-Aldrich) or plated on LB agar (Sigma-Aldrich) supplemented with 0.2% glycerol and the corresponding selection drug.

All mycobacterial strains in this study were derived from *M. abscessus* ATCC 19977 and were routinely cultured at 37°C in Middlebrook 7H9 broth (Sigma) supplemented with 10% ADS (albumin-dextrose-saline), 0.2% glycerol and 0.05% tyloxapol or Sauton's medium (HiMedia Laboratories) supplemented with 2% glycerol and 0.05% tyloxapol with the addition of 200 μ g/mL kanamycin (Sigma) for the overexpressing strains. Agar plates were made of Middlebrook 7H11 agar base (Sigma) or Sauton agar, consisting of Sauton's medium solidified with 1.5% Bacto™ Agar (Becton, Dickinson and Company).

Molecular cloning of mtr and mshC and construction of the pMV306_mtr, pMV306_TET-mtr and pMV306-mshC plasmid

The sequences of mycothione reductase (*mtr*; MAB_RS00460) and cysteine ligase (*mshC*; MAB_RS10805) were obtained using the National Center for Biotechnology Information (NCBI) platform. To isolate these genes from the genome of *Mab*, the bacteria were first grown until logarithmic phase and lysed by heating for 20 min at 90°C to make the DNA available. Then, PCR was performed using selected primers (**Table III.1**) to amplify the genes of interest while adding a N-terminal His-tag and restriction enzyme sites for EcoRI and Sall at the 5'-end and 3'-end, respectively, for cloning into the pMV306DIG13-

FFlucRT plasmid (Addgene 49998) or pMV306DIG13-FFlucRT-TET (Previously adjusted from pMV306DIG13-FFlucRT by Linda De Vooght). The PCR mixture (50 μ L) consisted of 25 μ L of Q5[®] High-Fidelity 2X Master Mix (NEB[®]), 2.5 μ L of each primer, 1 μ L of the lysed bacteria and 19 μ L Milli-Q, while the thermal cycles included a denaturation step (98°C, 30 sec), 35 amplification cycles (98°C for 5 sec; 72°C for 20 sec; 72°C for 35 sec), and a final extension step (72°C, 2 min). Next, the pMV306 expression plasmid was digested with EcoRI and Sall for 2h at 37°C and ligated together with the PCR products by NEBuilder[®] Hifi DNA assembly for 15 min at 50°C with help of the Hifi master mix (NEB[®]) to generate pMV306_*mtr*, pMV306_TET-*mtr* and pMV306-*mshC*. An overview of the method used to create the pMV306 plasmids is demonstrated in **Figure III.1**. The generated plasmids were then heat-shocked separately into *E. coli* DH5 α competent cells and correct recombinants were selected after confirmation by PCR using the previously mentioned primers (**Table III.1**). After selection, the plasmids were purified from the recombinants using the NucleoSpin[®] Plasmid QuickPure Miniprep kit (Machery-Nagel) and checked by Sanger sequencing (Neuromics Support Facility; University of Antwerp).

Table III.1. Overview of primers used to clone *mtr* and *mshC* from *Mab* into the pMV306 plasmids.

Name	Sequence*	Description
Mtr_For	acgcagcccacaaatgcacgcttg gtaaccgagagaaggagaagtac cgatgCACCATCACCATCAC CATATGTACGACCTCGTC ATCATCGGTTCCGG	Forward primer used to amplify the <i>mtr</i> gene while adding an N-terminal His-tag and a restriction enzyme site for EcoRI for cloning into the pMV306 plasmid.
Mtr_Rev	atttgatgcctggcagtcgacgta cgctagttaactacgCTAGAGG TCCAGACCCAGC	Reverse primer used to amplify the <i>mtr</i> gene while adding a restriction enzyme site for Sall for cloning into the pMV306 plasmid.
MshC_For	acgcagcccacaaatgcacgcttg gtaaccgagagaaggagaagtac cgatgCACCATCACCATCAC CATATGCAGTCGTGGGCG TCGGCGCCGGTTCC	Forward primer used to amplify the <i>mshC</i> gene while adding an N-terminal His-tag and a restriction enzyme site for EcoRI for cloning into the pMV306 plasmid.
MshC_Rev	atttgatgcctggcagtcgacgta cgctagttaactacgCTACAAC TGCACTCCC	Reverse primer used to amplify the <i>mshC</i> gene while adding a restriction enzyme site for Sall for cloning into the pMV306 plasmid.

*Upper case letters in the sequences refer to sequences originating from the bacterial genome while lower case letters refer to sequences originating from a plasmid.

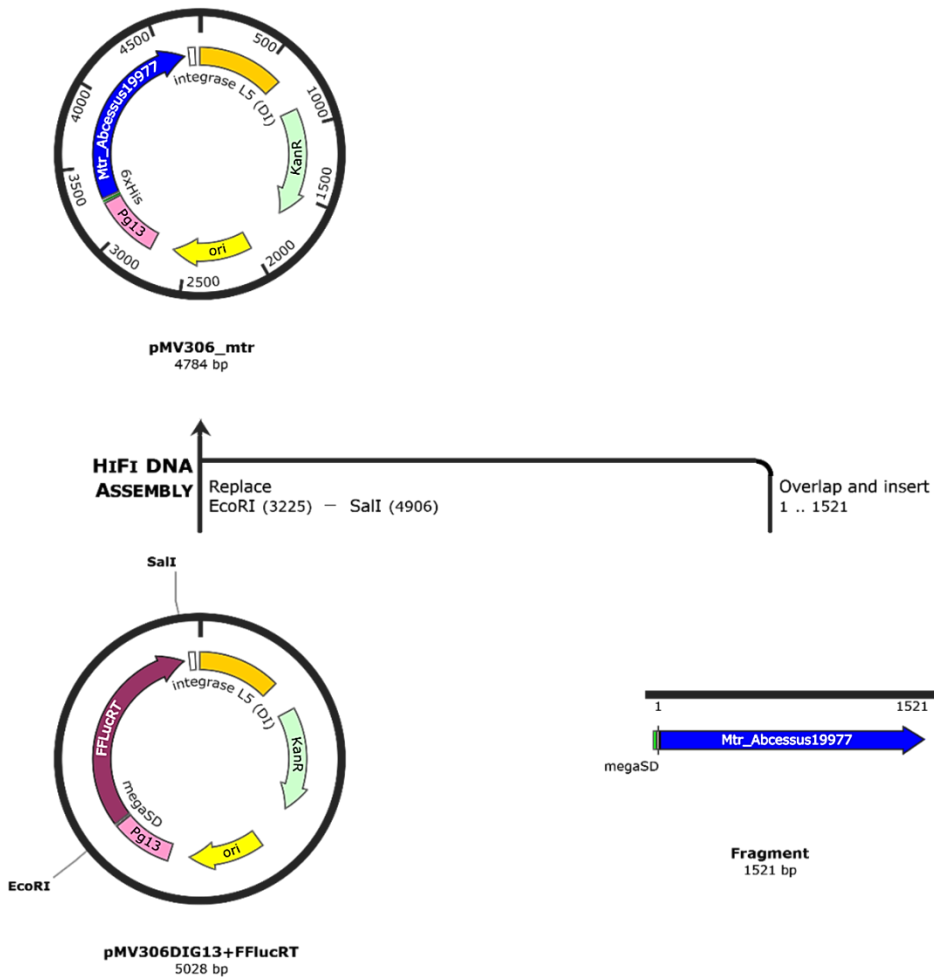


Figure III.1. Overview of the methodology used to create pMV306_mtr. The figure is a representative for all pMV306 plasmids generated. Created with SnapGene®.

Creation of Mab::mtr, Mab::TET-mtr and Mab::mshC

Mab was grown in a shaking incubator (New Brunswick Scientific; 175 rpm) in 7H9 supplemented with 10% OADC (oleic acid-albumin-catalase-dextrose; Thermo Fisher Scientific), 0.2% glycerol and 0.05% tyloxapol at 37°C until reaching an optical density at 600 nm (OD_{600}) between 0.2 and 0.8 and was made electrocompetent by washing three times with 10% glycerol. Then, 1 μ g

of the pMV306_ *mtr*, pMV306_TET-*mtr* or pMV306-*mshC* integrating plasmid was transformed together with 0.5 µg of the pBS-Int suicide plasmid expressing an integrase (Addgene 50000) into the electrocompetent bacteria by using the Gene Pulser Xcell Total System (Bio-Rad; 1.25 kV, 1000 Ω and 25 µF). Following electroporation, *Mab* was resuspended in 7H9 medium containing 20% OADC and incubated at 37°C for 4h before it was plated out on 7H11 agar containing 10% OADC, 0.2% glycerol and 200 µg/mL kanamycin (Sigma). The 7H11 agar plates were incubated for 3 days to 1 week at 37°C until the presence of colonies. Successful incorporation of the pMV306 plasmids into the L5 site of *Mab* and thus creation of *Mab::mtr*, *Mab::TET-mtr* and *Mab::mshC* was confirmed by PCR and Sanger sequencing (Neuromics Support Facility; University of Antwerp) utilizing primers to amplify the L5 integration site (Table III.2).

Table III.2. Overview of the primers used to amplify the L5 region of *Mab*.

Name	Sequence	Description
L5_For	CCGATCGGGTTCTCCACCTG	Forward primer used to amplify the L5 site of <i>Mab</i> .
L5_Rev	GCCCCGGCGCTGTACATTCA	Reverse primer used to amplify the L5 site of <i>Mab</i> .

RNA isolation

Mab strains were grown in 7H9 supplemented with 10% ADS, 0.2% glycerol and 0.05% tyloxapol until reaching their logarithmic phase and diluted to an OD₆₀₀ of 0.1 in the same medium. Half of the culture of *Mab::TET-mtr* was induced after dilution with 500 ng/µL µM ATc (Anhydrotetracycline; Takara Bio). After 48h of growth in a shaking incubator (New Brunswick Scientific; 175 rpm) at 37°C, the pellets of the strains were harvested and incubated in TRIzol reagent (Invitrogen) for 5 min at room temperature (RT). Next, the bacteria were lysed with BeadBug™ beads (Sigma; 0.1 mm Zirconium beads) by shaking

at a speed of 6 m/s twice for 45 seconds using the FastPrep 24 Classic (MP biomedical) followed by incubation at -80°C overnight. In order to separate the samples from the TRIzol reagent, Phasemaker tubes (Invitrogen) were used together with the addition of chloroform to the sample. Once separated, RNA isolation of the samples was completed using the RNeasy Plus Mini Kit (Qiagen) followed by a DNase treatment with TURBO DNAase (Qiagen) and ezDNase (Invitrogen). The final RNA concentration was measured using the NanoDrop™ 2000 spectrophotometer (Thermo Scientific) and the RNA samples were stored at -80°C until further use.

Real-time quantitative PCR

All RT-qPCR were performed combining 10 µL of 2× SensiFAST™ SYBR® No-ROX One-Step mix (Biotech), 0.6 µL of each primer (0.3 µM final concentration; **Table III.3**), 0.2 µL of reverse transcriptase (Biotech), 0.4 µL of RNase inhibitor (Biotech), 3 µL of RNA template, and 5.2 µL of DEPC-treated water (diethylpyrocarbonate; Biotech) in each well to reach a finale volume of 20 µL. Next, the mRNA expression was measured using the LightCycler® 480 system (Roche) with predetermined cycle conditions (Reverse T1 (45°C, 10 min, 1×), 2-step Amplification (95°C, 5 sec; 60°C, 30 sec, Single, 40×) and Melting (95°C, 10 sec; 45°C, 1 min; 95°C, continuous, 1×)) and analyzed relative to the expression of the housekeeping gene, *rpoB*, with the LightCycler® 480 SW 1.5.1 software. The normalized relative expression levels were further analyzed using GraphPad software 8.0. All primers are listed in **Table III.3**.

Table III.3. Primers used to measure the relative expression levels of the genes of interest.

Name	Sequence	Description
rpoB_qPCR_For	CAGCACTCCATCTCACCGAA	Forward primer needed for mRNA quantification of <i>rpoB</i> .
rpoB_qPCR_Rev	TGGTCGACGACAAGATCCAC	Reverse primer needed for mRNA quantification of <i>rpoB</i> .
Mtr_qPCR_For	CACCAACGACGACATCATGC	Forward primer needed for mRNA quantification of <i>mtr</i> .
Mtr_qPCR_Rev	AATCACGGTGACCTTCGAGC	Reverse primer needed for mRNA quantification of <i>mtr</i> .
MshC_qPCR_For	CATCATCGAGCTCGTCGAGAA	Forward primer needed for mRNA quantification of <i>mshC</i> .
MshC_qPCR_Rev	CCGACTCATAGCCGAAGTGT	Reverse primer needed for mRNA quantification of <i>mshC</i> .

Quantification of intracellular reduced thiol levels

For quantification of the intracellular reduced thiol levels, the Thiol Fluorescent Detection Kit (Thermo Fisher Scientific) was used. Briefly, mycobacterial strains were grown in 7H9 broth supplemented with 10% ADS, 0.2% glycerol and 0.05% tyloxapol until reaching their logarithmic phase, diluted in the same medium to match an OD₆₀₀ of 0.1 and incubated at 37°C for 48h. After 48h, the cultures were brought back to the same OD₆₀₀, washed twice with DPBS (Dulbecco's Phosphate Buffered Saline; Gibco) supplemented with 0.05% tyloxapol and resuspended in 1X Assay Buffer (Thiol Fluorescent Detection Kit; Thermo Fisher Scientific). Next, the mycobacterial cell wall was disrupted with BeadBug™ beads (Sigma; 0.1 mm Zirconium beads) by shaking at a speed of 6 m/s twice for 60 seconds using the FastPrep 24 Classic (MP biomedical) followed by centrifugation of the cultures and isolation of the supernatans. The samples were diluted two-fold by using the 1X Assay Buffer after which 100 µL of each diluted sample was added to a black half area 96-well plate together with 25 µL Detection Reagent (Thiol Fluorescent Detection Kit; Thermo Fisher

Scientific). The plate was incubated for 30 min at RT in the dark before reading the fluorescent signal with the Tecan plate reader (Infinite F plex) at an emission of 510 nm and excitation of 390 nm. For determination of the thiol levels, the fluorescent values of the samples were plotted according to a standard curve obtained with an N-Acetylcysteine Standard (Thermo Fisher Scientific).

Growth curves

The bacteria were grown until logarithmic phase in 7H9 broth supplemented with 10% ADS, 0.2% glycerol and 0.05% tyloxapol or Sauton's medium supplemented with 2% glycerol and 0.05% tyloxapol and diluted to an OD₆₀₀ of 0.05 before being incubated in a shaking incubator (New Brunswick Scientific; 175 rpm) at 37°C. Growth of the strains was evaluated every 24h by measuring the OD₆₀₀ with a cell density meter (Biochrom WPA Biowave).

Oxidative stress-induced viability assay

Logarithmic-phase mycobacterial strains were cultured in Sauton's medium supplemented with 2% glycerol and 0.05% tyloxapol after which they were diluted to an OD₆₀₀ of 0.05. At that moment, all strains were divided in two groups whereas one group was subjected to 7.5 or 15 mM H₂O₂ (Sigma) before they were all incubated in a shaking incubator (New Brunswick Scientific; 175 rpm) at 37°C. At 0h, 4h, 8h and 24h after addition of H₂O₂, part of each culture was harvested to determine the ATP levels and CFU count. The ATP levels of the cultures were measured using the BacTiter-Glo™ kit (Promega) and a 10-fold serial dilution of each culture was plated on 7H11 agar plates supplemented with 10% ADS and 0,2% glycerol for measurement by CFU count.

RAW 264.7 macrophage infection

RAW 264.7 murine macrophages were cultured in Dulbecco's modified Eagle's medium (DMEM; Thermo Fisher Scientific) containing 10% heat-inactivated Fetal Calf Serum (iFCS; Thermo Fisher Scientific), 10% Penicillin-Streptomycin (P/S; Thermo Fisher Scientific; 10000 U/mL) and 10% L-Glutamine (Glutamax; Thermo Fisher Scientific; 200 nM) at 37°C. To determine the infectivity of the different mycobacterial strains, the macrophages were seeded in DMEM supplemented with 5% iFCS at a concentration of 5×10^5 cells/mL and incubated overnight at 37°C. Next, the cells were infected at a multiplication of infection (MOI) of 5 during 4h at 37°C in the presence of 5% CO₂. After infection, 200 µg/mL amikacin (Sigma) was added to the cells, and they were incubated once more in the same conditions for 45 min to kill all extracellular bacteria. The bacterial load was analyzed immediately after infection (0h) and 24h post-infection by first lysing the cells with 0.1% Triton-X-100 for 10 min and then plating out a serial dilution on 7H11 agar plates supplemented with 10% ADS and 0.2% glycerol to determine the CFUs.

Galleria mellonella infection

G. mellonella larvae were purchased from Anaconda Reptiles (Kontich, Belgium) and stored in boxes filled with wood chips at 4°C. The protocol followed was adapted from Cools et al. and Meir et al. (84, 172). Before infection, the bacterial strains were washed and resuspended in DPBS (Dulbecco's Phosphate Buffered Saline; Gibco).

To characterize infection progression, a total of 13 larvae were injected in the last left proleg with 5×10^4 bacteria of the luminescent *Mab* FF_scarlet strain in a total volume of 10 µL by a 31G needle using a Hamilton syringe. After injection, the larvae were incubated at 37°C and infection was assessed by bioluminescent imaging (BLI) every 24h.

To compare infection of *Mab* WT with *Mab::mtr*, larvae were injected in the penultimate pro-leg with 5×10^3 CFU in a volume of 10 μ l by a 31G needle using a Hamilton syringe. At the same time, the control group was injected with 10 μ l DPBS. Next, the larvae were incubated at 37°C until they were sacrificed or until the end of the experiment. To generate a Kaplan-Meier curve, a total of 20 larvae per strain received a dead-or-alive score every 24h based on absence of movement in response to external stimuli and melanization of the larvae. For CFU count of the bacteria per larvae, a total of 4 to 7 larvae of each infected group were sacrificed by freezing for 30 min on day 2, 4 and 6. Then, these larvae were decontaminated with 70% ethanol, homogenized by the Qiagen TissueRuptor and plated out in a serial dilution on 7H11 agar containing 10% ADS, 0.2% glycerol, 2 μ g/mL vancomycin (Sigma) and 8 μ g/mL ceftazidime (Sigma). The plates were incubated at 37°C until colonies could be counted properly.

Bioluminescent imaging

Imaging of the larvae was performed 1 to 10 min after injection of 0.05 μ g/g D-Luciferin (Firefly Luciferin Potassium Salt; AAT Bioquest) using the IVIS® Spectrum In Vivo Imaging system. D-Luciferin was administered in the last left proleg of the larvae in a volume ranging between 10 and 20 μ L by a 31G needle using a Hamilton syringe. After imaging, the luminescence signal of each larva was analyzed with the LivingImage v4.3.1 software and quantified as relative luminescence units (RLU).

Biofilm formation

The biofilm formation protocol was adapted from Rodríguez-Sevilla et al. (173). Briefly, all *Mab* strains were grown in 7H9 supplemented with 10% ADS and 0.2% glycerol up to logarithmic phase, washed with DPBS (Dulbecco's

Phosphate Buffered Saline; Gibco) and diluted in DPBS to an OD₆₀₀ of 0.2. Then, 5 µL of each strain was spotted on a sterile Isopore Polycarbonate membrane (Carl Roth Belgium; pore size: 0.22 µm, diameter: 13 mm, white) present on an 7H11 agar plate supplemented with 10% ADS and 0.2% glycerol followed by incubation of the agar plates side-up at 37°C with 5% CO₂. After 24h, 48h, 72h and 96h of incubation, an image was taken of each membrane containing the biofilm, the area of the biofilm was calculated with ImageJ and the biofilm was extracted from the membranes to determine the bacterial load per membrane by CFU count. Sampling of the biofilm was accomplished by placing each membrane containing a biofilm in 10 mL DPBS and detaching the biofilm from the membrane by vortexing for 30 sec, sonicating for 2 min and vortexing again for 30 sec.

Statistical analysis

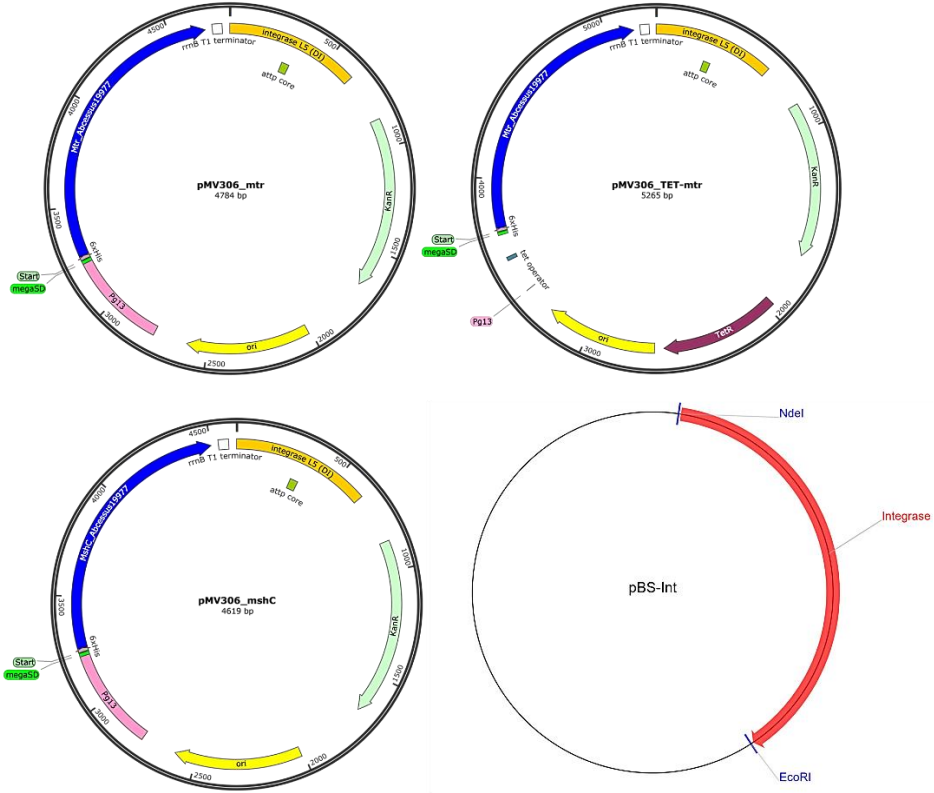
Mann-Whitney test was applied to statistically evaluate the results obtained by RT-qPCR, oxidative stress assay, macrophage assay, *G. mellonella* infection and biofilm formation, and was followed by correction for multiple testing when required. Interpretation of a decline or increase of the results over time was statistically analyzed with a non-linear regression. The Kaplan-Meyer curve was analyzed using the Log-rank (Mantel-Cox) test. Results were considered significantly different when $p < 0.05$. All statistical analysis was performed using the Graphpad software 8.0.

III.4 Results

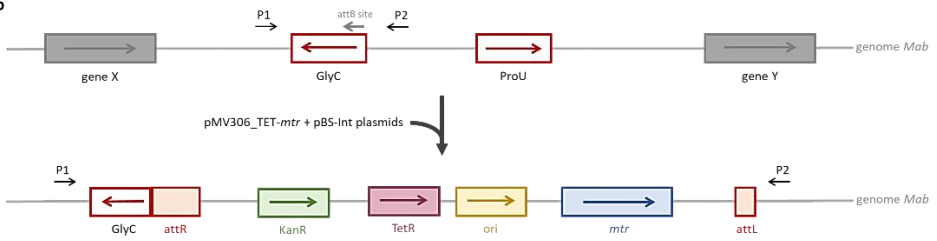
Successful integration of pMV306_mtr, pMV306_TET-mtr and pMV306-mshC plasmids into the L5 site of Mab

To create *mtr* and *mshC* overexpressing strains, pMV306 plasmids were created that constitutively express *mtr* or *mshC* via a strong G13 promoter (pMV306_mtr or pMV306-mshC) or express *mtr* via a Tet-On promoter (pMV306_TET-mtr). These integrating pMV306_mtr, pMV306_TET-mtr and pMV306-mshC plasmids were each transformed together with the integrase-expressing pBS-Int suicide plasmid inside *Mab* (**Figure III.2a**). After transformation, the constructed plasmids were integrated in the L5 site of the bacterial genome, as presented on **Figure III.2b**, to create *Mab::mtr*, *Mab::TET-mtr* and *Mab::mshC*. To confirm successful integration of the plasmids, primer 1 and 2 (P1 and P2; L5_For and L5_Rev respectively; **Table III.2**), were used to amplify the L5 integration site of *Mab*. For the WT strain, a 170 bp fragment is generated while integration of pMV306_mtr, pMV306_TET-mtr or pMV306-mshC plasmids results in the amplification of a 4954 bp, 5435 bp or 4789 bp fragment, respectively. As demonstrated on **Figure III.2c**, *Mab::mtr*, *Mab::TET-mtr* and *Mab::mshC* all show bands corresponding to the integration of the pMV306 plasmids into their L5 sites. Next, the PCR fragments were further analyzed by Sanger sequencing, confirming the correct integration of the respective plasmids (**Figure III.2d**). Perfect alignment is demonstrated by a filled, red-colored arrow while a transparent area displays a mismatch. All point mutations deducted from the Sanger sequencing analysis could be ruled out as a repeated Sanger sequencing of the same sites did not yield the same point mutations. However, an additional sequence of 19 bp located before the kanamycin-resistant cassette (KanR) and a gap of 14 bp located after the T1 terminator were observed in all plasmids without yielding any visible consequences on the performance of the plasmids.

a



b



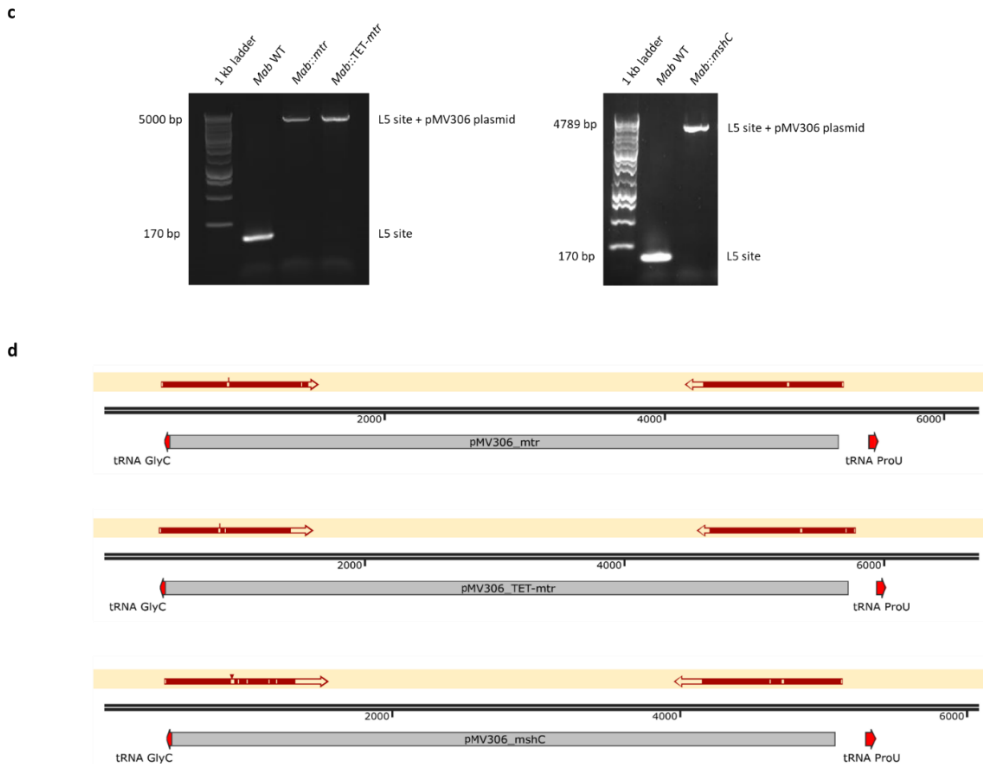


Figure III.2. pMV306_mtr, pMV306_TET-mtr and pMV306_mshC plasmids were successfully integrated into the L5 site. a) Overview of the integrating pMV306_mtr, pMV306_TET-mtr and pMV306_mshC plasmids that were separately transformed into *Mab* together with the integrase-expressing pBS-Int suicide plasmid. **b)** Schematic representation of the integration of pMV306_TET-mtr plasmid into the L5 site. The black arrows with P1 and P2 show the places where the L5_For and L5_Rev primers (**Table III.2**) anneal to amplify the L5 site. **c)** PCR amplification of the L5 site with the previously mentioned primers. After amplification of the L5 site, a fragment of 170 bp is expected for the WT while the integration of the pMV306_mtr, pMV306_TET-mtr and pMV306_mshC plasmids should provide a fragment of 4954 bp, 5435 bp or 4789 bp respectively. The results obtained from the PCR show the expected fragments at the expected height for all created strains. **d)** Sanger sequencing performed using the same primers to further confirm the correct integration of the pMV306 plasmids into the L5 site. The sequence of interest was aligned to a reference sequence in which a filled, red-colored arrows show an overlapping sequence with the expected sequence while transparent gaps in the arrow show mismatched. Repeated Sanger sequencing results of the same fragment did not show overlapping point mutation, hereby excluding the possibility of point mutations. ori: origin of replication, TetR: tetracycline repressor, KanR: kanamycin-resistant cassette

Confirmed increased expression of mtr or mshC in the overexpressing strains

To confirm higher expression of *mtr* or *mshC* in the created overexpressing strain, the expression of both genes was evaluated relative to that of the housekeeping gene, *rpoB*, using RT-qPCR. In *Mab::mtr* a markedly higher expression of *mtr* was observed compared to the WT strain, i.e. 263-fold higher, while the inducible strain demonstrated a 116-fold increase of *mtr* expression after addition of ATc (**Figure III.3**). However, the non-induced *Mab::TET-mtr* showed a 3.8-fold *mtr* upregulation compared to the WT, which may be the result of leaky expression. Due to the possibility of leaky expression, *Mab::TET-mtr* was excluded from further experiments. Finally, a 94-fold higher *mshC* expression was detected in *Mab::mshC* when compared to *Mab* WT. Overall, these results confirm that the correct integration of the pMV306 plasmids, harboring a second copy of the *mtr* or *mshC* gene, into the L5 site of *Mab* led to the construction of *mtr* and *mshC* overexpressing strains.

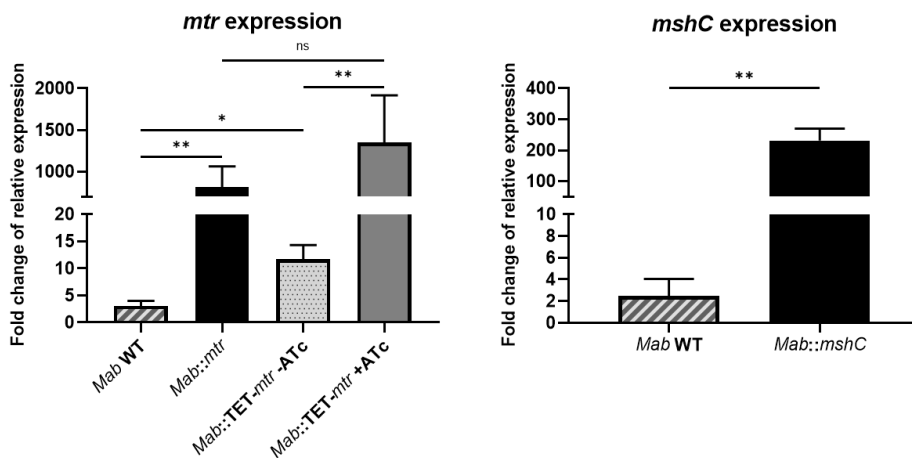


Figure III.3. *mtr* and *mshC* overexpressing strains display an increased expression of *mtr* or *mshC* respectively. RNA was isolated from all strains and the expression of the genes of interest were analyzed relative to the expression of the housekeeping gene *rpoB* by RT-qPCR. A 263-fold higher expression of *mtr* was demonstrated in *Mab::mtr* compared to *Mab* WT while *Mab::TET-mtr* displayed a 116-fold increased expression of *mtr* after being induced by ATc. However, a 3.8-fold higher expression of *mtr* was detected in the non-induced *Mab::TET-mtr* compared to the WT, possibly due to leaky expression. Furthermore, *Mab::mshC* presented a 94-

fold increase in *mshC* expression in comparison to *Mab* WT. Results are shown as mean \pm SEM from six independent experiments. Statistical significance was obtained with the Mann-Whitney test after which the p-values were corrected for multiple testing. * $p < 0.05$, ** $p < 0.01$, ns = non-significant

Intracellular reduced thiol levels are unaltered after overexpressing mtr and mshC

As Mtr and MshC are part of the MSH biosynthesis and recycling pathway, it would be interesting to investigate whether an increased expression of *mtr* or *mshC* leads to higher levels of intracellular MSH. However, due to the unavailability of such a test, the overall intracellular reduced thiol levels present in each strain were measured instead. Before measurement, the mycobacterial strains were grown for 48h, normalized by OD₆₀₀, and lysed to release their intracellular content. The results illustrated that the total concentration of reduced thiols present in 100 μ l WT *Mab* culture was around 2100 nM (**Figure III.4**). Furthermore, the strains overexpressing *mtr* or *mshC* present similar levels of intracellular reduced thiols compared to the WT.

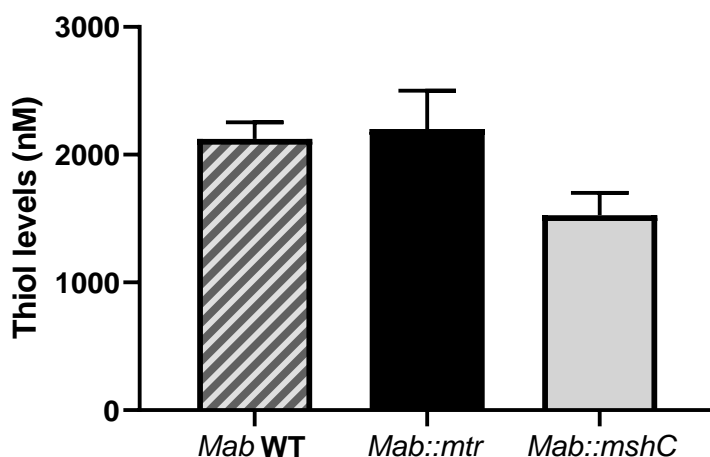


Figure III.4. Intracellular reduced thiol levels stay the same in *mtr* and *mshC* overexpressing strains. Intracellular reduced thiol levels of the lysed bacterial strains were

measured after growing for 48h. WT *Mab* culture presented intracellular thiol concentrations of around 2100 nM in a sample of 100 μ l. Moreover, no difference in intracellular reduced thiol levels was observed between WT *Mab* and the *mtr* or *mshC* overexpressing strain. Results are shown as mean \pm SEM from three independent experiments.

The overexpression of mtr leads to a reduced survival of Mab in a nutrient-poor medium

Mab is an environmental bacterium that can survive in various places including in soil, water, dust and inside a host (35), meaning that this bacteria must survive and grow under different conditions. In this experiment, the growth of the *mtr* and *mshC* overexpressing strains was analyzed in both nutrient-rich and nutrient-poor medium, Middlebrook 7H9 broth and Sauton's medium, respectively. The strains were grown until their logarithmic phase and diluted back to an OD₆₀₀ of 0.05 before being incubated in a shaking incubator at 37°C. Then, bacterial growth was determined each day by measuring the OD₆₀₀. During growth in the nutrient-rich 7H9 broth, *Mab::mtr* displayed a longer lag-phase and a higher plateau-phase compared to the WT whereas *Mab::mshC* showed comparable lag- and log-phase to *Mab* WT but a plateau-phase reaching a lower OD₆₀₀ (**Figure III.5a**). The doubling time of WT *Mab* ranged between 9.8h and 10.9h while *Mab::mtr* and *Mab::mshC* illustrated a doubling time of 11.7h and 11.8h, respectively. In contrast to the results obtained in 7H9 broth, growth of *Mab::mtr* in the nutrient-poor medium Sauton was compromised as the bacteria was unable to reach an OD₆₀₀ higher than 1.5 within 6 days of growth while *Mab::mshC* was able to grow in that medium but reached a plateau at a lower OD₆₀₀ compared to the WT (**Figure III.5b**).

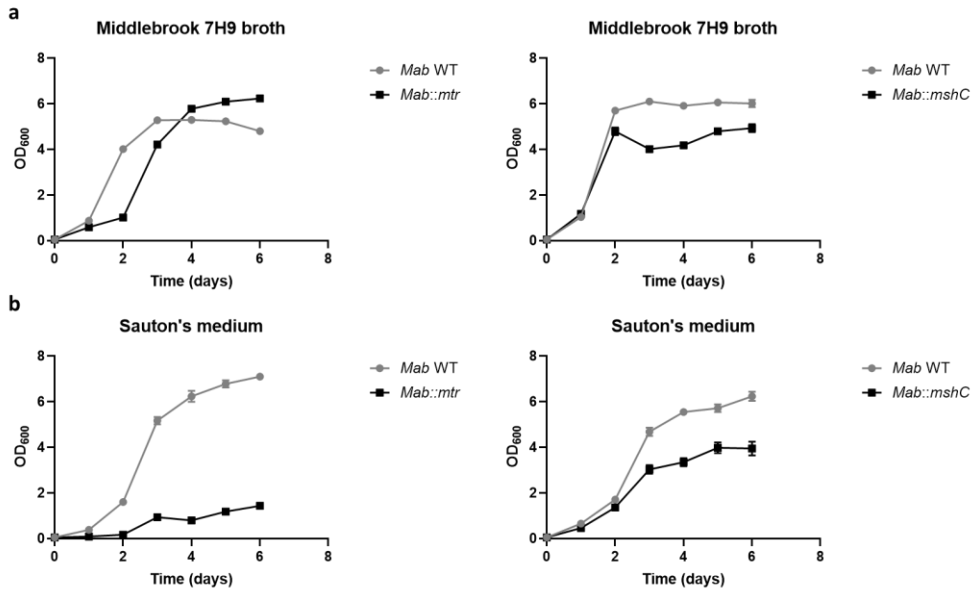
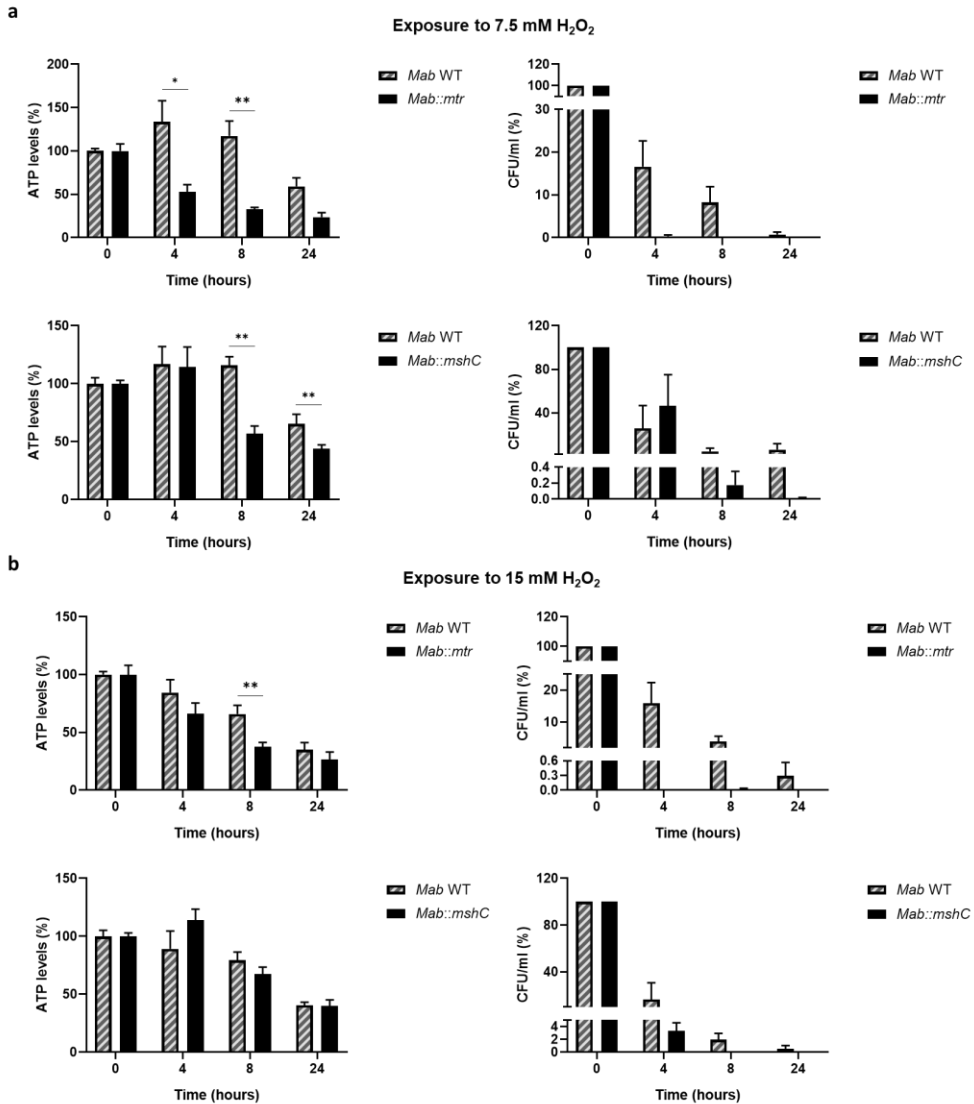


Figure III.5. *Mab::mtr* has a reduced ability to grow in the nutrient-poor medium Sauton. *Mab* overexpressing strains were grown in the nutrient-rich 7H9 broth (a) or the nutrient-poor medium Sauton (b), diluted to an OD₆₀₀ of 0.05 and incubated while shaking at 37°C. Bacterial growth was evaluated every 24h by measuring the OD₆₀₀. a) Both *Mab::mtr* and *Mab::mshC* demonstrate a slightly different growth curve in 7H9 broth compared to the WT. b) Growth of *Mab::mtr* is compromised in Sauton's medium as this strain is unable to reach a high OD₆₀₀ while *Mab::mshC* was able to grow in Sauton's medium but illustrated a plateau phase at a lower OD₆₀₀ compared to the WT. Results are shown as mean ± SEM from three independent experiments. A non-linear regression for Gompertz growth with least square fit was used to analyze the curves of *Mab::mtr* in 7H9 broth and *Mab::mshC* in Sauton's medium. A non-linear regression for Logistic growth with least square fit was used to analyze the curves of *Mab::mtr* in Sauton's medium and *Mab::mshC* in 7H9 broth.

Overexpressing mtr and mshC in Mab leads to lower ATP levels after exposure to 7.5 mM H₂O₂

As *Mab* is exposed to oxidative stress when infecting a host and Mtr and MshC are key enzymes of the pathway needed to neutralize ROS, all strains were exposed to different concentrations of H₂O₂, a direct source of ROS, in the nutrient-poor medium Sauton. *Mab* WT, *Mab::mtr* and *Mab::mshC* were diluted

to an OD_{600} of 0.05 after which 7.5 mM or 15 mM H_2O_2 was added to part of the cultures before being incubated while shaking at 37°C. As a control, the same cultures without any addition of H_2O_2 were included in the experiment. After 0h, 4h, 8h and 24h of incubation, ATP levels of all cultures were quantified using the BacTiter-Glo™ kit whereas the viability of the strains was determined by CFU count. Both overexpressing strains showed significantly lower ATP levels ($p < 0.05$ and $p < 0.01$) after exposure to 7.5 mM H_2O_2 with *Mab::mtr* having reduced levels at 4h and 8h after exposure while the ATP levels of *Mab::mshC* were decreased after 8h and 24h of exposure (**Figure III.6a**). Interestingly, the lower metabolic state of *Mab::mshC* did not lead to a difference in viability of the strain. *Mab::mtr* on the other hand demonstrated a faster decline in its survival compared to the WT when exposed to 7.5 mM H_2O_2 in Sauton's medium. When exposed to 15 mM H_2O_2 , only *Mab::mtr* showed reduction in ATP levels after 8h and overall viability (**Figure III.6b**).



the decay in viability of each strain, a non-linear regression for a one phase decay with least square fit was used. * $p < 0.05$, ** $p < 0.01$

Proliferation inside macrophages is not affected by overexpression of mtr or mshC

To further understand to role of Mtr and MshC during *Mab* infection, the intracellular proliferation of the overexpressing strains was evaluated inside macrophages, i.e. the primary host-cells of *Mab*. Here, RAW 264.7 macrophages were infected using an MOI of 5 of each bacterial strain. After infection, the bacterial load was evaluated by CFU count directly (0h) to determine the actual infection and 24 hpi (hours post infection) to measure the extend of intracellular proliferation after 24h. The bacteria were released from the macrophages after lysis of the cells. As presented in **Figure III.7**, the overexpression of *mtr* or *mshC* did not lead to a varying proliferation of *Mab*.

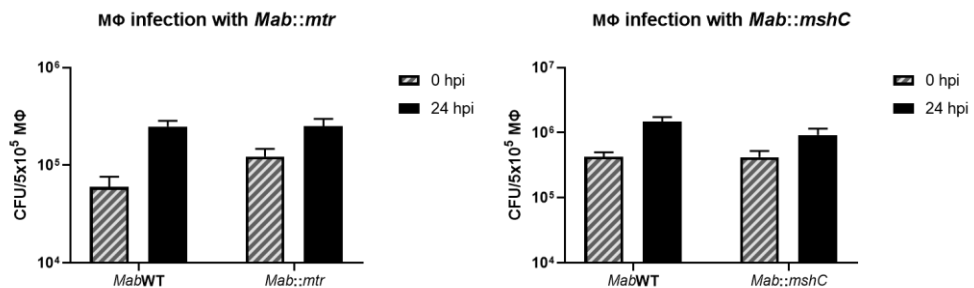


Figure III.7. Overexpressing *mtr* or *mshC* does not alter intracellular proliferation of *Mab*.

Mab WT, *Mab::mtr* and *Mab::mshC* were used to infect RAW 264.7 macrophages with an MOI of 5 and lysed 0 and 24 hours post infection (hpi) to determine the intracellular bacterial load. The figure illustrated the absence of a change in proliferation inside macrophages after the overexpression of *mtr* or *mshC*. Results are shown as mean \pm SEM from three independent experiments with *Mab::mtr* and two independent experiments with *Mab::mshC*. Each independent experiment was performed in duplicates.

Overexpressing mtr does not provide Mab with an advantage for proliferation inside G. mellonella larvae

As macrophages are only part of the components that play a role during *Mab* infection, *G. mellonella* larvae were used as a more complete *in vivo* infection model for *Mab*. To characterize the ability of *Mab* to infect *G. mellonella* larvae and determine infection progression within this organism, the luminescent strain *Mab* FF_scarlet was used. Hereby, a total of 13 larvae were infected with 5×10^4 bacteria and incubated at 37°C for 96h. Every 24h, BLI was performed on the larvae to assess the bacterial infection and the luminescent signal was quantified. It was demonstrated that *Mab* FF_scarlet is able to infect *G. mellonella* larvae as a luminescent signal can be detected inside the larvae, and that the signal is maintained over the course of the infection (**Figure III.8a**). Moreover, a clear tendency for progression of infection was established in **Figure III.8b**, with the luminescence inside the larvae being significantly higher at 2 days post-infection (dpi), 3 dpi and 4 dpi when compared to 1 dpi.

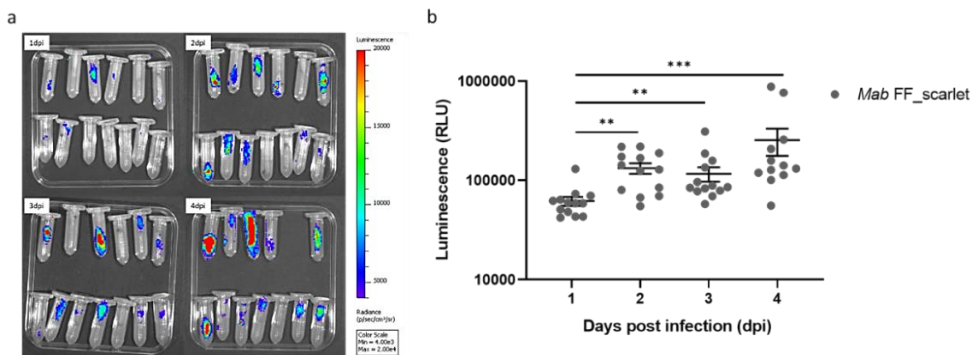


Figure III.8. *Mab* is able to proliferate inside *G. mellonella* larvae. A total of 13 *G. mellonella* larvae were infected with 5×10^4 *Mab* FF_scarlet bacteria and incubated for 96h at 37°C. Infection inside the larvae was determined every 24h by BLI followed by quantification of the measured luminescence signal. **a)** *Mab* FF_scarlet is able to successfully infect *G. mellonella* larvae while the luminescence signal of the strain maintains throughout the infection. **b)** Infection of *Mab* FF_scarlet progresses inside the larvae with the luminescence at 2, 3 and 4 dpi being significantly higher than at 1 dpi. Results are shown as mean \pm SEM from one single experiment. Statistical significance was obtained with the Mann-Whitney test after which the p-values were corrected for multiple testing. **p < 0.01, ***p < 0.001

Next, to compare infection of *G. mellonella* between WT and *Mab::mtr*, the larvae were infected with 5×10^3 of either *Mab* WT or *Mab::mtr* and the bacterial load was evaluated after 3 and 6 days of infection using viable plate count (VPC). In parallel, another experiment was set up in which 20 larvae were infected with either *Mab* WT, *Mab::mtr* or PBS to determine the virulence of the different strains. These larvae received a dead-or-alive score every 24h. **Figure III.9a** depicts the change in appearance that larvae undergo after death and **Figure III.9b** demonstrates the penultimate pro-leg, i.e. the site of injection. The results obtained by CFU count showed that overexpressing *mtr* did not lead to a higher proliferation 3 and 6 days after infection whereas proliferation of the WT in the larvae was increased after 6 days, although not significantly (**Figure III.9c**). Moreover, no effect of the different strains was perceived on the survival of the larvae (**Figure III.9d**). However, more repeats need to be performed for both experiments in order to correctly draw conclusions.

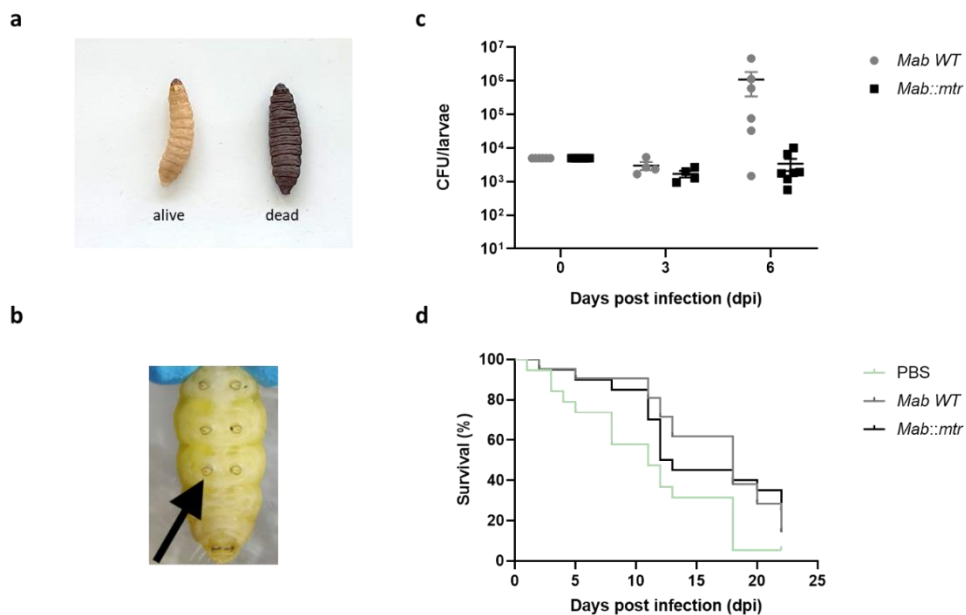


Figure III.9. Overexpressing *mtr* is not advantageous for proliferation inside *G. mellonella* larvae. *G. mellonella* larvae were infected with 5×10^3 bacteria of either *Mab* WT or *Mab::mtr*. After 3 and 6 days of incubation at 37°C, 4 and 7 larvae per condition respectively were sacrificed to determine the bacterial load by CFU (c). In parallel, 20 larvae were infected with *Mab* WT,

Chapter III

Mab::mtr or PBS to evaluate the effect of the different strains on the survival of the larvae by using a dead-or-alive score every 24h (**d**). **a**) Difference in appearance between alive and dead *G. mellonella* larvae. Larvae that are alive and healthy demonstrate a beige skin color while larvae that are dead undergo a melanization reaction. **b**) Illustration of the penultimate pro-leg that is used for injection. **c**) No significant difference was observed in the proliferation of both strains inside the larvae at every timepoint after infection. **d**) Infection of the larvae with the different strains did not lead to a variation in the survival of the larvae. Nonetheless, more repeats are needed for both experiments before conclusions can be drawn. Results are shown as mean \pm SEM from one single experiment. Statistical significance of the Kaplan-Meier curve was obtained by performing a survival analysis with Log-rank (Mantel-Cox) test.

Biofilm formation is unaltered after mtr or mshC is overexpressed in Mab

Mab is known to form biofilms which may contribute to the persistent pulmonary infections caused by this bacteria (37). To investigate whether the overexpression of *mtr* or *mshC* alters biofilm formation in *Mab*, *Mab* WT, *Mab::mtr* and *Mab::mshC* were diluted to an OD₆₀₀ of 0.2 after which a 5 μ L spot was applied on polycarbonate membranes and incubated at 37°C in the presence of 5% CO₂. Every 24h, a picture was taken of the biofilms, area of the biofilms was determined and the bacterial load per membrane was assessed by CFU count. As depicted on **Figure III.10a** and **b**, both overexpressing strains were able to form biofilms, however, no statistical difference in bacterial load nor area was observed compared to the WT. Additionally, the biofilms formed by the overexpressing strains and the WT strain were also similar based on appearance (**Figure III.10c**).

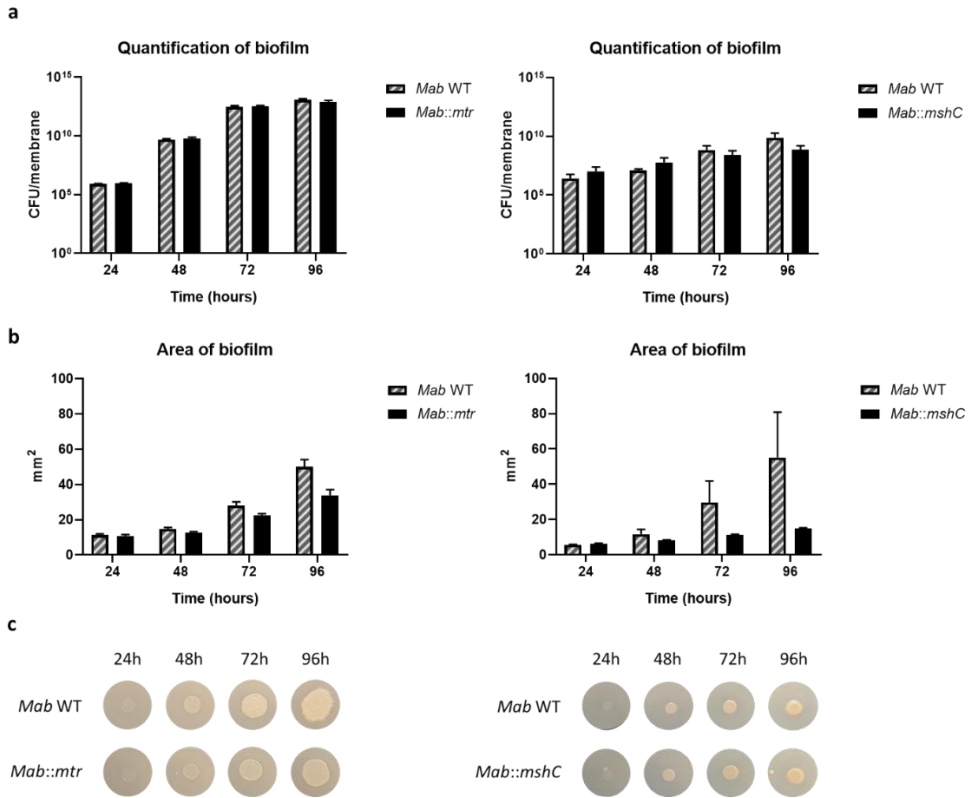


Figure III.10. Overexpression of *mtr* or *mshC* does not enhance biofilm formation. A 5 μ L spot of *Mab* WT, *Mab::mtr* or *Mab::mshC* was brought onto a polycarbonate membrane and incubated side-up at 37°C in the presence of 5% CO₂. Every 24h, the biofilms were assessed based on their bacterial load, area and appearance. The overexpression of *mtr* or *mshC* fails to enhance biofilm formation of *Mab* as no difference is seen in neither bacterial load (**a**), area (**b**) or appearance (**c**) of the biofilms. Results are shown as mean \pm SEM from three independent experiments. Images of the biofilms represent one of three independent repeats.

III.5 Discussion

MSH plays an important role in the protection of *Mab* and other mycobacteria against oxidative stress since it acts as an antioxidant that will neutralize reactive intermediates and thus keeping a balanced redox homeostasis (88). Other than MSH, more thiols and ROS-scavenging enzymes have been reported to play a role in the protection against oxidative stress, including glutathione, ergothioneine and catalase (174). Several studies have already demonstrated that the overexpression of these thiols and ROS-scavenging enzymes lead to increased protection against oxidative stress and enhanced robustness of bacteria (175). Hereby, Zhang et al. proved that the overexpression of glutathione protects *Lactobacillus sanfranciscensis* against stress conditions (176). In *Streptomyces coelicolor*, overexpressing ergothioneine showed similar protective abilities (177). Moreover, higher levels of catalase reduces oxidative stress in *Saccharomyces cerevisiae* while overexpression of the heme-dependent catalase gene, *kata*, was shown to offer protection against oxidative stress in *Lactobacillus rhamnosus* (178, 179). Finally, *Corynebacterium glutamicum*, bacteria belonging to the same order as mycobacteria (171), overexpressing MSH or the MSH-recycling enzyme Mtr present an enhanced survival under oxidative stress (180, 181).

In this study, *Mab mtr* and *mshC* overexpressing strains were generated to examine the role of both enzymes in the protection and robustness of *Mab* while also investigating whether overexpressing *mtr* or *mshC* would lead to an increased fitness of *Mab* during stress conditions and infection. However, the *mtr* and *mshC* overexpressing strains generated in this study showed impaired or reduced growth during *in vitro* growth in nutrient-poor Sauton's medium (**Figure III.5b**). Compared to Middlebrook 7H9 broth, Sauton's medium is lacking several components, including biotin and pyridoxine (182, 183). Biotin is a cofactor required for the fatty acid synthesis, gluconeogenesis, and amino acid metabolism, and is hereby essential for the growth of mycobacteria (184). Pyridoxine, also known as vitamin B6, is an essential cofactor for the amino acid

metabolism and was found to be essential for the survival and virulence of *Mtb* (185, 186). The lack of some essential components needed for mycobacterial growth seem to be disadvantageous for *Mab* in combination with higher levels of *mtr* or *mshC*, especially *mtr*. Interestingly, both overexpressing strains also demonstrated a reduced metabolic state after exposure to 7.5 mM H₂O₂ with *Mab::mtr* illustrating a faster decline in survival after exposure (**Figure III.6a**). While lower ATP levels may be correlated to a decrease in viability as a result of a reduced fitness when overexpressing *mtr* or *mshC* in *Mab*, the obtained effect might also be presented as an artefact due to an increased use of ATP by the bacteria to enable the production of higher concentrations of Mtr or MshC. Additionally, the overexpression of both genes did not alter proliferation of *Mab* inside macrophages, *G. mellonella* larvae or during biofilm formation (**Figure III.7, III.9 and III.10**). These findings suggest that overexpressing the MSH-related enzymes, Mtr and MshC, fail to increase the fitness of *Mab* and is even unfavorable for the bacteria under certain conditions.

Intracellular MSH levels of the *mtr* and *mshC* overexpressing genes were not yet determined, however, our research investigated the total intracellular reduced thiol levels of each strain (**Figure III.4**). This experiment illustrated unaltered intracellular thiol levels in the *mtr* and *mshC* overexpressing strains suggesting that overexpressing only one component of the MSH biosynthesis or recycling pathway may not translate into an increase in MSH levels. On the other hand, to counteract the effect of reductive stress, an increase in MSH levels may also be compensated by a reduction in other intracellular thiols in the overexpressing strains, leading to the same total level of thiols in the *mtr* and *mshC* overexpressing strains as in the WT. Reductive stress is a phenomena in which the reducing equivalents, including MSH, of redox pairs accumulate inside the bacteria and a research conducted by Mavi et al. demonstrated that the cellular accumulation of such reducing agents can lead to inhibited respiration and growth inhibition (164). Nonetheless, more experiments, in which the

concentration of each individual thiol is investigated, are needed to further elucidate this occurrence.

The pMV306 integration system has been widely used in various mycobacterial strains to successfully overexpress genes (129, 132) and complement knockout strains (130, 131, 132), and was highly effective in our study to produce overexpressing strains (**Figure III.2**). The pMV306 plasmid used in this study contains a G13 promoter, a strong promoter that expresses genes in a high amount (128). This enabled the creation of a strain with a 263-fold and 94-fold higher expression of *mtr* and *mshC*, respectively, yielding a strong overexpressing strain (**Figure III.3**). However, generating overexpressing strains with such a higher expression compared to the original expression appeared to be disadvantageous for *Mab* in certain conditions, especially for *Mab::mtr* (**Figure III.5b and III.6**). Another disadvantage of using the strong G13 promoter is that creating a complementary strain would lead to overexpression instead of complementation due to the high expression levels obtained with this promoter. A possible solution is the use of a *hsp60* (heat-shock protein 60) promoter instead, which is another mycobacterial promoter that is commonly used in expression vectors integrating in the L5 integration site (133, 134). Expression by *hsp60* demonstrated to be 40 times lower compared to expression by G13 in *M. marinum* and significantly lower in *Mtb* as well (128, 135). In *Msm*, however, the difference in expression with the G13 promoter and *hsp60* promoter varied depending on the gene expressed (135), meaning that the level of expression of both promoters may vary between mycobacterial species. Besides being continuously expressed, a Tet-On system can be added to control the expression of the extra copy of the gene of interest (139). By using a Tet-On complementary plasmid, the expression of the gene of interest can be deactivated to enable for the detection of phenotypic changes when the gene of interest is lost. In case of an essential gene, the bacteria will not survive without expression of this particular gene. Yet, we showed potential leaky expression of the gene of interest after the incorporation of the Tet-On

system onto the pMV306 plasmid, illustrating a 3.8-fold higher expression of *mtr* in the non-induced *Mab::mtr* cultures compared to the WT (**Figure III.3**). As a consequence, using this system for the complementation of knockout strains in *Mab* would possibly lead to the constant expression of low amounts of the gene of interest, making this system unfavorable for the creation of complementary strains and determination of essentiality.

As a conclusion, this study generates more knowledge about the role of MSH-related enzymes during growth and proliferation of *Mab* by utilizing novel produced *mtr* and *mshC* overexpressing strains created with the pMV306 plasmid. Despite previous findings claiming that ROS-scavenging enzymes lead to enhanced survival of various bacteria during oxidative stress, our findings demonstrate that overexpressing key enzymes of the MSH biosynthesis or recycling pathway, Mtr and MshC, does not increase the overall intracellular thiol levels and is not favorable for *Mab*. To determine whether MSH levels are unaltered as well, more experiments need to be conducted.

CHAPTER IV

Implementation of the *Streptococcus thermophilus* CRISPRi-system to investigate the essentiality of *mtr* and *mshC* in *Mycobacterium abscessus*



These data have not yet been published.

Author contributions:

Tatiana Piller¹: conceptualization, methodology, investigation and formal analysis.

Linda De Vooght¹: conceptualization, formal analysis and supervision.

Davie Cappoen¹: conceptualization, methodology and supervision.

Paul Cos¹: conceptualization and supervision.

¹Laboratory of Microbiology, Parasitology and Hygiene (LMPH), University of Antwerp, Belgium

IV. Implementation of the *Streptococcus thermophilus* CRISPRi-system to investigate the essentiality of *mtr* and *mshC* in *Mycobacterium abscessus*

IV.1 Abstract

The suboptimal treatment of MABC infections keep on promoting the acquisition of drug tolerance. To alleviate the pressure of drug resistance, new bacterial targets need to be explored with the capability of reducing bacterial survival within the host, requiring better and adapted genetic manipulation systems. Recently, the generation of an improved *Streptococcus thermophilus* CRISPR interference (*Stth* CRISPRi) system has enabled target exploration in various mycobacteria by rapidly and efficiently reducing transcription of selected mycobacterial genes. Hence, this chapter explored this improved system for use in *Mab* by first targeting the *mmpl3* gene, i.e. an essential inner membrane transporter. Initially, this system seemed promising since targeting *mmpl3* led to a reduction in bacterial survival in the modified *Mab* compared to the WT. While determining the gene expression levels of the modified *Mab* strains would be the next step, the required method was still being optimized. In the meantime, the adapted system was further implemented to target the key enzymes of the MSH biosynthesis and recycling pathway, *Mtr* and *MshC*, to exploit their essentiality for bacterial survival. However, no effect in growth was perceived in the generated *mtr* and *mshC* strains. By the time the required method for gene expression determination was optimized, most modified *Mab* strains had lost the integrated CRISPRi plasmid, making the obtained results using the *Stth* CRISPRi system unreliable. In conclusion, we were not able to demonstrate essentiality using CRISPRi, thus alternative approaches should be investigated.

IV.2 Introduction

Infections caused by MABC are known for being very difficult to treat, as MABC is resistant to the standard antimicrobial agents, its treatment often leads to adverse drug effects, and various patients experience relapse after treatment or surgical removal of the pathogen (47, 63, 187). To improve treatment of MABC infections and relieve the burden of drug resistance, novel mycobacterial targets need to be explored, which effectively reduce the bacterial burden within the host. MSH has already been highlighted as an interesting novel drug target as it plays an important role in the detoxification of ROS, antibiotics and other reactive intermediates (88, 104).

One way of characterizing novel mycobacterial targets is to discover essential genes with the help of genome editing. In this respect, the CRISPR*i* technology is a genome-editing tool that has been successfully used over the last years to efficiently regulate gene-silencing of numerous organisms, including mycobacteria (145). This technology is derived and adapted from the CRISPR-Cas9 system, which was first discovered in prokaryotes as part of the adaptive immune system defending the organisms against foreign genetic elements (188). The two principal components of the adapted CRISPR*i* system consist of repetitive genomic elements (CRISPR) and a deactivated RNA-guided nuclease (dCas9) (189). A sgRNA is created here, which forms a complex with the dCas9 to direct the nuclease to a specific sequence in the genome in order to block transcriptional initiation or elongation through steric obstruction (157). As the CRISPR system derived from *S. pyogenes* (*Spy*) is the simplest one and is absent in mycobacteria, this system was the first one to be implemented in mycobacteria (188). Nevertheless, the use of a *Spy* derived dCas9 was not favorable, because of a relatively poor knockdown efficiency and proteotoxicity in the pathogen. In 2017, however, Rock et al. developed an improved CRISPR*i* system for *Mtb* by using the dCas9 protein from *S. thermophilus* (*Sth*) (dCas9_{Sth1}), leading to 20- to 100-fold knockdown of endogenous gene expression with minimal proteotoxicity (146). Recently, this

system has also been successfully implemented in *Mab* to demonstrate the essentiality of a gene (148).

In this chapter, we aim to implement the *Sth* CRISPRi system to produce *mtr* and *mshC* knockdown strains in *Mab* and investigate the role of these genes in bacterial survival. To achieve this, the pLJR965 plasmid expressing dCas9_{Sth1} was first transformed alone in *Mab* and evaluated for its toxicity, since the expression of dCas9 in mycobacteria is known to cause proteotoxicity in the pathogen. Then, the correct implementation of this system was tested by knocking down the essential *mmpL3* gene, leading to a growth defect of the created strain after induction. Finally, the system was used to target the *mtr* and *mshC* genes, which, unlike when targeting the *mmpL3* gene, did not lead to a growth defect of the created strains. However, the pLJR965 plasmid was lost over time in all created strains, disabling us to determine the exact expression of the genes after genetic manipulation and rendering this system unstable and unreliable.

IV.3 Materials and methods

Bacterial strains, media and culture conditions

Escherichia coli (*E. coli*) DH5 α cultures were grown in Luria-Bertani (LB) broth (Sigma-Aldrich) or plated on LB agar (Sigma-Aldrich) supplemented with 0.2% glycerol and the corresponding selection drug.

All knockdowns in this study were derived from *M. abscessus* ATCC 19977 and were routinely cultured at 37°C in Middlebrook 7H9 broth (Sigma) supplemented with 10% OADC (Thermo Fisher Scientific; oleic acid-albumin-dextrose-catalase), 0.2% glycerol and 0.05% tyloxapol and with the addition of 200 $\mu\text{g}/\text{mL}$ kanamycin (Sigma) for the knockdown strains. During growth of the Mtr and MshC knockdowns, the 10% OADC supplementation was replaced by 10% ADS (albumin-dextrose-saline). Agar plates were made of Middlebrook 7H11 agar base (Sigma).

Construction of the dsDNAs and insertion into pLJR965 and pLJR962 plasmids

The sequences of mycobacterial membrane protein Large 3 (*mmpL3*; MAB_RS22830), mycothione reductase (*mtr*; MAB_RS00460) and cysteine ligase (*mshC*; MAB_RS10805) were obtained through the National Center for Biotechnology Information (NCBI) platform. After obtaining the sequences of interest, sgRNAs were selected for each gene based on the permissive PAM sequences for dCas9_{Sth1} described by Rock et al (146). To express the sgRNAs, dsDNAs were constructed coding for the sgRNAs. Each dsDNA was created by annealing two single-stranded oligo's (purchased at Integrated DNA Technologies (IDT)) that are complementary to each other (**Table IV.1**). For this, a 50 μ L mixture, consisting of 4 μ L of each oligo (stock concentration: 100 μ M) and 42 μ L annealing buffer (50 mM Tris pH 7.5, 50 mM NaCl, 1 mM EDTA), was incubated using the following program: 2 min at 95°C followed by 0.1°C/sec to reach 25°C. Hereby, a total of 8 dsDNAs were constructed for the *mmpL3* sequence whereas 10 dsDNAs were constructed for either *mtr* or *mshC*. One sgRNA without any complementary parts on the genome of *Mab* was included as a negative control. Next, the double-stranded sgRNAs were inserted in either the pLJR965 (Addgene 115163; plasmid for *Mtb*) or the pLJR962 (Addgene 115162; plasmid for *Msm*) plasmid to determine which plasmid is better for use in *Mab*. First, both plasmids were digested with BsmBI for 4h at 55°C after which the restriction enzymes were heat-inactivated for 20 min on 80°C. Then, 0.5 μ L of the double-stranded sgRNAs and 9 ng of the BsmBI-digested CRISPRi backbones were ligated together for 30-45 min at 25°C by T7 DNA ligation (NEB). Correct insertion of the dsDNAs into the plasmids was evaluated by Sanger sequencing (Neuromics Support Facility; University of Antwerp) using a primer that anneals to the plasmids (**Table IV.1**). Confirmed plasmids were heat-shocked into chemocompetent DH5 α *E. coli* to obtain a higher quantity of the plasmids whereafter they were purified using the NucleoSpin® Plasmid QuickPure Miniprep kit (Machery-Nagel) and stored at 4°C until further use.

Table IV.1. Overview of all single-stranded oligo's needed to construct the dsDNAs coding for the sgRNAs directed against the *mmp13*, *mtr* and *mshC* genes and the primers used to evaluate correct integration of the dsDNAs into the pLJR962 and pLJR965 plasmids.

Name	Sequence	Description
CRISPRi primer	TTCCTGTGAAGAGCCATTGATAATG	Primer used to evaluate the correct integration of the dsDNAs coding for the sgRNAs into the pLJR962 or pLJR965 plasmids
NC_For	GGGAGGAGACGATTAATGCGTCTCG	Single-stranded oligo to create the dsDNA coding for NC sgRNA
NC_Rev	AAACCGAGACGCATTAATCGTCTCC	Single-stranded oligo to create the dsDNA coding for NC sgRNA
MMPL3.1_For	GGGAAGCGTGACCACGGGCTGGGC	Single-stranded oligo to create the dsDNA coding for <i>mmp13</i> sgRNA 1
MMPL3.1_Rev	AAACGCCAGCCCGTGGTCAGGCT	Single-stranded oligo to create the dsDNA coding for <i>mmp13</i> sgRNA 1
MMPL3.2_For	GGGAACTGACTCACTGTTGTCGGC	Single-stranded oligo to create the dsDNA coding for <i>mmp13</i> sgRNA 2
MMPL3.2_Rev	AAACGCCGACAACAGTGAGTCAGT	Single-stranded oligo to create the dsDNA coding for <i>mmp13</i> sgRNA 2
MMPL3.3_For	GGGAAAGTGGTCGATGACCTTCTT	Single-stranded oligo to create the dsDNA coding for <i>mmp13</i> sgRNA 3
MMPL3.3_Rev	AAACAAGAAGGTCATCGACCACTT	Single-stranded oligo to create the dsDNA coding for <i>mmp13</i> sgRNA 3
MMPL3.4_For	GGGAACGATGGTGATGGTCTCGGT	Single-stranded oligo to create the dsDNA coding for <i>mmp13</i> sgRNA 4
MMPL3.4_Rev	AAACACCGAGACCATCACCATCGT	Single-stranded oligo to create the dsDNA coding for <i>mmp13</i> sgRNA 4
MMPL3.5_For	GGGAGTCGCGGTGTGGACTGTGGC	Single-stranded oligo to create the dsDNA coding for <i>mmp13</i> sgRNA 5
MMPL3.5_Rev	AAACGCCACAGTCCACACCGCGAC	Single-stranded oligo to create the dsDNA coding for <i>mmp13</i> sgRNA 5
MMPL3.6_For	GGGAGAAACCACCGCGACCACGA	Single-stranded oligo to create the dsDNA coding for <i>mmp13</i> sgRNA 6
MMPL3.6_Rev	AAACTCGTGGTCGCCGGTGGTTTC	Single-stranded oligo to create the dsDNA coding for <i>mmp13</i> sgRNA 6

Chapter IV

MMPL3.7_For	GGGAGCTTCATCCACGCCGAGCCCA	Single-stranded oligo to create the dsDNA coding for <i>mmp13</i> sgRNA 7
MMPL3.7_Rev	AAACTGGGCTCCGGCGTGGATGAAGC	Single-stranded oligo to create the dsDNA coding for <i>mmp13</i> sgRNA 7
MMPL3.8_For	GGGAGATGCGGCGTCCCTCGCGGC	Single-stranded oligo to create the dsDNA coding for <i>mmp13</i> sgRNA 8
MMPL3.8_Rev	AAACGCCGCGAGGGACGCCGCATC	Single-stranded oligo to create the dsDNA coding for <i>mmp13</i> sgRNA 8
Mtr.1_For	GGGAGCCATCTCGCGAGCCGGAAT	Single-stranded oligo to create the dsDNA coding for <i>mtr</i> sgRNA 1
Mtr.1_Rev	AAACATTCGGCTCGCGAGATGGC	Single-stranded oligo to create the dsDNA coding for <i>mtr</i> sgRNA 1
Mtr.2_For	GGGAGCAGGGCGTTCTCGACCAACT	Single-stranded oligo to create the dsDNA coding for <i>mtr</i> sgRNA 2
Mtr.2_Rev	AAACAGTTGGTCGAGAACGCCCTGC	Single-stranded oligo to create the dsDNA coding for <i>mtr</i> sgRNA 2
Mtr.3_For	GGGAGTCGGCGAACCTATCGTCGGG	Single-stranded oligo to create the dsDNA coding for <i>mtr</i> sgRNA 3
Mtr.3_Rev	AAACCCCGACGATAGGTTCCGCGAC	Single-stranded oligo to create the dsDNA coding for <i>mtr</i> sgRNA 3
Mtr.4_For	GGGAAATGGTCTCGTCCTGAGCGC	Single-stranded oligo to create the dsDNA coding for <i>mtr</i> sgRNA 4
Mtr.4_Rev	AAACGCGCTCAGGACGAGACCATT	Single-stranded oligo to create the dsDNA coding for <i>mtr</i> sgRNA 4
Mtr.5_For	GGGAGCCGATGATGTGCGGCCCA	Single-stranded oligo to create the dsDNA coding for <i>mtr</i> sgRNA 5
Mtr.5_Rev	AAACTGGGCGCGCACATCATCGGC	Single-stranded oligo to create the dsDNA coding for <i>mtr</i> sgRNA 5
Mtr.6_For	GGGAGCCGCTTGCGGCGATCACCG	Single-stranded oligo to create the dsDNA coding for <i>mtr</i> sgRNA 6
Mtr.6_Rev	AAACCGGTGATCGCCGCAAGCGGC	Single-stranded oligo to create the dsDNA coding for <i>mtr</i> sgRNA 6
Mtr.7_For	GGGAGCCCGCGGCCATCTCGCGAG	Single-stranded oligo to create the dsDNA coding for <i>mtr</i> sgRNA 7
Mtr.7_Rev	AAACCTCGCGAGATGGCGCGCGGC	Single-stranded oligo to create the dsDNA coding for <i>mtr</i> sgRNA 7

Mtr.8_For	GGGAGGGCGTACGCCCCGTGGCGA	Single-stranded oligo to create the dsDNA coding for <i>mtr</i> sgRNA 8
Mtr.8_Rev	AAACTCGCCACGGGGCGTACGCC	Single-stranded oligo to create the dsDNA coding for <i>mtr</i> sgRNA 8
Mtr.9_For	GGGAGCTTCGTGATTGGCCACATGCT	Single-stranded oligo to create the dsDNA coding for <i>mtr</i> sgRNA 9
Mtr.9_Rev	AAACAGCATGTGGCCAATCACGAAGC	Single-stranded oligo to create the dsDNA coding for <i>mtr</i> sgRNA 9
Mtr.10_For	GGGAGGTGGCGAATCCCATCCGG	Single-stranded oligo to create the dsDNA coding for <i>mtr</i> sgRNA 10
Mtr.10_Rev	AAACCCGGATGGGATTCGCCGACC	Single-stranded oligo to create the dsDNA coding for <i>mtr</i> sgRNA 10
MshC.1_For	GGGAAACTGTTCGGTGGCATCGAC	Single-stranded oligo to create the dsDNA coding for <i>mshC</i> sgRNA 1
MshC.1_Rev	AAACGTCGATGCCACCGAACAGTT	Single-stranded oligo to create the dsDNA coding for <i>mshC</i> sgRNA 1
MshC.2_For	GGGAGCGGCGCTGTATTCTGGTG	Single-stranded oligo to create the dsDNA coding for <i>mshC</i> sgRNA 2
MshC.2_Rev	AAACCACCACGAATACAGCGCCGC	Single-stranded oligo to create the dsDNA coding for <i>mshC</i> sgRNA 2
MshC.3_For	GGGAACCACGTACGCGCCCCGGAGG	Single-stranded oligo to create the dsDNA coding for <i>mshC</i> sgRNA 3
MshC.3_Rev	AAACCGTCCGGGGCCGCTACGTGGT	Single-stranded oligo to create the dsDNA coding for <i>mshC</i> sgRNA 3
MshC.4_For	GGGAAACTCACGCAGCACAATCGC	Single-stranded oligo to create the dsDNA coding for <i>mshC</i> sgRNA 4
MshC.4_Rev	AAACGGGATTGTGCTGCGTGAGTT	Single-stranded oligo to create the dsDNA coding for <i>mshC</i> sgRNA 4
MshC.5_For	GGGAATCGGCACCTGCGCGCCGGCC	Single-stranded oligo to create the dsDNA coding for <i>mshC</i> sgRNA 5
MshC.5_Rev	AAACGGCCGGCGCAGGTGCGCGAT	Single-stranded oligo to create the dsDNA coding for <i>mshC</i> sgRNA 5
MshC.6_For	GGGAATCGGTCACCCAGTTATCCAGG	Single-stranded oligo to create the dsDNA coding for <i>mshC</i> sgRNA 6
MshC.6_Rev	AAACCCTGGATAACTGGGTGACCGAT	Single-stranded oligo to create the dsDNA coding for <i>mshC</i> sgRNA 6

MshC.7_For	GGGAGCGGCCACCACCGTCGAGTT	Single-stranded oligo to create the dsDNA coding for <i>mshC</i> sgRNA 7
MshC.7_Rev	AAACAACCTCGACGGTGGTGGGCCGC	Single-stranded oligo to create the dsDNA coding for <i>mshC</i> sgRNA 7
MshC.8_For	GGGAGTTCCCCGGCCTGGCGGCCGCC	Single-stranded oligo to create the dsDNA coding for <i>mshC</i> sgRNA 8
MshC.8_Rev	AAACGGCGGGCCGCCAGGCCCGGGAAC	Single-stranded oligo to create the dsDNA coding for <i>mshC</i> sgRNA 8
MshC.9_For	GGGAATCGGCCCGGTAGTGACCAG	Single-stranded oligo to create the dsDNA coding for <i>mshC</i> sgRNA 9
MshC.9_Rev	AAACCTGGTCACTACCGGGCCGAT	Single-stranded oligo to create the dsDNA coding for <i>mshC</i> sgRNA 9
MshC.10_For	GGGAGTCAGCCAACACCGCATCACT	Single-stranded oligo to create the dsDNA coding for <i>mshC</i> sgRNA 10
MshC.10_Rev	AAACAGTGATGCGGTGTTGGCTGAC	Single-stranded oligo to create the dsDNA coding for <i>mshC</i> sgRNA 10

Transformation of constructed CRISPRi plasmids into Mab

Mab was grown in a shaking incubator (New Brunswick Scientific; 175 rpm) in 7H9 medium supplemented with 10% OADC (oleic acid-albumin-catalase-dextrose; Thermo Fisher Scientific), 0.2% glycerol and 0.05% tyloxapol at 37°C until reaching an optical density at 600 nm (OD₆₀₀) between 0.2 and 0.8 and was made electrocompetent by washing three times with 10% glycerol. Then, 1 µg of each pLJR plasmid was transformed separately into the electrocompetent bacteria by using the Gene Pulser Xcell Total System (Bio-Rad; 1.25 kV, 1000 Ω and 25 µF). Following electroporation, *Mab* was resuspended in 7H9 medium containing 20% OADC and incubated at 37°C for 4h before it was plated out on 7H11 agar containing 10% OADC, 0.2% glycerol and 200 µg/mL kanamycin (Sigma). The 7H11 agar plates were incubated for 3 days to 1 week at 37°C until the presence of colonies. Successful incorporation of the pLJR plasmids into the L5 site of *Mab* was confirmed by PCR and Sanger sequencing (Neuromics Support Facility; University of Antwerp) utilizing primers to amplify the L5 integration site (**Table IV.2**).

Table IV.2. Overview of the primers used to amplify the L5 region of *Mab*.

Name	Sequence	Description
L5_For	CCGATCGGGTTCTCCACCTG	Forward primer used to amplify the L5 site of <i>Mab</i> .
L5_Rev	GCCCCGGCGCTGTACATTCA	Reverse primer used to amplify the L5 site of <i>Mab</i> .

Growth curves

The bacteria were grown until logarithmic phase in 7H9 broth supplemented with 10% OADC (*Mab* containing the pLJR965 plasmid or pLJR plasmids with the *mmp13* sgRNAs) or 10% ADS (*Mab* containing the pLJR965 plasmid with the *mtr* or *mshC* sgRNAs), 0.2% glycerol and 0.05% tyloxapol and diluted to an OD₆₀₀ of 0.1 or 0.05 before being incubated in a shaking incubator (New Brunswick Scientific; 175 rpm) at 37°C. Half of each culture was induced with 100 ng/mL anhydrotetracycline (ATc; Takara Bio) before incubation. Growth of the strains was evaluated every 24h or after 72h by measuring the OD₆₀₀ with a cell density meter (Biochrom WPA Biowave). In parallel, after the cultures were brought back to an OD₆₀₀ of 0.1 or 0.05, a series of spots was carried out in a ten-fold dilution on a 7H11 agar plate supplemented with 10% OADC (*Mab* containing the pLJR plasmids with the *mmp13* sgRNAs) or 10% ADS (*Mab* containing the pLJR965 plasmid with the *mtr* or *mshC* sgRNAs), 0.2% glycerol and with or without 100 ng/mL ATc.

RNA isolation

Mab strains were grown in 7H9 supplemented with 10% OADC, 0.2% glycerol and 0.05% tyloxapol until reaching their logarithmic phase and diluted to an OD₆₀₀ of 0.1 in the same medium. Half of the cultures were induced after dilution with 100 ng/ μ L μ M ATc (Anhydrotetracycline; Takara Bio). After 48h of growth in a shaking incubator (New Brunswick Scientific; 175 rpm) at 37°C, the pellets of the strains

were harvested and incubated in TRIzol reagent (Invitrogen) for 5 min at room temperature (RT). Next, the bacteria were lysed with BeadBug™ beads (Sigma; 0.1 mm Zirconium beads) by shaking at a speed of 6 m/s twice for 45 seconds using the FastPrep 24 Classic (MP biomedical) followed by incubation at -80°C overnight. To separate the samples from the TRIzol reagent, Phasemaker tubes (Invitrogen) were used together with the addition of chloroform to the sample. Once separated, RNA isolation of the samples was completed using the RNeasy Plus Mini Kit (Qiagen) followed by a DNase treatment with TURBO DNAase (Qiagen) and ezDNase (Invitrogen). The final RNA concentration was measured using the NanoDrop™ 2000 spectrophotometer (Thermo Scientific) and the RNA samples were stored at -80°C until further use.

Real-time quantitative PCR

All RT-qPCR were performed combining 10 µL of 2× SensiFAST™ SYBR® No-ROX One-Step mix (Biotech), 0.6 µL of each primer (0.3 µM final concentration; Table 3.3), 0.2 µL of reverse transcriptase (Biotech), 0.4 µL of RNase inhibitor (Biotech), 3 µL of RNA template, and 5.2 µL of DEPC-treated water (diethylpyrocarbonate; Biotech) in each well to reach a finale volume of 20 µL. Next, the mRNA expression was measured using the LightCycler® 480 system (Roche) with predetermined cycle conditions (Reverse T1 (45°C, 10 min, 1×), 2-step Amplification (95°C, 5 sec; 60°C, 30 sec, Single, 40×) and Melting (95°C, 10 sec; 45°C, 1 min; 95°C, continuous, 1×)) and analyzed relative to the expression of the housekeeping gene, *rpoB*, with the LightCycler® 480 SW 1.5.1 software. The normalized relative expression levels were further analyzed using GraphPad software 8.0. All primers are listed in **Table IV.3**.

Table IV.3. Primers used to measure the expression levels of the *mmp13* gene relative to *rpoB*.

Name	Sequence	Description
rpoB_qPCR_For	CAGCACTCCATCTCACCGAA	Forward primer needed for mRNA quantification of <i>rpoB</i> .
rpoB_qPCR_Rev	TGGTCGACGACAAGATCCAC	Reverse primer needed for mRNA quantification of <i>rpoB</i> .
Mmp13_qPCR_For	CGGTATCGGTTTCATCGTCGT	Forward primer needed for mRNA quantification of <i>mmp13</i> .
Mmp13_qPCR_Rev	ACTGACTCACTGTTGTCCGGC	Reverse primer needed for mRNA quantification of <i>mmp13</i> .

Statistical analysis

Mann-Whitney test was applied to statistically evaluate the growth of the *mmp13* knockdown strains expressing sgRNA NC, 5 and 8, and was followed by correction for multiple testing when required. Results were considered significantly different when $p < 0.05$. All statistical analysis was performed using the Graphpad software 8.0.

IV.4 Results

The presence of the pLJR965 plasmid does not inhibit growth in Mab

Before knocking down mycobacterial genes, the pLJR965 plasmid was incorporated into the L5 site of *Mab* to determine whether the presence of the pLJR965 plasmid is toxic for *Mab* when being induced, since the expression of dCas9 in mycobacteria is known to cause proteotoxicity. First, the pLJR965 plasmid was transformed into *Mab* and confirmed for successful integration by PCR with primers L5_For and L5_Rev (**Table IV.2**). When analyzing the PCR results, amplifying the WT L5 site of *Mab* is expected to give a fragment of 170 bp while the L5 site together with an integrated plasmid will generate an 8821 bp fragment. Once the integration of the plasmid was confirmed, the strain was

incubated at an OD₆₀₀ of 0.1 with and without the addition of ATc and evaluated every 24h to assess growth. As displayed on **Figure IV.1b**, the transformed strain was confirmed to have an integrated pLJR965 plasmid in the L5 site of *Mab*. However, the transformed strain still contained a fraction of the WT L5 site on top of the L5 site with integrated plasmid, indicating a mixed culture of transformed and untransformed bacteria. Surprisingly, *Mab* containing the pLJR965 plasmid was able to reach a higher plateau phase than WT *Mab* (**Figure IV.1c**). Additionally, no difference is observed between the induced and non-induced transformed strain suggesting that the presence of the induced pLJ965 plasmid is not toxic for *Mab* over a period of 7 days.

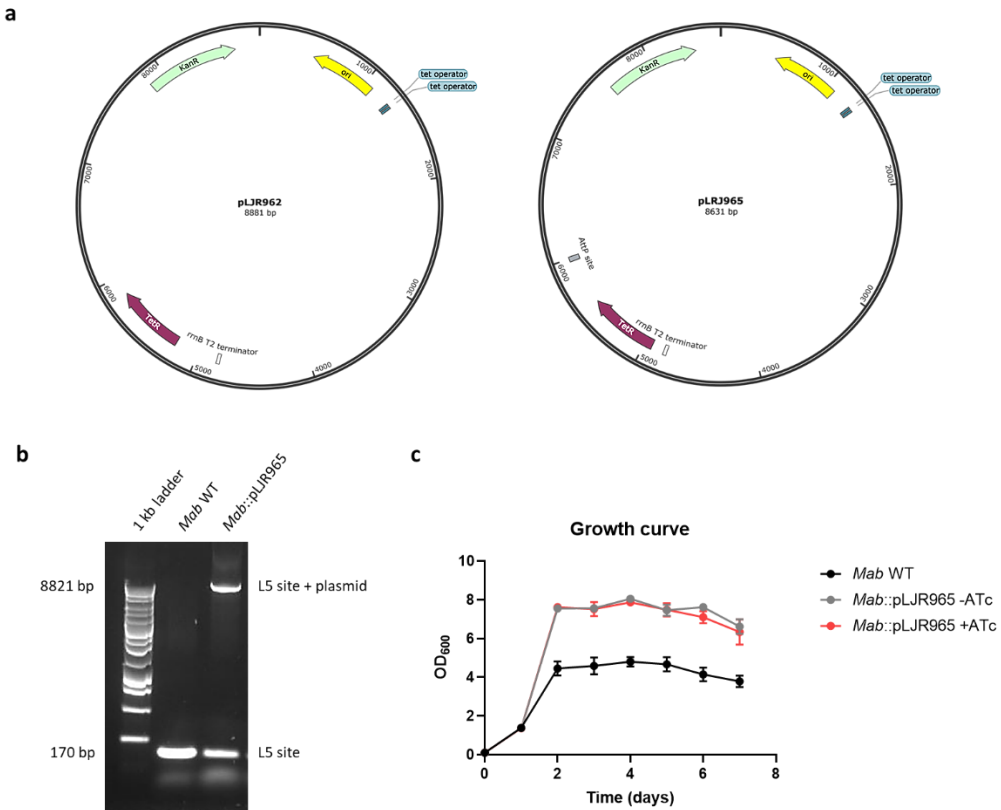


Figure IV.1. The presence of an induced pLJR965 plasmid is not toxic for *Mab*. To first determine what effect the integration of the knockdown plasmids has on the growth of *Mab*, the pLJR965 plasmid was transformed inside *Mab* and confirmed for successful integration in the L5 site with primers L5_For and L5_Rev (**Table IV.2**) by PCR (**b**). Next, the pLJR965-containing strain was diluted

to an OD₆₀₀ of 0.1 and incubated at 37°C in the presence or absence of ATc (c). **a)** Overview of the pLJR962 and pLJR965 CRISPRi integrating plasmids. Created with SnapGene®. **b)** The amplification of the WT L5 site generates a 170 bp fragment while an L5 site with an integrated plasmid is expected to generate a fragment of 8821 bp. The results indicate the presence of both bacteria containing the pLJR965 plasmid and WT bacteria. **c)** Growth was assessed every 24h by measuring the OD₆₀₀. The presence of the induced pLJR965 plasmid does not lead to growth inhibition in *Mab*. Results are shown as mean ± SEM from three independent experiments. KanR: kanamycin-resistant cassette, TetR: tetracycline repressor, ori: origin of replication

*WT bacteria remain present in the transformed culture when targeting the *mmp13* gene*

mmp13 is an essential gene for *Mab* (190), and was therefore selected as a target to confirm the correct use of the *Sth* CRISPRi-system. To achieve this, 8 different dsDNAs were constructed coding for sgRNAs that target *mmp13* and combined with both the pLJR962 and the pLJR965 plasmids. As the pLJR962 plasmid is designed for use in *Msm* and the pLJR965 plasmid for use in *Mtb*, both plasmids were tested to determine which one was more fit for use in *Mab*. Both plasmids with each of the dsDNAs were separately transformed into *Mab* after which correct integration of each plasmid in the L5 site was confirmed by PCR and Sanger sequencing. For both techniques, primers L5_For and L5_Rev (**Table IV.2**) were used. A successful integration of the plasmids is expected to generate a 9051 bp and 8821 bp fragment for the integrated pLJR962 and pLJR965 plasmids respectively, while the WT L5 site only generates a fragment of 170 bp. After PCR, the PCR-generated bands were further analyzed by Sanger sequencing. Sanger sequencing results show a successful integration of the plasmids when the sequence of interest, depicted by a red arrow, aligns to the reference sequence. Perfect alignment is illustrated by a filled, red-colored arrow while an unfilled area indicates a mismatch in the sequence of interest. The PCR results displayed the successful integration of both the pLJR962 and pLJR965 plasmids expressing sgRNA 1 as a fragment of 9051 bp and 8821 bp could be detected (**Figure IV.2a**). However, both strains still demonstrated the presence of a 170 bp fragment

corresponding to the WT L5 site, indicating once again the presence of a mixed culture containing both transformed and untransformed bacteria. Next, the Sanger sequencing results further confirmed successful integration of the plasmids into the L5 site of *Mab* as the sequences extracted from both 9051 bp and 8821 bp fragments aligned perfectly to the reference sequence containing an integrated plasmid into the L5 site (**Figure IV.2b**). Furthermore, these results also confirmed the presence of WT bacteria in both cultures as the DNA extracted from the 170 bp fragment aligned perfectly to the WT L5 reference sequence. **Figure IV.2** displays the PCR and sequencing results of pLJR962 and pLJR965 expressing sgRNA 1 and are representative for all created plasmids expressing *mmp13* sgRNAs.

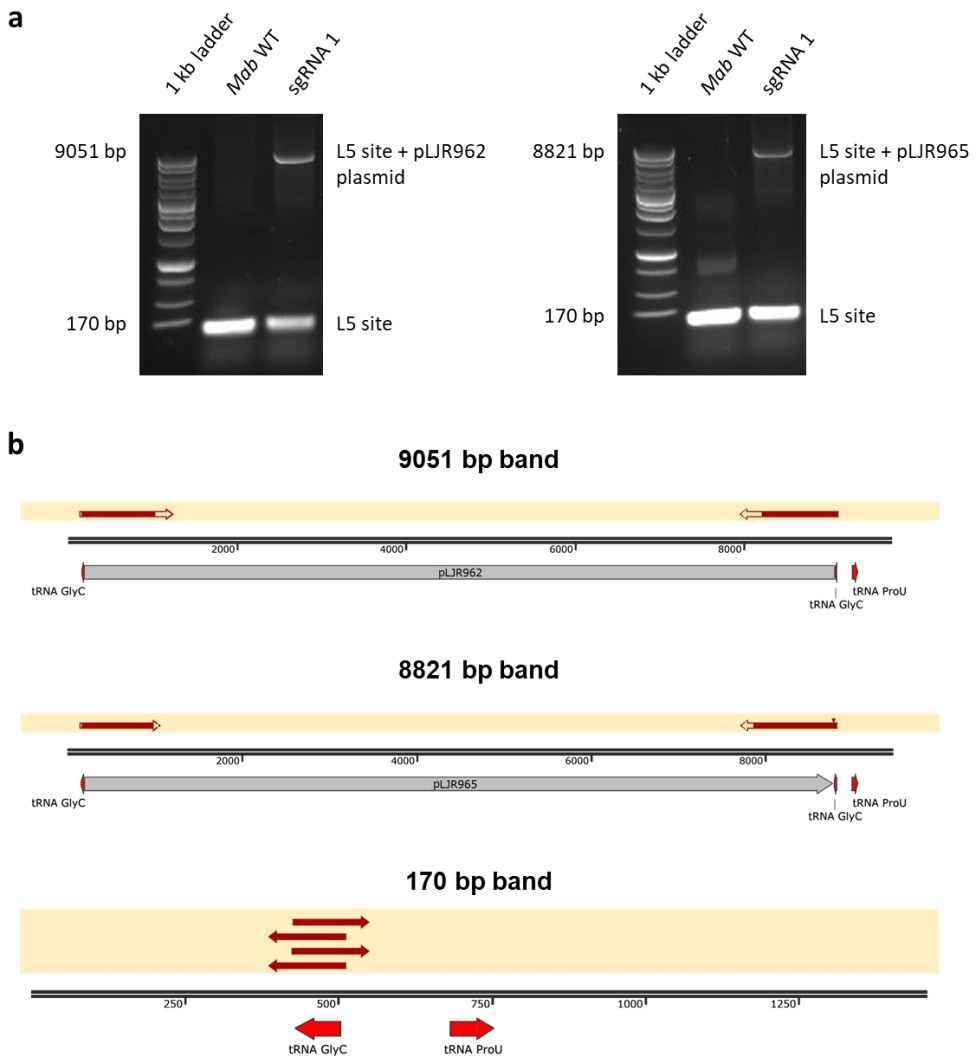


Figure IV.2. Transformed cultures still contain WT bacteria when targeting *mmpI3*. *mmpI3* was selected as a target to evaluate the correct use of the *Sth* CRISPRi-system. While the pLJR962 plasmid was designed for use in *Msm* and the pLJR965 plasmid for use in *Mtb*, both plasmids were implemented to determine which one is better for use in *Mab*. Both plasmids, each expressing one of the 8 different sgRNAs targeting *mmpI3*, were all separately transformed inside *Mab* and assessed by PCR (a) and Sanger sequencing (b) with primers L5_For and L5_Rev (Table IV.2). a) The PCR results are expected to show a 9051 bp and 8821 bp fragment for integration of the pLJR962 and pLJR965 plasmid, respectively, while the WT L5 site is characterized by a 170 bp fragment. Once again, a mixed culture of both bacteria containing the plasmid and WT bacteria was detected. b) The sequenced DNA from the fragments were aligned against a WT L5 site reference sequence or L5 site reference

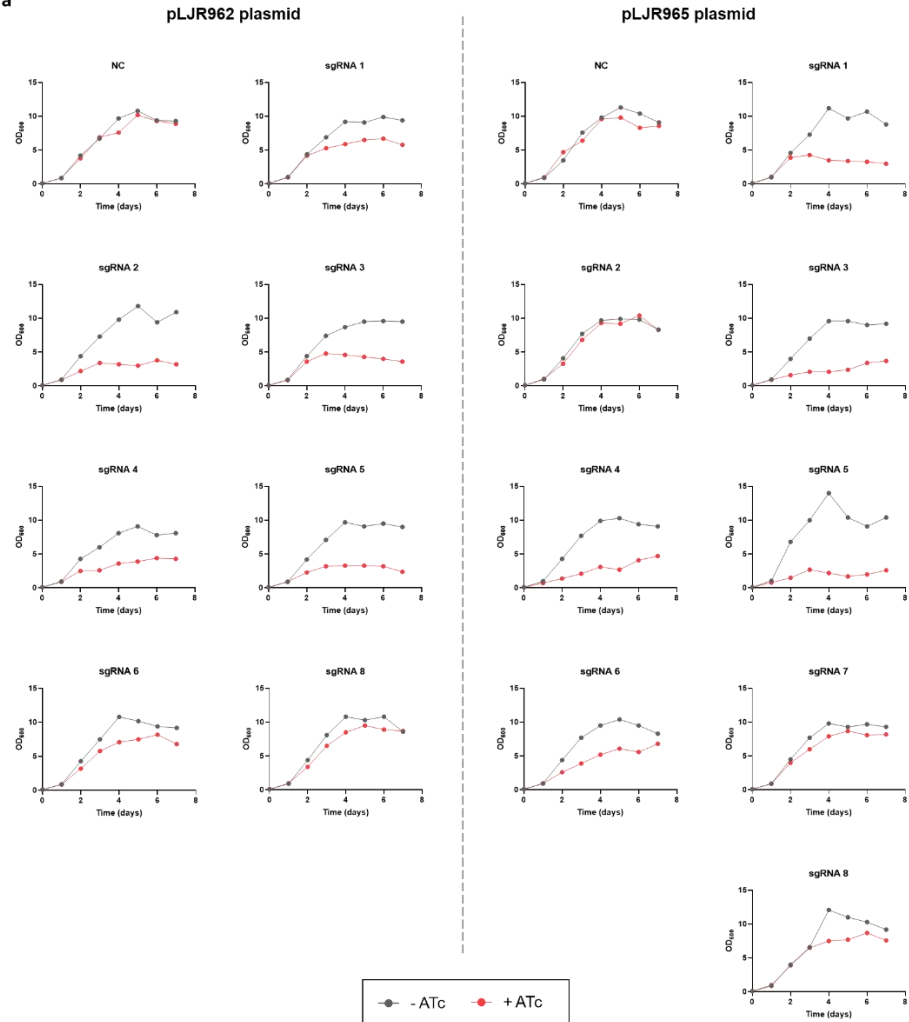
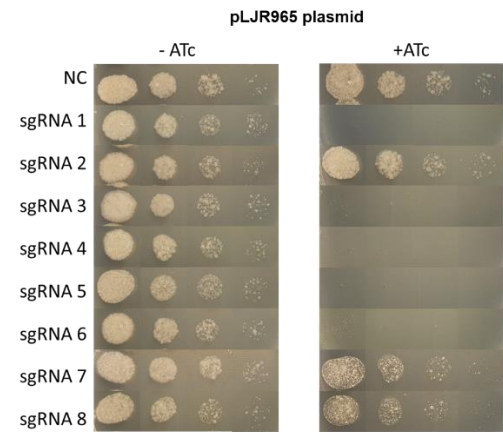
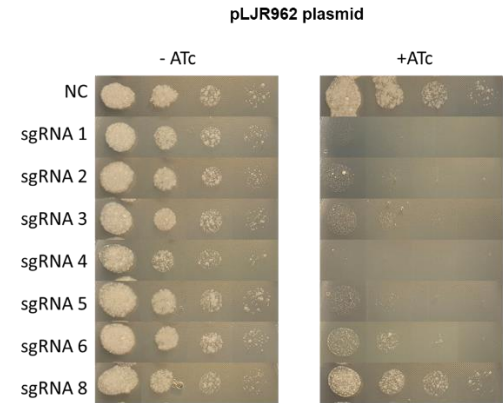
Chapter IV

sequence with an integrated pLJR plasmid. A filled, red-colored arrow indicates perfect alignment of the investigated sequence to the reference sequence while an unfilled area reveals a mismatch. Sanger sequencing results further confirmed the successful integration of both plasmids into the L5 site as well as the presence of the WT L5 site in the cultures. The figures display the PCR and Sanger sequencing results of the pLJR962 and pLJR965 plasmids expressing sgRNA 1 and are representative for all plasmids expressing *mmp13* sgRNAs generated and tested.

The growth effect perceived after induction of the transformed mmp13 strains is dependent of both the sgRNA and the plasmid

To determine which plasmid, pLJR962 or pLJR965, is suitable for use in *Mab* and if the different sgRNAs targeting *mmp13* have a varying effect on the growth of *Mab*, a growth curve was set up to compare all generated strains. The strains were diluted to an OD₆₀₀ of 0.1, incubated with and without the addition of ATc for 7 days and assessed every 24h for growth. In parallel, all strains were spotted on agar plates in the presence or absence of ATc in a ten-fold dilution, starting at an OD₆₀₀ of 0.1, and incubated for 3 days. A strain expressing a control sgRNA with no complementary sequence to the genome of *Mab* was included as a negative control (NC). As illustrated on **Figure IV.3a**, the induction of some plasmids influenced the growth of *Mab* while others did not. Furthermore, induction of sgRNA 2 expression had a varying effect on the growth depending on if it was expressed by pLJR962 or pLJR965. All remaining sgRNAs demonstrated a similar effect, whether it was expressed from the pLJR962 or pLJR965 plasmid. The observations noticed in medium could also be applied to the findings on agar (**Figure IV.3b**). However, growth of *Mab* was inhibited to a greater extent after sgRNA 3, 5 and 6 were expressed from the pLJR965 plasmid. Therefore, the pLJR965 plasmid was selected for further experiments in *Mab*. Furthermore, to significantly confirm the generation of a *mmp13* knockdown strains having a reduced *mmp13* expression and leading to a reduction in growth, *Mab* containing the pLJR965 expressing three different sgRNAs, NC, sgRNA 5 and sgRNA 8, was selected for the next experiment.

Page 110: Figure IV.3. Growth deficiency after induction of the transformed *mmp13* strains is dependent on the sgRNA and the plasmid from which it is expressed. Growth of *Mab* was compared between all created *mmp13* strains containing the pLJR962 or pLJR965 plasmid expressing the different sgRNAs. **a)** All strains were diluted to an OD₆₀₀ of 0.1, incubated for 7 days with or without ATc and evaluated based on growth every 24h. Induction of the transformed strains led to a difference in growth depending on which plasmid with sgRNA the strains possessed. **b)** In parallel, the diluted strains were also spotted in a ten-fold dilution on agar plates, with half of the plates supplemented with ATc, and incubated for 3 days. Results on agar illustrate the same results as in medium. This experiment was conducted as a preliminary experiment and was only performed once.

a**b**

Transformed mmpl3 strains lose the pLJR965 plasmid over time

To confirm successful creation of a *mmpl3* knockdown strain with lower *mmpl3* expression that lead to a decreased growth, *Mab* containing the pLJR965 plasmid expressing sgRNA NC, 5 or 8 was first grown until reaching its logarithmic phase and brought to an OD₆₀₀ of 0.1. Then, the strains were incubated with or without ATc and at the same time spotted on agar supplemented with or without ATc in a ten-fold dilution. The broth cultures and agar plates were both incubated for 3 days after which the extent of growth of the strains was determined. As observed on **Figure IV.4**, the bacterial growth of the transformed strain expressing sgRNA 5 was significantly reduced after induction while no difference was detected between the induced and non-induced strains expressing the sgRNA NC and 8. This reduced growing ability of the strains expressing sgRNA 5 was also observed on agar after induction. Remarkably, while growth of the strain expressing sgRNA 8 was not altered after induction in liquid medium, its growth was greatly reduced after induction on agar.

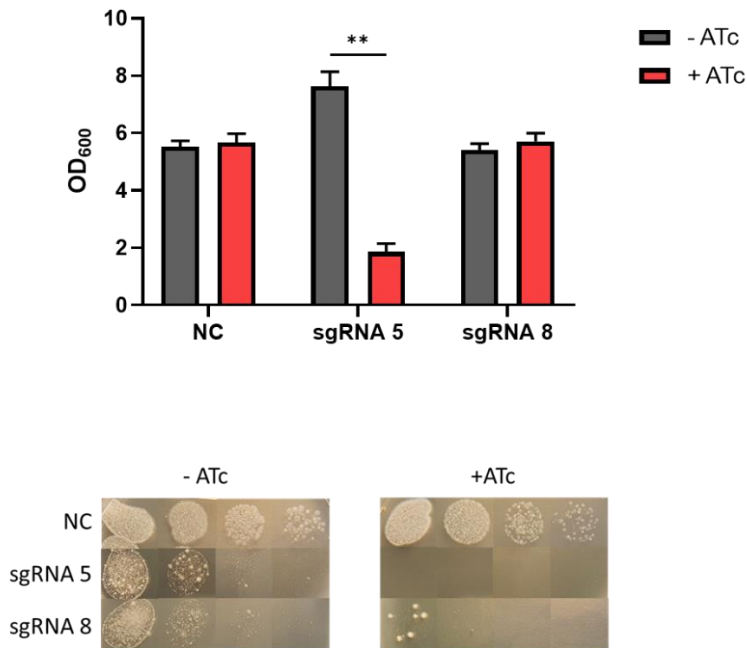


Figure IV.4. *Mab* strain expressing *mmp13* sgRNA 5 demonstrates a decreased growth. The transformed strains containing the pLJR965 plasmid expressing sgRNA NC, 5 and 8 were grown until reaching their logarithmic phase and incubated at an OD₆₀₀ of 0.1 with or without ATc for 3 days. In parallel, the strains were also spotted on an agar plate with or without ATc in a ten-fold dilution, starting from an OD₆₀₀ of 0.1. Bacterial growth of the transformed strain containing the pLJR965 plasmid expressing sgRNA 5 was significantly reduced in both liquid medium and agar after induction. Results are shown as mean \pm SEM from six independent experiments with the agar images being a representative of six independent repeats. Statistical significance was obtained with the Mann-Whitney test after which the p-values were corrected for multiple testing. **p < 0.01

After confirming that the induction of the strain containing the pLJR965 plasmid expressing sgRNA 5 leads to a significant growth impairment of *Mab*, the expression of *mmp13* was examined in the selected strains using RT-qPCR. The expression of *mmp13* was evaluated relative to that of the housekeeping gene, *rpoB*. Surprisingly, the obtained results demonstrated no change in *mmp13* expression after induction of the transformed strains (**Figure IV.5a**). Because the RT-qPCR was performed after the strains were subjected to multiple division cycles, the PCR

amplifying the L5 site using the L5 primers (**Table IV.2**) and the growth curve were repeated to ensure that the strains still contained the integrated plasmid and demonstrated the desired growth effect. This time, the strains were incubated starting from an OD₆₀₀ of 0.05. However, the results established that the selected transformed strains lost the pLJR965 plasmid and corresponding growth effect at the time that the RT-qPCR was performed (**Figure IV.5b**). Conclusively, the integration of the pLJR965 plasmids seems unstable and the plasmid is lost over time.

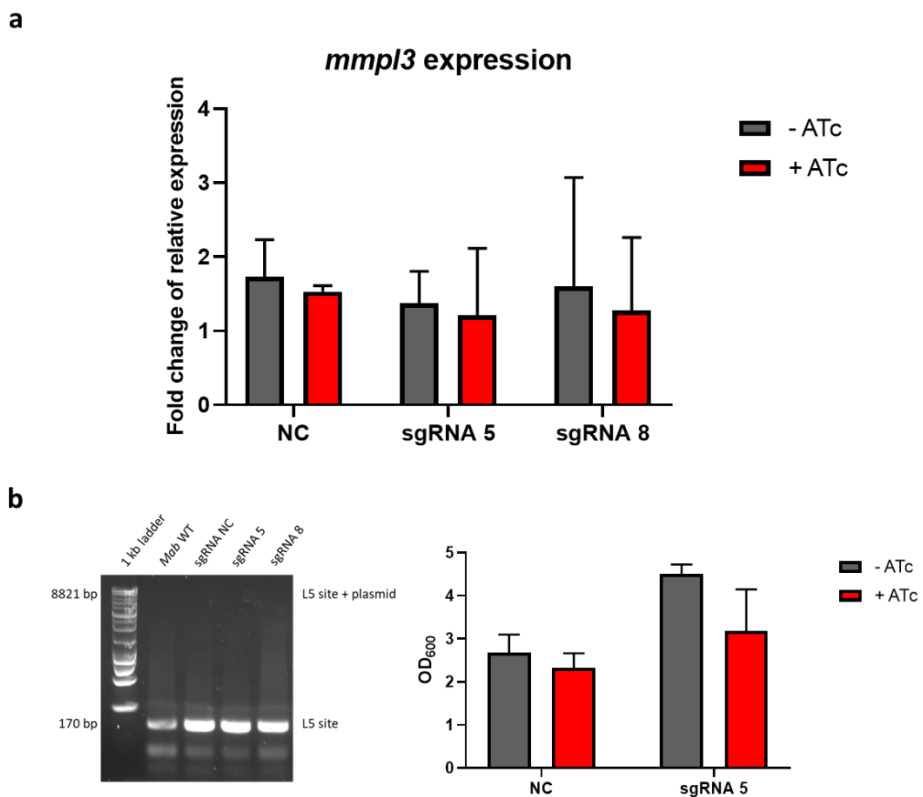


Figure IV.5. pLJR965 is lost over time in the transformed *mmp13* strains. **a)** RNA was extracted from the different induced and non-induced strains after which the expression of *mmp13* was investigated relative to *rpoB*. No difference in *mmp13* expression was observed in the strains after being induced. **b)** After establishing the *mmp13* expression levels in the strains, the PCR, amplifying the L5 site using the L5 primer (**Table IV.2**), and the growth curve, starting from an OD₆₀₀ of 0.05 and incubated for 3 days, were repeated to ensure that the plasmid and its activity was not lost after multiple division cycles. However, the integration of the pLJR965 plasmid seems unstable since the

Chapter IV

plasmid and its activity is lost after several division cycles. Growth curve results of the strain containing the pLJR965 plasmid expressing sgRNA 8 are not included. Results are shown as mean \pm SEM from two independent experiments.

mtr and *mshC* knockdown plasmids were successfully incorporated into the L5 site of *Mab*

Even though the integration of the pLJR965 seems unstable, the *Sth* CRISPRi-system was used to target *mtr* and *mshC* next. Here, a total of 10 dsDNAs coding for the sgRNAs were constructed for either *mtr* or *mshC* and transformed into *Mab* on the pLJR965 plasmid. After transformation, integration of the pLJR965 plasmids with the different dsDNAs was assessed by PCR and Sanger sequencing with primers L5_For and L5_Rev (**Table IV.2**). A PCR reaction using these primers is predicted to generate a fragment of 8821 bp when the pLJR965 plasmid is integrated into the L5 site while a 170 bp fragment is generated for the WT L5 site only. Next, the fragments generated by the PCR reaction were further analyzed by Sanger sequencing in which the sequences of interest were compared to a reference sequence. Here, a perfect alignment is depicted by a filled, red-colored arrow while a mismatch is demonstrated by an unfilled area. The results showed that the different pLJR965 plasmids were successfully integrated in the L5 site of *Mab* as a band of 8821 bp was generated during the PCR reaction (**Figure IV.6a**). Similarly to the transformed *mmp13* strains, the WT L5 site was still present in the transformed *mtr* and *mshC* strains as well, suggesting the presence of a mixed culture every time the pLJR965 plasmid is transformed into *Mab*. Successful integration of the plasmids was further confirmed by the sequencing results which demonstrated that the sequences of the 8821 bp fragment completely aligned with the reference sequence (**Figure IV.6b**). The figures display the PCR and sequencing results of pLJR965 expressing the *mtr* or *mshC* sgRNA 1 and are representative for all plasmids expressing *mtr* and *mshC* sgRNAs generated and tested in *Mab*.

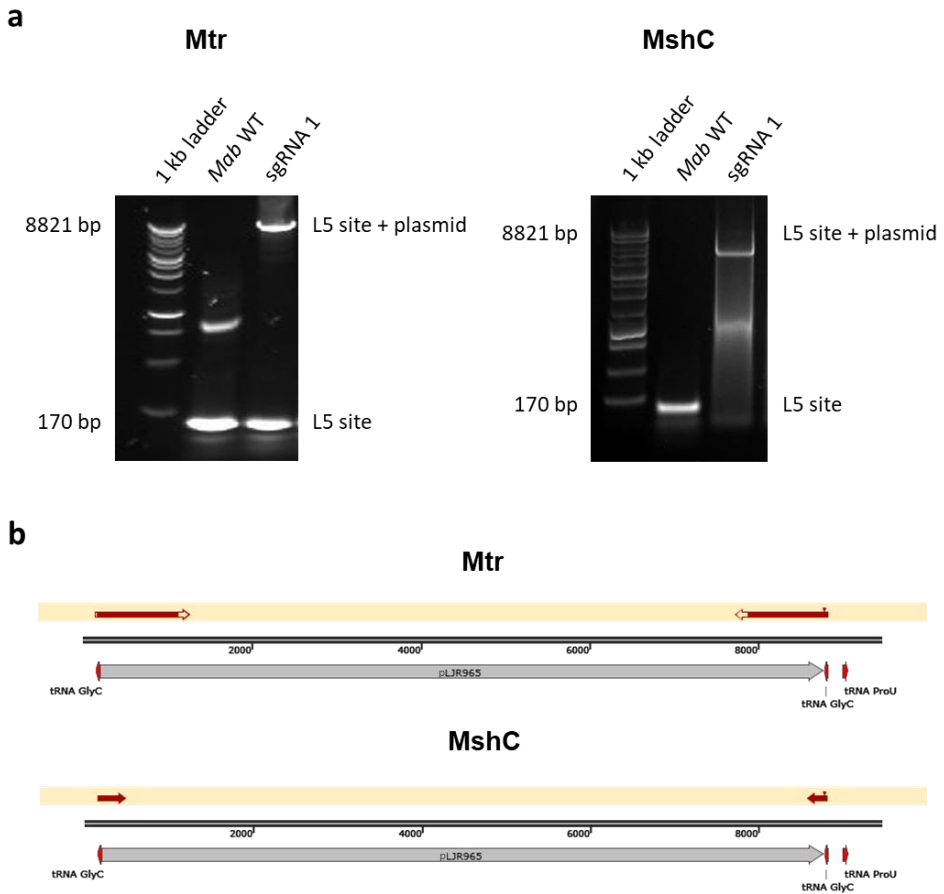


Figure IV.6. Plasmids needed to create *mtr* and *mshC* knockdowns were successfully integrated into the L5 site. To create *mtr* and *mshC* knockdown strains, 10 dsDNAs coding for the sgRNAs were constructed targeting each gene. The dsDNAs were transformed into *Mab* by first cloning them into the pLJR965 plasmid. After transformation, integration of the plasmid into the L5 site was investigated by PCR and Sanger sequencing with the use of the L5_For and L5_Rev primers (Table IV.2). **a)** The PCR results are expected to generate a fragment of 8821 bp if the pLJR965 plasmid is integrated into the L5 site of *Mab* while a fragment of 170 bp is expected for the WT L5 site. All pLJR965 plasmids expressing the different sgRNAs were integrated into the L5 site of *Mab*, however, the WT L5 site was still detected as well. **b)** The fragments were analyzed by Sanger sequencing. Here, the sequence of interest is being aligned to a reference sequence where a perfect alignment is illustrated by a filled, red-colored arrow and a mismatch by an unfilled area. Successful integration of the pLJR965 plasmids into the L5 site of *Mab* was further confirmed by Sanger sequencing. The figures display the PCR and Sanger sequencing results of the pLJR965 plasmids expressing *mtr* and *mshC* sgRNA 1 and are representative for all plasmids expressing *mtr* and *mshC* sgRNAs generated and tested in *Mab*.

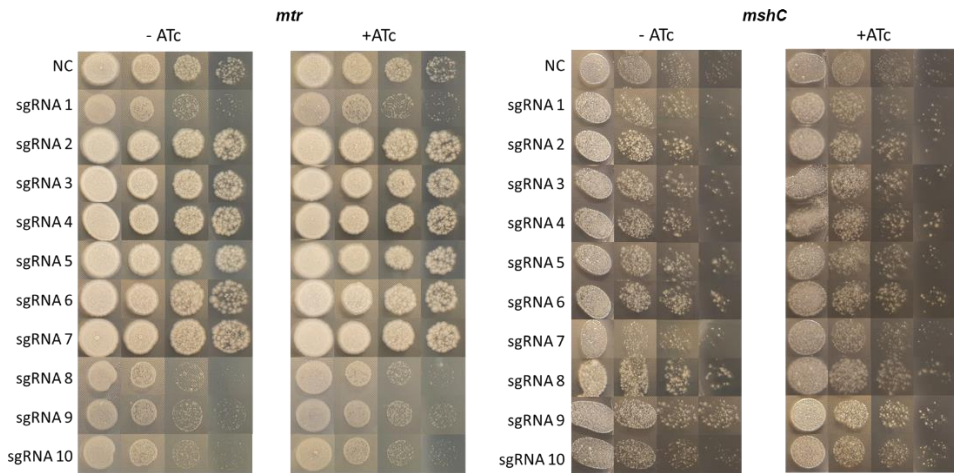
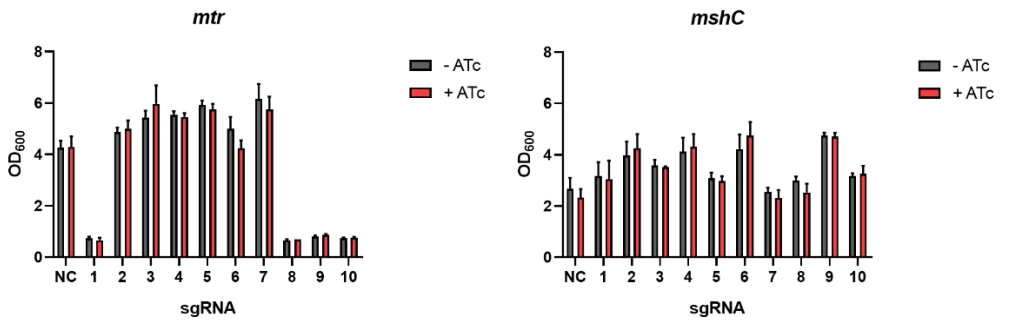
*Induction of the transformed *mtr* and *mshC* strains does not lead to an altered growth*

To examine whether targeting *mtr* or *mshC* using the *Sth* CRISPRi-system will translate into an altered phenotypic character, all the transformed *mtr* and *mshC* strains were brought to an OD₆₀₀ of 0.1 or 0.05 respectively, and incubated with or without ATc for 3 days before the growth was assessed based on the OD₆₀₀. In parallel, once all strains were brought back to an OD₆₀₀ of 0.1 or 0.05, they were spotted in a ten-fold dilution on agar with or without ATc and incubated for 3 days as well. Additionally, the PCR amplifying the L5 site using the L5 primers (**Table IV.2**) was repeated to determine whether the pLJR965 integration remained stable in the generated strains. Remarkably, no difference was seen in bacterial growth between the induced and non-induced transformed strains after 3 days (**Figure IV.7a**). Additionally, the spots on agar did not show any variation in growth either between the induced and non-induced strains. Similarly to the transformed *mmpI3* strains, some of the transformed *mtr* and *mshC* strains lost the pLJR965 plasmid after several division cycles (**Figure IV.7b**). This event makes it difficult to investigate the gene expression of the transformed strains and further confirms the instability of the pLJR965 integration, rendering this system unreliable.

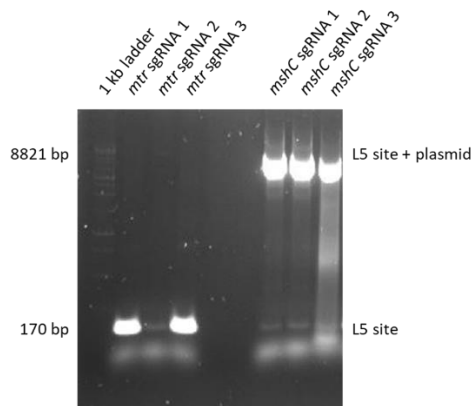
Page 117: Figure IV.7. Bacterial growth is unaltered after inducing the transformed *mtr* and *mshC* strains. a) All generated *mtr* and *mshC* strains were diluted to an OD₆₀₀ of 0.1 and 0.05 respectively, and incubated with or without ATc for 3 days before growth was assessed by the OD₆₀₀. At the same time, the diluted strains were spotted in a one-over-ten dilution on agar with or without ATc. No change was observed in bacterial growth between the induced and non-induced strains. **b)** A PCR amplifying the L5 site by using the L5 primers (**Table IV.2**) was performed to investigate whether the pLJR965 plasmid was still present in the generated strains after several division cycles. It was established that some of the generated *mtr* and *mshC* strains already lost the pLJR965 plasmid after several division cycles. Results are shown as mean ± SEM from three independent experiments for the generated *mtr* strains and two independent experiments for the generated *mshC* strains.

Implementing the CRISPRi-system

a



b



IV.5 Discussion

Almost all antibiotic targets are made up from essential bacterial genes (191). Thus, to examine Mtr and MshC as potential drug targets, their essentiality during growth and function in the survival of *Mab* need to be explored. Over the past years, CRISPRi has been extensively used to investigate essential genes since knocking out these genes is lethal for pathogens. Therefore, by using this technique to create knockdowns, the role and function of the genes can be thoroughly investigated during bacterial growth and stress conditions (147, 192). In this chapter, the *Sth* CRISPRi-system was implemented in *Mab* where a series of 28 sgRNAs were generated targeting *mmpl3*, *mtr* or *mshC*. Our findings illustrated the successful integration of all generated CRISPRi plasmids in the L5 integration site of the transformed strains (**Figure IV.1b, 2 and 6**). Furthermore, we demonstrated that the induction of the CRISPRi plasmids only affected the growth of some transformed *mmpl3* strains, while no change in growth was observed between the induced and non-induced transformed *mtr* or *mshC* strains (**Figure IV.3, 4 and 7a**). However, next to an integrated pLJR plasmid in all transformed strains, the obtained results also displayed the presence of the WT L5 site in the strains (**Figure IV.1b, 2 and 6a**). In 2009, Beatrice Saviola demonstrated that while mycobacterial plasmids containing the *attP* L5 attachment site are capable of integrating into the *attB* L5 site of the mycobacterial genome, these plasmids are unstably integrated and constantly found in an equilibrium between inserted and excised stage (193). Hence, a mixed culture of WT *Mab* and *Mab* containing the CRISPRi plasmids is continually existing within the cultures, possibly interfering with the capacity of knocking down the genes of interest and the results during experiments. This event may be caused by the presence of both the *attP* L5 attachment site and the L5 integrase on the pLJR plasmid. An approach for stabilizing the integrated plasmid has been the electroporation of two separate plasmids, i.e. an *attP*-containing integration plasmid and a nonreplicating Int-containing plasmid, since the nonreplicating Int-containing plasmid provides integrase activity which is lost over time, hereby stabilizing the integrated vector.

Another approach has been the removal of the *int* gene from the genome via the expression of site-specific recombinases after integration of the pLJR plasmid in the L5 site (133).

Beside the observation of both the WT and modified L5 site still being present in the transformed strains, we noticed that in some transformed strains the unstable integrated plasmid was also completely removed from the genome of *Mab* over time (**Figure IV.5b and 7b**). Springer et al. observed that excision of the integrated plasmid is mediated by the integrase and occurs more frequently than anticipated, but can be avoided by utilizing a second nonreplicating Int-containing plasmid (194). Furthermore, integrase-mediated excision of the L5 integrated plasmid can lead to plasmid loss in cases where the integrated plasmid is disadvantageous for the growth of the recombinant strain (195), indicating that the pLJR965 plasmid may be toxic for *Mab* over a longer period of time. Nevertheless, any loss of the integrated plasmid was not reported when applying the *Sth* CRISPRi-system on either *Msm*, *Mtb* or *Mab* (146, 148, 196, 197), yet Bosch et al. described the use of a suicide plasmid to express Int in order to enhance the stability of the L5 integration during long-term studies (191). It is unclear whether excision of the integrated plasmid occurs more frequently in *Mab* than in *Msm* or *Mtb*, we waited too long in between experiments leading to the loss of the unstable plasmid over time, or if we were unable to correctly translate the *Sth* CRISPRi-system for use in *Mab*. Yet, the instability of the integrated plasmid renders this system unreliable for our investigation.

As a conclusion, this chapter implemented the *Sth* CRISPRi-system to target *mtr* or *mshC* and investigate their essentiality for *Mab*. The results demonstrate the successful integration of the CRISPRi plasmids in the L5 site of *Mab*, but the induction of the integrated plasmids did not lead to an altered growth pattern of the strains. However, the plasmids proved to be unstably integrated in the L5 site since the plasmids were found in a constant equilibrium between inserted and excised stage. Furthermore, the integrated plasmid in some transformed strains was even completely lost after several division cycles. Due to the instability of the

Chapter IV

pLJR965 integration, the *Sth* CRISPRi-system is not reliable to investigate the essentiality of *mtr* and *mshC* in *Mab*. Therefore, other methodologies need to be explored.

CHAPTER V

Validating the p2NIL/pGOAL method in
Mycobacterium smegmatis



These data have not yet been published.

Author contributions:

Tatiana Piller¹: conceptualization, methodology, investigation and formal analysis.

Linda De Vooght¹: conceptualization, methodology, investigation of the *mtr* knockout strain in *Msm*, formal analysis and supervision.

Davie Cappoen¹: conceptualization and supervision.

Paul Cos¹: conceptualization and supervision.

¹Laboratory of Microbiology, Parasitology and Hygiene (LMPH), University of Antwerp, Belgium

V. Validating the p2NIL/pGOAL method in *Mycobacterium smegmatis*

V.1 Abstract

The creation of genetic mutants is essential to understand more about gene function and to validate a potential drug target. While genetic manipulations are challenging in mycobacteria, *Msm* can be used as a valuable alternative model for the development and validation of genetic tools. Over the past decades, various new genetic engineering tools have been developed to facilitate studying genes, including the p2NIL/pGOAL method. In this study, *Msm* was used as a model to validate the p2NIL/pGOAL method by aiming at creating *mtr* and *mshC* knockout strains. While this method was successfully implemented to create a *Msm* Δ *mtr* mutant strain, it remains a very lengthy and complicated method for use in *Msm*. Due to the remaining challenges of the p2NIL/pGOAL method in *Msm* and the fact that *Msm* is already more easily manipulatable than *Mab*, another recently developed method was suggested instead of the p2NIL/pGOAL method for the creation of *mtr* and *mshC* knockout strains in *Mab*, i.e. the ORBIT system.

V.2 Introduction

Genetic analysis and the creation of genetic mutants is essential to understand more about mycobacterial infection, individual gene function and validation of a drug target (120, 198). While *in silico* tools can help determine the importance and function of a certain gene, experimental validation with genetic manipulations is necessary (116). Genetic manipulation of mycobacteria is challenging due to the thick mycobacterial cell wall, slow growing nature of mycobacteria, high frequency of nonhomologous recombination and highly resistant character of mycobacteria, limiting the availability of antibiotic selection markers (120). Due to the many challenges concerning genetic engineering in mycobacteria, various studies use *Msm* as a valuable model for genetic tool development and validation in

mycobacterial studies, since *Msm* is easily modified and closely associated to other mycobacterial species in regard to its biochemical properties and genetic information (199–202).

Over the past decades, a variety of novel genetic engineering tools have been developed, hereby facilitating the study of genes (116). An interesting method that was developed in the early 2000s is the p2NIL/pGOAL system that combines the use of two vectors, p2NIL and pGOAL. Hereby, the p2NIL suicide plasmid is used for the actual genetic manipulation after the insertion of a disrupted copy of the gene of interest together with the marker genes originating from the pGOAL plasmid (154). The p2NIL/pGOAL system employs a two-step strategy in which the disrupted copy of a gene of interest is incorporated into the genome of mycobacteria during a SCO event, followed by the elimination of the WT or disrupted copy of the gene in a DCO event (154, 198). Elimination of the WT gene during the DCO event leads to the creation of marked or unmarked knockout mutants while persistent elimination of the disrupted copy can provide some indirect insight into the essentiality of a gene (120, 154). The p2NIL/pGOAL method is widely used in mycobacteria and has been successfully employed in *Msm* for various allelic replacement procedures (203–205).

In this chapter, *Msm* was used as an alternative model to evaluate and validate the p2NIL/pGOAL method before implementing it in *Mab*. Hereby, this chapter aims at determining the correct use and efficiency of this method by creating *mtr* and *mshC* knockout strains in *Msm*. By applying the p2NIL/pGOAL method, a *Msm* Δ *mtr* mutant was successfully generated while any attempts to create a *Msm* Δ *mshC* mutant were unsuccessful. However, even though *Msm* is more easily genetically manipulatable than *Mab* or other mycobacteria, creating mutants following this method remains a very lengthy and complex process in *Msm*. Therefore, another more recently discovered method which is less complex, i.e. the ORBIT system (**Chapter VI**), was suggested for the generation of *mtr* and *mshC* knockout strains in *Mab*.

V.3 Materials and methods

Bacterial strains, media and culture conditions

Escherichia coli (*E. coli*) DH5 α cultures were grown in Luria-Bertani (LB) broth (Sigma-Aldrich) or plated on LB agar (Sigma-Aldrich) supplemented with 0.2% glycerol and the corresponding selection drug.

All mycobacterial strains in this study were derived from *M. smegmatis* mc² 155 (ATCC 700084) and were routinely cultured at 37°C in Middlebrook 7H9 broth (Sigma) supplemented with 10% ADS (albumin-dextrose-saline), 0.2% glycerol and 0.05% tyloxapol. Agar plates were made of Middlebrook 7H11 agar base (Sigma).

Construction of a p2NIL suicide vector

A p2NIL suicide plasmid was generated carrying the mutant gene of interest as described by Krishnamoorthy Gopinath et al (119). Both the p2NIL_*mtr* and p2NIL_*mshC* suicide plasmids were created following a slightly different approach. To create p2NIL_*mtr*, three individual fragments were amplified by PCR; part of the sequences of *mtr* (MSMEG_RS12670) and the gene before *mtr* (MSMEG_RS12675; F1), part of the sequences of *mtr* (MSMEG_RS12670) and the gene after *mtr* (MSMEG_RS12665; F2), and a hygromycin-resistant cassette (HygR) that was amplified from a pSMT3-M plasmid (Addgene 26589). The PCR mixture (50 μ L) consisted of 25 μ L of Q5[®] High-Fidelity 2X Master Mix (NEB), 2.5 μ L of each primer (**Table V.1**), 1 μ L of the lysed bacteria and 19 μ L Milli-Q. PCR amplification was characterized by a denaturation step (98°C for 30 sec), 35 amplification cycles (98°C for 5 sec; 72°C for 20 sec; 72°C for 27.5 sec) and an extension step (72°C for 5 min). The three fragments were assembled and cloned into the digested p2NIL plasmid (Addgene 20188), with HindIII and SalI restriction enzymes, by NEBuilder[®] Hifi DNA assembly to create p2NIL_*mtr*.

To create p2NIL_*mshC*, the sequences of *mshC* (MSMEG_RS20270), the gene before *mshC* (MSMEG_RS20275) and the gene after *mshC* (MSMEG_RS20265) were amplified from the genome of *Msm* by PCR amplification (denaturation step: 98°C for 30 sec; 35 amplification cycles: 98°C for 5 sec; 72°C for 20 sec; 72°C for 35 sec; extension step: 72°C for 2 min) of a PCR mixture (50 µL) consisting of 25 µL of Q5® High-Fidelity 2X Master Mix (NEB), 2.5 µL of each primer (**Table V.1**), 1 µL of the lysed bacteria and 19 µL Milli-Q. Then, the amplified sequence was cloned into the p2NIL plasmid (Addgene 20188), which was first digested with HindIII and Sall, by NEBuilder® Hifi DNA assembly to create p2NIL_*mshC*. To generate a mutant gene on the plasmids, p2NIL_*mshC* was digested once again with BbsI and ligated with HygR that was amplified from a pSMT3-M plasmid (Addgene 26589) using specific primers (**Table V.1**).

Finally, the marker genes, *lacZ* and *sacB*, originating from the pGOAL17 plasmid (Addgene 20189) were cloned into the p2NIL plasmids by digesting both plasmids with PacI followed by ligation. Digestions were performed for 2h at 37°C and NEBuilder® Hifi DNA assemblies for 15 min at 50°C with help of the Hifi master mix (NEBuilder®). An overview of the method used to create the p2NIL plasmids is demonstrated in **Figure V.1**.

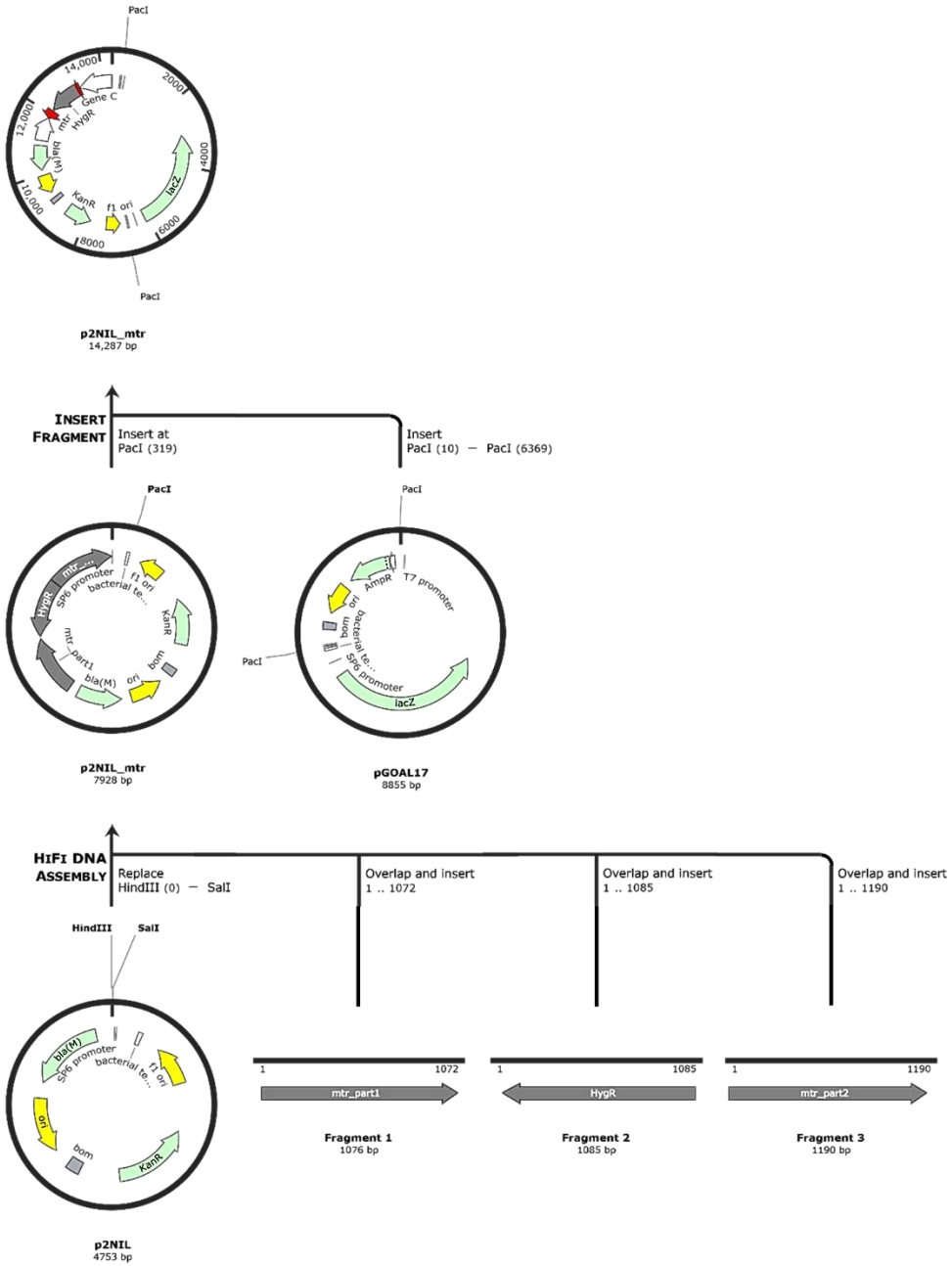
Table V.1. Overview of primers used to create a p2NIL suicide plasmid carrying a mutant *mtr* or *mshC* from *Msm*.

Name	Sequence*	Description
MtrF1_Msm_For	ACTGCGTTAGCAATTTAACTG TGATAAACTACCGCATTAAT GACCGACACGGCGAT	Forward primer used to amplify part of the <i>mtr</i> gene and <i>MSMEG_RS12675</i> from <i>Msm</i> .
MtrF1_Msm_Rev	caccgccccggcgcctgacCCAGAA CTACGGCGACACCGCTTACGGC	Reverse primer used to amplify part of the <i>mtr</i> gene and <i>MSMEG_RS12675</i> from <i>Msm</i> .
MtrF2_Msm_For	cagggattctgtgtcacagGCTCGCA GATCGCGAC	Forward primer used to amplify part of the <i>mtr</i> gene and <i>MSMEG_RS12665</i> from <i>Msm</i> .
MtrF2_Msm_Rev	ACATACGATTTAGGTGACACT ATAGAATACATAGGATCCGGT GACGTCACGGGAACCC	Reverse primer used to amplify part of the <i>mtr</i> gene and <i>MSMEG_RS12665</i> from <i>Msm</i> .
Hygro_Mtr_For	CGGTGTCGCGGTAGTTCTGGgt caggcgccgggggc	Forward primer used to amplify HygR from the PSMT3-M plasmid for cloning into <i>mtr</i> .
Hygro_Mtr_Rev	GAAGGTCGCGATCTGCGAGCct gtgacacaagaatccctgttactct	Reverse primer used to amplify HygR from the PSMT3-M plasmid for cloning into <i>mtr</i> .
MshC_Msm_For	ACTGCGTTAGCAATTTAACTG TGATAAACTACCGCATTAATC ACCGCTTCTCGATCGACT	Forward primer used to amplify the <i>mshC</i> , <i>MSMEG_RS20275</i> and <i>MSMEG_RS20265</i> genes from <i>Msm</i> .
MshC_Msm_Rev	ACATACGATTTAGGTGACACT ATAGAATACATAGGATCCGGT GACATCGACCGATGCCG	Reverse primer used to amplify the <i>mshC</i> , <i>MSMEG_RS20275</i> and <i>MSMEG_RS20265</i> genes from <i>Msm</i> .
Hygro_MshC_For	CCGAACGGCGAAGGCCAGCTG GGCTCGCCAGGACGCTCGGccg ggcgctcaggcgccggg	Forward primer used to amplify HygR from the PSMT3-M plasmid for cloning into p2NIL_ <i>mshC</i> .
Hygro_MshC_Rev	CCGCCGGGCAAGTCCGATCAA CTCGACGCGTTGCTGTGGgtgac acaagaatccctgttactct	Reverse primer used to amplify HygR from the PSMT3-M plasmid for cloning into p2NIL_ <i>mshC</i> .

*Upper case letters in the sequences refer to sequences originating from the bacterial genome while lower case letters refer to sequences originating from a plasmid.

Chapter V

a



b

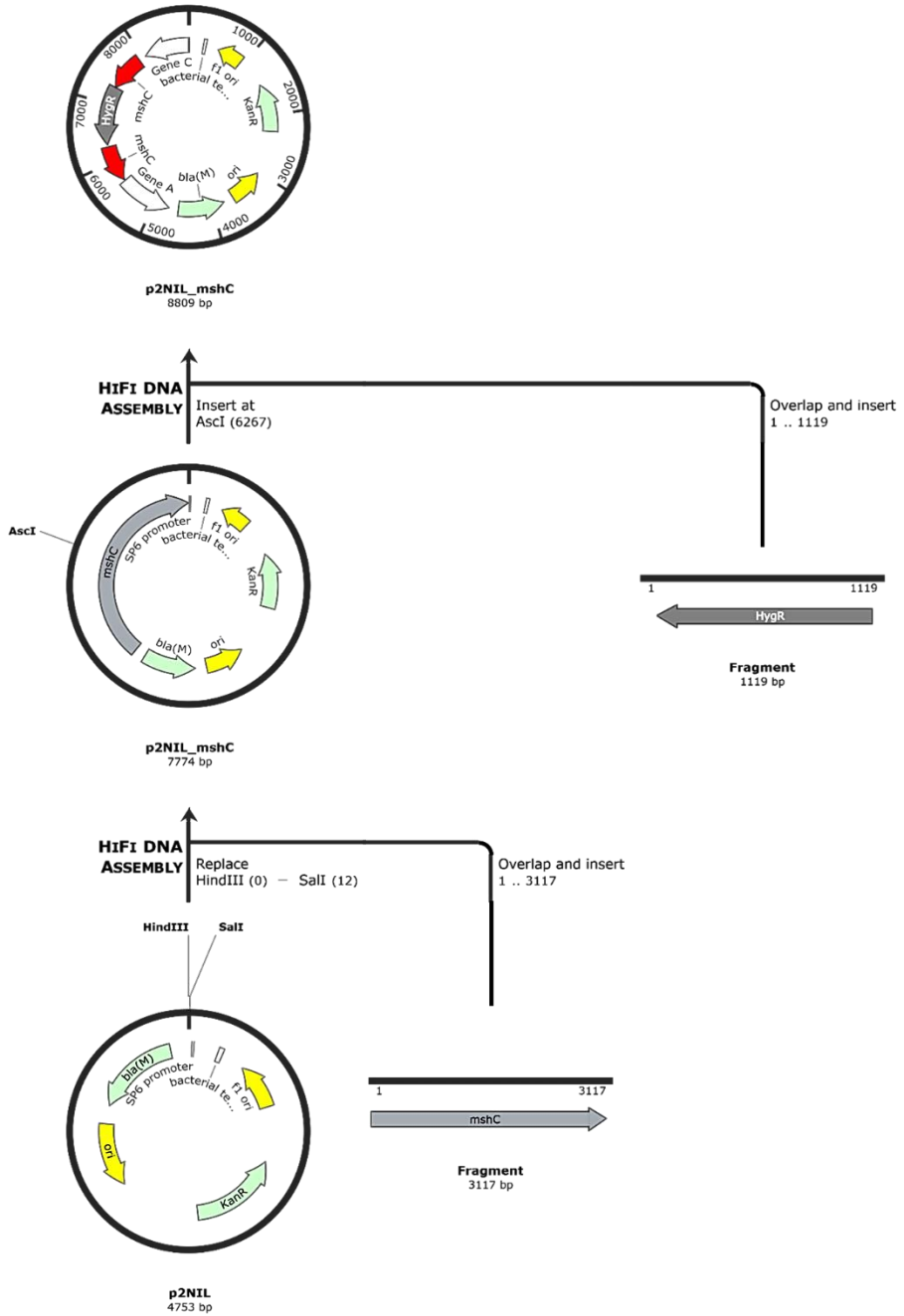


Figure V.1. Overview of the methodology used to create the p2NIL suicide plasmids. Generation of p2NIL_mtr (a) and p2NIL_mshC (b). Created with SnapGene®.

Construction of MsmΔmtr and MsmΔmshC mutants using the p2NIL/pGOAL system

MsmΔmtr and *MsmΔmshC* mutants were constructed in a two-step strategy using the p2NIL/pGOAL system as described by Krishnamoorthy Gopinath et al. (119). During the first step, *Msm* was allowed to grow in a shaking incubator (New Brunswick Scientific; 175 rpm) in 7H9 supplemented with 10% OADC (oleic acid-albumin-catalase-dextrose; Thermo Fisher Scientific) and 0.2% glycerol at 37°C until reaching an optical density at 600 nm (OD₆₀₀) between 0.2 and 0.8 and was made electrocompetent by washing three times with 10% glycerol. Then, 1 µg of the generated p2NIL plasmid carrying the mutant gene of interest (p2NIL_*mtr* or p2NIL_*mshC*) was transformed into the electrocompetent bacteria by using the Gene Pulser Xcell Total System (Bio-Rad; 2.5 kV, 1000 Ω and 25 µF) and 0.2 mm cuvettes (Bio-Rad Laboratories). Following electroporation, *Msm* was resuspended in 7H9 medium containing 20% OADC and incubated at 37°C for 4h before it was plated out on 7H11 agar containing 10% OADC, 0.2% glycerol, 50 µg/mL kanamycin (Sigma), 50 µg/mL hygromycin (Sigma) and 60 µg/ml X-gal (Thermo Fisher Scientific) for selection of SCO recombinants. The 7H11 agar plates were incubated at 37°C until the presence of colonies. Blue colonies resistant to kanamycin and hygromycin were labeled as possible SCO recombinants and were selected for the second step after confirmation. To confirm incorporation of the p2NIL plasmid carrying the mutant gene of interest into the genome of *Msm* and determining whether the incorporation happened before or after the WT gene of interest, PCR was performed using primer sets 1 and 2. Next, Sanger sequencing (Neuromics Support Facility; University of Antwerp) was performed using the reverse primer of primer set 1 and the forward primer of primer set 2 for the *mtr* SCO recombinant and primers that anneal in the middle of *mshC* for the *mshC* SCO recombinant (**Table V.2**).

The second step included allowing the formation of DCO recombinants. Here, the previously confirmed SCO recombinants were transferred to a 7H11 agar plate containing 10% OADC, 0.2% glycerol, 50 µg/mL hygromycin (Sigma), 2% sucrose (Merck) and 60 µg/ml X-gal (Thermo Fisher Scientific) and incubated at 37°C until

the presence of colonies. White colonies resistant to hygromycin and sucrose were labeled as possible DCO recombinants. To confirm whether DCO recombinants and thus whether *Msm* Δ *mtr* or *Msm* Δ *mshC* mutants were generated, the recombinants were checked by PCR and Sanger sequencing (Neuromics Support Facility; University of Antwerp) using the reverse primer of primer set 1 and the forward primer of primer set 2 or primers amplifying part of the hygromycin-resistant cassette. For the *mshC* DCO recombinant, the Sanger sequencing was performed using primers that anneal in the middle of *mshC* (**Table V.2**).

Table V.2. Overview of primers used for the characterization of *Msm* SCO and DCO recombinants created with the p2NIL/pGOAL system.

Name	Sequence*	Description
PrimerSet1_Mtr_For	AGTGGCTGGTTGCGGCGGTG CCGGTGAGCGCCGCGGTGCT	Forward primer used to confirm a SCO and DCO event for <i>mtr</i> in <i>Msm</i> .
PrimerSet1_Mtr_Rev	CTCGACCGGTGGCTCGACGA GTATCTGAGCCTGCAGAATC	Reverse primer used to confirm a SCO and DCO event for <i>mtr</i> in <i>Msm</i> .
PrimerSet2_Mtr_For	TCGAACTGCCCTGGGGCTTC GCGGTTCCGGAACGCTCGCG	Forward primer used to confirm a SCO and DCO event for <i>mtr</i> in <i>Msm</i> .
PrimerSet2_Mtr_Rev	CGTTGCGCTCATGATGCCGG CCCCACCAACACGACGTCA	Reverse primer used to confirm a SCO and DCO event for <i>mtr</i> in <i>Msm</i> .
PrimerSet1_MshC_For	ACAAGGATCCAGACCGGGAC GAGGATCGGGCGCAGACTGC	Forward primer used to confirm a SCO and DCO event for <i>mshC</i> in <i>Msm</i> .
PrimerSet1_MshC_Rev	CGTACCTTCCGGACTTCGTG ATGTGCCGCGTGAGCTGGC	Reverse primer used to confirm a SCO and DCO event for <i>mshC</i> in <i>Msm</i> .
PrimerSet2_MshC_For	GTGTCGGCGTGCGCCTTCAG GGCGTCGGCATCGACGTCCA	Forward primer used to confirm a SCO and DCO event for <i>mshC</i> in <i>Msm</i> .
PrimerSet2_MshC_Rev	GCACATCACCGACCGCGAGA TCGCCGCACTGCGCGCCAGA	Reverse primer used to confirm a SCO and DCO event for <i>mshC</i> in <i>Msm</i> .
Hygro_For	actgcatctcaacgccttcc	Forward primer used to amplify part of HygR.
Hygro_Rev	gtctcctcgaacacctcgaa	Reverse primer used to amplify part of HygR.
MshC_Mid_For	GCCGCCCTGGATGTCGAGGC CGGTGCCGATCCGCGTCAGG	Forward primer annealing to the middle of <i>mshC</i> .
MshC_Mid_Rev	GCCGCCCTGGATGTCGAGGC CGGTGCCGATCCGCGTCAGG	Reverse primer annealing to the middle of <i>mshC</i> .

*Upper case letters in the sequences refer to sequences originating from the bacterial genome while lower case letters refer to sequences originating from a plasmid.

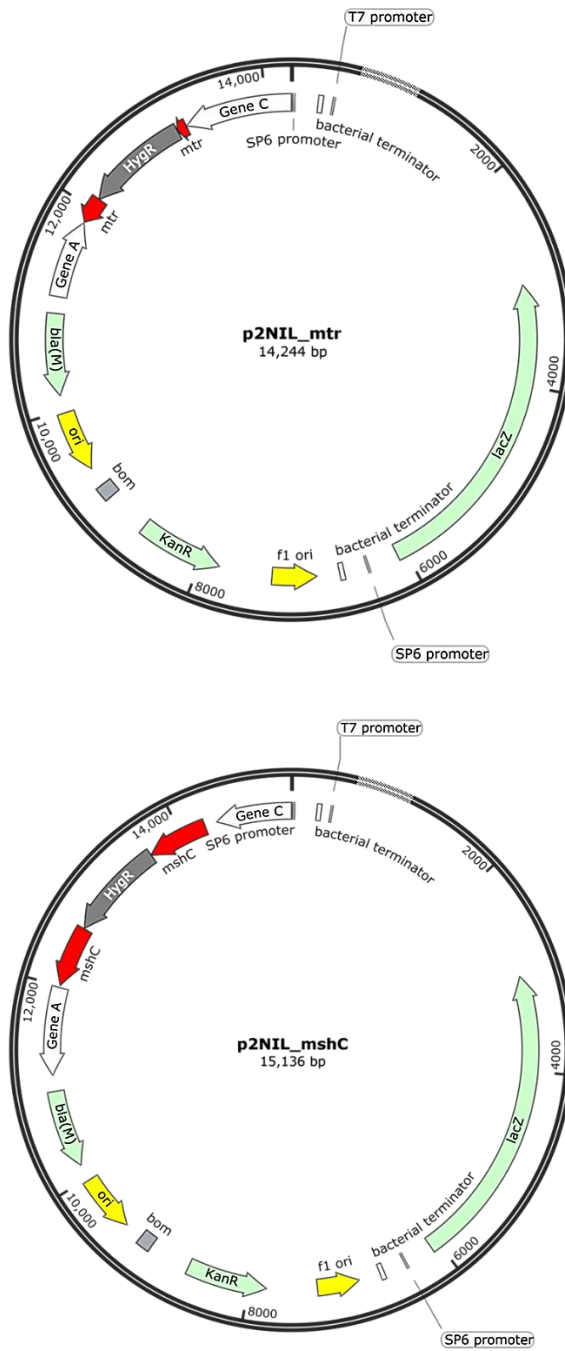
V.4 Results

p2NIL_mtr and *p2NIL_mshC* suicide plasmids were created for use in *Msm*

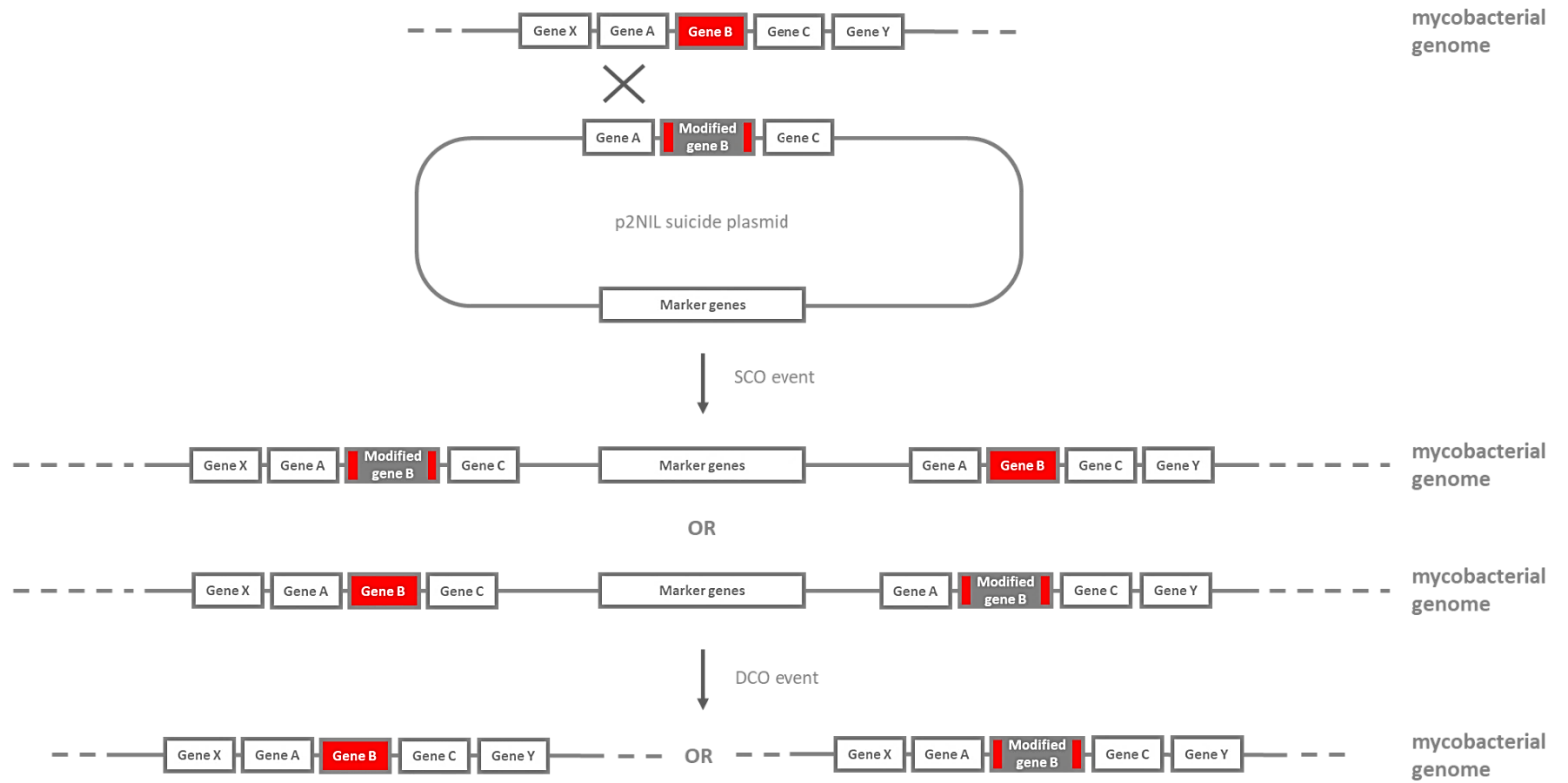
Because *Mab* is difficult to genetically manipulate, *Msm* was selected as an alternative model to evaluate and validate the p2NIL/pGOAL method before use in *Mab* by knocking out *mtr* and *mshC* in *Msm*. To achieve this, *p2NIL_mtr* and *p2NIL_mshC* plasmids were created carrying a modified copy of *mtr* or *mshC*, respectively, and the marker genes (**Figure V.2a**). Then, the p2NIL suicide plasmids were transformed individually into *Msm* to enable the recombination process to start (**Figure V.2b**). Although successful, the creation of *p2NIL_mtr* and *p2NIL_mshC* plasmids was time-consuming as it required multiple molecular cloning steps.

Page 134 and 135: Figure V.2. Overview of the *mtr* and *mshC* suicide plasmids and the expected recombination events occurring after transformation. a) Generated suicide plasmids needed to knock out *mtr* and *mshC* in *Msm*, i.e. *p2NIL_mtr* and *p2NIL_mshC* respectively. Created with SnapGene®. **b)** Overview of the recombination events to occur after transformation of the p2NIL suicide plasmids inside *Msm* and the possible outcomes after each event. This figure was adapted from Gopinath et al (119).

a



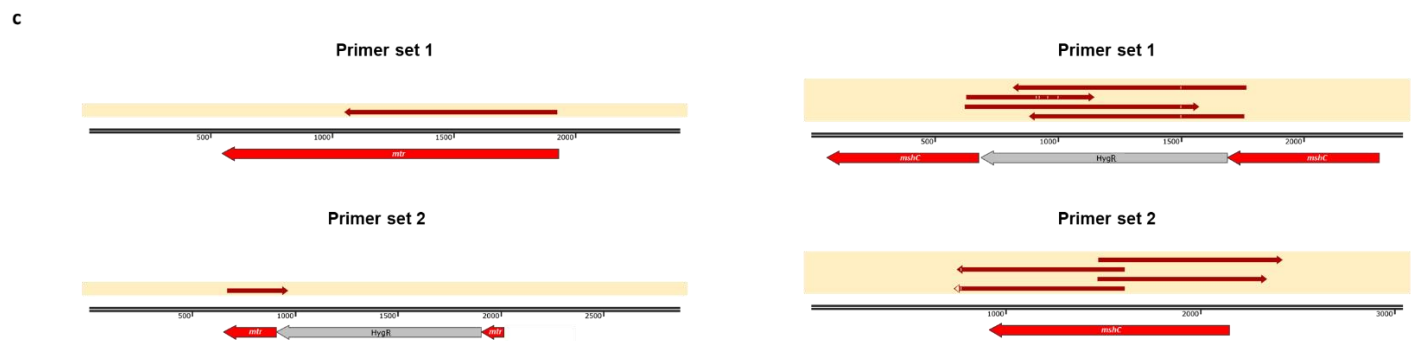
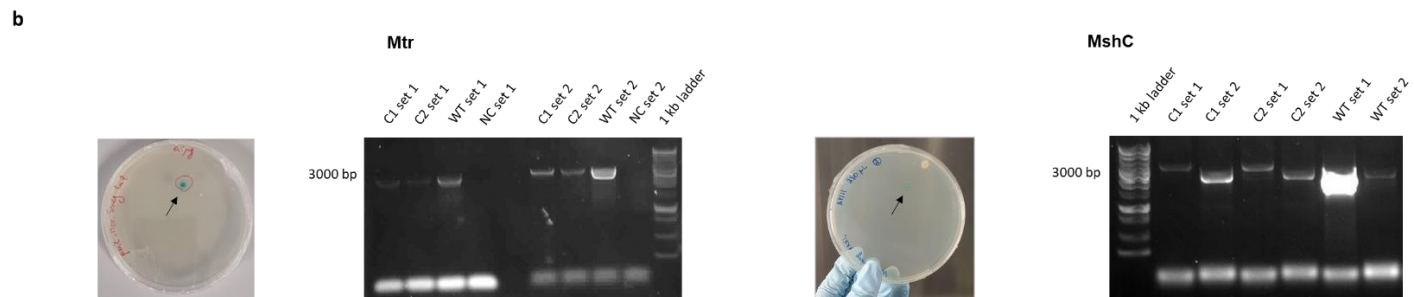
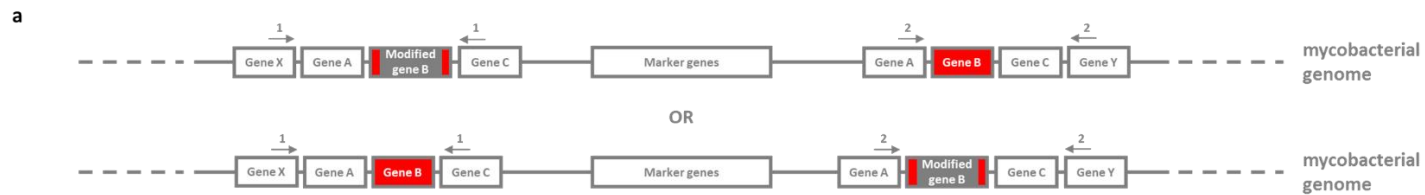
b



SCO recombinants were created for both mtr and mshC

Msm was transformed with the created suicide plasmids, p2NIL_ *mtr* or p2NIL_ *mshC*, after which the transformed bacteria were plated out on an agar plate containing kanamycin, hygromycin and X-gal to select for SCO recombinants. Blue colonies resistant to kanamycin and hygromycin were selected as possible SCO recombinants and assessed by PCR. By utilizing two primer sets, the integration place of the p2NIL plasmid could be determined, i.e., before or after the WT gene (**Table V.2**). Hereby, integration of the p2NIL plasmid before the WT gene is expected to generate a 2253 (*mtr*)/3401 (*mshC*) bp fragment with primer set 1 and a 2805 (*mtr*)/2564 (*mshC*) bp fragment with primer set 2 while integration after the WT gene generates a 2287 (*mtr*)/2405 (*mshC*) bp and 2771 (*mtr*)/3560 (*mshC*) bp fragment with primer set 1 and 2 respectively. When no SCO event occurred, a 2287 (*mtr*)/2405 (*mshC*) bp fragment is generated by primer set 1 and a 2805 (*mtr*)/2564 (*mshC*) bp fragment by primer set 2. After confirmation with PCR, the band generated with primer sets 1 and 2 was further examined by Sanger sequencing using the same primer sets. **Figure V.3a** gives a schematic overview of the possible outcomes of the SCO event and strategy implied to genotype the SCO recombinants with primer sets 1 and 2. To genotype SCO recombinants, two blue colonies for both *mtr* and *mshC* recombinant strains were selected to analyze the occurrence of a SCO event (**Figure V.3b**). As presented on the figure, the *mtr* SCO colonies exhibited a larger fragment with primer set 2 while *mshC* SCO colonies presented a larger fragment with primer set 1, indicating that the SCO event occurred after the WT gene in the *mtr* SCO colonies and before the WT gene in the *mshC* SCO colonies. This was further confirmed by the Sanger sequencing results where the sequences originating from the PCR were aligned to a reference sequence in which perfect alignment was depicted by a filled, red-colored arrow (**Figure V.3c**).

Page 138: Figure V.3. SCO recombinants were successfully obtained for both *mtr* and *mshC* in *Msm*. The p2NIL plasmid carrying a modified *mtr* or *mshC* was transformed into *Msm* after which the bacteria were plated out on agar plates supplemented with kanamycin, hygromycin and X-gal to select for SCO recombinants. **a)** Schematic overview of the two possible outcomes of a SCO event and the strategy implied to determine whether the p2NIL plasmid was incorporated before or after the WT gene. The gene of interest is shown as a red box (Gene B) and the modified gene as a red box interrupted by a grey box (Modified gene B). Primer set 1 and 2 are depicted as grey arrows. This figure was adapted from Gopinath et al. (119). **b)** A total of four blue colonies (black arrow) resistant to kanamycin and hygromycin were selected as possible *mtr* or *mshC* SCO recombinants and analyzed by PCR with primer sets 1 and 2. Integration of the p2NIL plasmid before the WT gene is expected to generate a fragment of 2253 (*mtr*)/3401 (*mshC*) bp with primer set 1 and 2805 (*mtr*)/2564 (*mshC*) bp with primer set 2. During integration after the WT gene, primer set 1 is expected to generate a 2287 (*mtr*)/2405 (*mshC*) bp fragment while primer set 2 a 2771 (*mtr*)/3560 (*mshC*) bp fragment. WT *Msm* containing no integrated plasmid is expected to generate a 2287 (*mtr*)/2405 (*mshC*) bp and 2805 (*mtr*)/2564 (*mshC*) bp fragment with primer set 1 and 2 respectively. The results demonstrated that the *mtr* SCO recombinant (C1) integrated the p2NIL plasmid after the WT gene while integration of the p2NIL plasmid in the *mshC* recombinants occurred before the WT gene. **c)** The sequences of the fragments generated by PCR were further analyzed by Sanger sequencing where the analyzed sequences were aligned to a reference sequence. A filled, red-colored area illustrated a perfect alignment while a mutation was shown as a transparent area. Sanger sequencing confirmed the findings shown by PCR.

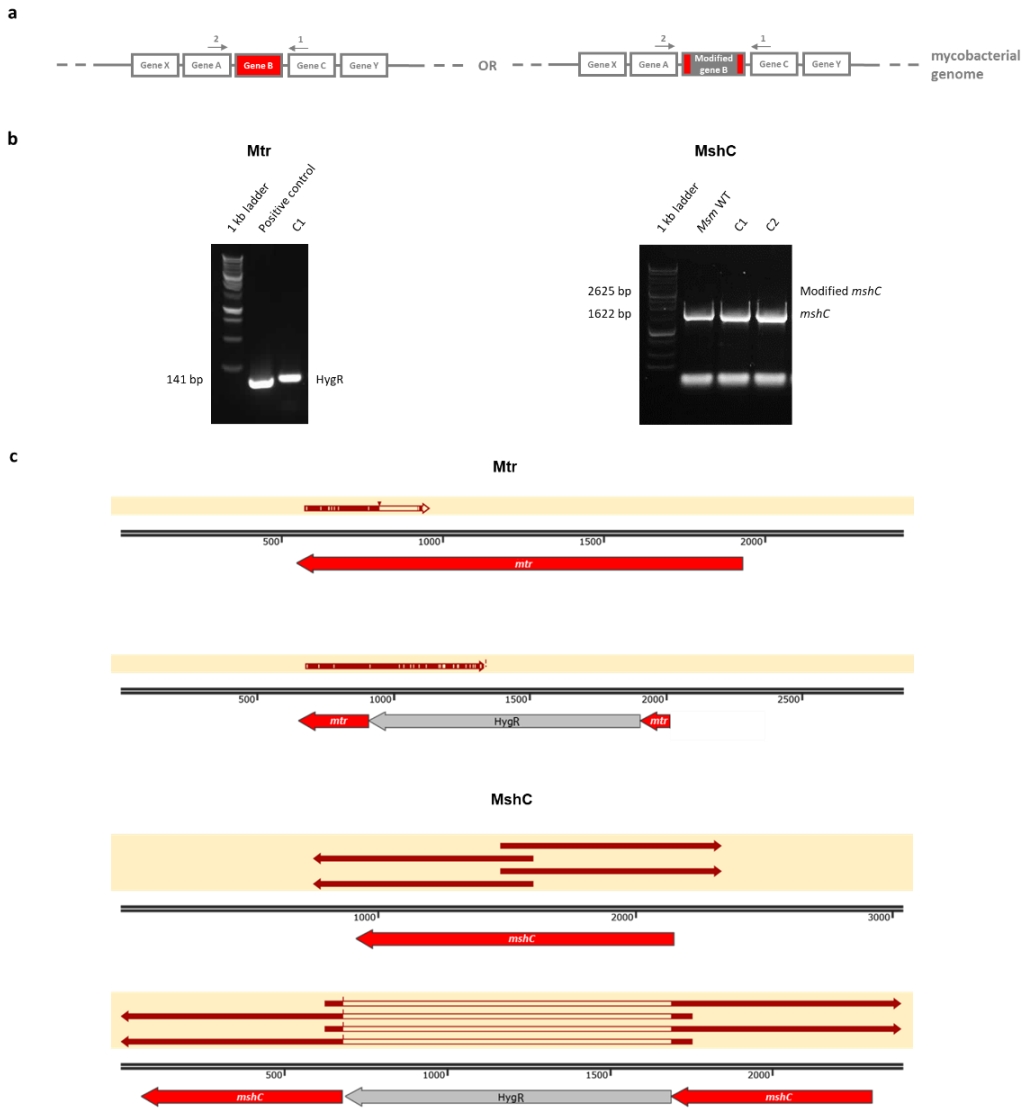


A MsmΔmtr mutant was generated using the p2NIL/pGOAL system

After characterization of the *mtr* and *mshC* SCO recombinants, the recombinants were transferred to another agar plate supplemented with hygromycin, sucrose and X-gal to allow for generation of DCO recombinants. Possible DCO recombinants were selected and analyzed by PCR and Sanger sequencing. To confirm the generation of DCO mutants by PCR, primers amplifying part of HygR were used that are expected to generate a 141 bp fragment as well as the forward primer of primer set 2 and reverse primer of primer set 1 to generate a 2625 bp fragment in the presence of a modified *mshC* or a 1622 bp fragment in the presence of a WT *mshC*. After analysis by PCR, fragments generated by using the forward primer of primer set 2 and the reverse primer of primer set 1 were further confirmed by Sanger sequencing. Here, the analyzed sequences were aligned against a reference sequence in which a filled, red-colored area represented a perfect alignment while misalignment was characterized by a transparent area. A schematic representation of the two possible results after a DCO event and the annealing place of the forward primer of primer set 2 and reverse primer of primer set 1 is depicted in **Figure V.4a**. Out of 23 colonies, only one *mtr* DCO recombinant was confirmed to possess HygR, creating a viable *MsmΔmtr* mutant (**Figure V.4b and c**). However, none of the 20 *mshC* DCO colonies tested retained the mutant *mshC*, failing to create a *MsmΔmshC* mutant. Although mutant strains need to be validated to confirm the generation of a successful mutant, validation of the *MsmΔmtr* is not the scope of this chapter.

Page 141: Figure V.4. *MsmΔmtr* was successfully created using the p2NIL/pGOAL system. The colonies of the SCO recombinants were transferred to an agar plate supplemented with hygromycin, sucrose and X-gal to allow for the occurrence of a DCO event. **a)** Schematic representation of the two possible outcomes of the DCO event. The primers used to characterize the DCO recombinants are depicted by a gray arrow, the WT gene of interest by a red box (Gene B) and the modified gene of interest by a red box interrupted by a gray box (Modified gene B). This figure was adapted from Gopinath et al. (119). **b)** All possible mutants were analyzed by PCR using primers amplifying part of HygR for the *mtr* DCO recombinants and the forward primer of primer set 2 together with the reverse primer of primer set 1 for the *mshC* DCO recombinants. If the *mtr* DCO recombinants retained the modified *mtr*, a 141 bp fragment is expected while no fragment is amplified if the WT gene is retained. Moreover, a 2625 bp fragment is expected if the modified *mshC* is present in the *mshC* DCO recombinants while a 1622 bp fragment demonstrates the retention of the WT *mshC*. *MsmΔmtr* was successfully generated whereas none of the *mshC* DCO colonies tested were *mshC* mutants. **c)** *mtr* and *mshC* DCO recombinants were further characterized by Sanger sequencing using the forward primer of primer set 2 or primers that anneal in the middle of *mshC*. The results confirmed previous findings claiming the successful creation of *MsmΔmtr* and loss of the modified *mshC* in all *mshC* DCO recombinants. The results of the two *mshC* DCO colonies displayed in the figure are representative for all *mshC* DCO colonies tested.

Validating the p2NIL/pGOAL method



V.5 Discussion

The creation of genetic mutants is of utmost importance to learn more about the function of a gene and to validate a gene as a drug target (120, 198). Recent development of new genetic tools, including the p2NIL/pGOAL method, have been facilitating the creation of mutants to study genes (116, 121, 123). The p2NIL/pGOAL method is described as an efficient tool to introduce specific mutations in mycobacteria (154). Furthermore, by incorporating markers into the backbone of the p2NIL suicide plasmid that are selectable (KanR), visual (*lacZ*) and counter-selectable (*sacB*), the p2NIL/pGOAL is an easy system that facilitates the identification and selection of allelic exchange mutants (206). In this chapter, the p2NIL/pGOAL method was employed to generate *Msm* Δ *mtr* and *Msm* Δ *mshC* mutant strains. While the occurrence of a SCO and DCO event was successful in both the *mtr* and *mshC* recombinant strains, only *Msm* Δ *mtr* was created (**Figure V.3 and V.4**). Hereby, **Figure V.4** demonstrated that all 20 *mshC* recombinants reverted back to a WT phenotype after the DCO event in *Msm*. This incidence may indicate gene essentiality since knockouts of essential genes are not viable (119). Yet, Xu et al. was able to create viable *mshC* mutants in *Msm* (207), questioning the ability of making predictions based on the outcome obtained with this method. Moreover, the fact that a DCO event does not always lead to the formation of mutants makes the p2NIL/pGOAL method inconvenient and time-consuming. Other time-consuming factors regarding this method are the lengthy molecular cloning procedures required to generate a p2NIL suicide plasmid carrying both the marker genes and the mutant gene of interest, and time necessary for the SCO and DCO event to occur. The p2NIL/pGOAL homologous recombination is mediated by the mycobacterial RecA protein, a large family of conserved, functional homologs of DNA strand exchange proteins (119, 208). However, homologous recombination techniques relying on the endogenous RecA are inefficient and laborious, mainly due to the requirement of long homology arms for the integration into a specific locus and the varying induction rate of RecA in different mycobacterial species (209, 210).

The DCO event of the p2NIL/pGOAL system enables for the selection of the WT or mutant copy of a gene (156). Thus, the generation of a knockout mutant is mainly dependent on the fitness cost the bacterium experiences when the WT copy of the gene is removed. Hereby, if a gene is essential or if its absence has a negative impact on the fitness of the bacterium, the mutant copy of the gene will most likely be removed from its genome. While this method was successfully implemented in *Msm*, multiple tryouts were still needed to successfully create a single *Msm* Δ *mtr* mutant and all attempts to generate a *Msm* Δ *mshC* mutant resulted in the reversion into WT (**Figure V.4b and c**). As a result of our observations, we concluded that this system is not the most convenient method to produce knockout mutants of potential novel targets in mycobacteria. Therefore, we decided not to implement the p2NIL/pGOAL system to create mutants in *Mab*, but instead apply a more recently discovered technique, i.e. the ORBIT system. The ORBIT system is a widely used system that combines both homologous recombination and site-specific integration. In contrary to the p2NIL/pGOAL method, the ORBIT system does not rely on the selected removal of a WT or mutant copy of a gene. Furthermore, it does not require multiple cloning steps for the construction of a suicide plasmid, but only involves the generation of a targeting oligonucleotide that can be easily purchased (116). Finally, the ORBIT system utilizes the provided RecT of phage Che9c for its recombineering and is therefore independent from host factors, increasing the recombineering efficiency (115, 116).

Altogether, the p2NIL/pGOAL method was validated by successfully applying this method to generate a *Msm* Δ *mtr* mutant. However, while validating the p2NIL/pGOAL method in *Msm*, this method proved to be laborious, inefficient and time-consuming. Therefore, the p2NIL/pGOAL method will not be implemented in *Mab* and will be replaced by a more recent and efficient technique, i.e. the ORBIT system.

CHAPTER VI

Creating *mtr* and *mshC* knockout strains to evaluate Mtr and MshC as potential drug targets



Part of this chapter has been published in:

Piller T, De Vooght L, Gansemans Y, Van Nieuwerburgh F, Cos P. Mycothione reductase as a potential target in the fight against *Mycobacterium abscessus* infections. *mSphere*. 2023 Dec 12:e0066923. doi: 10.1128/msphere.00669-23. Epub ahead of print. PMID: 38085034.

Author contributions:

Tatiana Piller¹: conceptualization, methodology, investigation and formal analysis.

Linda De Vooght¹: conceptualization, methodology, formal analysis and supervision.

Yannick Gansemans²: WGS investigation and formal analysis.

Filip Van Nieuwerburgh²: WGS investigation and formal analysis.

Paul Cos¹: conceptualization, methodology, formal analysis and supervision.

¹Laboratory of Microbiology, Parasitology and Hygiene (LMPH), University of Antwerp, Belgium

²Laboratory of Pharmaceutical Biotechnology, Faculty of Pharmaceutical Sciences, Ghent University, Ghent, Belgium

VI. Creating *mtr* and *mshC* knockout strains to evaluate Mtr and MshC as potential drug targets

VI.1 Abstract

While infections caused by MABC are rising worldwide, the current treatment of these infections is far from ideal due to its numerous shortcomings, thereby increasing the urge for novel drug targets. In this study, Mtr and MshC were evaluated for their potential as drug targets for MABC infections since they are key enzymes needed in the biosynthesis and recycling of MSH, the main LMW thiol protecting the bacteria against ROS and other reactive intermediates. First, a *MabΔmtr* mutant strain was generated, lacking *mtr* expression. Next, the *in vitro* sensitivity of *MabΔmtr* to oxidative stress and anti-mycobacterial drugs was determined. Finally, we evaluated the intramacrophage survival and the virulence of *MabΔmtr* in *G. mellonella* larvae. *MabΔmtr* demonstrated a 39.5-fold reduction in IC₉₀ when exposed to bedaquiline *in vitro*. Furthermore, the *MabΔmtr* mutant showed a decreased ability to proliferate inside macrophages and larvae, suggesting that Mtr plays an important role during MABC infection. Lastly, biofilms generated by *MabΔmtr* show a more smooth-like phenotype, making them possibly less resistant to mechanical stress. Altogether, these findings support the assumption of Mtr being a potential target for anti-mycobacterial drugs. Regarding MshC, we were unable to generate an *mshC* knockout after many attempts.

VI.2 Introduction

Infections caused by MABC are known for being very difficult to treat, as this complex is resistant to the standard antimicrobial agents, its treatment displays a low success rate and often leads to adverse drug effects, and various patients experience relapse after treatment or surgical removal of the pathogen (47, 50, 187). Thus, current treatment is far from ideal and requires a long-term multidrug therapy including a macrolide together with 2 to 3 intravenous drugs during the

initial treatment phase or nebulized amikacin and 1 to 4 oral drugs during the continuation phase (47). Accordingly, in order to improve treatment of MABC infections and relieve the burden of drug resistance, novel mycobacterial targets need to be explored, which effectively reduce the bacterial burden within the host.

MSH plays a key role in the protection of mycobacteria against harmful endogenous and exogenous ROS generated by both aerobic respiration and the host's immune system (88, 104, 166). Macrophages, i.e. the primary host cells of MABC during pulmonary disease, will release ROS after phagocytosis to promote bacterial killing (211, 212). Since Mtr and MshC play a major role in the biosynthesis and recycling of MSH and hereby maintaining a balanced redox homeostasis, they are interesting targets for the development of anti-mycobacterial drugs (166, 170). Recently, several studies have shown that altered levels of MSH affect the susceptibility to oxidative stress and overall survival of other mycobacterial species, including *Mtb* and *Msm* (104, 164).

To validate a drug target and learn more about a gene, genetic mutants must be created with the use of genetic engineering techniques (120, 198). Recently, a new system called ORBIT was developed combining two efficient recombination systems (123). It involves the transformation of a plasmid expressing Che9c RecT annealase and Bxb1 integrase into mycobacteria followed by the co-transformation of a single-stranded targeting oligonucleotide containing an *attP* Bxb1 recombination site together with a payload plasmid containing both the selection markers and an *attB* Bxb1 integration site. First, Che9c RecT annealase integrates the oligonucleotide into the genome by homologous recombination. Subsequently, Bxb1 integrase incorporates the payload plasmid into the *attP*-site introduced earlier in the genome, hereby disrupting a gene of interest and creating a knockout (116, 120, 123).

In this study, we investigated the potential of Mtr and MshC as novel drug targets in *Mab*. While all attempts to generate an *mshC* knockout strain failed, we used a *MabΔmtr* knockout strain to deplete *mtr* expression and showed that although not

strictly essential for growth, elimination of *mtr* leads to an increased *in vitro* sensitivity towards oxidative stress and anti-mycobacterial drugs. Furthermore, in the absence of *mtr*, a decrease in intramacrophage replication and survival in *G. mellonella* was observed. Finally, biofilms formed by the *MabΔmtr* mutant showed a shift to a smoother phenotype compared to biofilms formed by the WT, possibly making them less resistant to mechanical stress factors. Collectively, these results validate Mtr as a potential drug target in *Mab* and demonstrate the potential for synergy by combining currently used anti-mycobacterial drugs with Mtr inhibitors.

VI.3 Material and Methods

Bacterial strains, media and culture conditions

All mycobacterial strains in this study were derived from *M. abscessus* ATCC 19977 and were routinely cultured at 37°C in Middlebrook 7H9 broth (Sigma) supplemented with 10% ADS (albumin-dextrose-saline), 0.2% glycerol and 0.05% tyloxapol or Sauton's medium (HiMedia Laboratories) supplemented with 2% glycerol and 0.05% tyloxapol with the addition of 100 µg/mL Zeocin™ (Fisher Scientific) for the *MabΔmtr* mutant and 50 µg/ml Zeocin™ (Fisher Scientific) for the *Mab* FF_scarlet. Agar plates were made of Middlebrook 7H11 agar base (Sigma) or Sauton agar, consisting of Sauton's medium solidified with 1.5% Bacto™ Agar (Becton, Dickinson and Company).

Construction of a MabΔmtr mutant

For construction of the *MabΔmtr* and *MabΔmshC* mutants, the ORBIT system was used as described by Murphy et al. (123). Briefly, *Mab* was grown in a shaking incubator (New Brunswick Scientific; 175 rpm) in 7H9 supplemented with 10% OADC (oleic acid-albumin-catalase-dextrose; Thermo Fisher Scientific), 0.2% glycerol and 0.05% tyloxapol at 37°C until reaching an optical density at 600 nm

(OD₆₀₀) between 0.2 and 0.8 and was made electrocompetent by washing three times with 10% glycerol. Then, 1 µg of the endogenous pKM444 plasmid (Addgene 108319) was transformed into the electrocompetent bacteria by using the Gene Pulser Xcell Total System (Bio-Rad; 1.25 kV, 1000 Ω and 25 µF). Following electroporation, *Mab* was resuspended in 7H9 medium containing 20% OADC and incubated at 37°C for 4h before it was plated out on 7H11 agar containing 10% OADC, 0.2% glycerol and 200 µg/mL kanamycin (Sigma). The 7H11 agar plates were incubated for 3 days to 1 week at 37°C until the presence of colonies. After confirming plasmid uptake by the candidate colonies by PCR using primers amplifying the KanR of the pKM444 plasmid, *Mab::pKM444* was grown in the same medium, induced for plasmid expression with 500 ng/mL anhydrotetracycline (ATc; Takara Bio Europe) 18h before electroporation and incubated in the shaking incubator at 37°C until reaching the previously mentioned OD₆₀₀. Next, the induced culture was made electrocompetent and transformed together with 1 µg of the *attP*-containing oligonucleotide and 200 ng of the *attB*-containing pKM496 plasmid (Addgene 109301) using the same system and settings as the previous transformation. The transformed bacteria was incubated in the shaking incubator in 7H9 medium containing 20% OADC at 37°C overnight to allow for homologous recombination before being spread out on 7H11 agar plates supplemented with 10% OADC, 0.2% glycerol and 100 µg/mL Zeocin™ and incubated for 1 to 2 weeks at 37°C. Colonies obtained from the transformation were confirmed for successful recombination and thus successfully obtained *MabΔmtr* by PCR and Sanger sequencing (Neuromics Support Facility; University of Antwerp) utilizing primers to amplify the WT *mtr* gene together with the fully incorporated pKM496 plasmid into the WT *mtr*. All primers and oligo's used are listed in **Table VI.1**.

Table VI.1. Overview of primers and oligos used for the construction of the *MabΔmtr* and *MabΔmshC* mutant.

Name	Sequence*	Description
Kana_For	tcaacgggaaacgtcttgct	Forward primer used to amplify KanR.
Kana_Rev	ggagaaaactcaccgaggca	Reverse primer used to amplify KanR.
Mtr_Oligo	CGTCACGGGCCCCTCAGGAGAT GGAGAGTAGATGTACGACCTCGT CATCATCGGTTCCGGCAGCGCAA g g t t g t c t g g t c a a c c a c c g g t c t c a g t g g t g t a c g g t a c a a a c c T G G T C G A G A A C G C C C T G C T G G G T C T G G A C C T C T A G C C C T A C T C A G C C G G C C A T G A A T T C G T C G T A G G C G G	The oligonucleotide containing the <i>attP</i> -site required for the homologous recombination between the WT <i>mtr</i> and the <i>attB</i> -containing pKM496 plasmid.
MshC_Oligo	GGGCGGCCTAACGACCCATAAG GTGTGGGTATGCAGTCGTGGGCG TCGGCGCCGGTTCCTGAACTCGAg g g t t g t c t g g t c a a c c a c c g g t c t c a g t g g t g t a c g g t a c a a a c c A T G C G G T G G A T G C C C T G C T G G G A G T G C A G T T G T A G C G T C G T C G C A T G G G T T C A A C G G C G A A C G G T G T T G C	The oligonucleotide containing the <i>attP</i> -site required for the homologous recombination between the WT <i>mshC</i> and the <i>attB</i> -containing pKM496 plasmid.
Mtr_For	CCGATCGGGTCTCCACCTG	Forward primer used to amplify the WT <i>mtr</i> and a few nucleotides before the gene.
Mtr_Rev	GCCCCGGCGCTGTACATTCA	Reverse primer used to amplify the WT <i>mtr</i> and a few nucleotides after the gene.

*Upper case letters in the sequences refer to sequences originating from the bacterial genome while lower case letters refer to sequences originating from a plasmid.

Whole genome sequencing and analysis

Genomic DNA concentration was determined using Quant-iT Picogreen dsDNA (Thermo Fisher) and integrity was inspected on a 1% E-gel (Invitrogen). About 120 - 800 ng input DNA was fragmented in a Covaris S2 sonicator, aiming for 400 bp fragments. For each sample, a sequencing library was constructed using the NEBNext Ultra II DNA Library Prep Kit for Illumina (NEB) using 90 - 400 ng of fragmented material. After adapter ligation, library fragments were size-selected for 400 - 800 bp on a 2% E-gel and purified using the Zymoclean Gel DNA Recovery Kit (Zymo Research). Half of the material was then submitted to 6 PCR cycles and purified using Ampure XP beads (Beckman Coulter). Quality was checked using a High Sensitivity DNA Kit on a Bioanalyzer (Agilent). Yield was determined by qPCR according to the 'Sequencing Library qPCR Quantification Guide' (Illumina). Sample libraries were pooled equimolar and a final size selection for 400-800 bp fragments was done on a 2% E-gel. The material was purified using Zymoclean Gel DNA Recovery Kit. The pooled libraries were sequenced as paired-end 150 on a NovaSeq device (Illumina).

Sequencing read quantity and quality was evaluated using FastQC (v0.11.9) (213). Contamination was checked using FastQ Screen (v0.15.1) (214) and genomes from a limited set of common lab organisms. Adapter and quality trimming was done with cutadapt (v3.7) (215) using a phred score threshold of 20 and removing reads with ambiguous bases. We used breseq (v0.37.0) (216) to perform structural variant analysis using either the *Mab L948* (ATCC 19977) reference genome (GCF_000069185.1_ASM6918v1_genomic.gbff GenBank file from NCBI) or the *Mtb H37Ra* (ATCC 25177) reference genome (GCF_001938725.1_ASM193872v1_genomic.gbff GenBank file from NCBI), together with plasmid sequences and putative genome-inserted sequences. Briefly, the tool first maps the trimmed reads on the reference sequences with bowtie2 (v2.4.5) (217), then performs a variant analysis and reports SNPs, as well as new junctions explaining larger deletions and insertions. Finally, it annotates all

detected mutations using the available genome information and results are reported as an interactive HTML document.

RNA isolation

Mab strains were grown in 7H9 supplemented with 10% ADS, 0.2% glycerol and 0.05% tyloxapol until reaching their logarithmic phase and diluted to an OD₆₀₀ of 0.1 in the same medium. After 48h of growth in a shaking incubator (New Brunswick Scientific; 175 rpm) at 37°C, the pellets of the strains were harvested and incubated in TRIzol reagent (Invitrogen) for 5 min at room temperature (RT). Next, the bacteria were lysed with BeadBug™ beads (Sigma; 0.1 mm Zirconium beads) by shaking at a speed of 6 m/s twice for 45 seconds using the FastPrep 24 Classic (MP biomedical) followed by incubation at -80°C overnight. In order to separate the samples from the TRIzol reagent, Phasemaker tubes (Invitrogen) were used together with the addition of chloroform to the sample. Once separated, RNA isolation of the samples was completed using the RNeasy Plus Mini Kit (Qiagen) followed by a DNase treatment completed with TURBO DNAase (Qiagen) and ezDNase (Invitrogen). The final RNA concentration was measured using the NanoDrop™ 2000 spectrophotometer (Thermo Scientific) and the RNA samples were stored at -80°C until further use.

Real-time quantitative PCR

All RT-qPCR were performed combining 10 µL of 2× SensiFAST™ SYBR® No-ROX One-Step mix (Biotech), 0.6 µL of each primer (0.3 µM final concentration; Table S1), 0.2 µL of reverse transcriptase (Biotech), 0.4 µL of RNase inhibitor (Biotech), 3 µL of RNA template, and 5.2 µL of DEPC-treated water (diethylpyrocarbonate; Biotech) in each well to reach a finale volume of 20 µL. Next, the mRNA expression was measured using the LightCycler® 480 system (Roche) with predetermined cycle conditions (Reverse T1 (45°C, 10 min, 1×), 2-step Amplification (95°C, 5 sec;

60°C, 30 sec, Single, 40×) and Melting (95°C, 10 sec; 45°C, 1 min; 95°C, continuous, 1×)) and analyzed relative to the expression of the housekeeping gene, *rpoB*, with the LightCycler® 480 SW 1.5.1 software. The normalized relative expression levels were further analyzed using GraphPad software 8.0. All primers are listed in **Table VI.2**.

Table VI.2. Overview of primers used to characterize the *MabΔmtr* mutant by RT-qPCR.

Name	Sequence	Description
rpoB_qPCR_For	CAGCACTCCATCTCACCGAA	Forward primer needed for mRNA quantification of <i>rpoB</i> .
rpoB_qPCR_Rev	TGGTCGACGACAAGATCCAC	Reverse primer needed for mRNA quantification of <i>rpoB</i> .
Mtr_qPCR_For	CACCAACGACGACATCATGC	Forward primer needed for mRNA quantification of <i>mtr</i> .
Mtr_qPCR_Rev	AATCACGGTGACCTTCGAGC	Reverse primer needed for mRNA quantification of <i>mtr</i> .
MshA_qPCR_For	CATCGGTGAGTTGTTGGTGC	Forward primer needed for mRNA quantification of <i>mshA</i> .
MshA_qPCR_Rev	CGGCCGTAGCTCGACAATAA	Reverse primer needed for mRNA quantification of <i>mshA</i> .
MshB_qPCR_For	ACGACTCGACGACTCATGC	Forward primer needed for mRNA quantification of <i>mshB</i> .
MshB_qPCR_Rev	AGGTCACCAACTGGACATCG	Reverse primer needed for mRNA quantification of <i>mshB</i> .
MshC_qPCR_For	CATCATCGAGCTCGTCGAGAA	Forward primer needed for mRNA quantification of <i>mshC</i> .
MshC_qPCR_Rev	CCGACTCATAGCCGAACTGT	Reverse primer needed for mRNA quantification of <i>mshC</i> .
MshD_qPCR_For	CCTGCTGCGTGCAACAATG	Forward primer needed for mRNA quantification of <i>mshD</i> .
MshD_qPCR_Rev	GTCATGCGCCAGGAACAATC	Reverse primer needed for mRNA quantification of <i>mshD</i> .

Quantification of intracellular reduced thiol levels

For quantification of the intracellular reduced thiol levels, the Thiol Fluorescent Detection Kit (Thermo Fisher Scientific) was used. Briefly, mycobacterial strains were grown in 7H9 broth supplemented with 10% ADS, 0.2% glycerol and 0.05% tyloxapol until reaching their logarithmic phase, diluted in the same medium to match an OD₆₀₀ of 0.1 and incubated at 37°C for 48h. After 48h, the cultures were washed twice with DPBS (Dulbecco's Phosphate Buffered Saline; Gibco) supplemented with 0.05% tyloxapol and resuspended in 1X Assay Buffer (Thermo Fisher Scientific). Next, the mycobacterial cell wall was disrupted with BeadBug™ beads (Sigma; 0.1 mm Zirconium beads) by shaking at a speed of 6 m/s twice for 60 seconds using the FastPrep 24 Classic (MP biomedical) followed by centrifugation of the cultures and isolation of the supernatans. The samples were diluted in a one-over-two manner by using the 1X Assay Buffer after which 100 µL of each diluted sample was added to a black half area 96-well plate together with 25 µL Detection Reagent (Thermo Fisher Scientific). The plate was incubated for 30 min at RT in the dark before reading the fluorescent signal with the Tecan plate reader (Infinite F plex) at an emission of 510 nm and excitation of 390 nm. For determination of the thiol levels, the fluorescent values of the samples were plotted according to a standard curve obtained with an N-Acetylcysteine Standard (Thermo Fisher Scientific).

Growth curves

The bacteria were grown until logarithmic phase in 7H9 broth supplemented with 10% ADS, 0.2% glycerol and 0.05% tyloxapol or Sauton's medium supplemented with 2% glycerol and 0.05% tyloxapol and diluted to an OD₆₀₀ of 0.05 before being incubated in a shaking incubator (New Brunswick Scientific; 175 rpm) at 37°C. Growth of the strains was evaluated every 24h by measuring the OD₆₀₀ with a cell density meter (Biochrom WPA Biowave). In parallel, the same experiment was conducted for 2 days in 7H9 broth and 3 days in Sauton's medium with growth

measured by both OD₆₀₀ and CFU count to determine the CFU-OD₆₀₀ proportion of each strain.

Oxidative stress-induced viability assay

Logarithmic-phase mycobacterial strains were cultured in Sauton's medium supplemented with 2% glycerol and 0.05% tyloxapol after which they were diluted to an OD₆₀₀ of 0.05. At that moment, all strains were divided in two groups whereas one group was subjected to 15 mM H₂O₂ before they were all incubated in a shaking incubator (New Brunswick Scientific; 175 rpm) at 37°C. A part of the cultures was harvested at 0h, 4h, 8h, and 24h after addition of H₂O₂. The ATP levels of the cultures were measured using the BacTiter-Glo™ kit (Promega) and a 10-fold serial dilution of each culture was plated on 7H11 agar plates supplemented with 10% ADS and 0,2% glycerol for measurement by CFU count.

Antimicrobial activity determination

The selected compounds, bedaquiline (Sigma), clofazimine (Sigma) and moxifloxacin (Sigma), were first solubilized in 100% dimethyl sulfoxide (DMSO; Sigma) at a concentration of 20 mM and stored at -20°C until further use. To determine the activity of the compounds against the mycobacterial strains, both *Mab* WT and *Mab*Δ*mtr* mutant in their logarithmic phase were diluted to an OD₆₀₀ of 0.05 with 7H9 supplemented with 10% ADS, 0.2% glycerol and 0.5% tyloxapol and inoculated in a 96-well plate. Then, each compound was added in a one-over-three dilution to the 96-well plates containing the bacteria to reach a final concentration starting from 100 μM and a maximal final DMSO concentration of 1%. The 96-well plates were incubated at 37°C for 3 days to allow for exposure to the compounds. After incubation, 0.001% (w/v) of resazurin (Sigma) was added to each well after which the plates were incubated again overnight at 37°C. Finally, the viability of the mycobacterial strains was assessed by measuring the

fluorescence signal emitted by each well at an excitation and emission of 550 and 590 nm respectively with the use of a Tecan plate reader (Infinite F plex).

RAW 264.7 macrophage infection

RAW 264.7 murine macrophages were cultured in Dulbecco's modified Eagle's medium (DMEM; Thermo Fisher Scientific) containing 10% heat-inactivated Fetal Calf Serum (iFCS; Thermo Fisher Scientific), 10% Penicillin-Streptomycin (P/S; Thermo Fisher Scientific; 10000 U/mL) and 10% L-Glutamine (Glutamax; Thermo Fisher Scientific; 200 nM) at 37°C. To determine the infectivity of the different mycobacterial strains, the macrophages were seeded in a 24-well plate (Greiner Bio-One) in DMEM supplemented with 5% iFCS at a concentration of 5×10^5 cells/mL and incubated overnight at 37°C. Next, the cells were infected at a multiplication of infection (MOI) of 5 during 4h at 37°C in the presence of 5% CO₂. After infection, 200 µg/mL amikacin (Sigma) was added to the cells, and they were incubated once more in the same conditions for 45 min to kill all extracellular bacteria. The bacterial load was analyzed 0h and 24h after infection by first lysing the cells with 0.1% Triton-X-100 for 10 min and then plating out a serial dilution on 7H11 agar plates supplemented with 10% ADS and 0.2% glycerol to determine the CFUs.

Galleria mellonella infection

G. mellonella larvae were purchased from Anaconda Reptiles (Kontich, Belgium) and stored in boxes filled with wood chips at 4°C. The protocol followed was adapted from Cools et al. and Meir et al. (84, 218). For infection, larvae were injected in the penultimate pro-leg with 5×10^3 CFU in a volume of 10 µl by a 31G needle using a Hamilton syringe. At the same time, the control group was injected with 10 µl DPBS (Dulbecco's Phosphate Buffered Saline; Gibco). Next, the larvae were incubated at 37°C until they were sacrificed or until the end of the

experiment. To generate a Kaplan-Meier curve, a total of 90 larvae received a dead-or-alive score every 24h based on absence of movement in response to external stimuli and melanization of the larvae. For CFU count of the bacteria per larvae, a total of 8 to 11 larvae of each infected group were sacrificed by freezing for 30 min on day 2, 4 and 6. Then, these larvae were decontaminated with 70% ethanol, homogenized by the Qiagen TissueRuptor and plated out in a serial dilution on 7H11 agar containing 10% ADS, 0.2% glycerol, 2 µg/mL vancomycin (Sigma) and 8 µg/mL ceftazidime (Sigma). The plates were incubated at 37°C until colonies could be counted properly.

Biofilm formation

The biofilm formation protocol was adapted from Rodríguez-Sevilla et al. (173). Briefly, all *Mab* strains were grown in 7H9 supplemented with 10% ADS and 0.2% glycerol up to logarithmic phase, washed with DPBS (Dulbecco's Phosphate Buffered Saline; Gibco) and diluted in DPBS to an OD₆₀₀ of 0.2. Then, 5 µL of each strain was spotted on a sterile Isopore Polycarbonate membrane (Carl Roth Belgium; pore size: 0.22 µm, diameter: 13 mm, white) present on an 7H11 agar plate supplemented with 10% ADS and 0.2% glycerol followed by incubation of the agar plates side-up at 37°C with 5% CO₂. After 24h, 48h, 72h and 96h of incubation, an image was taken of each membrane containing the biofilm, the area of the biofilm was calculated with ImageJ and the biofilm was extracted from the membranes to determine the bacterial load per membrane by CFU count. Sampling of the biofilm was accomplished by placing each membrane containing a biofilm in 10 mL PBS and detaching the biofilm from the membrane by vortexing for 30 sec, sonicating for 2 min and vortexing again for 30 sec.

Statistical analysis

Mann-Whitney test was applied to statistically evaluate the results obtained by RT-qPCR, thiol levels determination, oxidative stress assay, macrophage assay, *G. mellonella* infection and biofilm formation, and was followed by correction for multiple testing when required. Interpretation of a decline or increase of the results over time was statistically analyzed with a non-linear regression while the difference in the obtained results over time during *G. mellonella* infection was analyzed using the Kruskal-Wallis test. The Kaplan-Meier curve was analyzed using the Log-rank (Mantel-Cox) test. Results were considered significantly different when $p < 0.05$. All statistical analysis was performed using the Graphpad software 8.0.

VI.4 Results

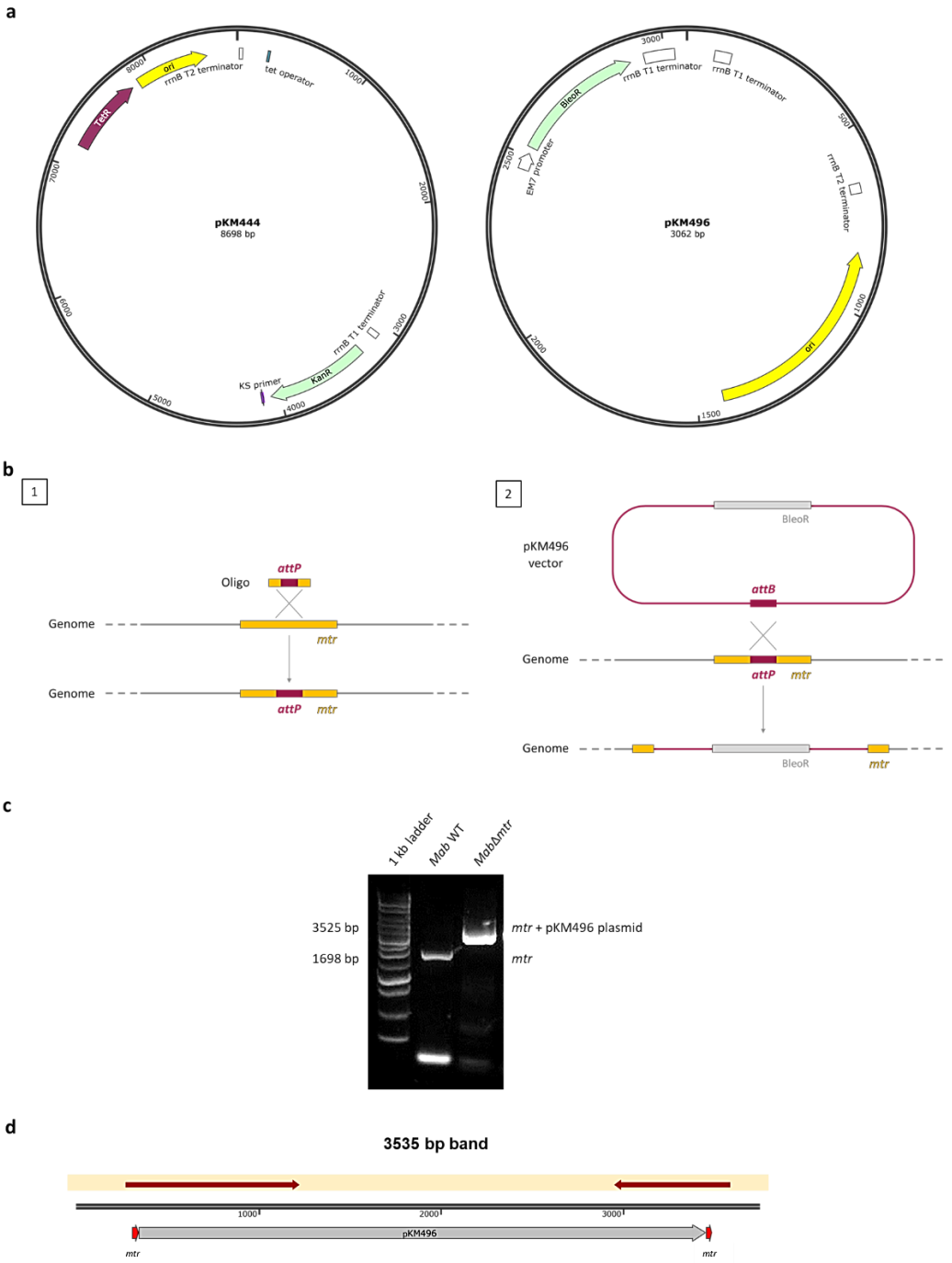
*Successful implementation of the ORBIT system resulted in the creation of a *MabΔmtr* mutant*

To create *mtr* and *mshC* knockout mutants, the ORBIT system was implemented to transform the bacteria with a total of two plasmids (pKM444 and pKM496) and an oligo (**Figure VI.1a and b**). After transformation, the colonies were investigated by PCR and Sanger sequencing using primers to amplify the gene of interest (**Table VI.1**). Unfortunately, no colonies were generated when trying to knock out *mshC*. On the other hand, *MabΔmtr* was successfully created when the pKM496 was incorporated in the middle of the gene of interest, generating a 3525 bp fragment by PCR while a WT generates a 1698 bp fragment. The PCR result showed a 1698 bp fragment generated for the WT while a 3525 bp fragment was generated for the tested colony, indicating that *mtr* was interrupted by the pKM496 plasmid in this colony (**Figure VI.1c**). The generation of a *MabΔmtr* mutant was further confirmed by the Sanger sequencing results in which the sequence of the 3535 bp fragment was perfectly aligned to a reference sequence including *mtr* interrupted by the

pKM496 plasmid (**Figure VI.1d**). Perfect alignment is illustrated by a filled, red-colored arrow.

Page 161: Figure VI.1. Successful implementation of the ORBIT system to create a *MabΔmtr* mutant. **a)** Overview of the plasmids used with the ORBIT system, pKM444 and pKM496. **b)** Schematic representation of the ORBIT system. Integration of the pKM496 plasmid is performed in a two-step process. First, an *attP* site is incorporated via the oligo in the gene of interest. Next, site-specific recombination occurs between the *attP*-containing genome and the *attB*-containing pKM496 vector, hereby interrupting the WT *mtr* gene. **c)** The PCR result showed that *mtr* was disrupted by the pKM496 plasmid, generating a *MabΔmtr* mutant. **d)** The generation of a *MabΔmtr* mutant was confirmed by the Sanger sequencing. Perfect alignment is illustrated by a filled, red-colored arrow. BleoR: cassette conferring resistance to bleomycin, phleomycin, and Zeocin, TetR: tetracycline repressor, KanR: kanamycin-resistant cassette, ori: origin of replication

Creating *mtr* and *mshC* knockouts



Part of the MSH biosynthesis pathway is upregulated when its recycling pathway is disabled

After establishing the correct implementation of the ORBIT system to produce a *MabΔmtr* mutant, the WT and *MabΔmtr* strains were analyzed by WGS to exclude the occurrence of off-target effects during transformation (**Table VI.3**). The WGS results confirmed that no off-target integration of the oligo and pKM496 plasmid occurred in the *MabΔmtr* mutant. Next, to confirm successful knocking out of the *mtr* gene in the *MabΔmtr* mutant, first the relative expression of *mtr* was evaluated in the WT and *MabΔmtr* using RT-qPCR (**Figure VI.2a**). As observed in the figure, the *MabΔmtr* mutant displayed no expression of *mtr*, hereby confirming the abolishment of *mtr* expression after deletion of the gene. To evaluate compensation of the loss of *mtr*, i.e. the MSH recycling pathway, the relative expression of *mshA*, *mshB*, *mshC* and *mshD* was analyzed as well. No significant difference was detected between the strains for the *mshA*, *mshC* and *mshD* gene expression (**Figure VI.2b**). Interestingly, the relative expression of *mshB* showed a 2.6-fold upregulation in *MabΔmtr* compared to the WT indicating that only part of the MSH biosynthesis pathway is upregulated when the recycling pathway is not expressed.

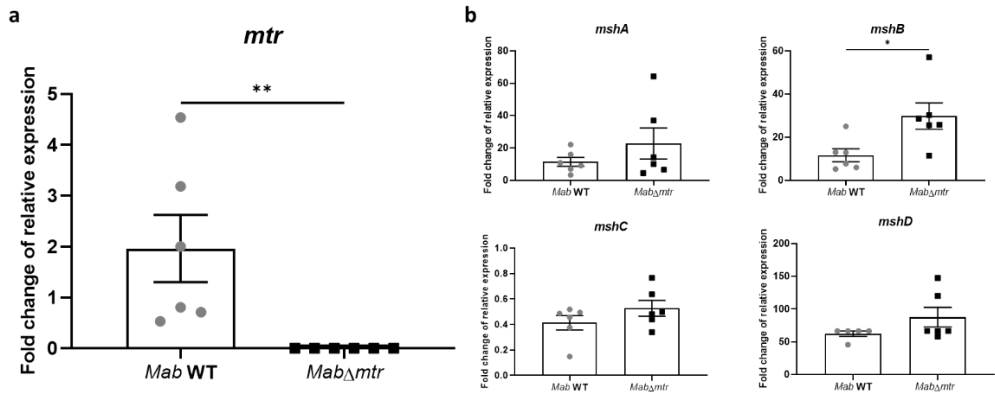


Figure VI.2. Part of the MSH biosynthesis pathway is upregulated in the confirmed *MabΔmtr* mutant. Log-phase bacteria were diluted to an OD₆₀₀ of 0.01 and incubated for 48h at 37°C before RNA was isolated. The RNA samples were examined by RT-qPCR after which mRNA expression of *mtr*, *mshA*, *mshB*, *mshC* and *mshD* was analyzed relative to the expression of the *rpoB* gene. **a)** Absence of *mtr* expression in the *MabΔmtr* confirmed successful development of a *mtr* knockout. **b)** Analysis of the mRNA expression of the MSH biosynthesis pathway genes *mshA*, *mshB*, *mshC* and *mshD*. A significant difference in relative expression between the WT and *MabΔmtr* was observed for the *mshB* gene alone meaning only part of the MSH biosynthesis pathway is upregulated when *mtr* is disabled. Results are shown as mean ± SEM from six independent experiments. Statistical significance was obtained with the Mann-Whitney test. *p < 0.05, **p < 0.01

Table VI.3. Overview of the additional mutations detected using WGS in *MabΔmtr* after transformation. As expected with every transformation, a few base pairs substitutions were detected in *MabΔmtr*, however, the biological relevance of these substitutions is not clear. The WT strain was used as reference.

Position	Mutation	Annotation	Gene	Description
378,895	G → T	V313L (<u>G</u> TG → <u>T</u> TG)	<i>glpK</i>	glycerol kinase GlpK
379,459	G → T	G501W (<u>G</u> GG → <u>T</u> GG)	<i>glpK</i>	glycerol kinase GlpK
678,272	C → G	T429S (<u>A</u> CC → <u>A</u> GC)	<i>MAB_RS03565</i>	HAMP domain-containing histidine kinase
936,703	deleted C	coding (1651/11094 nt)	<i>MAB_RS04905</i>	type I polyketide synthase
1,095,891	G → A	E138K (<u>G</u> AG → <u>A</u> AG)	<i>MAB_RS05625</i>	MspA family porin
3,708,848	deleted C	intergenic (-67/+52)	<i>MAB_RS18530</i> / <i>MAB_RS18535</i>	glycerol-3-phosphate dehydrogenase / oxidase / NAD(P)H-quinone dehydrogenase

Mab Δ *mtr* shows a decrease in the intracellular reduced thiol levels

To investigate whether knocking out *mtr* translates into a decrease in thiol levels, the intracellular reduced thiol levels were measured after lysis of the mycobacterial cell wall of cultures grown for 48h. It was observed in **Figure VI.3** that 100 μ l of the WT culture contained a total concentration of intracellular thiols of around 2100 nM. Moreover, *Mab* displayed a significant decrease of 1.9-fold in intracellular thiols after *mtr* is disabled.

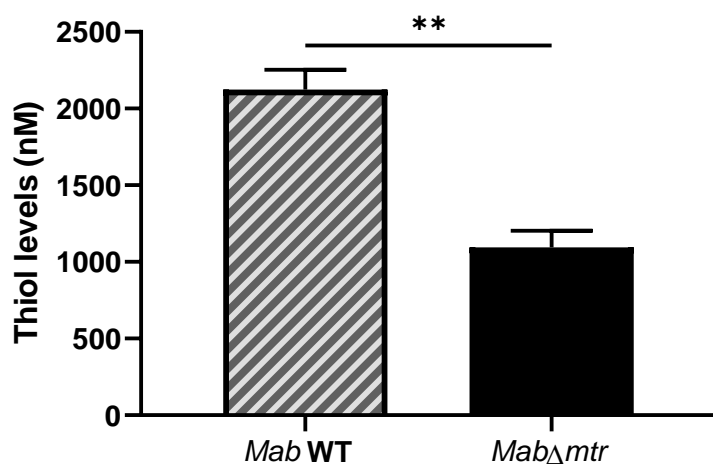


Figure VI.3. Intracellular reduced thiol levels are diminished in *Mab* Δ *mtr* mutant. The total intracellular reduced thiol levels were measured in the lysed *Mab* WT and *Mab* Δ *mtr* strains after growing for 48h. WT *Mab* culture presented intracellular thiol concentrations of around 2100 nM in a sample of 100 μ l. Additionally, a 1.9-fold decrease in intracellular thiols was detected after knocking out *mtr*. Results are shown as mean \pm SEM from three independent experiments. Statistical significance was obtained with the Mann-Whitney test. **p < 0.01

Knocking out mtr enables Mab to reach a higher plateau phase in a nutrient-poor medium

Since *Mab* can survive nutrient starvation for extended periods of time, bacterial growth of the WT and *Mab* Δ *mtr* mutant strains were assessed in a nutrient-rich and nutrient-poor medium, Middlebrook 7H9 broth and Sauton's medium, respectively. The strains were incubated starting from an OD₆₀₀ of 0.05 while shaking at 37°C and evaluated every 24h for their growth based on OD₆₀₀. When growing in a nutrient-rich medium, the absence of *mtr* expression had no effect on the growth of both strains. Surprisingly, a significant difference was observed in growth between WT *Mab* and *Mab* Δ *mtr* when growing in Sauton's medium with *Mab* Δ *mtr* reaching a higher plateau phase (**Figure VI.4a**). These observations were confirmed for both strains by CFU count while establishing that the mutation in *Mab* Δ *mtr* did not alter the CFU-OD₆₀₀ proportion of *Mab* in a nutrient-rich medium (**Figure VI.4b**).

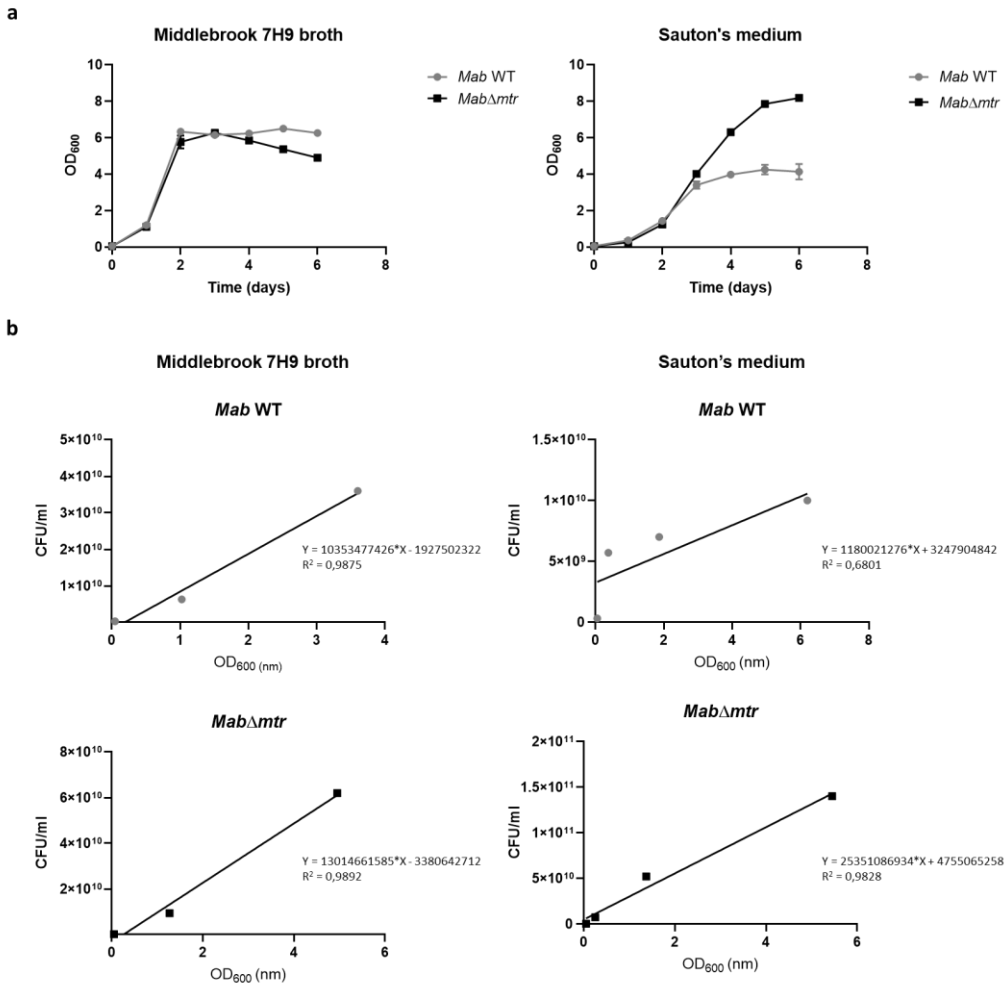


Figure VI.4. *Mab*Δ*mtr* mutant reaches higher plateau phase than *Mab* WT in a nutrient-poor medium. a) Growth curve of the WT and *Mab*Δ*mtr* mutant in Middlebrook 7H9 broth supplemented with 10% ADS, 0.2% glycerol and 0.05% tyloxapol and nutrient-poor medium Sauton supplemented with 2% glycerol and 0.05% tyloxapol shaking at 37°C. Before incubation, both strains were grown until their logarithmic phase and diluted in the corresponding medium to reach an OD₆₀₀ of 0.05. **b)** Measurement of the CFU-OD₆₀₀ proportion of the WT and *Mab*Δ*mtr* mutant in Middlebrook 7H9 broth supplemented with 10% ADS, 0.2% glycerol and 0.05% tyloxapol and nutrient-poor medium Sauton supplemented with 2% glycerol and 0.05% tyloxapol shaking at 37°C. Before incubation, both strains were diluted to an OD₆₀₀ of 0.05 in the corresponding medium. Results of (a) are shown as mean ± SEM from three independent experiments. A non-linear regression for Gompertz growth with least square fit was used to analyze the curves. Results of (b) are a representative of three independent experiments. A linear regression was used to analyze the curves. R² depicts the coefficient of determination.

MabΔmtr demonstrates fast reduction of ATP levels under oxidative stress conditions

When infecting a host, *Mab* is subjected to various types of endogenous and exogenous oxidative stress, including hydrogen peroxide (H_2O_2). Given the importance of Mtr in neutralizing this oxidative stress, both *Mab* WT and *MabΔmtr* strains were analyzed for their sensitivity against H_2O_2 in the nutrient-poor media Sauton. For this experiment, logarithmic-phase bacterial cultures were diluted to an OD_{600} of 0.05 followed by addition of 7.5 or 15 mM H_2O_2 to half of each culture and incubation while shaking at 37°C. After 0h, 4h, 8h and 24h of exposure, the ATP levels of the cultures were determined with the BacTiter-Glo™ kit as well as the viability of the strains by CFU count. It was observed in **Figure VI.5a** that *MabΔmtr* demonstrated lower ATP levels than the WT after 4h of exposure to 7.5 mM H_2O_2 . However, this reduction in ATP levels did not affect the CFU. After exposure to 15 mM H_2O_2 , the ATP levels of the mutant strain were lower than that of the WT after 4h and 8h after exposure to 15 mM H_2O_2 . Furthermore, a faster decay of ATP levels was perceived over time in *MabΔmtr* compared to the WT after H_2O_2 was added, corresponding to a reduction in the metabolic activity. This lower metabolic state of the *MabΔmtr* mutant strain had no effect on the viability of the strain (**Figure VI.5b**).

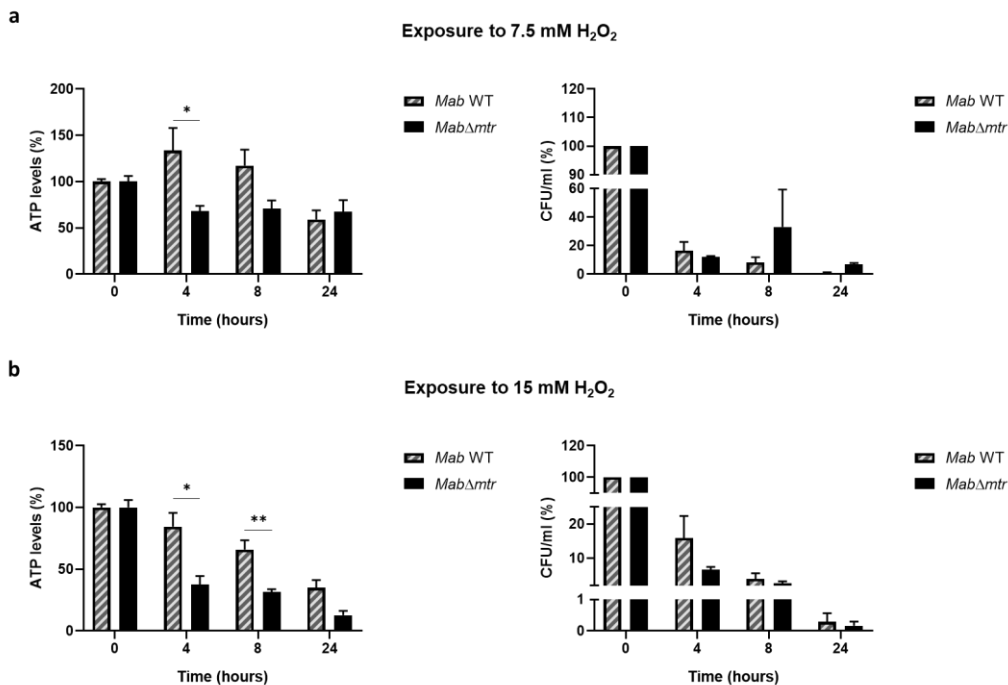


Figure VI.5. A fast reduction of ATP levels is observed in *MabΔmtr* after exposure to oxidative stress. As Mtr plays a key role in the protection mechanism of *Mab* against oxidative stress, both WT and *MabΔmtr* were exposed to 7.5 (a) or 15 mM (b) H₂O₂. After 0, 4, 8 and 24h of exposure, the ATP levels and viability of the strains were assessed. Results are shown as mean ± SEM from three independent experiments after normalization of the results collected after addition of 7.5 mM or 15 mM H₂O₂ relative to results acquired when no H₂O₂ was added to the cultures. Hereby, the cultures to which no H₂O₂ was added were displayed as 100% to enable the results to demonstrate the extent of change in ATP levels or CFU in % after the addition of H₂O₂ to each strain. Statistical significance was obtained with the Mann-Whitney test followed by correction for multiple testing. To analyze the decay of ATP or CFU/ml for each strain, a non-linear regression for a one phase decay with least square fit was used. *p < 0.05, **p < 0.01

The absence of mtr causes Mab to be more susceptible to bedaquiline

To further evaluate whether *MabΔmtr* is more susceptible to oxidative stress and reduced ATP levels, the strains were subjected to anti-mycobacterial compounds known to target the ATP synthase (bedaquiline), generate ROS (clofazimine) or target DNA replication (moxifloxacin) (219). For this purpose, logarithmic-phase

Mab WT and *MabΔmtr* were incubated at an OD₆₀₀ of 0.05 after which the compounds were added in a one-over-three dilution. Out of all compounds, bedaquiline generated the greatest shift in the susceptibility of the strains with *MabΔmtr* displaying a 5.1-fold reduction in IC₅₀ and a 39.5-fold reduction in IC₉₀ compared to the WT (**Table VI.4**). Moreover, a 2.4-fold decline of the IC₉₀ was observed in the *MabΔmtr* mutant when treated with moxifloxacin. Curiously, the activity of clofazimine remained unaltered after disabling *mtr*.

Table VI.4. A higher susceptibility to bedaquiline is obtained when *Mab* lacks *mtr*. A panel of three anti-mycobacterial drugs was selected targeting the ATP-synthase, generating oxidative stress or targeting the DNA replication; bedaquiline, clofazimine and moxifloxacin respectively. The compounds were added in a one-over-three dilution to WT and *MabΔmtr* cultures set at an OD₆₀₀ of 0.05. The results showed a considerable shift in the susceptibility of *MabΔmtr* compared to *Mab* WT when subjected to bedaquiline, demonstrating a 5.1-fold reduction in IC₅₀ and a 39.5-fold reduction in IC₉₀. Moxifloxacin demonstrated a higher activity against *MabΔmtr* as well with a 2.4-fold decrease in IC₉₀. However, no difference in activity was detected when clofazimine was added to the strains, further confirming that oxidative stress does not lead to a reduction in viability of *MabΔmtr*.

Results are expressed as the average of three individual experiments ± SD with $SD = \sqrt{\frac{\sum(x_i - \bar{x})^2}{n-1}}$. The IC₅₀ and IC₉₀ of each individual experiment was calculated using the GraphPad software 8.0.

	<i>Mab</i> WT		<i>MabΔmtr</i>	
	IC ₅₀ (μM)	IC ₉₀ (μM)	IC ₅₀ (μM)	IC ₉₀ (μM)
Bedaquiline	0,51 ± 0,33	9,08 ± 3,16	0,10 ± 0,05	0,23 ± 0,10
Clofazimine	4,36 ± 0,34	6,91 ± 1,75	3,28 ± 0,74	7,97 ± 0,80
Moxifloxacin	1,74 ± 0,36	4,97 ± 1,28	1,14 ± 0,21	2,05 ± 0,63

MabΔmtr lacks the ability to proliferate inside macrophages

Macrophages are natural host-cells of *Mab* during infection (212). Therefore, intracellular proliferation of both strains was characterized by setting up an *in vitro* macrophage assay in which RAW 264.7 macrophages were infected with an MOI of 5 with either *Mab* WT or *MabΔmtr*. After infection, part of the macrophages were lysed directly to evaluate the actual infection while the remaining

macrophages were lysed after 24h to determine the extent of intracellular replication. As displayed in **Figure VI.6**, a significant increase in proliferation of the WT inside macrophages was detected over time while *MabΔmtr* was not able to proliferate inside the macrophages after 24h. No difference was observed in the initial infection with the WT or *MabΔmtr*.

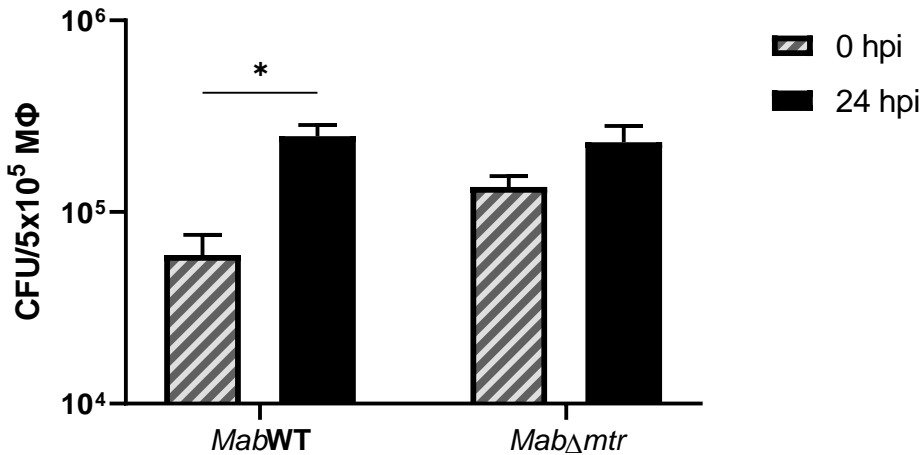


Figure VI.6. No proliferation of *MabΔmtr* is observed intracellularly. RAW 264.7 macrophages were infected with *Mab* WT and *MabΔmtr* at an MOI of 5 and were lysed at 0 and 24 hours post-infection (hpi) to determine the intracellular survival and replication. At 0 hpi, no difference was observed in the intracellular CFU of macrophages infected with either *Mab* WT or *MabΔmtr*. The intracellular replication of the WT strain showed a significant increase after 24h while *MabΔmtr* failed to proliferate. Results are shown as mean ± SEM from three independent experiments and each independent experiment was performed in duplicates. Statistical significance was obtained with the Mann-Whitney test followed by correction for multiple testing. *p < 0.05

Knocking out mtr inhibits proliferation of Mab inside G. mellonella larvae

To further unravel the role of Mtr during *Mab* infection, *G. mellonella* larvae were used as an *in vivo* infection model for *Mab*. Each larva was infected with 5x10³ bacteria with either WT or *MabΔmtr* and kept at 37°C. Eight to ten larvae per condition were sacrificed on day 2, 4 and 6 after infection to assess the bacterial

load in each larva by CFU count. In parallel, a total of 90 larvae injected with each strain and an additional 50 larvae injected with PBS received a dead-or-alive score every 24h to define whether infection with the different strains affect the survival of the larvae. The results indicate that larvae infected with the WT showed a significant higher CFU count compared to the *MabΔmtr* mutant strain at each timepoint after infection (**Figure VI.7a**). Furthermore, while WT *Mab* was able to proliferate inside the larvae over time, proliferation of *MabΔmtr* over time was absent (**Figure VI.7b**). However, the differential ability of both strains to proliferate within the larvae did not affect the survival of the larvae (**Figure VI.7c**). Neither was a difference observed in the survival between the larvae infected with the WT, *MabΔmtr* mutant and PBS.

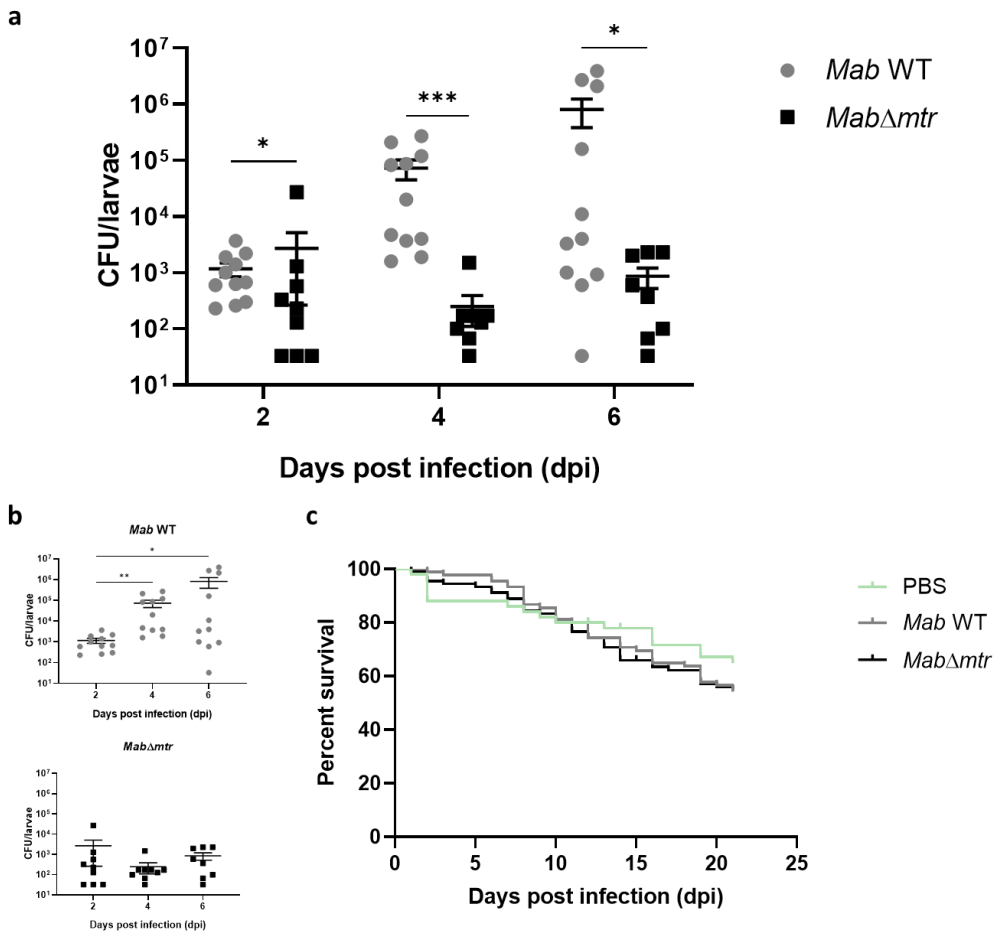


Figure VI.7. *Mab*Δ*mtr* has a reduced ability to proliferate inside *G. mellonella* larvae. *Mab* WT and *Mab*Δ*mtr* were used to infect *G. mellonella* larvae with 5×10^3 bacteria per larva. The larvae were incubated at 37°C until 8 to 10 larvae per condition were sacrificed 2, 4 and 6 days after infection and the CFU count was assessed to ascertain the internal bacterial load (**a** and **b**). In parallel, 90 larvae were infected with each strain to investigate whether the different strains influence the survival of the larvae (**c**). 50 larvae were injected with PBS as a control. Survival of the larvae was determined by a dead-or-alive score every 24h. Results are shown as mean \pm SEM from two independent experiments. Statistical significance was obtained with the Mann-Whitney test followed by correction for multiple testing or by performing a survival analysis with Log-rank (Mantel-Cox) test. * $p < 0.05$, *** $p < 0.001$

Biofilm area of Mab is decreased in MabΔmtr

As biofilm formation plays an important role in infection progression and persistence, biofilm formation was compared between *Mab* WT and *MabΔmtr*. To generate biofilms, 5μL of each strain at an OD₆₀₀ of 0.2 was spotted onto a polycarbonate membrane present on an agar plate and incubated at 37°C in the presence of 5% CO₂. Every 24h, the biofilms were assessed based on their bacterial load, area and visual characteristics. **Figure VI.8a** demonstrated that knocking out *mtr* did not lead to a difference in bacterial load of the individual biofilms at each timepoint. Surprisingly, despite not showing any difference in CFU, *MabΔmtr* biofilms had a reduced area compared to biofilms generated by WT *Mab* after 96h of biofilm formation (**Figure VI.8b**). It was observed that biofilms can grow either in height or in width, leading to the area differences obtained between both strains, without it affecting the bacterial load. Moreover, *MabΔmtr* biofilms appeared to have a smoother phenotype in comparison to WT biofilms (**Figure VI.8c**).

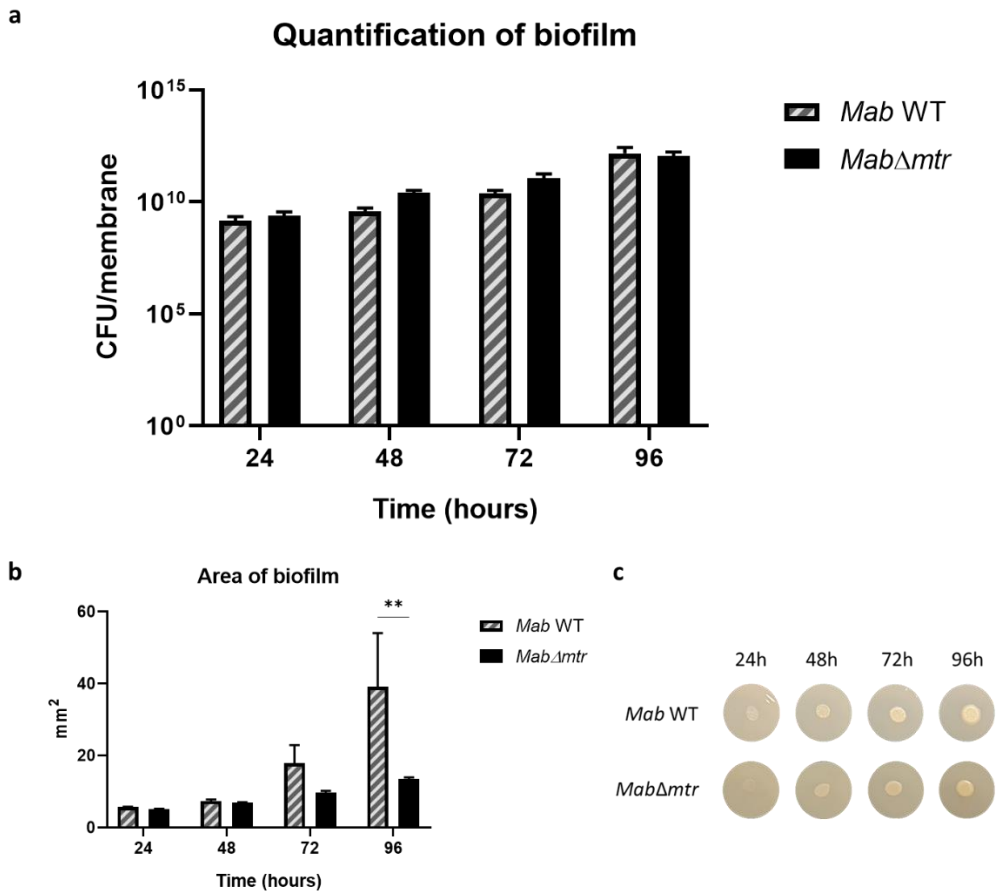


Figure VI.8. *Mab*Δ*mtr* displays a decrease in biofilm area compared to the WT. 5 μ l of *Mab* WT or *Mab*Δ*mtr* was spotted at an OD₆₀₀ of 0.2 on a polycarbonate membrane present on an agar plate and incubated at 37°C in the presence of 5% CO₂. Next, biofilms were assessed every 24h based on their bacterial load, area and visual characteristics. **a)** Bacterial load of the formed biofilms remained unaltered after knocking out *mtr*. **b)** The area of *Mab*Δ*mtr* biofilms was significantly reduced after 96h of biofilm formation. **c)** Biofilm formation results revealed that *Mab*Δ*mtr* biofilms have a smoother phenotype compared to *Mab* WT biofilms. Results are shown as mean \pm SEM from three independent experiments. Statistical significance was obtained with the Mann-Whitney test followed by correction for multiple testing. Images of the biofilms represent one of three independent repeats. ** $p < 0.01$

VI.5 Discussion

MABC outbreaks and nosocomial transmissions are rising worldwide, leading to a serious public health problem (35). Unfortunately, the current treatment of MABC infections is very limited due to the extensive drug resistant profile of this pathogen. As a result, treating these infections requires a lengthy and complex treatment which is frequently characterized by high failure rates, serious adverse drug effects and acquired drug resistance (13, 38, 50). Hence, there is an urgent need for novel mycobacterial drug targets and treatment options.

Mycobacteria are constantly exposed to endogenous and exogenous oxidative stress stimuli when infecting a host (88, 104, 166). They are described to be highly sensitive to oxidative stress (169, 220) but are able to neutralize most of it inside a host by means of MSH and other pathways (164). Several studies have already highlighted the importance of MSH together with its biosynthesis and recycling pathway and presented them as potential drug targets in *Mtb*, *Msm* and *M. intracellulare* (100, 220–222). Coulson et al. demonstrated that the growth of *Mtb* is inhibited when the MSH biosynthesis and MSH-dependent detoxification is lost (169). This role of MSH and MSH-dependent enzymes as protectors against oxidative and acidic stress was also confirmed in *Msm* (167, 168). Moreover, *Msm* deficient of MSH showed a lower survival and higher sensitivity to H₂O₂ (223). This study is the first to examine the direct role of the MSH-recycling enzyme, Mtr, on the survival of *Mab* *in vitro* and *in vivo*, and after exposure to oxidative stress. To obtain these results, a novel *Mab mtr* knockout mutant, *MabΔmtr*, was generated. The findings presented in this paper illustrate that *mtr* plays a role in the proliferation of *Mab* during macrophage and *G. mellonella* infection in which *Mab* missing *mtr* lacked the ability to proliferate inside both macrophages or larvae (**Figure VI.6 and VI.7**). Surprisingly, unlike MSH-deficient *Msm* being more sensitive to H₂O₂ (223), exposure of the *Mab* mutant to H₂O₂ lowered the metabolic state of the bacteria but did not affect its viability (**Figure VI.5a and b**).

Figure VI.2b demonstrated that one gene of the MSH biosynthesis, i.e. *mshB*, was upregulated when *mtr* was disabled in *Mab*. This may ensure the production of

more MSH and indicates the possibility of a compensation mechanism within *Mab* to keep the internal MSH levels stable when the MSH recycling pathway is lost. On the other hand, other components might also play a role in a possible compensation mechanism. It was established by Ta et al. that MshA-deficient *Msm* compensate for the loss of MSH by overexpressing an organic hydroperoxide resistance protein (Ohr) and ergothioneine (ESH) (107, 224). However, we also illustrated that *MabΔmtr* showed a decrease in the overall levels of the intracellular reduced thiol (**Figure VI.3**). Since this test does not give us more information about the levels of each individual thiol, a compensation mechanism could still be present in some manner which fails to fully compensate for the reduced MSH levels after knocking out *mtr*. Therefore, further research, including measurement of the internal MSH, ESH and Ohr levels, is necessary to unravel the possibility of a compensation mechanism in the *MabΔmtr* and to determine if *mshB*-upregulation is part of that compensation mechanism.

Another interesting discovery is the increased sensitivity of *MabΔmtr* to the anti-mycobacterial drugs bedaquiline and moxifloxacin *in vitro* (**Table VI.4**). The sensitivity of the *MabΔmtr* mutant to bedaquiline demonstrated a large shift, establishing a 5.1-fold reduction in IC₅₀ and a 39.5-fold reduction in IC₉₀ compared to WT *Mab*. This implies the possibility of a synergistic effect between Mtr-targeting drugs and bedaquiline. Bedaquiline, an inhibitor of the ATP-synthase, has been suggested as a potential drug for treatment of *Mab* infections (225) and has been proven to rapidly deplete ATP in the bacteria (226). Furthermore, the ATP synthase is reported to be essential for mycobacteria, likely due to the essentiality of ATP (227). As a result, combining bedaquiline and a drug targeting Mtr during *Mab* infection could lead to an even higher depletion of bacterial ATP levels as a faster and greater reduction of ATP is perceived in the *MabΔmtr* mutant when exposed to oxidative stress (**Figure VI.5a**). The same reason as for the higher sensitivity of *MabΔmtr* to bedaquiline might be presented for moxifloxacin since it inhibits the DNA replication by inhibiting DNA gyrase, an enzyme that works in an ATP-dependent manner (228). By inhibiting *mtr* as well

as DNA gyrase, less ATP becomes available to DNA gyrase that is already being mostly inhibited by moxifloxacin, hereby reinforcing the inhibition of the DNA replication.

Moreover, it has been recently demonstrated that biofilm formation may contribute to the persistent characteristics of *Mab* during pulmonary infection and leads to a decreased susceptibility to some first-line anti-mycobacterial drugs. Furthermore, biofilms formed by R colony types display a higher mechanical resistance than biofilms formed by S colony types (37, 229). Our results illustrated a shift from a rough-like biofilm to a more smooth-like biofilm after disabling *mtr* (**Figure VI.8c**). This finding indicates that biofilms formed by *Mab* Δ *mtr* may possibly be less resistant against mechanical stress factors (230). Therefore, targeting Mtr in *Mab* biofilms may improve cleaning procedures in an industrial or healthcare setting in order to clear the biofilms. However, additional experiments need to be performed to confirm this hypothesis.

Unlike *mtr*, any attempts in generating an *mshC* mutant in *Mab* by utilizing the ORBIT system were unsuccessful, hereby failing to generate colonies after transformation (**Figure VI.1**). Rock lab predicted that knocking out *mshC* in *Mab* would lead to a growth defect (159), possibly explaining the difficulties encountered when creating an *mshC* knockout. Accordingly, more attempts in creating an *mshC* knockout strain should be made as MshC may be a great potential target to fight off *Mab* infections.

As a conclusion, our findings suggest that Mtr plays a role in the proliferation of *Mab* during infection and support the hypothesis of Mtr being a possible target for anti-mycobacterial drugs. These findings were possible because of the generation of a novel *Mab* Δ *mtr* strain that will facilitate future research regarding the MSH biosynthesis and recycling pathway in *Mab*. Additionally, our results suggest the potential activation of a partial compensation mechanism in *Mab* when the MSH recycling pathway is disabled. Additionally, promising results were demonstrated regarding the use of a combined therapy including an anti-Mtr drug and

Chapter VI

bedaquiline, as *Mab* lacking *mtr* becomes more sensitive after exposure to bedaquiline *in vitro*. Finally, this study suggests the possibility that biofilms formed after disabling *mtr* may be less resistant to mechanical stress factors, which could improve the removal of biofilms in an industrial or healthcare setting.

CHAPTER VII

Discussion and Summary



VII. Discussion and Summary

VII.1 General discussion

In most cases, MABC disease remains untreatable. This is mainly due to the lack of an optimal treatment regimen together with the highly resistant nature of MABC, limiting the availability of antibiotics (35, 47). Treatment of MABC includes a long, multidrug therapy with a high probability of serious adverse drug effects and a success rate of less than 50%, leading to patient-noncompliance, relapse, and further development and spread of drug-resistant MABC (45, 47, 50, 63). Given these shortcomings and the fact that MABC infections are rising worldwide (28), there is an urgent need for the discovery of novel anti-mycobacterials that can shorten the treatment, reduce the adverse drug effects and prevent additional development of drug resistance. Nevertheless, development of novel anti-mycobacterials remains challenging due to the unique properties of mycobacteria. First, the unique and thick mycobacterial cell wall acts as a barrier that prevents the penetration of antibiotics. Secondly, the ability of mycobacteria to survive in different environments requires anti-mycobacterials to be active under various conditions. Finally the slow growth rate of mycobacteria decreases their susceptibility towards antibiotics (77, 231, 232). MABC belongs to the RGM, however, even compared to most other bacteria, RGM are still slow growing since their doubling time in a laboratory setting is higher than most bacteria (233–235).

An interesting novel target for the development of anti-mycobacterials is the MSH biosynthesis and recycling pathway. The primary function of this pathway is the detoxification of reactive intermediates originating from the host's immune system or the bacterial anaerobic respiration (88, 89). My PhD research employed a target-based approach for the investigation of Mtr and MshC, i.e. key enzymes of the MSH biosynthesis and recycling pathway, as potential novel targets for anti-MABC drugs. As part of a target-based approach, various genetic engineering tools were used to manipulate the mycobacterial genome, including L5 integration,

Chapter VII

CRISPRi, the p2NIL/pGOAL method and the ORBIT system. These tools were utilized to create *mtr* and *mshC* overexpressing strains to learn more about the function of these genes and their protective capacity (**Chapter III**), create *mtr* and *mshC* knockdown and knockout strains to assess the essentiality of these genes for bacterial survival, i.e. essential, conditionally essential or nonessential (**Chapters IV, V and VI**), and use the constructed *mtr* knockout strain to evaluate Mtr as a potential target for novel anti-mycobacterial drugs (**Chapter VI**)(**Figure VII.1**).

This chapter will discuss aspects of this thesis in a broader perspective to aim at better understanding the use of a target-based approach for the discovery and validation of novel targets in *Mab* as well as improving treatment of MABC infections.

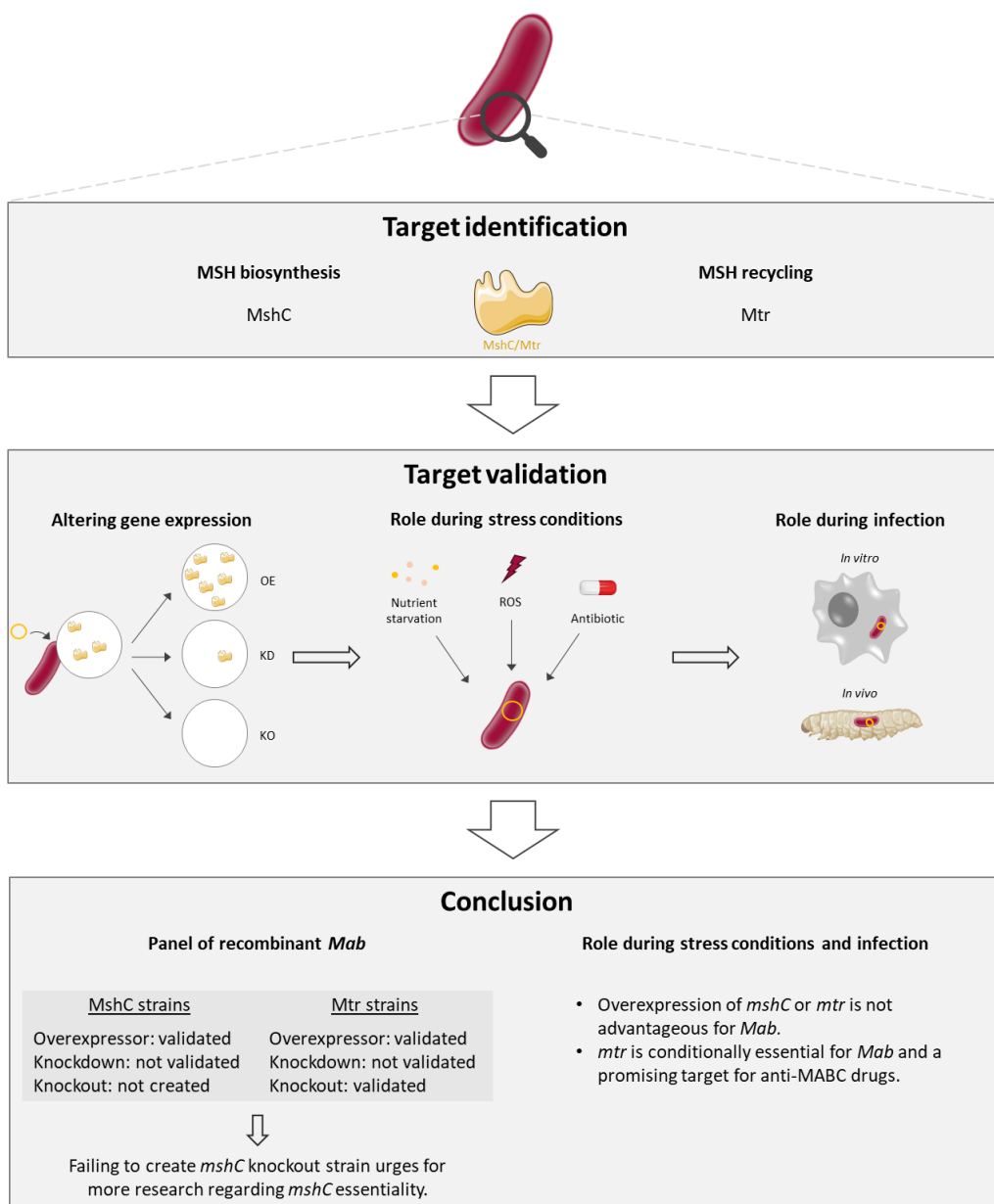


Figure VII.1. Overview of the mode of action and results of this thesis. This thesis followed a target-based drug discovery approach in which MshC and Mtr were identified as potential drug targets. Validation of these targets encompassed the creation of differentially-expressed strains and investigation of these strains during stress conditions and infection. Designed with PowerPoint, some images from Servier Medical Art and Biorender. OE: overexpressor, KD: knockdown, KO: knockout

VII.1.1 Using a target-based approach for anti-mycobacterial drug discovery

Target-based drug discovery is characterized by the selection of a drug target as a starting point for the development of novel therapeutics (236). The drug target is usually a single gene or gene product that is identified on the basis of biological observations and is considered a good target when disturbing the target leads to a significant therapeutic effect (237). During drug discovery, the identification of a target is of utmost importance as the absence of a known target can be challenging for optimizing compounds. Additionally, a target-based drug approach is often more efficient, easier to execute, faster, and less costly than other approaches. Furthermore, the use of a target-based approach for drug discovery has been highly successful in the past where 70% of the first-in-class drugs approved by the US FDA between 1999 and 2013 were identified by this approach (124, 174). This type of drug discovery has been favorable for various diseases, especially viral and non-communicable diseases, however, has not been very successful for bacterial infectious diseases, including mycobacterial diseases (238). While this approach has been widely used to successfully validate several mycobacterial targets, it failed to produce a single effective anti-mycobacterial drug (239, 240). This outcome can be the cause of several factors: i) the low number of druggable targets available, ii) the target develops resistance too quickly, iii) failing to translate cell-free assay activity to whole-cell activity, iv) the high levels of cytotoxicity of the obtained molecules, v) unavailability of specific inhibitors for a certain target and, vi) identifying lead compounds as non-specific inhibitors (73, 76, 231, 239).

Over the recent years, mycobacterial drug discovery has shifted to a phenotypic-based approach (231). In comparison to a target-based approach, a phenotypic-based approach showed to be much more promising regarding the discovery of anti-mycobacterials (76). Hereby, most currently used anti-mycobacterial drugs originate from a phenotypic-based drug discovery approach, including the four main used anti-TB drugs (ethambutol, isoniazid, pyrazinamide and rifampicin), some second-line anti-TB drugs or anti-MABC drugs (linezolid and clofazimine),

and new anti-TB drugs (delamanid, pretomanid and bedaquiline) (231, 239, 241). The favorable outcome of a phenotypic-based approach is mainly attributed to the use of a whole-cell screen involving intact pathogens, increasing the translatability (76, 232). The main advantages of working with a whole-cell screen is that no insight is required on the mode of action of a compound and a compound identified by a whole-cell screen undoubtedly displays the required cell-permeability (239). Furthermore, it enables researchers to include the screen of complex biological mechanisms, hereby identifying drugs and targets that would otherwise not be discovered (72, 242). However, a phenotypic-based approach also presents many disadvantages, such as an increased risk of rediscovering known inhibitor classes due to the limited chemical diversity used in the screening libraries (239). Moreover, target identification is not always possible and lead optimization can be difficult in the absence of known structural data for the target (239, 242). Another disadvantage of this approach is that it is slower and more costly than a target-based approach, with the hit rate of *Mab* screens being even slower than the ones obtained for *Mtb* screens (232, 243). Finally, a phenotypic-based approach gravitates towards the repeated discovery of inhibitors of promiscuous targets, i.e. targets that repeatedly show up in screens, instead of discovering compounds with novel targets and mode of action that aid in the avoidance of the further development of drug resistance (239).

Consequently, as both a target-based and phenotypic-based approach demonstrate various disadvantages, innovative strategies are being developed and employed that combine the two approaches. By combining both approaches, the advantages of the approaches are combined as well whereas the disadvantageous are outbalanced, leading to the accelerated discovery of novel anti-mycobacterials (73, 239). An example of such approach is using a target-based whole cell phenotypic high-throughput screen (HTS) in which a target gene is overexpressed and used to screen compound libraries. Hereby, increased resistance to a compound will indicate target involvement (73).

Besides target- and phenotypic-based drug discovery, artificial intelligence (AI)-integrated drug discovery has been emerging over the recent years aiding the acceleration of drug discovery. This type of drug discovery uses machine learning and AI as new tools and can be applied in different parts of the drug discovery process, including target identification and validation, drug design, polypharmacology, chemical synthesis, drug screening and drug repurposing. The applications of AI in these processes are diverse and can range from predicting the 3D structure of a target protein to predicting the bioactivity and toxicity of a novel drug, rendering drug discovery faster and cheaper (244, 245). Hereby, AI-integrated drug discovery has already led to the discovery of a novel narrow-spectrum antibiotic called aubacin and the identification of novel inhibitors against essential targets in *Mtb* (246).

VII.1.2 Mtr and MshC as potential drug targets

Investigating novel mycobacterial drug targets is of great interest to improve treatment of MABC infections and intercept the continuously rising resistance to anti-mycobacterials. To validate novel drug targets, the targets are studied based on their uniqueness, essentiality, 'druggability' and the possibility of conferring a synergistic effect with other anti-mycobacterials when being inhibited.

Uniqueness

The current treatment of MABC disease is far from optimal and produces many adverse drug effects, mainly due to antibiotic-related toxicity (45, 64). To increase drug efficiency and lower drug toxicity, it is important to have a drug that selectively targets the gene or gene product of interest (247). Hereby, as a gene or gene product is present in the pathogen but absent in the host, there are lower chances of encountering adverse drug effects during treatment. MSH and the MSH-dependent enzymes are highly specific components as they are only found in *Actinomyces* (248). The human-analog of MSH, GSH, is a protein with a similar function but which is not found in mycobacteria (249, 250). Although MSH and GSH exert a similar function, they possess certain differences; while GSH is a tripeptide of gamma-glutamyl-cysteinylglycine, MSH is a cysteinyl pseudo-disaccharide (101, 102). Additionally, GSH biosynthesis involves only two enzymes while MSH biosynthesis involves five (251, 252). Finally, a research conducted at the Colorado State University demonstrated that Mtr is not activated by the presence of glutathione in any detectable manner (253).

Essentiality

Essential genes or gene products are generally the focus for the development of novel anti-mycobacterials since their inhibition interrupts pathogen activity or mediates pathogen clearance, hereby limiting the damage caused by the pathogen

(75, 118). However, a gene can also be conditionally essential, in which these are essential only in certain growth conditions (78). The best way to determine the essentiality of a target is with the help of genetic engineering. Genetic engineering methods are used to manipulate the mycobacterial genome and generate strains characterized by the overexpression, knockdown or knockout of the gene of interest (118). During my PhD, the ORBIT system was implemented to generate *Mab* Δ *mtr* (**Figure VI.1**), a *Mab* strain lacking the expression of *mtr* (**Figure VI.2**). Since knockout mutants of genes essential for the survival are not viable (119), we can conclude that *mtr* is not essential for the overall survival of *Mab*. Next, further investigation aimed at determining whether *mtr* is conditionally essential for *Mab* during stress conditions and infection. We identified that *Mab* Δ *mtr* demonstrated lower levels of ATP compared to WT *Mab* after 4h of exposure to 7.5 mM H₂O₂ and after 4h and 8h of exposure to 15 mM H₂O₂, lowering the metabolic state of *Mab* (**Figure VI.5**). Furthermore, knocking out *mtr* affected the proliferation of *Mab* during infection in both macrophages and *G. mellonella* larvae (**Figure VI.6 and 7**). This indicates that although not essential for the overall survival of *Mab*, *mtr* is conditionally essential for the proliferation of *Mab* during stress conditions and infection of a host.

Together with the generation of a *mtr* knockout strain, many unsuccessful attempts have been conducted in the desire of creating an *mshC* knockout strain as well in both *Mab* and *Msm* (**Figure V.4 and VI.1**). This inability may imply that *mshC* is essential for the overall survival of *Mab* and *Msm*, making it an interesting target for anti-mycobacterial drugs. However, predictions made by a laboratory from Rockefeller University, Rock lab, state that inhibiting *mshC* in *Mab* will lead to growth deficiency but not complete growth impairment (94, 159). Furthermore, Xu et al. created a viable *mshC* knockout in *Msm* through allelic exchange using specialized transduction (207). Therefore, more research is required to determine the degree of essentiality of *mshC*. The generation of a complementary strain may facilitate further study of essentiality of *mshC*.

Druggability

A 'druggable' target is a target of which the activity can be modulated by a drug. The most used method to evaluate the druggability of a protein is by exploring the 3D-structure of that protein (254). After obtaining the 3D-structure, *in silico* models can be used to estimate an important parameter to define druggability, i.e. the likelihood that a target can bind a drug-like molecule with a high affinity (255, 256). The 3D-structure of MshC was previously determined by Tremblay et al. and Pang et al. in *Msm* and was labeled as a druggable target in *Mtb* (100, 109, 114). However, the 3D-structure and druggability of both enzymes are yet to be determined for *Mab*.

Synergy

To reduce the length and improve the efficiency of MABC treatment, two drugs can be given together during treatment that work in a synergistic manner. A synergistic effect is obtained when the acquired combined effect of both drugs is greater than the expected combined effect (257). In our study, we illustrate a shift in susceptibility of *Mab* to certain anti-mycobacterials after removing *mtr* expression (**Table VI.4**). Here we show that when *Mab* Δ *mtr* is exposed to bedaquiline, it demonstrates a 5.1-fold reduction in IC₅₀ and a 39.5-fold reduction in IC₉₀ compared to WT *Mab*. This suggests the possibility of a synergistic effect between Mtr-targeting drugs and bedaquiline.

VII.2 Future perspectives

This PhD uses a target-based approach to characterize Mtr and MshC in *Mab* and determine whether these are potential targets for novel anti-mycobacterial drugs. While the results obtained suggest that Mtr is a promising target for anti-mycobacterial drugs, further characterization and validation is needed before fully confirming Mtr as a suitable novel target. MshC on the other hand, has not been thoroughly characterized yet as any attempt in generating a knockout strain failed, raising questions about the essentiality of *mshC* in *Mab*. Finally, the exploitation of other future research options beyond targeting only Mtr or MshC are also being discussed.

Mtr

To further characterize and validate Mtr as a novel drug target, several additional experiments can be conducted. First, as Mtr is involved in the pathway that protects *Mab* against oxidative stress, the effect of Mtr inhibition after exposure to ROS can be elaborated to other types of ROS as well, i.e. hydroxyl and superoxide radicals. Furthermore, measuring the difference in ROS levels between *Mab* Δ *mtr* and *Mab* WT after ROS exposure can give us valuable information regarding the role of Mtr in the neutralization of ROS. Next, to increase the clinical relevance of this research and discover more potential synergism, the impact of the mutation can be tested on a broader panel of drugs or the whole panel of drugs used in the RAPMYCOI susceptibility test. The latter is intended for susceptibility testing of clinical isolates of rapidly-growing mycobacteria which is used to assist in the decision of the potential treatment options (258). Moreover, the infection and proliferation ability of *Mab* Δ *mtr* can also be tested in other *in vivo* models, including the nonmammalian zebrafish model (*Danio rerio*) and the mammalian mice model. The proposed zebrafish model for *Mab* can be utilized for the imaging and monitoring of *Mab* infection and establishment of the effect of a drug. In this model, zebrafish larvae are infected by a microinjection into the caudal vein and

exposed to water in a 96-well plate that contains a drug. In mice, *Mab* is rapidly cleared after infection, limiting the use of this model for drug discovery. However, severely immunocompromised mice with multiple deficits in innate and acquired immunity have been used to obtain a severe progression of *Mab* infection that resembles human NTM lung disease (259).

After complete validation of Mtr, the next steps of a target-based approach can be applied (**Figure I.9**). First, *in silico* virtual screening can be implemented to test a great quantity of compounds against Mtr *in silico*, enabling the selection of potential compounds. Then, Mtr can be expressed in predefined expression system, such as *E. coli*, and purified to exploit the enzyme's kinetics and 3D crystal structure (crystallography) (76)(Oorst et al., manuscript in preparation). The 3D crystal structure of Mtr will facilitate the determination of its druggability together with the design and development of anti-Mtr drugs (260, 261). Finally, HTS methods, including *in vitro* inhibition assays and whole-cell screens testing synthesized compounds, can be executed to identify hits and optimize lead compounds (76, 262–265).

MshC

Since generating an *mshC* knockout strain in *Mab* was unsuccessful, alternatives need to be implemented to determine whether *mshC* is essential for *Mab* and possibly a novel target for anti-mycobacterials. An option to address this is to try generating a knockout strain using a different genetic manipulation system, such as CRISPR-Cas9. Additionally, assuming *mshC* may be essential, the best approach is to generate a knockout starting from a complementary strain. By using an inducible promoter on the second copy, the WT gene can be knocked out while still expressing the gene of interest. Once the WT gene is knocked out, expression of the second copy can be halted which will give us more information about whether *mshC* is essential for the overall survival of *Mab* in normal conditions.

Other options

The MSH biosynthesis and recycling pathway is a process involving six different enzymes: MshA, MshA2, MshB, MshC, MshD and Mtr. While Mtr and MshC perform important steps of the pathway and were selected as potential targets for novel anti-mycobacterials, this study can be elaborated to the investigation of the other enzymes of the pathway as well. Many studies have already cited the importance of MshA, MshB and MshD for the survival of *Mtb* under oxidative stress conditions (94, 164, 266, 267). Moreover, eliminating only one component of the pathway may not be enough to induce a large effect on the survival of *Mab*, whereas targeting two or more components at the same time may work synergistically, especially when combining the inhibition of both the MSH biosynthesis and recycling pathway.

VII.3 Conclusion

Altogether, although many advances have been made in the recent years regarding the genetic engineering of mycobacteria, a target-based approach remains a challenging method for the discovery of novel anti-mycobacterials. Therefore, a more suitable approach would be to use a combined target-based and phenotypic-based approach to alleviate the disadvantages of both approaches. By following a target-based approach to validate a target with the available genetic engineering tools, our findings conclude that Mtr alone does not present the qualities needed to be a good target for novel anti-mycobacterial drugs, since it is only conditionally essential. However, as MABC treatment always requires a multidrug therapy and our results indicated that the inhibition of *mtr* may work synergistically with other anti-MABC drugs, Mtr is in fact a promising target in combination with other anti-MABC drugs.

VII.4 Summary

Mycobacterium abscessus complex (MABC) is the most common rapidly-growing nontuberculous mycobacteria (NTM) species causing disease in human, predominantly immunocompromised patients or patients with a preexisting lung condition. The incidence of MABC infections have been rising worldwide over the last decades and in most cases, MABC disease remains untreatable due to the absence of an optimal treatment and the highly resistant nature of MABC. Treatment of MABC consists of a long, multidrug therapy characterized by serious adverse drug effects and a success rate of only 45.6%. These treatment shortcomings urge for the discovery of novel anti-mycobacterial drugs and drug targets capable of reducing the adverse drug effects of the treatment, shortening the treatment and preventing further development of drug resistance. During this PhD, mycothione reductase (Mtr) and cysteine ligase (MshC), two key enzymes of the mycothiol (MSH) biosynthesis and recycling pathway, were selected as promising novel targets since this pathway is essential for the detoxification of harmful reactive intermediates (**Chapter I**). While the main objective of this thesis was to investigate Mtr and MshC as potential novel targets, three sub-objectives were applied.

The **first aim** of this thesis was to create a panel of recombinant *Mab* strains having a differential expression of *mtr* or *mshC*, i.e. overexpressing, knockdown and knockout strains. First, using the pMV306 vector to incorporate an extra copy of the genes into the L5 site of the bacterial genome, *Mab* overexpressing *mtr* or *mshC*, i.e. *Mab::mtr* or *Mab::mshC* respectively, was successfully created and validated (**Chapter III**). Next, the *Streptococcus thermophilus* CRISPRi-system was implemented to produce *mtr* and *mshC* knockdown strains in *Mab*. While integration of the CRISPRi-plasmids was successful at first, some of the generated strains lost the integrated plasmids over time, making this system unstable and unreliable for our research (**Chapter IV**). Finally, genetic engineering techniques, including the p2NIL/pGOAL method, were used to create *mtr* and *mshC* knockout strains. To validate the p2NIL/pGOAL method for use in *Mab*, this method was first

applied to create *mtr* and *mshC* knockout strains in *Mycobacterium smegmatis* (*Msm*), a widely used alternative model for genetic tool development and validation in mycobacterial studies (**Chapter V**). Although the p2NIL/pGOAL method was successfully validated in *Msm*, carrying out genetic manipulations using this method proved to be laborious, inefficient and time-consuming. Hence, another technique, i.e. the ORBIT system, was selected for use in *Mab* instead (**Chapter VI**). With this system, a *Mab* strain lacking the expression of *mtr*, i.e. *Mab* Δ *mtr*, was successfully created while any attempt at creating a *Mab* Δ *mshC* strain failed. Since knockout strains of essential genes are not viable, these results indicate that *mtr* is not essential for the overall survival of *Mab* while *mshC* may be essential. Nevertheless, more research is needed to prove this theory.

The **second** and **third aim** of this thesis was to determine the role of *mtr* and *mshC* during stress conditions and infection by using the previously created recombinant strains. Due to the protective ability of MSH, increased MSH levels was expected to enhance bacterial survival during stress conditions. However, overexpressing either *mtr* or *mshC* did not lead to higher levels of total reduced intracellular thiols nor an enhanced bacterial survival during stress conditions. Moreover, overexpressing *mtr* or *mshC* was even unfavorable for bacteria growth in certain conditions (**Chapter III**). Next, *Mab* Δ *mtr* was used to further investigate whether *mtr* is conditionally essential for *Mab*, i.e. essential for the survival of *Mab* in certain growth conditions. Hereby, *Mab* lacking *mtr* demonstrated to have a reducing ability to proliferate during infection in *G. mellonella* and became more sensitive to bedaquiline *in vitro*, thus being conditionally essential for the proliferation of *Mab* during stress conditions and infection (**Chapter VI**).

Collectively, although many advances have been made in the recent years regarding the genetic engineering of mycobacteria, a target-based drug discovery approach remains laborious and time-consuming. By implementing the available genetic engineering tools, *mtr* was proven to be conditionally essential for the proliferation of *Mab* in certain conditions and consequently a potential target for novel anti-mycobacterial drugs to be used in combination with the current drugs.

VII.5 Samenvatting

Het *Mycobacterium abscessus* complex (MABC) is de meest voorkomende, snelgroeïende niet-tuberculeuze mycobacteriën (NTM) groep die ziekten veroorzaakt bij mensen, voornamelijk patiënten met immunodeficiëntie of patiënten met een reeds bestaande longaandoening. De incidentie van MABC-infecties is de afgelopen decennia wereldwijd gestegen en in de meeste gevallen blijft het ziek zijn met MABC onbehandelbaar vanwege het ontbreken van een optimale behandeling en de zeer resistente aard van MABC. De behandeling van MABC bestaat uit een lange behandeling van meerdere geneesmiddelen en wordt gekenmerkt door ernstige bijwerkingen en een succespercentage van slechts 45,6%. De tekortkomingen van deze behandeling dringen aan op het ontdekken van nieuwe anti-mycobacteriële geneesmiddelen en doelwitten die in staat zijn de bijwerkingen van de behandeling te verminderen, de behandeling te verkorten en de verdere ontwikkeling van geneesmiddelresistentie te voorkomen. Tijdens dit doctoraat werden mycothione reductase (Mtr) en cysteïne ligase (MshC), twee belangrijke enzymen van de biosynthese en recycling pathway van mycothiol (MSH), geselecteerd als veelbelovende nieuwe doelwitten, aangezien deze pathway essentieel is voor het onschadelijk maken van reactieve tussenproducten (**Hoofdstuk I**). Hoewel het hoofddoel van dit proefschrift het onderzoeken van Mtr en MshC als potentiële nieuwe doelwitten was, werden drie subdoelstellingen toegepast.

Het **eerste doel** van dit proefschrift was het creëren van een panel van recombinante *Mab*-stammen met een differentiële expressie van *mtr* of *mshC*, d.w.z. overexpressie-, knockdown- en knockout-stammen. Eerst werd met behulp van de pMV306-vector, die in staat is een extra kopie van een gen in de L5-site van het bacteriële genoom te incorporeren, met succes een *Mab* stam gecreëerd en gevalideerd dat *mtr* of *mshC* tot overexpressie brengt, *Mab::mtr* of *Mab::mshC* respectievelijk (**Hoofdstuk III**). Vervolgens werd het *Streptococcus thermophilus* CRISPRi-systeem geïmplementeerd om in *Mab mtr* en *mshC* knockdown-stammen te produceren. Hoewel de integratie van de CRISPRi-plasmiden aanvankelijk

succesvol was, verloren sommige van de gegenereerde stammen de geïntegreerde plasmiden in de loop van tijd, waardoor dit systeem onstabiel en onbetrouwbaar werd voor ons onderzoek (**Hoofdstuk IV**). Ten slotte werden genetische manipulatietechnieken, waaronder de p2NIL/pGOAL-methode, gebruikt om *mtr* en *mshC* knockout-stammen te creëren. Om de p2NIL/pGOAL methode te valideren voor gebruik in *Mab*, werd deze methode eerst toegepast om *mtr* en *mshC* knockout-stammen te creëren in *Mycobacterium smegmatis* (*Msm*), een veelgebruikt alternatief model voor de ontwikkeling en validatie van genetische hulpmiddelen in mycobacteriële studies (**Hoofdstuk V**). Hoewel de p2NIL/pGOAL-methode met succes werd gevalideerd in *Msm*, bleek het uitvoeren van genetische manipulaties met deze methode arbeidsintensief, inefficiënt en tijdrovend. Daarom werd in plaats daarvan een andere techniek, namelijk het ORBIT-systeem, geselecteerd voor gebruik in *Mab* (**Hoofdstuk VI**). Aan de hand van dit systeem werd met succes een *Mab* stam gecreëerd waarbij de expressie van *mtr* ontbreekt, *Mab* Δ *mtr*, terwijl elke poging om een *Mab* Δ *mshC* stam te creëren mislukte. Omdat knockout-stammen van essentiële genen niet levensvatbaar zijn, geven deze resultaten aan dat *mtr* niet essentieel is voor de algehele overleving van *Mab*, terwijl *mshC* mogelijk essentieel is. Niettemin is er meer onderzoek nodig om deze theorie te bewijzen.

Het **tweede** en **derde** doel van dit proefschrift was het bepalen van de rol van *mtr* en *mshC* tijdens stressomstandigheden en infectie door gebruik te maken van de eerder gecreëerde recombinante stammen. Vanwege het beschermende vermogen van MSH werd verwacht dat verhoogde MSH-niveaus de overleving van bacteriën tijdens stressomstandigheden zouden verbeteren. Het tot overexpressie brengen van *mtr* of *mshC* leidde echter niet tot hogere niveaus van totaal gereduceerde intracellulaire thiolen, noch tot een verbeterde bacteriële overleving tijdens stressomstandigheden. Bovendien was de overexpressie van *mtr* of *mshC* onder bepaalde omstandigheden zelfs ongunstig voor de groei van de bacteriën (**Hoofdstuk III**). Vervolgens werd *Mab* Δ *mtr* gebruikt om verder te onderzoeken of *mtr* conditioneel essentieel is voor *Mab*, d.w.z. essentieel voor het overleven van

Mab onder bepaalde groeiomstandigheden. Hierbij bleek dat de *mtr*-deficiënte *Mab* een reducerend vermogen heeft om te prolifereren tijdens infectie in *G. mellonella* larven en gevoeliger werd voor bedaquiline *in vitro*, waardoor het conditioneel essentieel is voor de proliferatie van *Mab* tijdens stressomstandigheden en infectie (**Hoofdstuk VI**).

Als conclusie, hoewel er de afgelopen jaren veel vooruitgang is geboekt op het gebied van de genetische manipulatie van mycobacteriën, blijft een doelwitgerichte aanpak een moeilijke methode voor het ontdekken van geneesmiddelen in mycobacteriën. Door het implementeren van de beschikbare genetische manipulatiemethodes bleek *mtr* conditioneel essentieel te zijn voor de proliferatie van *Mab* onder bepaalde omstandigheden en bijgevolg een potentieel doelwit voor nieuwe anti-mycobacteriële geneesmiddelen die in combinatie met de huidige geneesmiddelen worden gebruikt.

References

1. Adedeji WA. 2016. THE TREASURE CALLED ANTIBIOTICS. Ann Ibadan Postgrad Med.
2. Browne K, Chakraborty S, Chen R, Willcox MDP, Black DS, Walsh WR, Kumar N. 2020. A new era of antibiotics: The clinical potential of antimicrobial peptides. Int J Mol Sci <https://doi.org/10.3390/ijms21197047>.
3. Sakai T, Morimoto Y. 2022. The History of Infectious Diseases and Medicine. Pathogens <https://doi.org/10.3390/pathogens11101147>.
4. De Clercq E, Li G. 2016. Approved antiviral drugs over the past 50 years. Clin Microbiol Rev <https://doi.org/10.1128/CMR.00102-15>.
5. WHO COVID19.
6. Shahraki AH, Mirsaeidi M. 2021. Phage therapy for mycobacterium abscessus and strategies to improve outcomes. Microorganisms <https://doi.org/10.3390/microorganisms9030596>.
7. Tippett E, Ellis S, Wilson J, Kotsimbos T, Spelman D. 2018. Mycobacterium abscessus complex: Natural history and treatment outcomes at a tertiary adult cystic fibrosis center. Int J Mycobacteriology https://doi.org/10.4103/ijmy.ijmy_55_18.
8. Ganapathy US, Dartois V, Dick T. 2019. Repositioning rifamycins for Mycobacterium abscessus lung disease. Expert Opin Drug Discov <https://doi.org/10.1080/17460441.2019.1629414>.
9. Degiacomi G, Sammartino JC, Chiarelli LR, Riabova O, Makarov V, Pasca MR. 2019. Mycobacterium abscessus, an emerging and worrisome pathogen among cystic fibrosis patients. Int J Mol Sci <https://doi.org/10.3390/ijms20235868>.
10. Scherr N, Nguyen L. 2009. Mycobacterium versus Streptomyces—we are different, we are the same. Curr Opin Microbiol <https://doi.org/10.1016/j.mib.2009.10.003>.
11. Khan O, Chaudary N. 2020. The use of amikacin liposome inhalation suspension (Arikayce) in the treatment of refractory nontuberculous mycobacterial lung disease in adults. Drug Des Devel Ther <https://doi.org/10.2147/DDDT.S146111>.
12. Koh W-J. 2017. Nontuberculous Mycobacteria—Overview. Microbiol Spectr <https://doi.org/10.1128/microbiolspec.tnmi7-0024-2016>.
13. López-Roa P, Esteban J, Muñoz-Egea MC. 2023. Updated Review on the Mechanisms of Pathogenicity in Mycobacterium abscessus, a Rapidly Growing Emerging Pathogen. Microorganisms <https://doi.org/10.3390/microorganisms11010090>.
14. Cao Yao JC, Navas Méndez J, Tórtola Fernández MT. 2023. Analysis of Phenotypic and Genotypic Susceptibility to Clarithromycin and Amikacin of Mycobacterium abscessus Complex Strains Isolated from Cystic Fibrosis Patients. Microorganisms 11.
15. Andrew EC, Connell T, Robinson P, Curtis N, Massie J, Robertson C, Harrison J, Shanthikumar S, Bryant PA, Starr M, Steer A, Ranganathan S, Gwee A.

2019. Pulmonary Mycobacterium abscessus complex in children with cystic fibrosis: A practical management guideline. *J Paediatr Child Health* <https://doi.org/10.1111/jpc.14427>.
16. Dahl VN, Mølhave M, Fløe A, van Ingen J, Schön T, Lillebaek T, Andersen AB, Wejse C. 2022. Global trends of pulmonary infections with nontuberculous mycobacteria: a systematic review. *Int J Infect Dis* <https://doi.org/10.1016/j.ijid.2022.10.013>.
 17. Cowman S, Van Ingen J, Griffith DE, Loebinger MR. 2019. Non-tuberculous mycobacterial pulmonary disease. *Eur Respir J* <https://doi.org/10.1183/13993003.00250-2019>.
 18. Victoria L, Gupta A, Gómez JL, Robledo J. 2021. Mycobacterium abscessus complex: A Review of Recent Developments in an Emerging Pathogen. *Front Cell Infect Microbiol* <https://doi.org/10.3389/fcimb.2021.659997>.
 19. Koh WJ, Stout JE, Yew WW. 2014. Advances in the management of pulmonary disease due to Mycobacterium abscessus complex. *Int J Tuberc Lung Dis* <https://doi.org/10.5588/ijtld.14.0134>.
 20. Horne D, Skerrett S. 2019. Recent advances in nontuberculous mycobacterial lung infections. *F1000Research* <https://doi.org/10.12688/f1000research.20096.1>.
 21. Ventura M, Canchaya C, Tauch A, Chandra G, Fitzgerald GF, Chater KF, van Sinderen D. 2007. Genomics of Actinobacteria : Tracing the Evolutionary History of an Ancient Phylum . *Microbiol Mol Biol Rev* <https://doi.org/10.1128/mnbr.00005-07>.
 22. Maitra A, Munshi T, Healy J, Martin LT, Vollmer W, Keep NH, Bhakta S. 2019. Cell wall peptidoglycan in Mycobacterium tuberculosis: An Achilles' heel for the TB-causing pathogen. *FEMS Microbiol Rev* <https://doi.org/10.1093/femsre/fuz016>.
 23. Jankute M, Cox JAG, Harrison J, Besra GS. 2015. Assembly of the Mycobacterial Cell Wall. *Annu Rev Microbiol* <https://doi.org/10.1146/annurev-micro-091014-104121>.
 24. Konyariková Z, Savková K, Kozmon S, Mikušová K. 2020. Biosynthesis of galactan in mycobacterium tuberculosis as a viable TB drug target? *Antibiotics* <https://doi.org/10.3390/antibiotics9010020>.
 25. Abrahams KA, Besra GS. 2021. Synthesis and recycling of the mycobacterial cell envelope. *Curr Opin Microbiol* <https://doi.org/10.1016/j.mib.2021.01.012>.
 26. Ferrell KC, Johansen MD, Triccas JA, Counoupas C. 2022. Virulence Mechanisms of Mycobacterium abscessus: Current Knowledge and Implications for Vaccine Design. *Front Microbiol* <https://doi.org/10.3389/fmicb.2022.842017>.
 27. Brown L, Wolf JM, Prados-Rosales R, Casadevall A. 2015. Through the wall: Extracellular vesicles in Gram-positive bacteria, mycobacteria and fungi. *Nat Rev Microbiol* <https://doi.org/10.1038/nrmicro3480>.
 28. To K, Cao R, Yegiazaryan A, Owens J, Venketaraman V. 2020. General overview of nontuberculous mycobacteria opportunistic pathogens: Mycobacterium avium and mycobacterium abscessus. *J Clin Med*

- <https://doi.org/10.3390/jcm9082541>.
29. Gutiérrez AV, Viljoen A, Ghigo E, Herrmann JL, Kremer L. 2018. Glycopeptidolipids, a double-edged sword of the Mycobacterium abscessus complex. *Front Microbiol* <https://doi.org/10.3389/fmicb.2018.01145>.
 30. Parmar S, Tocheva EI. 2023. The cell envelope of Mycobacterium abscessus and its role in pathogenesis. *PLoS Pathog* <https://doi.org/10.1371/journal.ppat.1011318>.
 31. Mukherjee R, Chatterji D. 2012. Glycopeptidolipids: Immuno-modulators in greasy mycobacterial cell envelope. *IUBMB Life* <https://doi.org/10.1002/iub.602>.
 32. Pereira AC, Ramos B, Reis AC, Cunha M V. 2020. Non-tuberculous mycobacteria: Molecular and physiological bases of virulence and adaptation to ecological niches. *Microorganisms* <https://doi.org/10.3390/microorganisms8091380>.
 33. Sepulcri C, Vena A, Bassetti M. 2023. Skin and soft tissue infections due to rapidly growing mycobacteria. *Curr Opin Infect Dis* <https://doi.org/10.1097/QCO.0000000000000905>.
 34. Marshall JS, Warrington R, Watson W, Kim HL. 2018. An introduction to immunology and immunopathology. *Allergy, Asthma Clin Immunol* <https://doi.org/10.1186/s13223-018-0278-1>.
 35. Abdelaal HFM, Chan ED, Young L, Baldwin SL, Coler RN. 2022. Mycobacterium abscessus: It's Complex. *Microorganisms* <https://doi.org/10.3390/microorganisms10071454>.
 36. Clary G, Sasindran SJ, Nesbitt N, Mason L, Cole S, Azad A, McCoy K, Schlesinger LS, Hall-Stoodley L. 2018. Mycobacterium abscessus smooth and rough morphotypes form antimicrobial-tolerant biofilm phenotypes but are killed by acetic acid. *Antimicrob Agents Chemother* <https://doi.org/10.1128/AAC.01782-17>.
 37. Gloag ES, Wozniak DJ, Stoodley P, Hall-Stoodley L. 2021. Mycobacterium abscessus biofilms have viscoelastic properties which may contribute to their recalcitrance in chronic pulmonary infections. *Sci Rep* <https://doi.org/10.1038/s41598-021-84525-x>.
 38. Hendrix C, McCrary M, Hou R, Abate G. 2023. Diagnosis and Management of Pulmonary NTM with a Focus on Mycobacterium avium Complex and Mycobacterium abscessus: Challenges and Prospects. *Microorganisms* <https://doi.org/10.3390/microorganisms11010047>.
 39. Lee MR, Chang LY, Ko JC, Wang HC, Huang YW. 2020. Nontuberculous mycobacterial lung disease epidemiology in Taiwan: A systematic review. *J Formos Med Assoc* <https://doi.org/10.1016/j.jfma.2020.05.019>.
 40. Lopeman RC, Harrison J, Desai M, Cox JAG. 2019. Mycobacterium abscessus: Environmental bacterium turned clinical nightmare. *Microorganisms* <https://doi.org/10.3390/microorganisms7030090>.
 41. Mi Wi Y. 2019. Treatment of extrapulmonary nontuberculous mycobacterial diseases. *Infect Chemother* <https://doi.org/10.3947/ic.2019.51.3.245>.
 42. Kwon YH, Lee GY, Kim WS, Kim KJ. 2009. A case of skin and soft tissue

- infection caused by mycobacterium abscessus. *Ann Dermatol* <https://doi.org/10.5021/ad.2009.21.1.84>.
43. Singh K, Kumari R, Tripathi R, Gupta S, Anupurba S. 2020. Detection of clinically important non tuberculous mycobacteria (NTM) from pulmonary samples through one-step multiplex PCR assay. *BMC Microbiol* <https://doi.org/10.1186/s12866-020-01952-y>.
 44. Ravnholt C, Kolpen M, Skov M, Moser C, Katzenstein TL, Pressler T, Høiby N, Qvist T. 2018. The importance of early diagnosis of Mycobacterium abscessus complex in patients with cystic fibrosis. *APMIS* <https://doi.org/10.1111/apm.12903>.
 45. Recchia D, Stelitano G, Stamilla A, Gutierrez DL, Degiacomi G, Chiarelli LR, Pasca MR. 2023. Mycobacterium abscessus Infections in Cystic Fibrosis Individuals: A Review on Therapeutic Options. *Int J Mol Sci* <https://doi.org/10.3390/ijms24054635>.
 46. Daley CL, Iaccarino JM, Lange C, Cambau E, Wallace RJ, Andrejak C, Böttger EC, Brozek J, Griffith DE, Guglielmetti L, Huitt GA, Knight SL, Leitman P, Marras TK, Olivier KN, Santin M, Stout JE, Tortoli E, Van Ingen J, Wagner D, Winthrop KL. 2020. Treatment of nontuberculous mycobacterial pulmonary disease: An official ats/ers/escmid/idsa clinical practice guideline. *Clin Infect Dis* <https://doi.org/10.1093/cid/ciaa241>.
 47. Weng YW, Huang CK, Sy CL, Wu KS, Tsai HC, Lee SSJ. 2020. Treatment for Mycobacterium abscessus complex–lung disease. *J Formos Med Assoc* <https://doi.org/10.1016/j.jfma.2020.05.028>.
 48. Broncano-Lavado A, Senhaji-Kacha A, Santamaría-Corral G, Esteban J, García-Quintanilla M. 2022. Alternatives to Antibiotics against Mycobacterium abscessus. *Antibiotics* <https://doi.org/10.3390/antibiotics11101322>.
 49. Griffith DE, Daley CL. 2022. Treatment of Mycobacterium abscessus Pulmonary Disease. *Chest* <https://doi.org/10.1016/j.chest.2021.07.035>.
 50. Ganapathy US, Dick T. 2022. Why Matter Matters: Fast-Tracking Mycobacterium abscessus Drug Discovery. *Molecules* <https://doi.org/10.3390/molecules27206948>.
 51. Doucet-Populaire F, Buriánková K, Weiser J, Pernodet JL. 2002. Natural and acquired macrolide resistance in Mycobacteria. *Curr Drug Targets - Infect Disord* <https://doi.org/10.2174/1568005023342263>.
 52. Van Der Paardt AF, Wilffert B, Akkerman OW, De Lange WCM, Van Soolingen D, Sinha B, Van Der Werf TS, Kosterink JGW, Alffenaar JWC. 2015. Evaluation of macrolides for possible use against multidrug-resistant Mycobacterium tuberculosis. *Eur Respir J* <https://doi.org/10.1183/09031936.00147014>.
 53. Kannan K, Kanabar P, Schryer D, Florin T, Oh E, Bahroos N, Tenson T, Weissman JS, Mankin AS. 2014. The general mode of translation inhibition by macrolide antibiotics. *Proc Natl Acad Sci U S A* <https://doi.org/10.1073/pnas.1417334111>.
 54. Gaynor M, Mankin A. 2005. Macrolide Antibiotics: Binding Site, Mechanism of Action, Resistance. *Curr Top Med Chem* <https://doi.org/10.2174/1568026033452159>.

55. Krause KM, Serio AW, Kane TR, Connolly LE. 2016. Aminoglycosides: An overview. *Cold Spring Harb Perspect Med* <https://doi.org/10.1101/cshperspect.a027029>.
56. Becker B, Cooper MA. 2013. Aminoglycoside antibiotics in the 21st century. *ACS Chem Biol* <https://doi.org/10.1021/cb3005116>.
57. Dowling, Aileen M Adley, C O'Dwyer J. 2017. Antibiotics: mode of action and mechanisms of resistance. *Nurs Stand*.
58. Worthington RJ, Melander C. 2013. Overcoming resistance to β -Lactam antibiotics. *J Org Chem* <https://doi.org/10.1021/jo400236f>.
59. Abeylath SC, Turos E. 2008. Drug delivery approaches to overcome bacterial resistance to β -lactam antibiotics. *Expert Opin Drug Deliv* <https://doi.org/10.1517/17425247.5.9.931>.
60. Glanzer S, Pulido SA, Tutz S, Wagner GE, Kriechbaum M, Gubensäk N, Trifunovic J, Dorn M, Fabian WMF, Novak P, Reidl J, Zangger K. 2015. Structural and functional implications of the interaction between macrolide antibiotics and bile acids. *Chem - A Eur J* <https://doi.org/10.1002/chem.201406413>.
61. Isanga J, Mukunzi D, Chen Y, Suryoprabowo S, Liu L, Kuang H. 2017. Development of a monoclonal antibody assay and immunochromatographic test strip for the detection of amikacin residues in milk and eggs. *Food Agric Immunol* <https://doi.org/10.1080/09540105.2017.1309361>.
62. El-Gamal MI, Brahim I, Hisham N, Aladdin R, Mohammed H, Bahaaeldin A. 2017. Recent updates of carbapenem antibiotics. *Eur J Med Chem* <https://doi.org/10.1016/j.ejmech.2017.03.022>.
63. Lee M-R, Sheng W-H, Hung C-C, Yu C-J, Lee L-N, Hsueh P-R. 2015. Mycobacterium abscessus Complex Infections in Humans . *Emerg Infect Dis* <https://doi.org/10.3201/2109.141634>.
64. Kumar K, Daley CL, Griffith DE, Loebinger MR. 2022. Management of Mycobacterium avium complex and Mycobacterium abscessus pulmonary disease: therapeutic advances and emerging treatments. *Eur Respir Rev* <https://doi.org/10.1183/16000617.0212-2021>.
65. Egorova A, Jackson M, Gavrilyuk V, Makarov V. 2021. Pipeline of anti-Mycobacterium abscessus small molecules: Repurposable drugs and promising novel chemical entities. *Med Res Rev* <https://doi.org/10.1002/med.21798>.
66. Dong Z, Abbas MN, Kausar S, Yang J, Li L, Tan L, Cui H. 2019. Biological Functions and Molecular Mechanisms of Antibiotic Tigecycline in the Treatment of Cancers. *Int J Mol Sci* <https://doi.org/10.3390/ijms20143577>.
67. Ferro BE, Srivastava S, Deshpande D, Pasipanodya JG, Van Soolingen D, Mouton JW, Van Ingen J, Gumbo T. 2016. Tigecycline is highly efficacious against Mycobacterium abscessus pulmonary disease. *Antimicrob Agents Chemother* <https://doi.org/10.1128/AAC.03112-15>.
68. Thomas S, Pethe K, Roquet-Banères F, Kremer L, Herrmann J-L, Dupont C, Viljoen A. 2017. Bedaquiline Inhibits the ATP Synthase in Mycobacterium abscessus and Is Effective in Infected Zebrafish. *Antimicrob Agents*

Chemother 61:1–15.

69. Pieroni M. 2019. Antituberculosis agents: Beyond medicinal chemistry rules Annual Reports in Medicinal Chemistry.
70. Riccardi N, Occhineri S, Matucci T, Marchetti G, Rindi L, Tiseo G, Cirillo DM, Falcone M. 2023. Bedaquiline-based all-oral regimen for macrolide-resistant Mycobacterium abscessus pulmonary disease. *Int J Tuberc Lung Dis* <https://doi.org/10.5588/ijtld.23.0220>.
71. Pinheiro M, Amenitsch H, Reis S. 2019. Antituberculosis drug interactions with membranes: A biophysical approach applied to bedaquiline. *Membranes (Basel)* <https://doi.org/10.3390/membranes9110141>.
72. Wang S, Wang Z, Fang L, Lv Y, Du G. 2022. Advances of the Target-Based and Phenotypic Screenings and Strategies in Drug Discovery. *Int J Drug Discov Pharmacol* <https://doi.org/10.53941/ijddp.v1i1.199>.
73. Abrahams KA, Besra GS. 2020. Mycobacterial drug discovery. *RSC Med Chem* <https://doi.org/10.1039/d0md00261e>.
74. Goff A, Cantillon D, Wildner LM, Waddell SJ. 2020. Multi-omics technologies applied to tuberculosis drug discovery. *Appl Sci* <https://doi.org/10.3390/app10134629>.
75. Ejalonibu MA, Ogundare SA, Elrashedy AA, Ejalonibu MA, Lawal MM, Mhlongo NN, Kumalo HM. 2021. Drug discovery for mycobacterium tuberculosis using structure-based computer-aided drug design approach. *Int J Mol Sci* <https://doi.org/10.3390/ijms222413259>.
76. Dalberto PF, de Souza E V., Abbadi BL, Neves CE, Rambo RS, Ramos AS, Macchi FS, Machado P, Bizarro C V., Basso LA. 2020. Handling the Hurdles on the Way to Anti-tuberculosis Drug Development. *Front Chem* <https://doi.org/10.3389/fchem.2020.586294>.
77. Kingdon ADH, Alderwick LJ. 2021. Structure-based in silico approaches for drug discovery against Mycobacterium tuberculosis. *Comput Struct Biotechnol J* <https://doi.org/10.1016/j.csbj.2021.06.034>.
78. Minato Y, Gohl DM, Thiede JM, Chacón JM, Harcombe WR, Maruyama F, Baughn AD. 2019. Genomewide Assessment of Mycobacterium tuberculosis Conditionally Essential Metabolic Pathways. *mSystems* <https://doi.org/10.1128/msystems.00070-19>.
79. Bosch-Guiteras N, van Leeuwen J. 2022. Exploring conditional gene essentiality through systems genetics approaches in yeast. *Curr Opin Genet Dev* <https://doi.org/10.1016/j.gde.2022.101963>.
80. Parish T. 2020. In vitro drug discovery models for Mycobacterium tuberculosis relevant for host infection. *Expert Opin Drug Discov* <https://doi.org/10.1080/17460441.2020.1707801>.
81. Saxena S, Spaink HP, Forn-Cuní G. 2021. Drug resistance in nontuberculous mycobacteria: Mechanisms and models. *Biology (Basel)* <https://doi.org/10.3390/biology10020096>.
82. Admella J, Torrents E. 2023. Investigating bacterial infections in Galleria mellonella larvae: Insights into pathogen dissemination and behavior. *J Invertebr Pathol* <https://doi.org/10.1016/j.jip.2023.107975>.
83. Ménard G, Rouillon A, Cattoir V, Donnio PY. 2021. Galleria mellonella as a

- Suitable Model of Bacterial Infection: Past, Present and Future. *Front Cell Infect Microbiol* <https://doi.org/10.3389/fcimb.2021.782733>.
84. Meir M, Grosfeld T, Barkan D. 2018. Establishment and validation of *Galleria mellonella* as a novel model organism to study *Mycobacterium abscessus* infection, pathogenesis, and treatment. *Antimicrob Agents Chemother* <https://doi.org/10.1128/AAC.02539-17>.
 85. Tsai CJY, Loh JMS, Proft T. 2016. *Galleria mellonella* infection models for the study of bacterial diseases and for antimicrobial drug testing. *Virulence* <https://doi.org/10.1080/21505594.2015.1135289>.
 86. Le Gal K, Schmidt EE, Sayin VI. 2021. Cellular redox homeostasis. *Antioxidants* <https://doi.org/10.3390/antiox10091377>.
 87. Tretter V, Hochreiter B, Zach ML, Krenn K, Klein KU. 2022. Understanding cellular redox homeostasis: A challenge for precision medicine. *Int J Mol Sci* <https://doi.org/10.3390/ijms23010106>.
 88. Torfs E, Piller T, Cos P, Cappoen D. 2019. Opportunities for overcoming *Mycobacterium tuberculosis* drug resistance: Emerging mycobacterial targets and host-directed therapy. *Int J Mol Sci* <https://doi.org/10.3390/ijms20122868>.
 89. Rani A, Saini KC, Bast F, Mehariya S, Bhatia SK, Lavecchia R, Zuorro A. 2021. Microorganisms: A potential source of bioactive molecules for antioxidant applications. *Molecules* <https://doi.org/10.3390/molecules26041142>.
 90. Ruhland BR, Reniere ML. 2019. Sense and sensor ability: redox-responsive regulators in *Listeria monocytogenes*. *Curr Opin Microbiol* <https://doi.org/10.1016/j.mib.2018.10.006>.
 91. Mandal M, Sarkar M, Khan A, Biswas M, Masi A, Rakwal R, Agrawal GK, Srivastava A, Sarkar A. 2022. Reactive Oxygen Species (ROS) and Reactive Nitrogen Species (RNS) in plants- maintenance of structural individuality and functional blend. *Adv Redox Res* <https://doi.org/10.1016/j.arres.2022.100039>.
 92. Liu Y, Li X, Luo J, Su T, Si M, Chen C. 2021. A novel mycothiol-dependent thiol-disulfide reductase in *Corynebacterium glutamicum* involving oxidative stress resistance. *3 Biotech* <https://doi.org/10.1007/s13205-021-02896-4>.
 93. Bhat SA, Singh N, Trivedi A, Kansal P, Gupta P, Kumar A. 2012. The mechanism of redox sensing in *Mycobacterium tuberculosis*. *Free Radic Biol Med* <https://doi.org/10.1016/j.freeradbiomed.2012.08.008>.
 94. Sao Emani C, Gallant JL, Wiid IJ, Baker B. 2019. The role of low molecular weight thiols in *Mycobacterium tuberculosis*. *Tuberculosis* <https://doi.org/10.1016/j.tube.2019.04.003>.
 95. Ganguli G, Mukherjee U, Sonawane A. 2019. Peroxisomes and oxidative stress: Their implications in the modulation of cellular immunity during mycobacterial infection. *Front Microbiol* <https://doi.org/10.3389/fmicb.2019.01121>.
 96. Naeem MA, Ahmad W, Tyagi R, Akram Q, Younus M, Liu X. 2021. Stealth strategies of *Mycobacterium tuberculosis* for immune evasion. *Curr Issues Mol Biol* <https://doi.org/10.21775/CIMB.041.597>.

97. Ellzey LM, Patrick KL, Watson RO. 2023. Mitochondrial reactive oxygen species: double agents in *Mycobacterium tuberculosis* infection. *Curr Opin Immunol* <https://doi.org/10.1016/j.coi.2023.102366>.
98. Sies H. 2020. Oxidative stress: Concept and some practical aspects. *Antioxidants* <https://doi.org/10.3390/antiox9090852>.
99. Gutteridge JMC, Halliwell B. 2018. Mini-Review: Oxidative stress, redox stress or redox success? *Biochem Biophys Res Commun* <https://doi.org/10.1016/j.bbrc.2018.05.045>.
100. Pang L, Lenders S, Osipov EM, Weeks SD, Rozenski J, Piller T, Cappoen D, Strelkov S V., Van Aerschot A. 2022. Structural Basis of Cysteine Ligase MshC Inhibition by Cysteinylnyl-Sulfonamides. *Int J Mol Sci* <https://doi.org/10.3390/ijms232315095>.
101. Narayanankutty A, Job JT, Narayanankutty V. 2019. Glutathione, an Antioxidant Tripeptide: Dual Roles in Carcinogenesis and Chemoprevention. *Curr Protein Pept Sci* <https://doi.org/10.2174/1389203720666190206130003>.
102. Zhao Q, Wang M, Xu D, Zhang Q, Liu W. 2015. Metabolic coupling of two small-molecule thiols programs the biosynthesis of lincomycin A. *Nature* <https://doi.org/10.1038/nature14137>.
103. Eberle RJ, Kawai LA, de Moraes FR, Tasic L, Arni RK, Coronado MA. 2018. Biochemical and biophysical characterization of a mycoredoxin protein glutaredoxin A1 from *Corynebacterium pseudotuberculosis*. *Int J Biol Macromol* <https://doi.org/10.1016/j.ijbiomac.2017.10.063>.
104. Fraternali A, Zara C, Pierigè F, Rossi L, Ligi D, Amagliani G, Mannello F, Smietana M, Magnani M, Brandi G, Schiavano GF. 2020. Redox homeostasis as a target for new antimycobacterial agents. *Int J Antimicrob Agents* <https://doi.org/10.1016/j.ijantimicag.2020.106148>.
105. Van Loi V, Rossius M, Antelmann H. 2015. Redox regulation by reversible protein S-thiolation in bacteria. *Front Microbiol* <https://doi.org/10.3389/fmicb.2015.00187>.
106. Rawat M, Maupin-Furlow JA. 2020. Redox and thiols in archaea. *Antioxidants* <https://doi.org/10.3390/antiox9050381>.
107. Reyes AM, Pedre B, De Armas MI, Tossounian MA, Radi R, Messens J, Trujillo M. 2018. Chemistry and Redox Biology of Mycothiol. *Antioxidants Redox Signal* <https://doi.org/10.1089/ars.2017.7074>.
108. Fan F, Luxenburger A, Painter GF, Blanchard JS. 2007. Steady-state and pre-steady-state kinetic analysis of *Mycobacterium smegmatis* cysteine ligase (MshC). *Biochemistry* <https://doi.org/10.1021/bi7011492>.
109. Tremblay LW, Fan F, Vetting MW, Blanchard JS. 2008. The 1.6 Å crystal structure of *Mycobacterium smegmatis* MshC: The penultimate enzyme in the mycothiol biosynthetic pathway. *Biochemistry* <https://doi.org/10.1021/bi801708f>.
110. Buchmeier NA, Newton GL, Fahey RC. 2006. A mycothiol synthase mutant of *Mycobacterium tuberculosis* has an altered thiol-disulfide content and limited tolerance to stress. *J Bacteriol* <https://doi.org/10.1128/JB.00393-06>.

111. Holsclaw CM, Muse WB, Carroll KS, Leary JA. 2011. Mass spectrometric analysis of mycothiol levels in wild-type and mycothiol disulfide reductase mutant *Mycobacterium smegmatis*. *Int J Mass Spectrom* <https://doi.org/10.1016/j.ijms.2010.10.027>.
112. Sareen D, Newton GL, Fahey RC, Buchmeier NA. 2003. Mycothiol Is Essential for Growth of *Mycobacterium tuberculosis* Erdman. *J Bacteriol* <https://doi.org/10.1128/JB.185.22.6736-6740.2003>.
113. Gutierrez-Lugo MT, Baker H, Shiloach J, Boshoff H, Bewley CA. 2009. Dequalinium, a new inhibitor of mycobacterium tuberculosis mycothiol ligase identified by high-throughput screening. *J Biomol Screen* <https://doi.org/10.1177/1087057109335743>.
114. Newton GL, Buchmeier N, La Clair JJ, Fahey RC. 2011. Evaluation of NTF1836 as an inhibitor of the mycothiol biosynthetic enzyme MshC in growing and non-replicating *Mycobacterium tuberculosis*. *Bioorganic Med Chem* <https://doi.org/10.1016/j.bmc.2011.05.028>.
115. Armianinova DK, Karpov DS, Kotliarova MS, Goncharenko A V. 2022. Genetic Engineering in Mycobacteria. *Mol Biol* <https://doi.org/10.1134/S0026893322060036>.
116. Chimukuche NM, Williams MJ. 2021. Genetic Manipulation of Non-tuberculosis Mycobacteria. *Front Microbiol* <https://doi.org/10.3389/fmicb.2021.633510>.
117. Pashley CA, Parish T. 2003. Efficient switching of mycobacteriophage L5-based integrating plasmids in *Mycobacterium tuberculosis*. *FEMS Microbiol Lett* [https://doi.org/10.1016/S0378-1097\(03\)00823-1](https://doi.org/10.1016/S0378-1097(03)00823-1).
118. Adefisayo OO, Curtis ER, Smith CM. 2023. Mycobacterial Genetic Technologies for Probing the Host- Pathogen Microenvironment. *Infect Immun* <https://doi.org/10.1128/iai.00430-22>.
119. Gopinath K, Warner DF, Mizrahi V. 2015. Targeted gene knockout and essentiality testing by homologous recombination. *Methods Mol Biol* https://doi.org/10.1007/978-1-4939-2450-9_8.
120. Borgers K, Vandewalle K, Festjens N, Callewaert N. 2019. A guide to *Mycobacterium* mutagenesis. *FEBS J* <https://doi.org/10.1111/febs.15041>.
121. Liu K, Gao Y, Li ZH, Liu M, Wang FQ, Wei DZ. 2022. CRISPR-Cas12a assisted precise genome editing of *Mycobacterium neoaurum*. *N Biotechnol* <https://doi.org/10.1016/j.nbt.2021.10.003>.
122. Rahman K, Jamal M, Chen X, Zhou W, Yang B, Zou Y, Xu W, Lei Y, Wu C, Cao X, Tyagi R, Naeem MA, Lin D, Habib Z, Peng N, Fu ZF, Cao G. 2022. Reprogramming *Mycobacterium tuberculosis* CRISPR System for Gene Editing and Genome-wide RNA Interference Screening. *Genomics, Proteomics Bioinforma* <https://doi.org/10.1016/j.gpb.2021.01.008>.
123. Murphy KC, Nelson SJ, Nambi S, Papavinasasundaram K, Baer CE, Sasseti CM. 2018. Orbit: A new paradigm for genetic engineering of mycobacterial chromosomes. *MBio* <https://doi.org/10.1128/mbio.01467-18>.
124. Hussain W, Yang X, Ullah M, Wang H, Aziz A, Xu F, Asif M, Ullah MW, Wang S. 2023. Genetic engineering of bacteriophages: Key concepts, strategies, and applications. *Biotechnol Adv*

- <https://doi.org/10.1016/j.biotechadv.2023.108116>.
125. Fels U, Gevaert K, Van Damme P. 2020. Bacterial Genetic Engineering by Means of Recombineering for Reverse Genetics. *Front Microbiol* <https://doi.org/10.3389/fmicb.2020.548410>.
 126. Grindley NDF, Whiteson KL, Rice PA. 2006. Mechanisms of site-specific recombination. *Annu Rev Biochem* <https://doi.org/10.1146/annurev.biochem.73.011303.073908>.
 127. Blakely GW. 2014. Mechanisms of Horizontal Gene Transfer and DNA Recombination *Molecular Medical Microbiology*.
 128. Rubelj I. 2013. Specialized Recombination *Brenner's Encyclopedia of Genetics: Second Edition*.
 129. Le Bourgeois P, Cornet F. 2013. Chromosome Dimer Resolution by Site-Specific Recombination *Brenner's Encyclopedia of Genetics: Second Edition*. Elsevier Inc. <http://dx.doi.org/10.1016/B978-0-12-374984-0.00241-2>.
 130. Mong Hong Lee, Pascopella L, Jacobs WR, Hatfull GF. 1991. Site-specific integration of mycobacteriophage L5: Integration-proficient vectors for *Mycobacterium smegmatis*, *Mycobacterium tuberculosis*, and bacille Calmette-Guerin. *Proc Natl Acad Sci U S A* <https://doi.org/10.1073/pnas.88.8.3111>.
 131. Mong Hong Lee, Hatfull GF. 1993. Mycobacteriophage L5 integrase-mediated site-specific integration in vitro. *J Bacteriol* <https://doi.org/10.1128/jb.175.21.6836-6841.1993>.
 132. Golichenari B, Yari S, Tasbiti AH, Behravan J, Vaziri F, Ghazvini K. 2022. First conjugation directed traverse of gene cassettes harboring α 1,3GT from fast-growing *Mycobacterium smegmatis* mc2 155 to slow-growing pathogen *Mycobacterium tuberculosis* H37Rv, presumably opening up new scopes in tuberculosis treatment. *Enzyme Microb Technol* <https://doi.org/10.1016/j.enzmictec.2022.110003>.
 133. Huff J, Czyz A, Landick R, Niederweis M. 2010. Taking phage integration to the next level as a genetic tool for mycobacteria. *Gene* <https://doi.org/10.1016/j.gene.2010.07.012>.
 134. Roy RB, Sambou B, Uhía I, Roetynck S, Robertson BD, Kampmann B. 2019. An auto-luminescent fluorescent BCG whole blood assay to enable evaluation of paediatric mycobacterial responses using minimal blood volumes. *Front Pediatr* <https://doi.org/10.3389/fped.2019.00151>.
 135. Wang T, Li Y, Li J, Zhang D, Cai N, Zhao G, Ma H, Shang C, Ma Q, Xu Q, Chen N. 2019. An update of the suicide plasmid-mediated genome editing system in *Corynebacterium glutamicum*. *Microb Biotechnol* <https://doi.org/10.1111/1751-7915.13444>.
 136. Zhou X, Zhang Y, Shen Y, Zhang X, Zan Z, Xia M, Luo J, Wang M. 2020. Efficient repeated batch production of androstenedione using untreated cane molasses by *Mycobacterium neoaurum* driven by ATP futile cycle. *Bioresour Technol* <https://doi.org/10.1016/j.biortech.2020.123307>.
 137. Ko EM, Oh J Il. 2020. Induction of the *cydAB* Operon Encoding the *bd* Quinol Oxidase Under Respiration-Inhibitory Conditions by the Major cAMP Receptor Protein MSMEG_6189 in *Mycobacterium smegmatis*. *Front*

- Microbiol <https://doi.org/10.3389/fmicb.2020.608624>.
138. Barker LP, Porcella SF, Wyatt RG, Small PLC. 1999. The Mycobacterium marinum G13 promoter is a strong sigma 70-like promoter that is expressed in Escherichia coli and mycobacteria species. FEMS Microbiol Lett [https://doi.org/10.1016/S0378-1097\(99\)00169-X](https://doi.org/10.1016/S0378-1097(99)00169-X).
 139. Mouhoub E, Domenech P, Ndao M, Reed MB. 2021. The Diverse Applications of Recombinant BCG-Based Vaccines to Target Infectious Diseases Other Than Tuberculosis: An Overview. Front Microbiol <https://doi.org/10.3389/fmicb.2021.757858>.
 140. Gordon O, Ruiz-Bedoya CA, Ordonez AA, Tucker EW, Jain SK. 2019. Molecular imaging: A novel tool to visualize pathogenesis of infections in situ. MBio <https://doi.org/10.1128/mBio.00317-19>.
 141. Wei H, Ma Y, Chen Q, Cui Y, Du L, Ma Q, Li Y, Xie X, Chen N. 2018. Identification and application of a novel strong constitutive promoter in Corynebacterium glutamicum. Ann Microbiol <https://doi.org/10.1007/s13213-018-1344-0>.
 142. T. Das A, Tenenbaum L, Berkhout B. 2016. Tet-On Systems For Doxycycline-inducible Gene Expression. Curr Gene Ther <https://doi.org/10.2174/1566523216666160524144041>.
 143. Liu G, Lin Q, Jin S, Gao C. 2022. The CRISPR-Cas toolbox and gene editing technologies. Mol Cell <https://doi.org/10.1016/j.molcel.2021.12.002>.
 144. Koonin E V., Makarova KS. 2019. Origins and evolution of CRISPR-Cas systems. Philos Trans R Soc B Biol Sci <https://doi.org/10.1098/rstb.2018.0087>.
 145. Agarwal N. 2020. Construction of a novel CRISPRi-based tool for silencing of multiple genes in Mycobacterium tuberculosis. Plasmid <https://doi.org/10.1016/j.plasmid.2020.102515>.
 146. Rock JM, Hopkins FF, Chavez A, Diallo M, Chase MR, Gerrick ER, Pritchard JR, Church GM, Rubin EJ, Sasseti CM, Schnappinger D, Fortune SM. 2017. Programmable transcriptional repression in mycobacteria using an orthogonal CRISPR interference platform. Nat Microbiol <https://doi.org/10.1038/nmicrobiol.2016.274>.
 147. Zhang R, Xu W, Shao S, Wang Q. 2021. Gene Silencing Through CRISPR Interference in Bacteria: Current Advances and Future Prospects. Front Microbiol <https://doi.org/10.3389/fmicb.2021.635227>.
 148. Gupta R, Rohde KH. 2023. Implementation of a mycobacterial CRISPRi platform in Mycobacterium abscessus and demonstration of the essentiality of ftsZMab. Tuberculosis <https://doi.org/10.1016/j.tube.2022.102292>.
 149. McNeil MB, Cook GM. 2019. Utilization of CRISPR interference to validate MmpL3 as a drug target in mycobacterium tuberculosis. Antimicrob Agents Chemother <https://doi.org/10.1128/AAC.00629-19>.
 150. Stachler AE, Schwarz TS, Schreiber S, Marchfelder A. 2020. CRISPRi as an efficient tool for gene repression in archaea. Methods <https://doi.org/10.1016/j.ymeth.2019.05.023>.
 151. Collias D, Beisel CL. 2021. CRISPR technologies and the search for the PAM-free nuclease. Nat Commun <https://doi.org/10.1038/s41467-020-20633->

- y.
152. Zhang D, Zhang B. 2020. SpRY: Engineered CRISPR/Cas9 Harnesses New Genome-Editing Power. *Trends Genet* <https://doi.org/10.1016/j.tig.2020.05.001>.
 153. Qi LS, Larson MH, Gilbert LA, Doudna JA, Weissman JS, Arkin AP, Lim WA. 2013. Repurposing CRISPR as an RNA-guided platform for sequence-specific control of gene expression. *Cell*.
 154. Parish T, Stoker NG. 2000. Use of flexible cassette method to generate a double unmarked *Mycobacterium tuberculosis* tlyA plcABC mutant by gene replacement. *Microbiology* <https://doi.org/10.1099/00221287-146-8-1969>.
 155. Kendall SL, Frita R. 2008. Construction of targeted mycobacterial mutants by homologous recombination. *Methods Mol Biol* https://doi.org/10.1007/978-1-59745-207-6_20.
 156. Gordhan BG, Parish T. 2003. Gene Replacement using Pretreated DNAMycobacterium Tuberculosis Protocols.
 157. Meijers AS, Troost R, Ummels R, Maaskant J, Speer A, Nejentsev S, Bitter W, Kuijl CP. 2020. Efficient genome editing in pathogenic mycobacteria using *Streptococcus thermophilus* CRISPR1-Cas9. *Tuberculosis* <https://doi.org/10.1016/j.tube.2020.101983>.
 158. Nilewar SS, Kathiravan MK. 2014. Mycothiol: A promising antitubercular target. *Bioorg Chem* <https://doi.org/10.1016/j.bioorg.2013.11.004>.
 159. Rockefeller.
 160. Bronson RA, Gupta C, Manson AL, Nguyen JA, Bahadirli-Talbott A, Parrish NM, Earl AM, Cohen KA. 2021. Global phylogenomic analyses of *Mycobacterium abscessus* provide context for non cystic fibrosis infections and the evolution of antibiotic resistance. *Nat Commun* <https://doi.org/10.1038/s41467-021-25484-9>.
 161. Ruis C, Bryant JM, Bell SC, Thomson R, Davidson RM, Hasan NA, van Ingen J, Strong M, Floto RA, Parkhill J. 2021. Dissemination of *Mycobacterium abscessus* via global transmission networks. *Nat Microbiol* <https://doi.org/10.1038/s41564-021-00963-3>.
 162. Rai LS, van Wijlick L, Chauvel M, d'Enfert C, Legrand M, Bachellier-Bassi S. 2022. Overexpression approaches to advance understanding of *Candida albicans*. *Mol Microbiol* <https://doi.org/10.1111/mmi.14818>.
 163. Saeki N, Yamamoto C, Eguchi Y, Sekito T, Shigenobu S, Yoshimura M, Yashiroda Y, Boone C, Moriya H. 2023. Overexpression profiling reveals cellular requirements in the context of genetic backgrounds and environments. *PLoS Genet* <https://doi.org/10.1371/journal.pgen.1010732>.
 164. Mavi PS, Singh S, Kumar A. 2020. Reductive Stress: New Insights in Physiology and Drug Tolerance of *Mycobacterium*. *Antioxidants Redox Signal* <https://doi.org/10.1089/ars.2019.7867>.
 165. Canton M, Sánchez-Rodríguez R, Spera I, Venegas FC, Favia M, Viola A, Castegna A. 2021. Reactive Oxygen Species in Macrophages: Sources and Targets. *Front Immunol* <https://doi.org/10.3389/fimmu.2021.734229>.

166. Kumar A, Subramanian Manimekalai MS, Grüber G. 2018. Substrate-induced structural alterations of Mycobacterial mycothione reductase and critical residues involved. *FEBS Lett* <https://doi.org/10.1002/1873-3468.12984>.
167. Rawat M, Johnson C, Cadiz V, Av-Gay Y. 2007. Comparative analysis of mutants in the mycothiol biosynthesis pathway in *Mycobacterium smegmatis*. *Biochem Biophys Res Commun* <https://doi.org/10.1016/j.bbrc.2007.08.142>.
168. Rawat M, Newton GL, Ko M, Martinez GJ, Fahey RC, Av-Gay Y. 2002. Mycothiol-deficient *Mycobacterium smegmatis* mutants are hypersensitive to alkylating agents, free radicals, and antibiotics. *Antimicrob Agents Chemother* <https://doi.org/10.1128/AAC.46.11.3348-3355.2002>.
169. Coulson GB, Johnson BK, Zheng H, Colvin CJ, Fillinger RJ, Haiderer ER, Hammer ND, Abramovitch RB. 2017. Targeting *Mycobacterium tuberculosis* Sensitivity to Thiol Stress at Acidic pH Kills the Bacterium and Potentiates Antibiotics. *Cell Chem Biol* <https://doi.org/10.1016/j.chembiol.2017.06.018>.
170. Meiru S, Chao Z, Bing Z, Dawei W, Keqi C, Xu Y, He X, Xihui S. 2016. Overexpression of Mycothiol Disulfide Reductase Enhances *Corynebacterium glutamicum* Robustness by Modulating Cellular Redox Homeostasis and Antioxidant Proteins under Oxidative Stress. *Sci Rep*.
171. Nakamura Y, Nishio Y, Ikeo K, Gojobori T. 2003. The genome stability in *Corynebacterium* species due to lack of the recombinational repair system *Gene*.
172. Cools F, Torfs E, Vanhoutte B, Bidart De Macedo M, Bonofiglio L, Mollerach M, Maes L, Caljon G, Delputte P, Cappoen D, Cos P. 2018. *Streptococcus pneumoniae* galU gene mutation has a direct effect on biofilm growth, adherence and phagocytosis in vitro and pathogenicity in vivo. *Pathog Dis* <https://doi.org/10.1093/femspd/fty069>.
173. Rodríguez-Sevilla G, García-Coca M, Romera-García D, Aguilera-Correa JJ, Mahillo-Fernández I, Esteban J, Pérez-Jorge C. 2018. Non-Tuberculous *Mycobacteria* multispecies biofilms in cystic fibrosis: development of an in vitro *Mycobacterium abscessus* and *Pseudomonas aeruginosa* dual species biofilm model. *Int J Med Microbiol* <https://doi.org/10.1016/j.ijmm.2018.03.003>.
174. Fahey RC. 2013. Glutathione analogs in prokaryotes. *Biochim Biophys Acta - Gen Subj* <https://doi.org/10.1016/j.bbagen.2012.10.006>.
175. Sun WJ, Wang L, Liu HH, Liu YJ, Ren YH, Wang FQ, Wei DZ. 2019. Characterization and engineering control of the effects of reactive oxygen species on the conversion of sterols to steroid synthons in *Mycobacterium neoaurum*. *Metab Eng* <https://doi.org/10.1016/j.ymben.2019.09.004>.
176. Zhang J, Du GC, Zhang Y, Liao XY, Wang M, Li Y, Chen J. 2010. Glutathione protects *Lactobacillus sanfranciscensis* against freeze-thawing, freeze-drying, and cold treatment. *Appl Environ Microbiol* <https://doi.org/10.1128/AEM.00026-09>.
177. Nakajima S, Satoh Y, Yanashima K, Matsui T, Dairi T. 2015. Ergothioneine

- protects *Streptomyces coelicolor* A3(2) from oxidative stresses. *J Biosci Bioeng* <https://doi.org/10.1016/j.jbiosc.2015.01.013>.
178. Abbott DA, Suir E, Duong GH, De Hulster E, Pronk JT, Van Maris AJA. 2009. Catalase overexpression reduces lactic acid-induced oxidative stress in *Saccharomyces cerevisiae*. *Appl Environ Microbiol* <https://doi.org/10.1128/AEM.00009-09>.
 179. An H, Zhou H, Huang Y, Wang G, Luan C, Mou J, Luo Y, Hao Y. 2010. High-level expression of heme-dependent catalase gene *katA* from *Lactobacillus Sakei* protects *Lactobacillus Rhamnosus* from oxidative stress. *Mol Biotechnol* <https://doi.org/10.1007/s12033-010-9254-9>.
 180. Si M, Zhao C, Zhang B, Wei D, Chen K, Yang X, Xiao H, Shen X. 2016. Overexpression of Mycothiol Disulfide Reductase Enhances *Corynebacterium glutamicum* Robustness by Modulating Cellular Redox Homeostasis and Antioxidant Proteins under Oxidative Stress. *Sci Rep* <https://doi.org/10.1038/srep29491>.
 181. Liu Y, Yang X, Yin Y, Lin J, Chen C, Pan J, Si M, Shen X. 2016. Mycothiol protects *Corynebacterium glutamicum* against acid stress via maintaining intracellular pH homeostasis, scavenging ROS, and S-mycothiolating MetE. *J Gen Appl Microbiol* <https://doi.org/10.2323/jgam.2016.02.001>.
 182. Sauton components BD.
 183. Control Q. Sautons Fluid Medium Base M1276 Sautons Fluid Medium is used for the cultivation and enumeration of Mycobacteria in accordance with I Composition**.
 184. Hu Z, Cronan JE. 2020. The primary step of biotin synthesis in mycobacteria. *Proc Natl Acad Sci U S A* <https://doi.org/10.1073/pnas.2010189117>.
 185. Dick T, Manjunatha U, Kappes B, Gengenbacher M. 2010. Vitamin B6 biosynthesis is essential for survival and virulence of *Mycobacterium tuberculosis*. *Mol Microbiol* <https://doi.org/10.1111/j.1365-2958.2010.07381.x>.
 186. Mittenhuber G. 2001. Phylogenetic analyses and comparative genomics of vitamin B6 (pyridoxine) and pyridoxal phosphate biosynthesis pathways. *J Mol Microbiol Biotechnol*.
 187. Brugha R, Spencer H. 2021. *Mycobacterium abscessus* in cystic fibrosis . *Science (80-)* <https://doi.org/10.1126/science.abi5695>.
 188. Choudhary E, Thakur P, Pareek M, Agarwal N. 2015. Gene silencing by CRISPR interference in mycobacteria. *Nat Commun* <https://doi.org/10.1038/ncomms7267>.
 189. Kirchner M, Schneider S. 2015. CRISPR-Cas: From the Bacterial Adaptive Immune System to a Versatile Tool for Genome Engineering. *Angew Chemie - Int Ed* <https://doi.org/10.1002/anie.201504741>.
 190. Li W, Yazidi A, Pandya AN, Hegde P, Tong W, de Moura VCN, North EJ, Sygusch J, Jackson M. 2018. MmpL3 as a target for the treatment of drug-resistant nontuberculous mycobacterial infections. *Front Microbiol* <https://doi.org/10.3389/fmicb.2018.01547>.
 191. Bosch B, DeJesus MA, Poulton NC, Zhang W, Engelhart CA, Zaveri A, Lavalette S, Ruecker N, Trujillo C, Wallach JB, Li S, Ehrt S, Chait BT,

- Schnappinger D, Rock JM. 2021. Genome-wide gene expression tuning reveals diverse vulnerabilities of *M. tuberculosis*. *Cell* <https://doi.org/10.1016/j.cell.2021.06.033>.
192. Shapiro RS, Chavez A, Collins JJ. 2018. CRISPR-based genomic tools for the manipulation of genetically intractable microorganisms. *Nat Rev Microbiol* <https://doi.org/10.1038/s41579-018-0002-7>.
193. Saviola B. 2009. Phage L5 integrating vectors are present within the mycobacterial cell in an equilibrium between integrated and excised states. *Cancer Ther*.
194. Springer B, Sander P, Sedlacek L, Ellrott K, Böttger EC. 2001. Instability and site-specific excision of integration-proficient mycobacteriophage L5 plasmids: Development of stably maintained integrative vectors. *Int J Med Microbiol* [https://doi.org/10.1016/S1438-4221\(01\)80004-7](https://doi.org/10.1016/S1438-4221(01)80004-7).
195. Pham TT, Jacobs-Sera D, Pedulla ML, Hendrix RW, Hatfull GF. 2007. Comparative genomic analysis of mycobacteriophage Tweety: Evolutionary insights and construction of compatible site-specific integration vectors for mycobacteria. *Microbiology* <https://doi.org/10.1099/mic.0.2007/008904-0>.
196. Nguyen TQ, Heo BE, Park Y, Jeon S, Choudhary A, Moon C, Jang J. 2023. CRISPR Interference-Based Inhibition of MAB_0055c Expression Alters Drug Sensitivity in *Mycobacterium abscessus*. *Microbiol Spectr* <https://doi.org/10.1128/spectrum.00631-23>.
197. Kurepina N, Chen L, Composto K, Rifat D, Nuermberger EL, Kreiswirth BN. 2022. CRISPR Inhibition of Essential Peptidoglycan Biosynthesis Genes in *Mycobacterium abscessus* and Its Impact on b-Lactam Susceptibility. *Antimicrob Agents Chemother* <https://doi.org/10.1128/aac.00093-22>.
198. Parish T, Stoker NG. 2000. *glnE* is an essential gene in *Mycobacterium tuberculosis*. *J Bacteriol* <https://doi.org/10.1128/JB.182.20.5715-5720.2000>.
199. T JAS, J R, Rajan A, Shankar V. 2020. Features of the biochemistry of *Mycobacterium smegmatis*, as a possible model for *Mycobacterium tuberculosis*. *J Infect Public Health* <https://doi.org/10.1016/j.jiph.2020.06.023>.
200. Sparks IL, Derbyshire KM, Jacobs WR, Morita YS. 2023. *Mycobacterium smegmatis*: The Vanguard of Mycobacterial Research. *J Bacteriol* <https://doi.org/10.1128/jb.00337-22>.
201. Yamada H, Yamaguchi M, Igarashi Y, Chikamatsu K, Aono A, Murase Y, Morishige Y, Takaki A, Chibana H, Mitarai S. 2018. *Mycobacterium smegmatis*, Basonym *Mycobacterium smegmatis*, Expresses Morphological Phenotypes Much More Similar to *Escherichia coli* Than *Mycobacterium tuberculosis* in Quantitative Structome Analysis and CryoTEM Examination. *Front Microbiol* <https://doi.org/10.3389/fmicb.2018.01992>.
202. Singh AK, Reyrat JM. 2009. Laboratory maintenance of *Mycobacterium smegmatis*. *Curr Protoc Microbiol* <https://doi.org/10.1002/9780471729259.mc10c01s14>.
203. Grigorov A, Bychenko O, Salina EG, Skvortsova Y, Mazurova A, Skvortsov T,

- Kaprelyants A, Azhikina T. 2021. Small rna f6 provides mycobacterium smegmatis entry into dormancy. *Int J Mol Sci* <https://doi.org/10.3390/ijms222111536>.
204. Do TT, Rodríguez-Beltran J, Cebrián-Sastre E, Rodríguez-Rojas A, Castañeda-García A, Blázquez J. 2022. Inactivation of a New Potassium Channel Increases Rifampicin Resistance and Induces Collateral Sensitivity to Hydrophilic Antibiotics in Mycobacterium smegmatis. *Antibiotics* <https://doi.org/10.3390/antibiotics11040509>.
 205. Maslov DA, Shur K V., Vatlin AA, Danilenko VN. 2020. Mmps5-MmpL5 transporters provide Mycobacterium smegmatis resistance to imidazo[1,2-b][1,2,4,5]tetrazines. *Pathogens* <https://doi.org/10.3390/pathogens9030166>.
 206. Kana BD, Mizrahi V. 2004. Molecular genetics of Mycobacterium tuberculosis in relation to the discovery of novel drugs and vaccines Tuberculosis.
 207. Xu X, Vilchèze C, Av-Gay Y, Gómez-Velasco A, Jacobs WR. 2011. Precise null deletion mutations of the mycothiol synthesis genes reveal their role in isoniazid and ethionamide resistance in Mycobacterium smegmatis. *Antimicrob Agents Chemother* <https://doi.org/10.1128/AAC.00020-11>.
 208. Ganesh N, Muniyappa K. 2003. Mycobacterium smegmatis RecA protein is structurally similar to but functionally distinct from Mycobacterium tuberculosis RecA. *Proteins Struct Funct Genet* <https://doi.org/10.1002/prot.10433>.
 209. Filsinger GT, Wannier TM, Pedersen FB, Lutz ID, Zhang J, Stork DA, Debnath A, Gozzi K, Kuchwara H, Volf V, Wang S, Rios X, Gregg CJ, Lajoie MJ, Shipman SL, Aach J, Laub MT, Church GM. 2021. Characterizing the portability of phage-encoded homologous recombination proteins. *Nat Chem Biol* <https://doi.org/10.1038/s41589-020-00710-5>.
 210. Papavinasundaram KG, Anderson C, Brooks PC, Thomas NA, Movahedzadeh F, Jenner PJ, Colston MJ, Davis EO. 2001. Slow induction of RecA by DNA damage in Mycobacterium tuberculosis. *Microbiology* <https://doi.org/10.1099/00221287-147-12-3271>.
 211. Forman HJ, Torres M. 2001. Redox signaling in macrophages. *Mol Aspects Med* [https://doi.org/10.1016/S0098-2997\(01\)00010-3](https://doi.org/10.1016/S0098-2997(01)00010-3).
 212. Sun S, See M, Nim HT, Strumila K, Ng ES, Hidalgo A, Ramialison M, Sutton P, Elefanty AG, Sarkar S, Stanley EG. 2022. Human pluripotent stem cell-derived macrophages host Mycobacterium abscessus infection. *Stem Cell Reports* <https://doi.org/10.1016/j.stemcr.2022.07.013>.
 213. Andrews S. 2010. FastQC: a quality control tool for high throughput sequence data. <http://www.bioinformatics.babraham.ac.uk/projects/fastqc>.
 214. Wingett SW, Andrews S. 2018. Fastq screen: A tool for multi-genome mapping and quality control [version 1; referees: 3 approved, 1 approved with reservations]. *F1000Research* 7:1–13.
 215. Martin M. 2011. Cutadapt removes adapter sequences from high-throughput sequencing reads. *EMBnet.journal*

- <https://doi.org/10.14806/EJ.17.1.200>.
216. Barrick JE, Colburn G, Deatherage DE, Traverse CC, Strand MD, Borges JJ, Knoester DB, Reba A, Meyer AG. 2014. Identifying structural variation in haploid microbial genomes from short-read resequencing data using breseq. *BMC Genomics* 15:1–17.
 217. Langmead B, Wilks C, Antonescu V, Charles R. 2019. Scaling read aligners to hundreds of threads on general-purpose processors. *Bioinformatics* 35:421–432.
 218. Cools F, Torfs E, Aizawa J, Vanhoutte B, Maes L, Caljon G, Delputte P, Cappoen D, Cos P. 2019. Optimization and characterization of a *Galleria mellonella* larval infection model for virulence studies and the evaluation of therapeutics against *Streptococcus pneumoniae*. *Front Microbiol* <https://doi.org/10.3389/fmicb.2019.00311>.
 219. Peloquin CA, Davies GR. 2021. The Treatment of Tuberculosis. *Clin Pharmacol Ther* <https://doi.org/10.1002/cpt.2261>.
 220. Vargas D, Hageman S, Gulati M, Nobile CJ, Rawat M. 2016. S-nitrosomycothiols reductase and mycothiol are required for survival under aldehyde stress and biofilm formation in *Mycobacterium smegmatis*. *IUBMB Life* <https://doi.org/10.1002/iub.1524>.
 221. Tateishi Y, Minato Y, Baughn AD, Ohnishi H, Nishiyama A, Ozeki Y, Matsumoto S. 2020. Genome-wide identification of essential genes in *Mycobacterium intracellulare* by transposon sequencing — Implication for metabolic remodeling. *Sci Rep* <https://doi.org/10.1038/s41598-020-62287-2>.
 222. Patel K, Song F, Andreana PR. 2017. Synthesis of substrate analogues as potential inhibitors for *Mycobacterium tuberculosis* enzyme MshC. *Carbohydr Res* <https://doi.org/10.1016/j.carres.2017.10.014>.
 223. Newton GL, Unson MD, Anderberg SJ, Aguilera JA, Oh NN, Delcardayre SB, Av-Gay Y, Fahey RC. 1999. Characterization of *mycobacterium smegmatis* mutants defective in 1-D-myo-inosityl-2-amino-2-deoxy- α -D-glucopyranoside and mycothiol biosynthesis. *Biochem Biophys Res Commun* <https://doi.org/10.1006/bbrc.1999.0156>.
 224. Ta P, Buchmeier N, Newton GL, Rawat M, Fahey RC. 2011. Organic hydroperoxide resistance protein and ergothioneine compensate for loss of mycothiol in *Mycobacterium smegmatis* mutants. *J Bacteriol* <https://doi.org/10.1128/JB.01402-10>.
 225. Vesenbeckh S, Schönfeld N, Roth A, Bettermann G, Krieger D, Bauer TT, Rüssmann H, Mauch H. 2017. Bedaquiline as a potential agent in the treatment of *Mycobacterium abscessus* infections. *Eur Respir J* <https://doi.org/10.1183/13993003.00083-2017>.
 226. Dupont C, Viljoen A, Thomas S, Roquet-Banères F, Herrmann JL, Pethe K, Kremer L. 2017. Bedaquiline inhibits the ATP synthase in *mycobacterium abscessus* and is effective in infected zebrafish. *Antimicrob Agents Chemother* <https://doi.org/10.1128/AAC.01225-17>.
 227. Lu P, Lill H, Bald D. 2014. ATP synthase in mycobacteria: Special features and implications for a function as drug target. *Biochim Biophys Acta* -

- Bioenerg <https://doi.org/10.1016/j.bbabi.2014.01.022>.
228. Bahuguna A, Rawat DS. 2020. An overview of new antitubercular drugs, drug candidates, and their targets. *Med Res Rev* <https://doi.org/10.1002/med.21602>.
 229. Dokic A, Peterson E, Arrieta-Ortiz ML, Pan M, Di Maio A, Baliga N, Bhatt A. 2021. Mycobacterium abscessus biofilms produce an extracellular matrix and have a distinct mycolic acid profile. *Cell Surf* <https://doi.org/10.1016/j.tcs.2021.100051>.
 230. Boudarel H, Mathias JD, Blaysat B, Grédiac M. 2018. Towards standardized mechanical characterization of microbial biofilms: analysis and critical review. *npj Biofilms Microbiomes* <https://doi.org/10.1038/s41522-018-0062-5>.
 231. Grzelak EM, Choules MP, Gao W, Cai G, Wan B, Wang Y, McAlpine JB, Cheng J, Jin Y, Lee H, Suh JW, Pauli GF, Franzblau SG, Jaki BU, Cho S. 2019. Strategies in anti-Mycobacterium tuberculosis drug discovery based on phenotypic screening. *J Antibiot (Tokyo)* <https://doi.org/10.1038/s41429-019-0205-9>.
 232. Hoffner S, Chan MM, Chan ED, Ordway D. 2020. Drug discovery targeting drug-resistant nontuberculous mycobacteria. *Drug Discovery Targeting Drug-Resistant Bacteria*.
 233. Shankar P, Singh S, Boorgula GD, Gumbo T, Heysell SK, Srivastava S. 2022. Challenges and a potential solution to perform drug susceptibility testing of omadacycline against nontuberculous mycobacteria. *Tuberculosis* <https://doi.org/10.1016/j.tube.2022.102269>.
 234. Gibson B, Wilson DJ, Feil E, Eyre-Walker A. 2018. The distribution of bacterial doubling times in the wild. *Proc R Soc B Biol Sci* <https://doi.org/10.1098/rspb.2018.0789>.
 235. Strnad L, Winthrop KL. 2018. Treatment of Mycobacterium abscessus Complex. *Semin Respir Crit Care Med* <https://doi.org/10.1055/s-0038-1651494>.
 236. Swinney DC, Lee JA. 2020. Recent advances in phenotypic drug discovery. *F1000Research* <https://doi.org/10.12688/f1000research.25813.1>.
 237. Sams-Dodd F. 2005. Target-based drug discovery: Is something wrong? *Drug Discov Today* [https://doi.org/10.1016/S1359-6446\(04\)03316-1](https://doi.org/10.1016/S1359-6446(04)03316-1).
 238. Kana BD, Karakousis PC, Parish T, Dick T. 2014. Future target-based drug discovery for tuberculosis? *Tuberculosis* <https://doi.org/10.1016/j.tube.2014.10.003>.
 239. Fernandes GFS, Thompson AM, Castagnolo D, Denny WA, Dos Santos JL. 2022. Tuberculosis Drug Discovery: Challenges and New Horizons. *J Med Chem* <https://doi.org/10.1021/acs.jmedchem.2c00227>.
 240. Childers WE, Elokely KM, Abou-Gharbia M. 2020. The Resurrection of Phenotypic Drug Discovery. *ACS Med Chem Lett* <https://doi.org/10.1021/acsmedchemlett.0c00006>.
 241. Fekadu G, Tolossa T, Turi E, Bekele F, Fetensa G. 2022. Pretomanid development and its clinical roles in treating tuberculosis. *J Glob Antimicrob Resist* <https://doi.org/10.1016/j.jgar.2022.09.001>.

242. Vincent F, Nueda A, Lee J, Schenone M, Prunotto M, Mercola M. 2022. Phenotypic drug discovery: recent successes, lessons learned and new directions. *Nat Rev Drug Discov* <https://doi.org/10.1038/s41573-022-00472-w>.
243. Quang NT, Jang J. 2021. Current Molecular Therapeutic Agents and Drug Candidates for *Mycobacterium abscessus*. *Front Pharmacol* <https://doi.org/10.3389/fphar.2021.724725>.
244. Paul D, Sanap G, Shenoy S, Kalyane D, Kalia K, Tekade RK. 2021. Artificial intelligence in drug discovery and development. *Drug Discov Today* <https://doi.org/10.1016/j.drudis.2020.10.010>.
245. Hasselgren C, Oprea TI. 2024. Artificial Intelligence for Drug Discovery: Are We There Yet? *Annu Rev Pharmacol Toxicol* 64.
246. Liu GY, Yu D, Fan MM, Zhang X, Jin ZY, Tang C, Liu XF. 2024. Antimicrobial resistance crisis: could artificial intelligence be the solution? *Mil Med Res* 11:1–23.
247. Shen L, Liao K, Yang E, Yang F, Lin W, Wang J, Fan S, Huang X, Chen L, Shen H, Jin H, Ruan Y, Liu X, Zeng G, Xu JF, Pi J. 2023. Macrophage targeted iron oxide nanodecoys augment innate immunological and drug killings for more effective *Mycobacterium Tuberculosis* clearance. *J Nanobiotechnology* 21:1–26.
248. Yoshizumi T, Shibui Y, Kogo M, Honma S, Ito S, Yajima S, Sasaki Y. 2023. Mycothiol maintains the homeostasis and signalling of nitric oxide in *Streptomyces coelicolor* A3(2) M145. *BMC Microbiol* 23:285.
249. Gibango L, Oosthuizen CB, Lall N. 2020. Potential implications of the use of *Rapanea melanophloeos* (L.) Mez against mycobacteria. *South African J Bot* <https://doi.org/10.1016/j.sajb.2020.06.003>.
250. Oosthuizen CB, Gasa N, Hamilton CJ, Lall N. 2019. Inhibition of mycothione disulphide reductase and mycobacterial biofilm by selected South African plants. *South African J Bot* <https://doi.org/10.1016/j.sajb.2018.09.015>.
251. Copley SD, Dhillon JK. 2002. Lateral gene transfer and parallel evolution in the history of glutathione biosynthesis genes. *Genome Biol* <https://doi.org/10.1186/gb-2002-3-5-research0025>.
252. Vilchèze C, Av-Gay Y, Attarian R, Liu Z, Hazbón MH, Colangeli R, Chen B, Liu W, Alland D, Sacchettini JC, Jacobs WR. 2008. Mycothiol biosynthesis is essential for ethionamide susceptibility in *Mycobacterium tuberculosis*. *Mol Microbiol* <https://doi.org/10.1111/j.1365-2958.2008.06365.x>.
253. Hendricks AR, Guilliams BF, Cohen RS, Tien T, McEwen GA, Borgognoni KM, Ackerson CJ. 2023. Cloneable inorganic nanoparticles. *Chem Commun* <https://doi.org/10.1039/d3cc01319g>.
254. Gashaw I, Ellinghaus P, Sommer A, Asadullah K. 2011. What makes a good drug target? *Drug Discov Today* <https://doi.org/10.1016/j.drudis.2011.09.007>.
255. Owens J. 2007. Determining druggability. *Nat Rev Drug Discov* <https://doi.org/10.1038/nrd2275>.
256. Leach AR, Thomas PJ. 2017. Protein Structure Prediction and Homology Modeling *Comprehensive Medicinal Chemistry III*.

257. Caesar LK, Cech NB. 2019. Synergy and antagonism in natural product extracts: When 1 + 1 does not equal 2. *Nat Prod Rep* <https://doi.org/10.1039/c9np00011a>.
258. Borek A, Zabost A, Głogowska A, Filipczak D, Augustynowicz-Kopeć E. 2022. New RAPMYCOI Sensititre™ Antimicrobial Susceptibility Test for Atypical Rapidly Growing Mycobacteria (RGM). *Diagnostics* <https://doi.org/10.3390/diagnostics12081976>.
259. Rampacci E, Stefanetti V, Passamonti F, Henao-Tamayo M. 2020. Preclinical models of nontuberculous mycobacteria infection for early drug discovery and vaccine research. *Pathogens* <https://doi.org/10.3390/pathogens9080641>.
260. Taylor LS, Braun DE, Steed JW. 2021. Crystals and Crystallization in Drug Delivery Design. *Cryst Growth Des* <https://doi.org/10.1021/acs.cgd.0c01592>.
261. Fauman EB, Rai BK, Huang ES. 2011. Structure-based druggability assessment-identifying suitable targets for small molecule therapeutics. *Curr Opin Chem Biol* <https://doi.org/10.1016/j.cbpa.2011.05.020>.
262. Keseru GM, Makara GM. 2006. Hit discovery and hit-to-lead approaches. *Drug Discov Today* <https://doi.org/10.1016/j.drudis.2006.06.016>.
263. Togre NS, Vargas AM, Bhargavi G, Mallakuntla MK, Tiwari S. 2022. Fragment-Based Drug Discovery against Mycobacteria: The Success and Challenges. *Int J Mol Sci* <https://doi.org/10.3390/ijms231810669>.
264. Blay V, Tolani B, Ho SP, Arkin MR. 2020. High-Throughput Screening: today's biochemical and cell-based approaches. *Drug Discov Today* <https://doi.org/10.1016/j.drudis.2020.07.024>.
265. Smiejkowska N, Oorts L, Van Calster K, De Vooght L, Geens R, Mattelaer H-P, Augustyns K, Strelkov S V., Lamprecht D, Temmerman K, Sterckx YG-J, Cappoen D, Cos P. 2024. A high-throughput target-based screening approach for the identification and assessment of Mycobacterium tuberculosis mycothione reductase inhibitors. *Microbiol Spectr* 12:1–22.
266. Zhai W, Wu F, Zhang Y, Fu Y, Liu Z. 2019. The immune escape mechanisms of Mycobacterium Tuberculosis. *Int J Mol Sci* <https://doi.org/10.3390/ijms20020340>.
267. Cumming BM, Lamprecht DA, Wells RM, Saini V, Mazorodze JH, Steyn AJC. 2014. The Physiology and Genetics of Oxidative Stress in Mycobacteria. *Microbiol Spectr* <https://doi.org/10.1128/microbiolspec.mgm2-0019-2013>.



TATIANA PILLER

PhD researcher



Wilrijk, Belgium



+32475399727



www.linkedin.com/in/tatiana-piller



tatiana@pillar.be



French (Native)

Dutch (Native)

English (Fluent)

Hebrew (Proficient)

WORK EXPERIENCE

- 2019 - 2023 **PhD in Pharmaceutical Sciences**
Laboratory for Microbiology, Parasitology and Hygiene - University of Antwerp
Research topic: Mycobacteria
- 05/2019 - 04/2020 **RESPIRI-TB**
IMI AMR Accelerator Program
853903
- 08/2018 - 02/2019 **Voluntary Internship in Bacteriology**
Laboratory for Microbiology, Parasitology and Hygiene - University of Antwerp
- 11/2017 - 06/2018 **Master Thesis Internship in Molecular Parasitology**
I3s, Instituto de Investigação e inovação em Saúde, Porto, Portugal
Research topic: Leishmaniasis
- 09/2016 **Voluntary Internship in Proteomics**
Laboratory of Protein Chemistry, Proteomics and Epigenetic Signalling (PPES) - University of Antwerp

EDUCATION

- 2016 - 2018 **Master in Biomedical Sciences: Infectious and Tropical Diseases**
University of Antwerp
Minor: Research
Great Distinction
- 2013 - 2016 **Bachelor in Biomedical Sciences**
University of Antwerp
Distinction

VOLUNTEERING

- 08/2011 - 08/2013 **Leadership position**
Hanoar Hatzioni youth movement, Antwerp

ACCOMPLISHMENTS

- 11/2019 **FWO fellowship strategic basic research**
1S68720N

COURSES AND CERTIFICATES

- 2023 **Attest medical blood sampling**
Technique of venous blood sampling with vacutainer system
UZA
- 2022 **Grow your future career**
University of Antwerp
- 2022 **Personal effectiveness**
University of Antwerp
- 2021 **Basic principles of statistics**
StatUA, University of Antwerp
- 2021 **Writing academic papers**
University of Antwerp
- 2019 **Giving presentations in English**
University of Antwerp
- 2017 **FELASA C**
University of Antwerp

PUBLICATIONS

Cappoen D, Torfs E, Meiresonne T, Claes P, Semina E, Holvoet F, Bidart de Macedo M, Cools F, **Piller T**, Matheussen A, Van Calster K, Caljon G, Delputte P, Maes L, Neyrolles O, De Kimpe N, Mangelinckx S, Cos P. The synthesis and in vitro biological evaluation of novel fluorinated tetrahydrobenzo[j]phenanthridine-7,12-diones against *Mycobacterium tuberculosis*. *Eur J Med Chem*. 2019;118:111549. Doi: 10.1016/J.ejmech.2019.07.052.

Torfs E, **Piller T**, Cos P, Cappoen D. Opportunities for Overcoming *Mycobacterium tuberculosis* Drug Resistance: Emerging *Mycobacterial* Targets and Host-Directed Therapy. *Int J Mol Sci*. 2019;20.12:2868. Doi: 10.3390/ijms20122868. Review.

Pang L, Lenders S, Osipov EM, Weeks SD, Rozenski J, **Piller T**, Cappoen D, Strelkov SV, Van Aerschot A. Structural Basis of Cysteine Ligase MshC Inhibition by Cysteiny-Sulfonamides. *International Journal of Molecular Sciences*. 2022; 23(23):15095. <https://doi.org/10.3390/ijms232315095>

Piller T, De Vooght L, Gansemans Y, Van Nieuwerburgh F, Cos P. Mycothione reductase as a potential target in the fight against *Mycobacterium abscessus* infections. *mSphere*. 2023 Dec 12:e0066923. doi: 10.1128/msphere.00669-23. Epub ahead of print. PMID: 38085034.

Bento C, Van Calster K, **Piller T**, Oliveira G, De Vooght L, Cappoen D, Cos P, Gomes M S, Silva T. Characterization of novel double-reporter strains of *Mycobacterium abscessus* for drug discovery: a study in mScarlet. **Submitted**

PRESENTATIONS

Oral

Piller T., De Vooght L., Cappoen D., Cos P.
Title: Mycothione reductase: a novel target in the fight against *Mycobacterium abscessus* infections?
Research Day FBD 2022
Antwerp, Belgium

Poster

Piller T., De Vooght L., Cos P, Cappoen D.
Title: Mycothione reductase as a novel target in the fight against *M. abscessus* biofilm-related pulmonary infections
EMBO 2022
Paris, France

SUPERVISION OF STUDENTS

Master students

Jeroen Roelant
Title: Targeting the mycothiol pathway in *Mycobacterium avium* by using the pNIL/pGOAL system.
2020-2021

Iris Jacobs
Title: Investigating the role of MshC and Mtr as potential targets in the fight against *Mycobacterium abscessus* infections.
2022-2023

SUPERVISION PRACTICAL COURSE

Geïntegreerd Practicum

1st Master Biomedical Sciences
2021

ACKNOWLEDGEMENTS



“Sometimes life is like this dark tunnel.

*You can’t always see the light at the end of the tunnel, but if
you just keep moving you will come to a better place.”*

~ Uncle Iroh

Although these words were said by a fictional character, they couldn’t be more accurate. Most of you already know that I haven’t had the easiest time during my PhD. However, this thesis is proof that with perseverance and the right people around you, you can achieve anything.

~

First, I would like to express my gratitude to the members of my doctoral committee and external jury, **prof. dr. Wim Martinet**, **prof. dr. ir. Yann Stercks**, **prof. dr. Leen Rigouts** and **prof. dr. Maria Salomé Gomes**, for their invested time, thorough evaluation and invaluable feedback.

~

The ones I spent most of my time with at the LMPH is the **bacterio team**. Except from sharing the same boss, we’ve also shared the same lab, office, experiments, materials, meetings and/or sometimes problems. That last one gave us always a lot to talk, laugh and cry about, and definitely brought us closer together. **Freya**, dankzij jou voelde ik me direct welkom in het bacterio team en het delen van een bureau heeft gezorgd voor talrijke babbeltjes en veel gelach. Dank u om met jouw positieve uitstraling altijd een glimlach op mijn gezicht te toveren! **Matthias**, zingen en dansen in het labo was vanzelfsprekend een deel van onze dag, momenten die elke dag op het LMPH leuker hebben gemaakt. Het bacterio labo was véél stiller en saaier zonder jou!

Agnese, thank you for lighting up my days with cute videos of your nephew, our endless conversations in the office, making me laugh with your favorite word “JESUS”, our videocall exercise session when we both had COVID, and sharing your passion for music through your headphones XD. You made me laugh a lot during the past 4.5 years, keep on making people laugh. **Kevin**, dank u voor alle leuke momenten in het bureau, and let’s not forget de “venting” en gossip sessies! **Nele**, met jou klikte het al sinds dag 1. Even iets komen vragen kon al snel uitdraaien in lange conversaties. Dank u voor de luchtige gesprekken maar ook om me altijd te steunen! Ook bedankt om een stekje van jouw pannenkoekenplant met mij te willen delen, ik hoop dat de volgende die ik krijg iets langer blijft leven XD. **Laurence**, ik heb jou de laatste jaren beter leren kennen en daar ben ik heel blij om. Je bent aardig, behulpzaam en hardwerkend, de bacterio team is lucky dat je blijft. **Laure en Milan**, met jullie heb ik het kortst samengewerkt op het LMPH maar ik kon toch altijd bij jullie terecht om even goed te lachen en voor leuke gesprekken.

Besides the bacterio team, I’ve also spent lots of time with the other teams at the LMPH. **Parasito**, in spite of not being part of your team, I’ve always felt very welcome hanging out with you. Thank you for all the times that I could join you in your office for a lunch or coffee break, for the talks in the hallway, and for my last few days at the LMPH with a warm spot in your office. **Viro**, I’ve spent most of my Komida lunch breaks together with you and I loved every one of them. Our numerous talks about cats, babies and other subjects were the perfect breaks before continuing the afternoon in the lab. **Labtechs**, from talks in the lab or during lunch to learning more about birds and bees, it was always fun spending time with each one of you! A special thanks to **An and Natascha** for always helping me out with administrative stuff and making work at the LMPH so much easier.

Thank you LMPH for all the memories and fun times!

~

Of course I wouldn't have had the opportunity of doing a PhD or finishing it without the help of my promotors: **Paul and Linda**. Dank u om in mij te geloven, mij altijd te steunen en mij te helpen navigeren doorheen mijn doctoraat. Linda, naast mijn promotor ben je ook jaren mijn buurvrouw geweest in ons bureau, dank u voor alle luchtige gesprekken maar ook om altijd tijd te hebben voor mijn vragen.

~

I would also like to thank my **family and friends** for always supporting me throughout these last years. **Mam**, merci de m'avoir inspirée à faire de la recherche sur la Mycobactérie. **Mimi**, merci de m'avoir toujours écouter quand je l'avais besoin et d'être là pour moi.

~

Finally, I would like to thank some special people I couldn't have done this PhD without.

Eveline, hoewel er eerst vermeden wou worden dat we vriendinnen werden, werd het al snel duidelijk dat jij en ik veel gemeen hadden. Hierdoor werden we natuurlijk echt friends en dit is ook zo gebleven doorheen de jaren. Ik herinner me ons allereerst lang gesprek in het bureau tot laat na de werkuren en sindsdien kunnen we altijd bij elkaar terecht voor steun in goede en slechte momenten. Dank u voor een leuk jaar samen op het LMPH, wandeldates met Marceleke, babbeldates op restau, en er ook buiten het labo voor me te zijn.

Natalia en Lauren, MtrGirls, onze jaren op het LMPH worden het best gekarakteriseerd door een rollercoaster; goede en slechte labodagen, up en down momenten, gelukke en gefaalde experimenten. Toch had ik dit parcours met niemand anders willen afleggen dan met jullie. Doorheen de jaren konden we altijd bij elkaar terecht voor vragen, steun, babbeltjes, lachmomenten en voornamelijk gezamenlijke frustratiemomenten. En als onze mood tegen dan nog niet verbeterd was, konden we altijd rekenen op elkaars GIFs achteraf. Dank u girls voor al die jaren, ik had dit nooit allemaal gekund zonder jullie!

Ju-Li Moon, I am forever grateful for the LMPH to have led me to a friend like you. From our first conversation at our desk, where we bonded over our shared passion for Disney, I knew you and I would get along perfectly. Working alongside you in the lab made lab work so much fun; we spent our days singing and dancing in the lab with Matthias and our waiting times making agar art. But our friendship did certainly not stop after working hours and has only been growing since. I will always cherish our walks in the park, quick rollerblade sessions during my writing breaks, and the evenings with Laura filled with dancing, art, therapy, Ghibli movies and your amazing cooking skills. Thank you for everything and I can't wait to make more memories with you. Te amo.

Laura, my soulsister, I don't even know where to start. Toen ik 7 jaar geleden hoorde dat we samen op Erasmus mochten vertrekken naar Porto was ik zo blij; 7 maand lang dagelijks samen met mijn beste vriendin in een mega toffe stad. Ik had dan ook nooit gedacht dat we één jaar later samen aan onze PhD gingen beginnen in hetzelfde labo en elkaar nog 4.5 jaar elke dag zouden kunnen blijven zien. I'm so happy we did and I'm going to miss this so much! Het waren voor mij geen makkelijke 4.5 jaren maar je had altijd snel door als er iets was en wist altijd wat je moest doen of zeggen om me terug aan het lachen te maken. Dank u om er altijd voor me te zijn, voor alle leuke momenten samen op het labo zoals het maken van tiktoks of onze movie nights in de vergaderzaal, alle recharge avondjes na lange dagen op het labo, maar vooral thank you for being you. Ik had mezelf beloofd om het niet te emotioneel te maken, but here we are XD. I purple you.

Suki, my little companion while writing my thesis. Thank you for all the relaxing belly massages, purring therapy sessions and cuddles when I was stuck at home writing.

Eder, je n'ai pas toujours eu aussi facile les dernières années mais tu étais toujours à mes côtés pour me remonter le morale après une longue journée. Merci de toujours vouloir me faire rire, de m'accompagner au labo au milieu de la nuit quand je pense avoir oublier quelque chose ou juste d'écouter les histoires sur ma journée. I couldn't have done it without your endless support, positive energy, infectious humor, inspiring peptalks and caring nature. You know it all, je t'aime.



~

